BRUNEL UNIVERSITY

The Use of Macro Fiber Composite Transducers for Ultrasonic Guided Wave Based Inspection

by

Alexander George Haig

A thesis submitted in partial fulfillment for the
degree of Engineering Doctorate

in the
School of Engineering and Design

June 2013

Abstract

Sound can propagate for long distances with a low loss of intensity in objects whose geometry acts as a guide for the sound waves; a phenomenon that can be utilised for long range testing of structures. The guided sound waves can be used to conduct materials evaluation or to detect flaws, which can be done for a relatively large region of coverage from a relatively small region of access. In particular this technology can be used to inspect or monitor large engineering structures whose structural integrity is critical for safety and the environment, such as wind turbine towers, ship hulls, and pipelines.

The use of guided waves for structural inspection is complicated by the existence of many wave modes. In this thesis, the Macro Fiber Composite (MFC) is characterised for its frequency, wavelength, wave mode and direction dependent sensitivity. These devices are flexible, light and thin, and, here have been shown to have wave mode sensitivity characteristics that are favourable for some applications. The MFC is a piezoelectric actuator that can be used to excite and sense in-plane vibrations at a structures surface. The surface area of an MFC is significantly large with respect to typical wavelengths used in ultrasonic guided wave applications, which combined with their in-plane extensional nature gives rise to a significantly wave mode, frequency and direction dependent sensitivity. This can limit their application, but can also potentially be exploited for greater wave mode control.

A method for simulating the output from hypothesised transducer behaviour is shown and validated for the MFC. This allows their behaviour to be predicted for new structures. It is shown that their frequency response can depend on the waveguide and can vary with direction, which can lead to wave mode transmission and reception characteristics that may be advantageous for some methods of application and detrimental to others.

A novel method of adapting a flexible transducer, such as the MFC, has been developed and its characterisation is given. It is shown that through the use of a decoupling membrane, an MFC can be caused to have very different wave mode sensitivity characteristics whilst retaining their light and flexible nature. These altered characteristics are favourable for applications where shear horizontal wave modes are required.

Both fully coupled MFC transducers and the adapted MFC transducers are considered for application to pipeline testing. Fully coupled MFC transducers are used for inspection using longitudinal waves, whilst the adapted MFC transducers are used with torsional waves. These arrays are compared to a current commercial tool.

Acknowledgements

The author extends his gratitude to all those who have aided him during the EngD Programme at Brunel University, the University of Surrey, and TWI Ltd. The work could not have been completed without the help and support of the project supervisors Professor Wamadeva Balachandran and Peter Mudge. The friendship and tutelage from the fellow students have been treasured and thanks go to them, particularly Hugo Marques who used much time to aid me. Gratitude is extended to all staff at TWI Ltd. particularly those I worked with closely. Thanks and recognition for project funding goes to The Engineering and Physical Sciences Research Council (EPSRC) and TWI Ltd., who made the research possible.

Special thanks go to Dr Phil Catton and Dr Ruth Catton (née Sanderson) who have been invaluable colleagues and friends. Special thanks must also go to Martin Atkins, who as a friend taught me a great deal, which was valuable preparation for this research and for the rest of my career.

I am grateful to my family who encouraged me and patiently waited for me to finish after long period where I had little time for them. My greatest appreciation is for my most patient supporter of all, my fiance Kelly Tarrant.

Contents

List of Figures

Symbols

$L(0,q)$	qth longitudinal cylindrical wave mode
$T(0,q)$	qth torsional cylindrical wave mode
$F(p,q)$	qth flexural cylindrical wave mode of the pth circumferential order
d_{ij}	Piezoelectric modulus: strain in i by applied electric field in j, C/N
ω	Angular Frequency, radians
t	Time, seconds
$A_V(\omega)$	Signal voltage amplitude as a function of angular frequency, volts
$\phi(\omega)$	A signal phase off-set for each frequency, radians
E	Electric field, N/C
r_e	Distance between MFC electrode pairs, meters
w	The width of an MFC electrode finger, meters
σ	Material stress matrix (or scalar in the 1D case), pascal
ε	Material strain matrix (or scalar in the 1D case)
ζ_σ	Permittivity of a material when under zero stress
s	Compliance, the inverse of stiffness, m/N
n	An arbitrary wave mode
x	A position along the Cartesian x-axis, meters
y	A position along the Cartesian y-axis, meters
x_{min}	The position of the left hand edge of an MFC in the fibre axis, meters
x_{max}	The position of the right hand edge of an MFC in the fibre axis, meters
x_{rx}	A position of measurement on the Cartesian x-axis, meters
$k_n(\omega)$	Angular wavenumber for wave mode n at frequency ω, radians/meter
$\beta_n(\omega)$	The relative excitability of wave mode n, arbitrary units
$\alpha_n(\omega)$	The attenuation rate of wave mode n, decibels/meter
s_n	Surface displacement of an actuated MFC for wave mode n, meters
$s_{n,Point}$	Surface displacement field of wave mode n excited by a point, meters
$s_{n,tx}$	Surface displacement field of wave mode n excited by an MFC, meters
$A_n(\omega)$	A coefficient to represent the amplitude of an arbitrary wave
g_{ij}	Piezoelectric constant: electric field in i by applied stress in j, Vm/N
m	An arbitrary segment of an MFC
M	The last segment of an MFC in the positive x-axis direction
V_{rx}	The voltage developed by an MFC when receiving, volts

A_{AFL}	The transmission amplitude as influenced by Active Fibre Length
Λ	The Young's modulus (the modulus of elasticity)

Executive Summary

Introduction

Ultrasonic guided waves can be used for the inspection or condition monitoring of structures throughout engineering for detecting, locating and characterising structural defects. Any prismatic or plate-like structure can support the propagation of ultrasonic guided waves, which are capable of travelling relatively long distances. Typical structures tested with this technology include plates, beams, rods, rails, plates and tubes. It has been applied across many industries including food production, manufacturing, oil and gas, transport, power generation, aerospace and civil engineering. One of the most successful applications is the inspection of oil and gas pipe lines, which has been used commercially for over a decade. The long range capability of ultrasonic guided waves allows the development of techniques that can screen large areas of a structure whilst requiring limited access and relatively few sensors.

This technology facilitates the early detection of growing defects, which can allow for timely repair and avoid catastrophic failures. The long range capability also allows the inspection of areas of a structure that are otherwise in accessible. For example, it is common practise to use ultrasonic guided waves to inspect oil and gas pipelines that pass underground at a location where their route crosses a road. An inspection tool is placed around the pipe at an accessible location above ground, and from that position a length of that pipe that is submerged (typically tens of meters) is screened for defects. The prevention of structural failure in this scenario alone is of critical importance. In fact, corrosion was not detected in a pipeline that in 2006 led to the largest oil spill on Alaska's North Slope on record. Incidents like this can be reduced with the greater use of inspection and monitoring methods such as through the use of ultrasonic guided waves. When also considering the risks of structural failure in other areas, such as shipping, civil engineering and aviation, it is clear that any technology that can be used to give early warnings of structural failure is of great value. It is a technology that has really become popular for use and as a research topic from the end of the 20^{th} century onwards, making it a relatively new field of non-destructive testing. The research in this thesis aims at improving this technology so that it may be used better and for a wider range of applications.

In structures that can support ultrasonic guided waves, there are a great number of possible wave modes that can exist. That is, sound waves can propagate in different shapes of oscillation and there are many possible shapes. These wave modes vary by velocity and their velocities often vary with frequency. Any technique that makes use of ultrasonic guided waves must be carefully developed to make use of the most appropriate wave mode over the most appropriate frequency range.

One of the most crucial issues for many ultrasonic guided wave techniques is wave mode control. Generally arrays of transducers are designed such that a single wave mode (or selected set of wave modes) is transmitted in a desired direction without significant transmission of other modes or in other directions. This is made simpler if a transducer type can be selected for use in the array that has directional characteristics that suit the requirements of the application.

A new type of transducer has been identified in the literature as having potential benefits for ultrasonic guided wave techniques, which is the Macro Fiber Composite transducer. This transducer combines piezocomposite and interdigital electrode technologies to create a flexible, thin film device that is relatively robust and low weight. It has been hypothesised that, due to its size and nature, it may also have wave mode selective behaviour that once characterised could be used to create transducer arrays with superior wave mode control. In this thesis these devices are characterised in this way and they have been developed into an array for the application of pipe line testing.

Thesis Goal

Characterise MFC transducers so that they can be better used to produce transducer arrays that are effective at exciting a desired wave mode without exciting unwanted wave modes and demonstrate how this may lead to improved inspection technology.

Specific Objectives

- Analyse the MFC transducers sensitivy and its dependency on:
  - Wave mode
  - Wavelength
  - Frequency
  - Direction
- Produce a analytical model to represent this sensitivity variation, particularly with respect to MFC size dependency.

- Valiated the model's predictions against experiemental measurement of the transducer sensitivity.
- Develop a method of adapting the MFC to give it alternative wave mode sensitivity characteristics so that it has a wider range of potential applications.
- Design and produce a pipe inspection array using the characterised transducers.
- Demonstrate the MFC inspection tool's capabilities against the state of the art.

Contributions to Knowledge

Development of Parametric Characterisation Methods for Evaluating MFC Transducer Performance For 1D and 2D Waveguides

It has been shown that at low ultrasonic frequencies the sensitivity of an MFC transducer varies with wave mode (for each waveguide), wavelength, frequency and direction, and that reasonable predictions can be made for choosing optimal MFC size to suit the wave mode selectivity required. An analytical approach to explore the superpositional cancellation effects that occur for a transducer that is large with respect to wavelength and strains non-uniformly across its contact surface was used. Initially a 1D scenario was considered for the problem of transmission and reception from an MFC transducer in the direction of the MFC transducer's main axis (the fibre axis). The MFC transducer's length to wavelength dependency was shown through a pulse-echo test on an aluminium rod and a pitch-catch test on a steel plate both using broadband chirp signals and mode specific spectral analysis. This was followed with a 2D evaluation to assess the MFC transducer's performance for all in-plane directions for a steel plate waveguide. The MFC transducer's wave mode, wavelength and direction dependency was measured over a range of low ultrasonic frequencies commonly used in Long-Range Ultrasonic Testing (40-80 kHz). Characteristics such as the MFC transducer's low lateral sensitivity to shear horizontal wave modes and relatively high lateral sensitivity to Lamb modes were identified as important features to be known for transducer arrays of MFC transducer to be optimally designed for wave mode control. These characteristics were compared to those of a conventional in-plane shear transducer (a type commonly used for commercial guided wave inspection) to demonstrate the novel nature of the MFC transducer.

MFC Adaptation through Partial Decoupling With a Weak Shear Coupling Membrane For Tailored Wave Mode Sensitivity

Following the evaluation of the MFC transducer's size dependent characteristics, it was hypothesised that their directional wave mode sensitivity could be altered by partially

decoupling them in such a way that would give them wave mode sensing characteristics that would be advantageous in some applications. A method of MFC partial decoupling was developed that would allow the MFC to be dry coupled with a normal pressure such that only a portion of the MFC active area was acoustically coupled to a test structure. Since it was necessary to preserve the MFC transducers' light, low profile and flexible nature, a thin latex membrane was developed for use as a decoupling interface. The performance of an MFC partially decoupled in this way was assessed using a combination of finite element analysis, analytical simulation and experimental measurement. It was shown that an MFC transducer at low ultrasonic frequencies could be given the wave mode sensitivity characteristics similar to a point source transducer through the use of partial decoupling. The most significant advantage of this adaptation is that it allows MFC transducers to transmit and receive shear horizontal wave modes in a direction in which its sensitivity to Lamb modes is weak. This allows the transmission and reception of shear horizontal with a good degree of mode purity, which is the favoured move for many inspection techniques.

Development and Validation of a Point Source Superposition Model for Directional Ultrasonic Guided Wave Transducers

It was shown that a discrete analytical model could be used to make predictions about the nature of MFC transducers and how superposition effects determine their sensitivity on transmission and reception. In this model a transmitting or receiving MFC transducer could be represented by a set of in-plane point source transducers. This model was used to simulate the characteristics of the MFC transducer with and without the application of a partial decoupling interface layer. These results were compared to the experimental testing done for both the 1D and the 2D cases, and were found to achieve reasonable agreement. This model is fast to run and can be used to validate the hypothesised nature of a transducer, as has been demonstrated here, or, if this nature is known, to evaluate configurations of transducers or transducer arrays.

Pipe Inspection Array using Macro Fiber Composites to Improve upon the State-of-the-art

MFC transducers have been used to create a pipe inspection tool that was compared with a state-of-the-art commercial inspection tool, and the MFC tool's advantages were demonstrated. This device demonstrated the use of MFC transducers with and without partial decoupling to make use of both longitudinal and torsional axisymmetric waves for pipe inspection. The MFC transducers have form characteristics that offer practical advantages, namely they are thin film devices that have a relatively low weight and are flexible, and so equipment made with them will also have a low profile and weight, which

is of benefit to industry. Design challenges against achieving high mode purity were identified and overcome. It was shown that with partially decoupled MFC transducers it was necessary to have a high density of transducers to eliminate their sensitivity to circumferential waves over the frequency range of interest, and that this was less severe for the fully coupled MFC transducers because of their lateral cancellation of shear horizontal waves.

Publications Arising from the EngD

- A. Haig, W. Balachandran, P. Mudge and TH Gan. *Advanced Transducer Development for Long Range Ultrasonic Inspection Systems.* 4th International Conference on Emerging Technologies in NDT, Stuttgart, Germany. 2^{nd}-4^{th} April, 2007.
- P. Mudge and A. Haig. *Acoustic Transducer Assembly.* Patent Application. Publication Number: WO/2009/022130. International Application Number: PCT/GB2008/002737. International Filing Date: 13^{th} August 2008.
- A. Haig, P. Mudge and W. Balachandran. *The Use of Long-Range Ultrasonic Technology for the Evaluation of Engineering Structures.* Brunel University and Surrey University EngD Conference. Surrey University, Guildford, Surrey. 30^{th} June 2008.
- A. Haig, W. Balachandran, P. J. Mudge, and P. Catton. *Innovative Transducers for Condition Monitoring Using Ultrasonic Guided Waves.* 6th International Conference on Condition Monitoring and Machinery Failure Prevention Technologies. Dublin, Ireland. 23^{rd}-25^{th} June 2009.
- P. Catton, A. Haig, R. Sanderson, P. Mudge, and W. Balachandran. *Enhanced Signal Processing and Characterization Using Guided Waves.* The Review of Progress in Quantitative Nondestructive Evaluation, University of Rhode Island - Kingston (URI), Rhode Island. 26^{th}-31^{st} July, 2009.
- A. Haig, P. Catton, P. Mudge, and W. Balachandran. *Portable Ultrasonic Guided Wave Inspection with Macro Fiber Composite Actuators.* The Review of Progress in Quantitative Nondestructive Evaluation, University of Rhode Island - Kingston (URI), Rhode Island. 26^{th}-31^{st} July, 2009.
- Y. Gharaibeh, P. J. Mudge, P. Catton, R. M. Sanderson, and A. Haig. *Developments in Long Range Ultrasonic Testing for Pipes Using Guided Waves for Enhanced Detection and Evaluation of Metal Loss Defects.* European Conference on Non-Destructive Testing. Moscow. 7^{th}-10^{th} June, 2010.
- A. Haig, R. M. Sanderson, P. J. Mudge, and W Balachandran. *Experimental Validation of a Point Source Superposition Model for the Analysis of Transducer*

Directionality. Insight Journal of the British Institute of Non-Destructive Testing. *Accepted, In Press 2012.*

Chapter 1

Introduction

1.1 Non-Destructive Testing

Nothing is engineered with the expectation that it will last forever, but a long functional life is very often important. To assure that a structure lasts a long time it is necessary to test that it is made without significant flaws and to regularly check that flaws have not developed. If flaws have developed it is necessary to know how severe they are and at what rate they are developing. This testing must not reduce the life of the structure. It must be non-destructive and must keep disruption to a minimum.

Non-Destructive Testing is used throughout civil engineering, railway, shipping, manufacturing, aerospace, defence, sustainable energy, oil and gas, nuclear power and virtually all other areas of engineering. Monitoring the remaining life of a structure and preventing catastrophic failure can be critical for efficiency and for the protection of human life and the environment.

Non-Destructive Testing has many branches, each of which exploits a number of physical phenomena, including fluid flow, chemistry, magnetism, electricity, EM radiation (x-rays, light, microwaves, and radio waves) and sound (audible and ultrasonic). Ultrasonic testing is one of the most widely used and has been established since World War 1. It is most commonly used for the short range inspection of metal structures, particularly to test the integrity of welds. However, more recently techniques have been developed that take advantage of how some structures naturally form acoustic waveguides, which allows for the long-range inspection. This is the field of Ultrasonic Guided Waves, which this thesis aims to contribute to.

1.1.1 Ultrasonic Testing

Sound waves have many uses beyond hearing. In marine engineering they have been used for communications and for sensing objects. In engineering and health care they have been used for sensing, cleaning, and for melting and destroying material. It is most common that sound at ultrasonic frequencies is used, which has lead to the field being known as Ultrasonics.

Propagating sound waves are effected by discontinuities in the medium as they encounter them; most importantly discontinuities cause reflections. The excitation and sensing of ultrasonic waves allows for these effects to be measured, allowing for discontinuities to be detected and characterised. In nature, some creatures (such as some bats and toothed whales) use echo-location (biosonar) for sensing objects, where ultrasonic pulses are transmitted and the arrival time of reflections are sensed. Similar concepts enable watercraft to sense objects in water (SONAR), doctors to harmlessly visualise the inside of patients (Diagnostic Ultrasonography), and engineers to find defects inside of solid objects without causing damage (Ultrasonic Testing).

Ultrasonic Testing (UT) is now used throughout many engineering sectors for finding defects, both after manufacturing and in service. Whilst the inspection of steel structures is most common, ultrasonics can be applied to any material and has been used with metals, polymers, composites, wood, food products, concrete and more. Ultrasonic testing typically uses either compression waves or shear waves that propagate through the bulk of the media. For these two bulk wave modes, the velocity is dependent on the material, but not the frequency. It is typical for frequencies of 0.5 to 10 MHz to be used, but some applications expand upon this range.

Waves that travel close to the boundaries of the media in which they travel have different properties to the bulk modes and have special applications within ultrasonic testing. These modes are known as Ultrasonic Guided Waves (UGWs) and are commonly used at lower frequencies than conventional ultrasonic testing (approximately 20 kilohertz to 1 megahertz).

1.1.2 Ultrasonic Guided Waves

Some objects can act as waveguides where elastic vibration waves constrained within the boundaries of the structure are guided to propagate in only one or two axes. These propagating vibrational shapes are the result of harmonious vibration. These are similar to normal modes except the geometry of the structure is elongated in one or two axes. This facilitates propagation of the vibrational shapes and hence they are known as wave modes. The shapes and relative positions of the boundaries dictate the nature of the harmonic motion and, as the interaction of the vibration with the boundaries can depend on wavelength, the nature of these modes can be frequency dependent.

These wave modes can only propagate along the boundaries, and, as such, are collectively known as guided waves. Objects in which these waves propagate are known as waveguides. Waveguides have either one flat boundary (free surfaces and interface surfaces), multiple parallel flat boundaries (plates), or have a set of boundaries that form an enclosed cross-section (rod, tube, beam, etc). Surface and plate guided waves can only propagate in the axes parallel to the boundaries, which mean these waves can only diverge in two dimensions; the amplitude loss due to divergence is inversely proportional to distance (not the square of the distance). Guided waves that propagate in waveguides formed by a regular cross-section cannot diverge at all, and so there is no amplitude loss due to divergence. This lack of divergence means that Ultrasonic Guided Waves (UGWs) experience a great deal less amplitude loss with propagation in comparison to bulk waves.

Like bulk waves, ultrasonic guided waves are affected by discontinuities in the media in they travel. As a guided wave encounters a change in the cross-sectional shape or material of the medium it is scattered. It is possible for a wave of one mode to scatter into any other possible modes. The scattered guided waves will have the same directional limitations imposed on them by the boundaries of the object; some waves continue in the original direction, whilst some others are returned in the reverse direction.

Ultrasonic Guided Wave testing, also known as Long-Range Ultrasonic Testing (LRUT), has been commercially applied for over 10 years. In this time it has also been widely researched for use as part of Structural Health Monitoring systems. Throughout the literature it has been applied to the inspection of many kinds of engineering structures, including bridge components, train rails, fuel storage tanks, pipelines, wind turbine structures, aircraft and ships.

1.1.3 Transducers For Ultrasonic Guided Waves

There are many physical phenomena used in systems that create and sense acoustic guided waves. Transmitter devices for this application are generally required to create a controlled displacement in the test specimen, generally in close proximity to the device. And, in a similar manner, a receiver device would be required to sense displacements in a localised area. To reduce the physical complexity of inspection tools it is often advantageous to have co-located transmitters and receivers, and better still to use transducers that function effectively as both a transmitter and a receiver.

For field applications piezoelectric devices are most common and there are a wide variety of piezoelectric devices available, but there is also a great range of other technologies that have been researched and applied to ultrasonic guided waves. To understand the breadth of choice available when selecting a method of transduction an overview of the available technologies is given in Chapter 2.4. All transducer technologies for guided wave inspection reviewed interchanged between an electrical and a mechanical disturbance and/or

the reverse between the same two domains. The phenomena exploited in the literature for this purpose include electromagnetics (particularly lasers), electrostatics, electrostriction, magnetostriction and piezoelectricity. Magnetostriction and piezoelectricity are common in ultrasonic testing, and devices using both technologies are available at relatively low cost and can be produced on a large scale.

1.1.4 Macro Fiber Composites For Ultrasonic Guided Waves

Of all these potential technologies the Macro Fibre Composite transducers have been selected for study because their offers physical advantages for a variety of guide wave applications. The MFC transducers are comprised of a layer of aligned piezoceramic fibres housed in an epoxy matrix that is sandwiched between two layers of polyimide that have been printed with an electrode pattern. Their piezocomposite design makes them less brittle than conventional piezoceramics, and their film form affords them physical flexibility. Their flexibility reduces the challenge of achieving coupling as they can conform to surfaces that are not highly flat. The film form also gives them a low weight which offers an advantage for portable inspection equipment or for the monitoring of structures with weight carrying limitations.

The electrode layers consist of a pattern of interdigital electrode fingers that is the same for both layers. This creates top-bottom pairs of electrodes sandwiching the piezofibres. The polarity of the pairs alternate along the length of the piezofibres. Since these electrodes are used both to initially polarise the fibres and then to actuate them, they effectively enable an electric field to be manipulated along the fibre length. This enables a high field magnitude because the gap between the electrodes can be much shorter than the fibre length, which enables the MFCs to be highly efficient. The MFC transducers used for this study were provided by Smart Material GmbH and their data sheet is available in Appendix A [Daue, 2011].

1.2 Aims and Objectives

Characterise MFC transducers so that they can be better used to produce transducer arrays that are effective at exciting a desired wave mode without exciting unwanted wave modes and demonstrate how this may lead to improved inspection technology.

1.2.1 Specific Objectives

- Analyse the MFC transducer's sensitivity and its dependency on:
  - Wave mode

  - Wavelength
  - Frequency
  - Direction
- Produce an analytical model to represent this sensitivity variation.
- Validated the model's predictions against experimental measurement of the transducer sensitivity.
- Develop a method of adapting the MFC to give it alternative wave mode sensitivity characteristics so that it has a wider range of potential applications.
- Design and produce a pipe inspection array using the characterised transducers.
- Demonstrate the MFC inspection tool's capabilities against the state of the art.

1.3 Research Method

Prior to the research, a review in the area of non-destructive testing found value in expanding the use of ultrasonic guided waves. An initial study of this field identified a number of works relating to different transduction methods. This indicated the development of transducers can yield both ultrasonic improvements, but also practical improvements that can lead to the technology being better applied and more widely applied.

A review of transducer technology and phenomena used for transduction was carried out and the MFC devices were identified as having potential benefits for the technology. The course of the research was to characterise MFCs so they could be used optimally for guided wave applications.

Following the initial literature study, the research was designed to flow in four consecutive stages as indicated in Figure 1.1. First the MFC evaluation for one dimensional wave excitation and reception was planned, as the simplicity of a one dimensional waveguide provides the most feasible for frequency response measurement. This would then this would be expanded with the evaluation of MFC directionality for 2D (plate-like) waveguides, as directionality is an additional area of characterisation needed once the frequency response was understood. At this stage a method of MFC adaption was conceived and evaluated with the frequency and direction characterisation methods developed from the previous two stages. Finally the application of pipeline inspection was selected as a target for MFC application as this appeared the widest area of interest.

The method for each stage is similar and is centred on a series of experiments using MFC transducers to transmit and receive guided waves, alongside partnering analysis

for demonstrating how the parameters of the MFCs, their adaption housing and their use in arrays can influence their use.

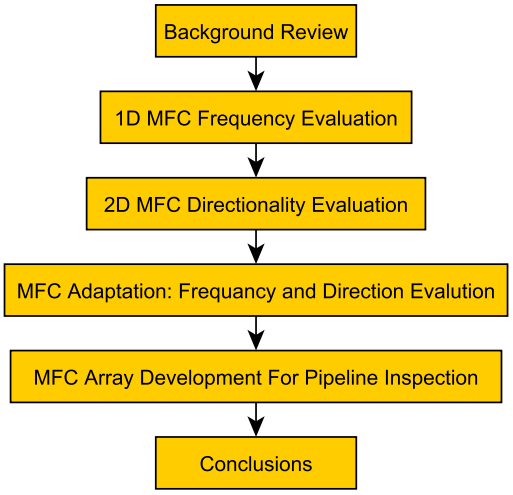

FIGURE 1.1: The planned flow of the research, as relefected in the structure of the thesis.

1.4 Organisation of Thesis

This chapter introduces the scope of the research and briefly prepares the reader for the technical chapters that follow. Chapter 2.4 provides further review of the background technology and literature. Chapter 3 covers the use of MFC transducers for exciting and receiving ultrasonic guided waves parallel to their fibre axis, and how various aspects effect their sensitivity. In particular this looks at the how their sensitivity varies with frequency, nature of the wave mode and size of the MFC. Chapter 4 expands upon this, by investigating the use of MFC transducers for exciting guided waves in any in-plane direction. In Chapter 5, a method of adapting the MFC transducer for to give it an alternative wave mode sensitivity in such a way that it acts more like a point source transducer at low ultrasonic frequencies. The use of the characterisation of the MFC and the adapted MFC for the development of an array for pipe line inspection is described in Chapter 6. Here a state-of-the-art commercial equivalent and an MFC based prototype are compared for their inspection ability using both longitudinal and torsional wave modes, and the advantages of the MFC approach are given. The final chapter, Chapter 7, gives the conclusions of the research and some recommendations for future work.

Chapter 2

Background Review

2.1 Introduction to Ultrasonic Guided Waves

It is well known that solid structures of suitable shapes can act as waveguides for the conduction of mechanical waves as propagating wave modes [Graff, 1991, Rose, 1999, Soutas-Little, 2012]. These guided waves are constrained to propagate within the boundaries of the structure and, as they experience reduced or no divergence, they can maintain their amplitude for relatively long distances. The wave interaction with the structure's boundaries leads to a variety of propagating wave modes, which differ by the shape of the structure's distortion due to the mode's vibration and by the velocity at which each mode propagates.

Most wave modes have a frequency dependent velocity. When a wave mode is transmitted with a frequency bandwidth that has little variation in velocity, that mode can propagate for relatively long distances without distortion. However, when a mode experiences a range of velocity for the transmitted bandwidth, then the transmitted wave mode will disperse as it propagates. It is typical to analyse the nature of potential wave modes in a given waveguide by producing a graph displaying the velocity-frequency characteristics of each mode. These are known as the dispersion curves. When propagating wave modes encounter a discontinuity, they may be caused to scatter and convert to other modes. The amount of proportions of the scattering and mode conversion depend on the mode, the frequency and the geometry and material of the discontinuity.

The interaction of wave modes with structural features has been used for the diagnosis of flaws in engineering structures. Most examples of this make use of ultrasonic frequencies and operate within the linearly elastic regime. This field of research is generally known as Ultrasonic Guided Waves for Non-Destructive Testing and Structural Health Monitoring.

2.2 Ultrasonic Guided Waves for Testing

Work on predicting a solid object's response to mechanical stimuli has been carried out for many centuries [Soutas-Little, 2012]. Knowledge of the behaviour of sound in bound solids was developed in particular from the late 18^{th} century to the early 20^{th} century by mathematicians such as Euler, Bernoulli, Laplace, Cauchy, Cayley, Lamb, Love, and Strutt (3^{rd} Baron Rayleigh). It wasn't until the 20^{th} century that they were extensively considered for industrial application.

Industrial application was made possible through the development of both electronics and piezoelectric materials in the 20^{th} century. Pierre and Jacques Curie discovered the direct piezoelectric effect in a number of materials in 1880, and in 1881 also discovered the inverse piezoelectric effect. Rochelle salt (Potassium Sodium Tartrate) was one of the materials the Curie brothers demonstrated as piezoelectric and it became the most popular material for work with actuated vibration until the development of better materials came along. The first of the high efficiency piezoelectric materials, Potassium Dihydrogen Phosphate (KDP), was developed in 1935, which opened up greater opportunities for industrial application [Busch and Scherer, 1935].

The first engineering application of ultrasound was SONAR, which was developed during the First World War, but it wasn't until 1942 when Firestone developed the first pulse-echo method of flaw detection in metal structures using Lamb waves [Firestone, 1942]. Firestone's patent covers the details of using angled probes to produce and manipulate the longitudinal plate waves that Lamb predicted to detect flaws in engineering structures. Firestone and Frederick also compared the use of longitudinal and shear waves for thickness measurement [Firestone and Frederick, 1946]. In the same paper they discuss the generation of Lamb waves and the use of different cuts of piezoelectric crystal to achieve either compression or shearing excitations for bulk or plate wave based inspection. Hudson analysed the characteristics of guided waves in rods with a circular cross-section and Morse later did the same for rods with a rectangular cross-section [Hudson, 1943, Morse, 1948]. In both cases good agreement between numerical predictions and experimental measurements were found. Gazis was the first to produce a full three dimensional analytical solution for characterising the shape and velocity of both axi-symmetric and flexural wave modes in tubular structures, and he compared his results to those produced by other previously researched methods based on shell theory, however he did not provide experimental validation [Gazis, 1959a,b]. His calculation was used to characterise the frequency-wavelength behaviour for all axi-symmetric modes and first order flexural modes for various values of the ratio of wall thickness to the average radius (the mean of the internal and external radii). He showed the limitations of shell theory for correctly calculating the behaviour of higher order modes with short wavelengths (relative to the thickness).

Mancuso [1957] describes a technique for using Lamb waves to inspect fuel elements (components in power generation) to detect and measure the size of voids caused by lack of bonding [Mancuso, 1957]. In the same year, Worlton presented work on water coupled angled transducers for measuring Lamb waves for the detection of laminar flaws (again in fuel elements).

Oliver [1957] conducted experimental measurements on the effects of dispersion of guided wave modes in rods with a circular cross-section and was the first to use short time duration pulses, which would later become common practise. He identified waveguide end resonance as a source of previously unidentified sound in experiments, which he showed occurs as an end experiences some resonance which gradually leaks propagating guided waves.

In one paper, the interaction of Lamb waves in a 1/32 inch (0.8 mm) steel plate with various saw cut defects was investigated [Grigsby and Tajchman, 1961]. They demonstrated a pitch-catch method where Lamb waves are sent directly between a transmitter and receiver transducer, and amplitude measurements are used to detect and size flaws. This work also includes a formula for calculating group velocity from phase velocity. At a similar time, Worlton provided a detailed experimental characterisation of Lamb waves, which validated previous predictions about wave mode behaviour [Worlton, 1961]. Numerical predictions about mode shape and velocity, along with experimental measurements were later made for a solid round rod [Zemanek, 1971].

Meitzler [1961] discusses how localised flaws can cause mode conversion, which can be severe at certain critical frequencies for specific wave modes, and that general imperfections throughout a waveguide, such as surface roughness, can lead to mode coupling at critical frequencies, where continuous mode conversion occurs during propagation, which leads to chaotic signals being received. Surface roughness may be a significant cause of distortion in narrow wires (such as the 1 mm and 2 mm diameter wires used in Meitzler's work) at megahertz frequencies due to the scale of the imperfections to the waveguide geometry and the wavelengths used. However, for larger structures the critical frequencies are likely to exist only at very high frequencies that are unlikely to be used for inspection. The work has greater implications for the development of ultrasonic delay lines, which makes use of ultrasonic guided waves in waveguides with such small dimensions. Demer and Fentnor [1969] provide an evaluation of Lamb waves and their applications with particular interest for the use of ultrasonic guided waves in cylindrical structures for the detection of flaws.

Horton and Mechler [1971] did the first numerical predictions of the velocity of circumferentially oriented waves that included experimental validation. Whilst they only predicted the first wave mode, they experimentally measured multiple modes, which experimentally demonstrated circumferential wave modes exist (with some equivalency to plate wave modes).

Mohr and Höller [1976] were the first to publish work on tube testing with axial guided waves for the detection of defects. They used a pulse-echo technique where the transmitter and the receiver devices are in close proximity (or a single transmitter/receiver transducer is used) and sound waves are propagated into the tube and reflections are used to determine the presence of flaws. This is now the basis of most modern commercial pipe inspection systems that use ultrasonic guided waves. The present a type of Electromagnetic Acoustic Transducer (EMAT) which makes use of wire coils (one transmit and one receive). Either both coils can be outside or with one inside and one outside the tube. The EMAT makes use of permanent magnets to apply Lorentz forces to the eddy currents that are induced in the tube by the coils, which is the common approach used for EMATs. The winding configuration of the coils is used to target a particular wavelength of sound in order to bias a desired wave mode. The coils are wound traversing half the circumference and also some distance axially. Pole shoes are used to direct the fields of either the axial runs of the coils or the circumference runs of the coils in order to excite respectively either torsional waves or longitudinal waves. Using the naming convention explained in the next section, they designed the longitudinal tests to use the L(0,2) mode and the torsional test to use the T(0,1) mode (although in their naming scheme they refer to it as T(0,0)). They study the reflection amplitude of the L(0,2) mode for tangential saw cut flaws of various depths, and the amplitude of the reflected T(0,1) signal from axial flaws. They do not fully study the effect of defect geometry on amplitude response, but they do show an increase in amplitude with increasing flaw size.

Silk and Bainton also studied the use of guided waves for the inspection of pipes. They used a transducers to excite either L(0,1) and L(0,2) [Silk and Bainton, 1979]. As discussed in the next section, it was this paper that defined the pipe mode nomenclature that is most commonly used and will be used in this work. The transducer involves a steel internal stop that has a pointed tip. The space next to this tip if filled with liquid and a piezoelectric transducer is used to excite axially propagating waves in the liquid towards the pointed stop. The slope of the point reflects the sound waves into the wall of the tube. The angle of the point is set to manipulate Snell's law in order to preferentially excite a particular wavelength in the tube. By selecting both the wavelength and frequency a significant bias towards the excitation of one mode is possible. They tested both the excitation with a single sudden voltage change (to excite the transducer resonance) and also a short-duration sinusoid burst, and found the latter to give better signal control (albeit requiring more elaborate electronics). There transducer design was shown to function well at mode biasing, but suffered from ringing effects, where sound trapped in the coupling fluid would be continuously received and would appear as noise early in the received signals. They did however provide some design modifications that went some way to improve this situation. They conducted velocity measurements in both a straight tube and a U-form tube that is realistic of those found in heat exchangers in industry, and they discuss the influence of the bend on guided wave propagation. They

provide discussion on using calculations of the modes' vibrational shapes through the cross-section (based on the work of Viktorov [1967]) to predict the influence of defects on the guided wave modes, but they do not provide experimental validation.

Böttger et al. [1987] present another tube inspection system and this time included experimental results for flaw detection and sizing. They discuss the need to for a strong bias towards a single mode and the need for selecting a frequency and wave mode to achieve low dispersion and a high spatial resolution. They built a pitch catch system using EMAT transducers designed to excite L(0,2) and tested on several hundred tubes in the field with some containing real flaws. They also measured the amplitude response for a number of real and artificial flaws, and compared them by depth. They showed a relationship between depth and the reflected amplitude, but did not fully explain the influence of other aspects of flaw geometry on the scattering of the wave modes nor did they consider the flaws' various influences on mode conversion.

Nayfeh and Chimenti [1988] were the first to analyse and experimentally study ultrasonic guided waves in fibre composite plates. They demonstrated the an agreement between their predictions and their experiment, with only sight exception which they stated was likely due to the influence of water loading on the composite plate in their experiment. Nagy and Adler [1989] considered the use of ultrasonic guided waves for inspecting bonded multi-layered plates for disband flaws and demonstrated a successful technique for using leaky guided waves for detecting such flaws..

Alleyne [1991] developed quantitative methods of plate testing using Lamb modes. He developed a method of using time-domain data sampled for many positions along a propagation axis with a two-dimensional Fourier transform in order to extract wavelength-frequency data for various wave modes despite signals including multiple, dispersive modes. He used Finite Element Models to simulate the propagation of Lamb modes and their interaction with various defects. He predicted the nature of the defect interaction would be dependent on the wave mode, frequency, plate thickness and defect geometry and verified their influences by modelling guided wave interaction with defects of various shapes and proportions. He used the same 2D FFT technique experimentally to validate his modelling method [Alleyne and Cawley, 1992]. Cho et al. [1997] later used a Boundary Element Method to further analyse and quantify the scattering effect on Lamb waves due to pit like defects.

Alleyne and Cawley [1996b] used Finite Element Models and experimentation with bonded piezoelectric transducers to study the interaction of the L(0,2) wave mode with Butt welds, Notches, Corrosion Patches, Pipe Supports, Flanges and pipe insulation. Most notably, they showed flanges give close to a complete reflection, whereas the butt welds gave between 5% and 20% of the incident L(0,2) mode. Bonded transducers cannot be for inspection systems as they are not easily moved between locations. The work on tubes described easier relied on fluid coupling or the use of EMATs, however coupling

fluid requires time to apply and EMATs can be large and inefficient. In another paper, Alleyne and Cawley [1996a] developed a piezoelectric transducer for exciting guided waves that was to be applied without a fluid coupling fluid by achieving coupling through force loading. L(0,2) was their target wave mode and it was their aim to avoid other wave modes. They discuss designing the transducer's contact length to be inefficient at generating L(0,1) at a desired frequency and the use of a circumferential array of such transducers to reduce the excitation of flexural modes. They demonstrated the excitation of L(0,2) in a tube with a noise flaw of 1% of the received L(0,2) mode. The construction of wide band, low frequency transducers is also later covered by Allin and Cawley [2003].

Alleyne et al. [1996] looked at the field application of pipeline inspection for the oil and gas industry. These tubes require a higher average tube radius and to a less extent a greater wall thickness, than the tube work done for heat exchanger tubes. They used a ring array of dry coupled piezoelectric transducers to excite only axisymmetric modes. They used two rings of these arrays with appropriate time delays applied to one ring in order to achieve testing in a single direction. They state that the number of transducers per ring must be higher than the highest order of flexural mode at the test frequency, in order to avoid uncontrolled transmission of flexural modes. By comparing Finite Element Models with experimental results, they showed the reflection coefficient of L(0,2) and it's mode conversion to F(1,2), F(1,2), and F(1,3) for a notch with varying circumferential extent. They also tested a number of pipes containing flaws on industrially used pipes and with the technique were able to detect all flaws with depths great than 50% of the thickness and with extending of 16% of the circumference or more. They determined that their system had a maximum range of 30m for pipes with significant general corrosion. They identified that when high mode control is not achieved, L(0,1) can be miss-detected as L(0,2), which can lead to false defect detection. They also suggested the use of flexural wave modes to provide more information about flaws. Lowe et al. [1998] gives an overview of pipeline inspection with guided waves for various works conducted at that time and gives an analysis for the techniques ability to detect open-crack like notches.

Shin and Rose [1999] use a normal expansion technique to predict the wave mode proportions excited by loading on a tube over varying circumferential and axial extents. They show that specifically constructed area loading can give rise to axisymmetric modes without significant flexural modes, and that the proportion of modes contains information that could be used for defect sizing (as was indicated by Alleyne et al. [1996]). They used a comb transducer to experimentally demonstrate their predictions.

Wilcox et al. [2001] consider the process of developing an inspection technique using ultrasonic guided waves for a new structure to provide abstracted guidelines for development. They divide the process into two stages where firstly the properties of the ultrasound to be used are decided and secondly the properties of the transducers are chosen. The wave mode selection process involves choosing a wave mode and frequency that is optimally will experience little dispersion and attenuation, which is also sensitive to the types of

flaws that are to be detected. Then the relative excitability of the desired mode and the undesired modes are considered for a range of frequencies and various orientations of point disturbance. Then a transducer is chosen that optimises the excitation over an area to capitalise on the selected excitability characteristics and to make use of acting over an area to further bias the desired mode. They also consider the use of angled transducers to manipulate the phase of the excitation of the given area (using Snell's law). This process should lead to relatively long range, high mode purity, high spatial resolution, and high defect sensitivity.

Whilst previous studies had mainly been on volume-loss flaws, Clézio et al. [2002] looked at crack detection using Lamb waves (specifically the S0 mode). The conducted analysis and experimentation to predict and measure the reflection coefficient from varying depths of crack. They used 0.7mm notches to simulate open cracks (the crack interior walls could not close and interact). They used symmetry to reduce the complexity of the calculations, and so the flaws used occurred symmetrically on both sides of the plate. They showed the reflection coefficient increases exponentially to 1 as the depth of the flaw increases to the full thickness.

In the new millennium the breadth of research on guided wave applications and related fields has reached new heights and it is at this time when Rose [2002] ties together various research papers on related issues in order to review the field and encourage knowledge transfer. However, tube and metal plate inspection remain two the most studied general areas. It was also around this time when commercial systems for pipe inspection became commercially available [Mudge, 2000, Alleyne et al., 2000]. Alleyne et al. describes a method of using three rings of transducers to both transmit L(0,2) in one axial direction and to suppress L(0,1) in both directions. The combined use of L(0,2) testing and T(0,1) testing is also discussed, indicating how ones advantages may be used to cover the others pit falls.

After guided wave inspection became widely used, interest in structural health monitoring followed. In particular, the use of spare arrays of transducers on plates and on tubes for tomographic imaging for detecting the presence has been studied by various authors [Malyarenko and Hinders, 2001, Song et al., 2003, Leonard and Hinders, 2005, Hay et al., 2006, Michaels, 2008, Clarke, 2009, Clarke et al., 2009, Clarke et al., 2010]. A review of general guided wave structural health monitoring is provided by Raghavan and Cesnik [2007a].

Research in pipe inspection has also continued. Long et al. [2002] looked at guided waters in water-carrying pipes for the detection of flaws and leaks. They analysed the mode characteristics in the pipe walls and the water in the bore, and evaluated the influence on various soil conditions on the attenuation of various modes. They confirmed the presence of an additional mode that existing in fluid filled pipes, which involves displacement only in the fluid. They investigated the wave interaction with pipe features, such as joints.

They use analytical models and Finite Element Models for these investigations which were validated with lab experimentation. Rose [2003] also discusses the influence of fluid loading on the propagation of guided waves in structures, and in particular highlights the T(0,1) mode's immunity to attenuation influences of fluids in pipes because the mode's entirely in-plane displacements.

Lee and Staszewski [2003a,b] used the Local Interaction Simulation Approach to simulate Lamb wave propagation as a cylindrical wave front in an isotropic plate and its interaction with notch defects, and they validated this simulation experimentally achieving a high degree of similarity.

Demma et al. [2003] conducted finite element models of the T(0,1) mode interacting with various defects. They studied the reflection coefficients for defects separately varying by depth, circumferential extend and axial extent, and did so for a range of frequencies. They showed that defects of varying thickness, the reflection coefficient always increases with depth, although the rate of increase is frequency dependent. The circumferential extent is shown to be proportional at high frequencies, however at low frequencies conversion to other modes makes the extent influence on reflection non-linear. The axial extent is shown to have a cyclic influence on the reflection coefficient caused by interference from reflections due to the beginning and end of the flaw. This shows that the circumferential extent of a flaw can be calculated by the ratio of the measured T(0,1) reflection amplitude to the amplitude of the reflected flexural modes (assuming the flaw has a consistent depth). This work is taken forward by Demma et al. [2004] with a maps giving the T(0,1) reflection coefficient for a given test configuration against both depth and axial extent. They provide a correction factor that can take into account the location of the flaw and the frequency of the wave mode used. This can also be used to adapt the results for the first few orders of flexural mode. They have also evaluated defects with non-uniform depths to establish possible ranges of reflection coefficient that enables the extent of any flaw to be estimated. The use of received mode proportions has been used to create maps of pipe feature locations in a tested pipe. Liu et al. [2006] use the combined proportions of reflected longitudinal and torsional wave modes to enhance the defect sizing. The axial influence on reflection coefficient has been studied in plates for the two fundamental Lamb modes [Benmeddour et al., 2008a,b]. They considered a flaw to consist separately of a step down change in thickness followed by a step up in thickness, and showed the reflected wave is the result of interactions of reflected waves from the two. Wang et al. [2010] conducted a study in pipes for again for the leading and ending edge face of a defect on the reflection coefficients of guided waves.

Another area of study is the transmission of multiple flexural modes in order to achieve energy focusing at a desired location on the pipe. If a reflector exists at the focus position, then a high proportion of reflected wave modes are expected. This is essentially the transmission reciprocal of measuring the proportions of modes received from a scattering feature. The use of both varying the circumferential extent of the excited portion of the

pipe and phased array methods for achieving flexural mode focusing Rose et al. [2003], Li and Rose [2006].

Alleyne et al. [2009] discuss the choice between pipe inspection with L(0,2) and T(0,1). They argue that T(0,1) outweighs L(0,2) for benefits and that in a majority of cases using T(0,1) would be sufficient. The principle issues with L(0,2) is that firstly mode conversion into L(0,1) and then back to L(0,2) is possible making signal interpretation challenging and secondly that L(0,2) can be influenced by the presence of liquid materials surrounding the pipe. Longitudinal testing also generally involves greater potential for unwanted flexural modes to be excited (as there are two flexural mode families stemming from L(0,1) and L(0,2)), which in equipment that doesn't significantly suppress these modes can lead to relatively high levels of noise. However, testing with L(0,2) does potentially offer extra information and if the practical obstacles with the equipment can be overcome then using both methods could be considered.

Ultrasonic guided wave testing of pipes, plates and other structures is now established as a research field and for industrial use. Enhancements in this area will allow for improved defect finding capability that can enhance many areas of engineering. The characteristics of guided waves in structures and their interaction with features and flaws are well understood. The success in deploying them in a technique often comes down to what is achieved with the amplitude and mode purity of the transmission and reception of the desired wave modes. Enhancements in this areas are likely to come from transducer development, array design, phased array and signal processing methods. This thesis will focus on the transducer and array aspects, with particular focus on plate and pipe inspection.

2.3 Wave Mode Nomenclature

For a given waveguide type, there are a number of classes of wave mode within which there are many modes. Whilst the characteristics of each mode varies with the geometry and elastic properties of each waveguide, generalisations can be made for a given waveguide type and individual modes can be uniquely identified by a naming scheme that draws upon their general distinctive characteristics. In the literature there is a naming scheme commonly used for plates and a naming scheme commonly used for pipes. This nomenclature is used in this thesis and is defined below.

2.3.1 Plate Mode Nomenclature

Plate testing with ultrasonic guided waves is often used on plates that are much wider and longer than they are thick. The propagation of the ultrasonic waves is considered

for regions of plates that are many wavelengths away from the plate's edges, which is done by analysing the wave modes that could exist in a theoretical infinite plate.

There are two major classes of plate wave mode. Firstly there are Lamb waves, named after Lamb [1917] for his original analysis of them, and shear horizontal waves. Lamb waves cause mainly displacement in the out-of-plane axis and in the axis of propagation, whereas shear horizontal waves cause mainly displacement in the in-plane axis orthogonal to the axis of propagation. These modes differ by their variation in displacement pattern through the plate thickness; each wave mode as a unique frequency dependent vibrational shape. The velocities of each wave mode can be described as a function of frequency, but since this characteristic scales with plate thickness the velocity for each mode can be defined as dependent on product of frequency and thickness. In this way, the wave mode velocities can be defined for a plate (with given elastic moduli and density) of any thickness. The displacement through the thickness of a plate caused by a guided wave is always a harmonious pattern with a half integer multiple of phase variations; the movement caused by a single wave mode at a point on the top of a plate is either in-phase or in anti-phase with a point on the bottom. A line of symmetry is taken half way through the plate thickness, and wave modes that have a vibrational shape symmetric about this line are known as symmetric modes, whilst the others are the asymmetric modes. Only three waves modes exist for all frequencies (the so called fundamental modes), whilst the others can only exist above their cut-off frequency (the so called higher order modes).

These modes are classed first by whether they are Lamb or shear horizontal modes, then by whether they are symmetric or asymmetric and finally by the order in which they occur with increasing frequency. In this thesis a common naming scheme is followed. Lamb modes are denoted with a letter S for symmetric or a letter A for asymmetric. This is the same for shear horizontal modes except they gain a following H letter to distinguish them from Lamb modes. This is then followed by a number to indicate their order of occurrence with increasing frequency. For example, S3 is the third symmetric Lamb mode and AH6 is the sixth asymmetric shear horizontal mode. The three fundamental modes are SH0, A0 and S0. Further information and graphs depicting the velocity characteristics of plate modes is given by Krautkrämer, J. and Krautkrämer, H. [1983].

2.3.2 Pipe Mode Nomenclature

Ultrasonic guided waves that propagate axially along tubular structures are categorised into three classes, following the naming scheme used by Silk and Bainton [1979]; these are torsional waves, longitudinal waves and flexural waves. These wave modes exist throughout the cross-section of the pipe they propagate in. Wave modes that fall into the torsional and longitudinal classes are known as axisymmetric modes because their vibrational characteristics do not vary with circumferential position, whereas all flexural

modes do. The major axis for material displacement caused by torsional waves is the circumferential axis, hence these modes are characterised by a twisting vibrational shape. Conversely the longitudinal modes predominantly displace in the axial and radial axes. In any pipe there are an infinite number of possible torsional, longitudinal and flexural wave modes. Whilst all torsional modes are axisymmetric and are dominated by a twisting motion, each torsional mode is distinguished by how the material displacement varies through the thickness of the pipe wall. All longitudinal modes can be distinguished by the way the vibration varies through the thickness, particularly by the proportion of axial and radial displacement at each point.

Fundamental wave modes are modes that can exist for all frequencies, whereas higher order modes can only exist above a so called cut-off frequency, which varies between wave modes. For axially propagating pipe wave modes, there is one longitudinal, one torsional and one flexural fundament wave mode.

Amongst each wave mode class, the wave modes are nominally ordinated by the order they occur with increasing frequency. For each torsional and longitudinal wave mode, there is a group of related flexural modes. The vibrational characteristic that makes each axisymmetric mode can also exist in a similar form with phase varying circumferentially. This phase variation cannot change suddenly with circumferential position; it can only vary smoothly between states going through whole cycles of phase change. Any natural number of phase shift cycles can occur around the circumference, and, theoretically, there is a flexural wave mode for each possibility. Each wave mode is named by its order of circumferential varying: axisymmetric modes vary zero times, and flexural modes vary with any natural number above that. The cut-off frequency for each flexural mode in a related group will increase with the order of circumferential variation.

As wave modes vary with class (torsional, longitudinal, and flexural), with circumferential order and come into existence in order of increasing cut-off frequency, a naming scheme was devised that denotes each unique wave mode by these characteristics. Each wave mode name consists of a letter and two comma separated numbers within parenthesises. The letter T is used for torsional modes, L for longitudinal modes and F for flexural modes. This gives each wave mode of the form *(p,q), where the * is replaced with the letter for the corresponding class, p is an integer representing the order of circumferential phase variation, and q is the order of occurrence with increasing frequency (for that class and circumferential order).

The fundamental wave modes are then T(0,1), L(0,1) and F(1,1). By way of example, T(0,1) is the first torsional wave mode. It has a 0 for the first parameter as it is an axisymmetric mode and a 1 for the second parameter as it is the first of its kind to be possible as frequency increases. F(1,1) is related to L(0,1) as (at most frequencies) the material displacement through the pipe wall thickness is similar for both modes and the wave mode velocity of both of them tend to the same value as frequency increases.

F(1,2) is the second type of flexural mode that can exist and is related to T(0,1). One downside of this naming scheme is that it is not clear which axisymmetric wave mode each flexural group relates to. However, this is often made when the wave modes' frequency/velocity relationships are displayed and compared graphically. Flexural modes can involve three-dimensional material displacement that does not occur for the related axisymmetric mode.

2.4 Transduction Methods For Long-Range Ultrasonics

There are many physical phenomena used in systems that create and sense acoustic guided waves. Transmitter devices for this application are generally required to create a controlled displacement in the test specimen, generally in close proximity to the device. And, in a similar manner, a receiver device would be required to sense displacements in a localised area. To reduce the physical complexity of inspection tools it is often advantageous to have co-located transmitters and receivers, and better still to use transducers that function effectively as both a transmitter and a receiver.

For frequency control and wave mode selection, it is required that such devices have directional sensitivity and can reproduce a narrow band signal within a desired frequency range. The frequency range required greatly depends on the application and the nature of the waveguide, however it is common to operate between 20 and 300 kilohertz.

There are various advantages and disadvantages to each technique and within each technique there are a great many possible approaches to device design. The best approach will depend heavily on the specific application. In particular, aspects that will strongly affect the requirements for device design are the physical nature of the test specimen (such as material and geometry) and practical limitations of the test location (such as accessibility and temperature).

The most common and successful devices make use of one or more of the following physical phenomena:

- Laser/Microwave
- Electromagnetic
- Electrostatic
- Active Materials
- Electrostrictive
- Magnetostrictive

- Piezoelectric

For field applications piezoelectric devices are most common, particularly for fixed tools, but there are many circumstances where the use of an alternative would be superior. The following sections will give an introduction to each approach and discuss the relative merits. There will be particular emphasis on piezoelectric methods as they are most prevalent in the literature and in commercial application.

2.4.1 Laser/Microwave

Nano-scale displacements in a specimen's surface can be measured through methods that make use of an optical interferometer. Generally a laser beam is reflected off the test specimen surface and received by a sensor that measures intensity, phase or wavelength variations to detect the velocity or displacement of a subject's surface. Some techniques require surface preparation for the laser measurement to be taken correctly.

Excitation can be achieved by rapidly heating a localised area on the specimen's surface with a laser or microwave beam that is pulsed with the desired frequency of the output wave. The heating causes localised thermal expansion, which results in the propagation of an elastic wave. The position and frequency control is precise. A point source target spot can be chosen or a line (or arc) shaped target can be used for directional transmission [Kim et al., 2006].

These methods offer greater precision than most other approaches. There is usually no-contact involved and the test piece can be monitored without being mechanically effected. One advantage of laser generation is that the angle of incidence can vary and mirrors can be used to change the target point easy. Iterative methods that require a sweep of the excitation point can be performed quickly, even with structures with complex surfaces.

However, laser equipment is often large and delicate. There is usually a high power requirements and requires caution towards human safety. Equipment also tends to be relatively expensive. Whilst it is often a very good lab approach, it is rarely a practical field solution for regular inspection. It is an approach sometimes used in research and development and for bespoke inspection problems in high-tech industry, such as the inspection of composite materials. It is possible that a permanent laser tool could be used to regularly monitor a structure as part of an SHM system, however, there are no current examples known to the author.

There are a number of popular types of interferometer for laser sensing. Fabry-Perot interferometers are sensitive to wavelength and by means of the Doppler effect and can be used to measure displacement. Michelson interferometers are sensitive to phase variation and give a time-varying signal for phase change. This can be used to measure

the velocity of a surface reflecting a laser beam into a Michelson interferometer. Fabry Perot are generally more sensitive to the available light and require a beam with a lower intensity, however, they are more sensitive to low frequency environmental optical noise [Staszewski et al., 2004].

2.4.2 ElectroMagnetic Acoustic Transducer

The most common electromagnetic device for ultrasonic testing is the ElectroMagnetic Acoustic Transducer (EMAT). This term specifically applies to a type of transducer that induces Eddy Currents into a conductive material and by exposing these currents to a static magnetic field, creates Lorentz forces that result in displacements. A coil is used near a test piece and is driven with an alternating current at the desired frequency. The arrangement of the coil and magnetic field dictate the direction of sensitivity. This phenomenon has a converse effect and so it is possible to use the same device for transmission and reception.

In comparison to other approaches EMATs are generally less sensitive, but unlike some of these approaches they are both practical in the field and do not require mechanical contact. This may remove the need for a mechanical loading mechanism and eliminates the need for couplant fluid. The distance from the test piece affects the sensitivity, but if this is carefully controlled then the sensitivity does not suffer from variation due to varying coupling conditions. This is very useful where multiple amplitude measurements must be comparable. There are no acoustic waves occurring in the EMAT body, so will have less design constraints and can be very rugged. EMATs are often used in applications where environmental conditions are harsh or where the test piece surface is coated, too rough or too hot for piezoelectric approaches.

An EMAT can only affect a test piece if it is electrically conductive. It is possible to couple a conductive material to a test piece to be used as an intermediate layer, however as this introduces new complexity to the problem and mitigates the non-contact advantages of EMATs it is not often the best approach available.

As the direction of the displacement can be selected through the EMAT design, it is possible for EMATs to excite any desired wave mode. They also offer both wavelength and frequency control, which further makes wave mode selection more precise and they have been successfully in use for guided wave inspection for many years [Hirao and Ogi, 1999].

EMAT's require a relatively high current and low voltage. A typical system consists of a pulse generator, a transmitter/receiver unit and an amplifier.

2.4.3 Electromagnetic: Solenoid

Current in a coiled wire will cause a magnetic field which can be used to displace a ferrous body with magnetic force. The magnetic force could apply to the test specimen or to an object coupled to the test specimen (as long as the material can be effected by a magnetic field). This object could include a component acting as a solid to gas interface.

Generally separate transmitter and receiver devices of this kind are used, although potentially even a single device, can be used for the transmission of ultrasonic waves. However, this technology suffers increasing sensitivity and signal distortion problems as the required frequency increases into the ultrasonic range. One guided wave approach using this technology excites an airborne wave inside a gas filled pipe, which reflects when the internal cross-section changes in area, thus indicating fouling build up, particularly blockages [Morgan and Crosse, 1978].

Good for low frequency, fluid coupled application. This technology suffers increasing sensitivity and signal distortion problems as the required frequency increases into the ultrasonic range. Conical and other solenoid type sensors are very widely available and often a cheap solution.

A doubtlessly familiar technology is the conical speaker, used in many household devices for the generation of audible sound. Microphone (and some hydrophone) devices use the same technology for the reception of audible sound in many common applications.

2.4.4 Electrostatic

Electrostatic transducers are based on capacitor technology. Two conductive parallel plates are placed in close proximity. Initially a static voltage is applied to one plate, then an applied cyclic variation in the voltage difference will cause the plates to contract and separate at the given frequency. Conversely, variations in separation distance will be sensed as an alternative voltage. Typically, one plate is fixed to the device's body and the other is an unrestrained membrane. This technology is commonly used for gas coupled applications, where sensitivity and frequency control is better than solenoid approaches at high frequencies [Hutchins et al., 1998]. They can be used for solid object inspection using air as the coupling medium. There are also many solid coupled applications, particularly for delay lines in electronics, where the specimen to be excited is a thin polymer plate [Badi, 2004].

They also offer higher sensitivity for air coupling than other methods because the membranes used have a good acoustic impedance match with air. Although air coupling is often unfavourable as the acoustic impedance mismatch between air and solid material causes it to suffer from poor efficiency. Shear waves cannot be generated in air. Shear

waves can only be generated through air coupling through mode conversion at the air/solid interface, which is not efficient and difficult to control.

Electrostatic transducers for solid coupling tend to be customised for each application and are bespoke. However, electrostatic transducers for air coupling are used in many sensor applications (particularly through air distance measurement) and are widely available with ranging frequency (ranging from the low kilohertz range to tens of megahertz), amplitude and clarity of signal capabilities and can be cheap to obtain [Castaings and Cawley, 1996].

2.4.5 Active Materials

Some materials exhibit coupling phenomena by which stress is isometrically coupled to the material's electrical, magnetic or thermal properties. For some materials the coupling is effective enough to be measurable and therefore useful for sensing stress variation.

The four well known phenomena are Pyrostriction, Electrostriction, Magnetostriction and Piezoelectricity. Pyrostriction is demonstrated when a material develops a stress variation under a change in temperature. As temperature variations are difficult to measure, there are few acoustic applications that make use of Pyrostriction and so will not be discussed further. However, the last three are very widely researched for acoustic applications and will be discussed in the following sections.

These techniques all use electrodes to create and sense electric and magnetic fields within the material. The material is then in mechanically coupled in some way to a test piece and caused to change shape at the desired frequency of the acoustic output. The change in shape will cause deformations that will result in propagation of elastic waves.

2.4.6 Magnetostriction

All ferrous materials will experience a change in shape when exposed to a magnetic field and, reciprocally, such materials will experience a change in magnetic state when exposed to stress. Materials in which this effect is so strong that it is measurable are called magnetostrictive materials and can be used as transmitters and receivers of acoustic waves. To excite a guided wave in a test subject, a magnetostrictive material must be mechanically coupled to the subject and then manipulated through an encapsulating magnetic field. Magnetostriction is used by equipment that is commercially available and in common use for pipeline inspection with ultrasonic guided waves Kwun et al. [2001].

The magnetic domains within a ferrous material can be oriented with a magnetic field. However, in a magnetostrictive material, the domains orientation is linked to the elastic

properties of the material and reorientation of the magnetic domains via a magnetic field will cause an isovolumetric change in shape and vice versa. Certain alloys, such as Terfenol-D, this effect is far more significant than is noticed in any element and has been specifically developed for transducer and actuator applications John et al. [2001].

Unlike piezoelectrics, the properties of magnetostrictive materials will not degrade over time through usage. They can be produced to be flexible, small (particularly low profile), and light. Some magnetostrictive materials are widely available and at low cost. Magnetostrictive approaches are found to be most competitive with other approaches when a low frequency method is needed [Kwun and Bartels, 1998]. Voltage requirement is usually relatively low.

Although alloys developed specifically for magnetostriction have the strongest effect, some materials developed for other applications have been found to be very useful. In particular materials developed for use in magnetic recording, such as Nickel and Iron Oxide based films (video tape), have been found to work well (largely due to their flexibility allowing them to be conformable) and they are very cheaply available [Kannan et al., 2007].

2.4.7 Electrostriction

All dielectric materials will to some degree change shape when placed in an electric field Turik et al. [2007]. The electric field encompassing the material causes the domains within the material to have polarised charge. Essentially the effect occurs when the charges are out of alignment with the electric field. Under an electric field the two opposing charges within each domain are pulled towards alignment and stress occurs resulting in displacement. There is no measurable converse effect and so sensing with such devices is not possible.

The strain developed per unit charge is quadratic and reversing the electric field does not reverse the direction of deformation. Approximate linear deformation can be achieved by using a narrow range and a DC offset. However, the presence on non-linear behaviour will make frequency control difficult. High voltage is generally required.

One advantage of this approach is that electrostrictive materials generally experience less creep in comparison to other active material methods. Creep is the delay that follows the application of a direct electric field before the material reaches it static shape governed by that field. This aids the signal generation at high frequencies. However, they generally are less sensitive than piezoelectric equivalents.

The amount by which a material changes shape depends on its electrostrictive constants. There are a number of man made ceramics that exhibit a high electrostrictive constant, such as the so called ''relaxor ferroelectrics'' [Damjanovic and Newnham, 1992, Uchino,

2000]. There are a number of companies that produce devices for actuation for active vibration control and ultrasonic thickness gauging. There are few commercial applications of electrostrictive materials for low frequency ultrasonic transduction, however, the research does indicate its potential for such applications [Sherrit and Mukherjee, 1998].

2.4.8 Piezoelectricity

Unlike electrostriction, piezoelectricity makes use of the anisotropic crystal structure of specific materials to generate linear and very directional deformation. The orientation of the deformation can selected for specific applications. Specifically, a piezoelectric material can be made to shear or expand in any orthogonal axis.

Piezoelectric materials each have a temperature, the Curie temperature, above which the electric domains have no dipole moment. If such a material is brought close to or above this point, exposed to a significant electric field and then allowed to cool, the dipole moment of all the domains will share a single orientation. This process is called polarisation. Following polarisation, each domain will develop a charge in the same direction when caused to deform and, through the inverse effect, will deform in the same direction when exposed to an equal electric field. When the domains are all acting in the same orientation, these effects have a net result and a deformation of the entire material is measurable.

Material Selection

Only a small number of crystalline materials have useful piezoelectric properties. Many of those used for industrial applications are man-made ceramics, most common of all are variations of Lead-Zinc-Titanate (PZT). The selection of material is largely dependant on cost, curie temperature, operating voltage, desired deformation mode and brittleness.

Alternatively, a small number of polymer materials have been found to piezoelectric characteristics, of which Polyvinylidene Fluoride (PVDF) is known to be most effective [Monkhouse et al., 1997]. Although the sensitivity of these materials are generally around one tenth that of the piezoceramic alternatives, sensitivity is not always of major and such materials are advantageous. PVDF for example can be produced as a flexible film at very low cost.

Material flexibility is very advantageous as it allows conformance with the test structure and affords superior mechanical coupling, particularly when the contact area is a curved surface, where a rigid device could only achieve tangential contact.

Electrode Arrangement

If uniform electric field strength is assumed, it can be expected that a piezoelectric materials would experience uniform strain and so an increase in material size would result in greater displacements. However, the electric field strength is partially determined by the separation distance of the electrodes and larger piezoelectric materials are likely to have wide electrode separation distances and lower field strengths. The type of deformation is determined by the direction of polarisation and the relative direction of the electric field used for actuation. The placement of the electrodes is therefor crucial in piezoelectric transducer design.

The efficiency of the electromechanical coupling is dependent on the matching of mechanical and electrical impedance. The electric field strength is also dependent on the permittivity of the material between the electrodes and material included other than the piezoelectric material can hamper sensitivity.

Rather than using a single pair of electrodes over a large piece of piezoelectric material, it is possible to increase the field intensity by dividing that material into sections which each have a pair of electrodes. If the sections are joined then the displacement will still be cumulative (as if a single piece), but the displacement will be higher as field strength will be greater.

An advanced approach is to use InterDigital Electrodes (IDE), where the sections of piezoelectric material are interspersed with electrodes alternating in polarity. With IDEs the positioning of electrodes not only effects field strength but also wavelength selection and directionality too [Monkhouse et al., 2000, Jin et al., 2005]. When the spacing of positive and negative electrode pairs is equal to the wavelength of a mode that is present at the target frequency, then that mode will be efficiently excited.

By varying the field strength used across a piezoelectric material it is possible to reduce the wavelength bandwidth, just as a window function will reduce the frequency bandwidth on a short pulse. Varying the field strength for separate electrodes is difficult, but can be achieved by varying the electrode size or shape.

Deformation Mode Selection

The type of piezoelectric deformation used will be chosen to suit the type of excitation required. To create a particular wave mode, the displacement of the contact surface of the piezoelectric should be similar to the displacement of that wave mode at the contact surface of the test piece.

Piezoelectric material can be made to deform in one of six degrees of freedom ; three of these are extension and constriction in the orthogonal axis and three are rotation

(effectively shearing) about the orthogonal axis(as shown in Figure 2.1). In common piezoelectric nomenclature the former three degrees of freedom are labelled 1 , 2 and 3, where 3 is the axis of initial polarisation, and the later three are labelled 4, 5 and 6, corresponding to rotation about 1, 2 and 3 respectively [BSE].

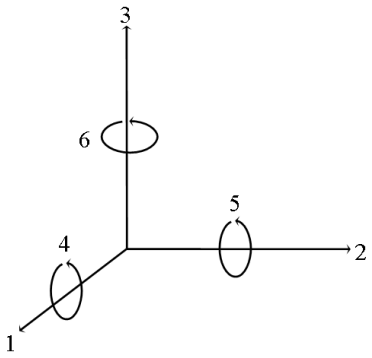

FIGURE 2.1: The six degrees of freedom for piezoceramics

Some deformation modes are more efficient than others. For example, there are two extensional modes; one where the actuation electric field is in the same direction to the polarisation and one where it is orthogonal to it. The former mode is known to be approximately three times more efficient, but often the geometry is harder to achieve.

For example, if a wave had significant displacement lateral to a contact surface, then a shearing element may be used such that this contact surface is caused to displace laterally. As a shearing piezoelectric element will have two parallel sides that displace in opposite directions, one of these sides can be coupled to a surface to create uniform lateral movement.

The coupling of normal displacements in a piezoelectric with a test piece can be supported through the use of couplant fluid. However, lateral displacements are transmitted as shear vibrations and are not supported well by fluids. Very viscous fluids can bridge small gaps, however, improved coupling can be achieved through mechanical loading, where high pressure is used to provide a mechanical connection between the two materials.

Extensional piezoelectric elements can be arranged to displace into a surface or in parallel to it. However, when placed to create a parallel displacement these devices will not have uniform displacement across the contact surface because the extension is cumulative from the centre position. An extensional element will expand from the centre point outwards in one axial direction with the extremes moving in separate directions. One side of the contact surface will be moving in an opposing direction to the other, effectively transmitting an equal and oppositely phased signal (Figure 2.2). This method is often more efficient at directly causing surface displacement than using a shear element, however, causes many difficulties in exciting a desired mode. A previous solution has been to lean the element onto one edge such that only one pole of this bipolar displacement is making contact with the surface.

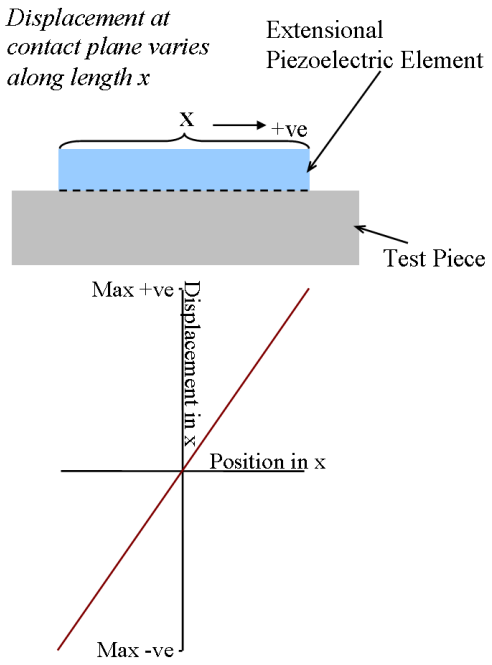

FIGURE 2.2: Simplified relative displacement along contact surface.

Interface

Another approach to the excitation of a particular wave mode is to use an interface to convert one mode of excitation into another. One very successful interface is that of the wedge interface. A transducer held against one face of the wedge is used to create a wave that propagates in the normal direction to that surface, which will then reach another outer boundary at an angle. The wave is transmitted through that boundary to the test piece and, as it is passing through at an angle and is a change of material, is subject to Snell's law of refraction. This can be used to generate a surface wave or a directional beam within the test piece. Wedges very good wave mode selection, as the angle is tailored to suit the narrow wavelength bandwidth. However the interface will reduce the overall sensitivity and often involves a tall profile.

Interfaces can also be used to direct the desired vibration to a desired point. The problem of a bipolar transducer having equal and opposite displacement mentioned before can also be solved by using an interface to couple one pole to a test piece better than its counterpart (patent pending: 0716047.6). Also, for many applications of guided waves, accessibility is considerable issue and interfaces can be used to connect transducers to areas where direct access is not possible.

Available Technology

Due to the material, polarisation, geometry, electrode placement and array design optimisation possibilities a number of advanced Piezoelectic transducers will be explored in following sections and the relative merits will be discussed separately.

Monolithic Piezoelectric Device

The standard monolithic piezoelectric ceramic transducer for SHM involves and piezoelectric element housed between two electrodes, which in turn are housed between a wear plate and a backing mass (Figure 2.3). A backing mass is required to dampen the transducer to prevent it continuing to vibrate after an excitation pulse has been applied. Many commercial compression transducers designed for a range of applications, such as megahertz range ultrasonic generation or fine placement actuation can actually be used for kilohertz range generation of ultrasonic guided waves.

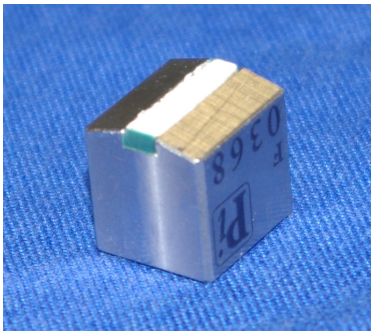

FIGURE 2.3: Conventional monolithic transducer for Long Range Ultrasonic Testing (LRUT).

A basic piezoelectric device is monolithic, which means it is from a single piece of piezoelectric material. Such transducers will have a single pair of electrodes surrounding the material in order to sense and control the electric field within it. This well established technique is cheap and relatively simple to produce. Best practice manufacturing, characterisation and quality control techniques are well known. There are a number of materials that can be selected to optimise the transducer development for a specific application, such as temperature durability. As this method involves a single piece of piezoelectric ceramic and a large backing mass, these devices are invariably rigid and bulky. Wear plates are essential due to the soft brittle nature of typical piezoelectric ceramics. In comparison to other active material devices, there are a very large number of suppliers of compression and probes. As mentioned above in the optimisation section, these transducers can be easily used with a wedge, which makes them more cumbersome, but allows good wave mode and direction control at low cost. Monolithic transducers have poor sensitivity to hydrostatic pressure.

Stacked Actuator

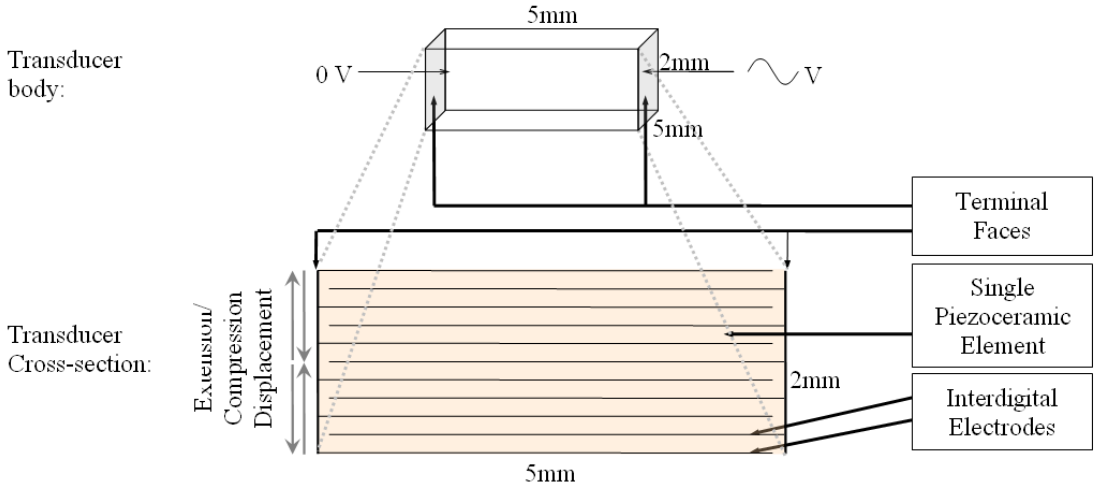

FIGURE 2.4: Stacked actuator cross-section view of InterDigital Electrode (IDE) pattern.

As mentioned above, IDEs allow for narrowly spaced electrodes and cumulative displacement. Also mentioned was the fact that extra material layers between the electrodes and the piezoelectric material will reduce the electric field strength in the piezoelectric material. Stacked Actuators are devices that include planar IDEs interposed within piezoelectric ceramic material (Figure 2.4). This is achieved by embedding electrodes into the piezoelectric ceramic before it has been sintered [Heinzmann et al., 2002].

The actuators have been shown to be highly reliable devices for both fine position and vibration control applications [Pertsch et al., 2006]. Whilst this advanced production method is more expensive, the sensitivity is much higher than that of a standard compression piezoelectric element of the same size. Production methods have developed over the last 10 years and they are now available at relatively low cost [Florian and Ragossnig, 2007].

A number of companies produce transducer using this technology. A variety, for example, are available from One example is the PICMA series from Physik Instrumente GbmH, which can be used a small, cheap and highly sensitive compression transducers (Figure 2.5).

Piezoceramic-Polymer Composites

Piezoceramic-polymer composites originated as a solution to the problem of producing a piezoelectric transducer that was sensitive to hydrostatic pressure for submerged use in fluids [Tressler et al., 1998]. The same principle can be applied to other materials and is sometimes referred to as active-inactive composites. Hyrostatic pressure will apply to all faces of a body evenly and may cause a change in size, but not shape. The sensitivity

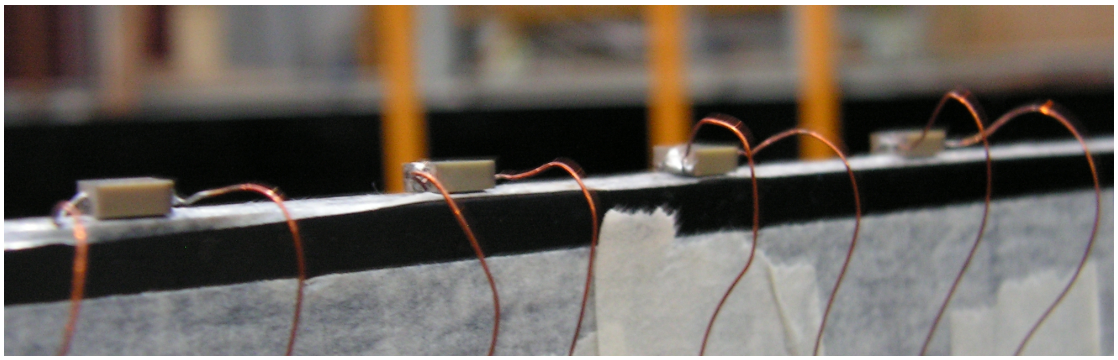

FIGURE 2.5: Array of four PICMA multilayer cofired transducers for plate wave generation and sensing.

of piezoelectric material in the axis of polarisation tends to be approximately inversely proportional to twice the sensitivity inversely of the other two orthogonal axes. The net charge will be approximately neutralised (effectively very low). By using a two phase material of piezoelectric ceramic (piezoceramic) and polymer can be used to provide stress transfer from the piezoceramic to the polymer in one or more axes. This serves to decouple the sensitivity in one axis to one or both of the other two axes, thus making the piezoelectric more sensitive to hydrostatic pressure.

Designs of Piezoceramic-polymer composites are classified by the number of axes in which either material is continuous in. The nomenclature for this uses two digits; the first for piezoceramic and the second for polymer, where digits 0, 1, 2, and 3 represent the number of axes each is continuous in. For example, a 3-2 piezoceramic polymer composite would signify a device made from a two phase material with piezo-ceramic running in all three orthogonal axes and polymer embedded within it running in two axes.

The research of this concept has lead to the optimisation of piezoelectric transducers for many applications. A composite approach allows for specialised electrode layouts, and can change the durability, flexibility, deformation shape and mechanical impedance of the active material's body.

1-3 composites are one of the most researched type of piezoceramic polymer composite. These usually involve a number of parallel piezoceramic fibres, which are polarised along their length and aligned in this axis. The spacing between rods is filled with a polymer. Stress in the axial direction of the fibres is transferred between the polymer and the fibres by shear stress, which increases their sensitivity in that direction [Tressler et al., 1998].

They have lower mechanical impedance than monolithic piezoelectric devices. Impedance, resonant frequency, sensitivity, piezoelectric coefficients and other properties can be made to be optimised in each axis. Production is often bespoke and high optimised for each application. Research has found ways to reduce cost of production, but costs remain

high in comparison to monolithic transducers. Another advantage is their ability to be shaped to have the curvature of the contact surface of a test subject.

There are a number of methods for creating the fiber patterns and housing them in a polymer. The cheapest methods tend to involve a cutting apparatus used to shape a block of piezoelectric material which is then injected with a polymer filler. A number of complete piezocomposite devices are commercially available for a variety of applications.

Patch transducers and Macro Fiber Composites

One type of piezoceramic-polymer composite is the 2-2 lamina piezocomposite, or piezoelectric patch transducer. This device consists of essentially a monolithic piezoelectric wafer layer held between layers of electrodes, and polymer housing. Although thin piezoceramic wafers are very brittle the polymer layers improve their flexibility. They are a device offering all the benefits of a monolithic transducer, but with improved flexibility. Flexibility allows the contact surface of the patch to conform to the surface of the test piece and, where the test piece is curved, direct coupling is greatly improved.

These transducers found applications in many fields including structural actuation, energy harvesting, active vibration control and acoustic non-destructive testing. This spawned two more approaches which would then be brought together to create the Active Fibre Composite transducers (Figure 2.6).

The first was a device that uses interdigital electrodes in place of the electrode layers. Top and bottom layers of electrodes are identical, with electrode fingers run across the surface in one axis and alternative between positive and negative along the other axis. This allows for an electric field to be manipulated in the plane of the wafer and benefits from the advantages of narrowly spaced electrodes. The wafer could then be used to expand through one of its wide axes whilst making use of the efficient D_{33} mode of piezoelectric actuation.

The second approach took advantage of 1-2 composite design and replaced the wafer layer with axially aligned fibres that have a circular cross-section. This demonstrates improved flexibility and durability. It also allows the patches to be optimised for lateral sensitivity and many other properties that a designer may wish to optimise for a specific application.

Active Fiber Composite (AFC) transducers combine the interdigital electrode approach with the fibre composite approach, gaining the inherent advantages of both. This allows for a durable, flexible and highly sensitive device. Fibres are housed within epoxy that is in turn housed between two polyimide layers with interdigital electrode patterns printed on. However, AFC fibre production and AFC part assembly are expensive and not optimised for large scale production.

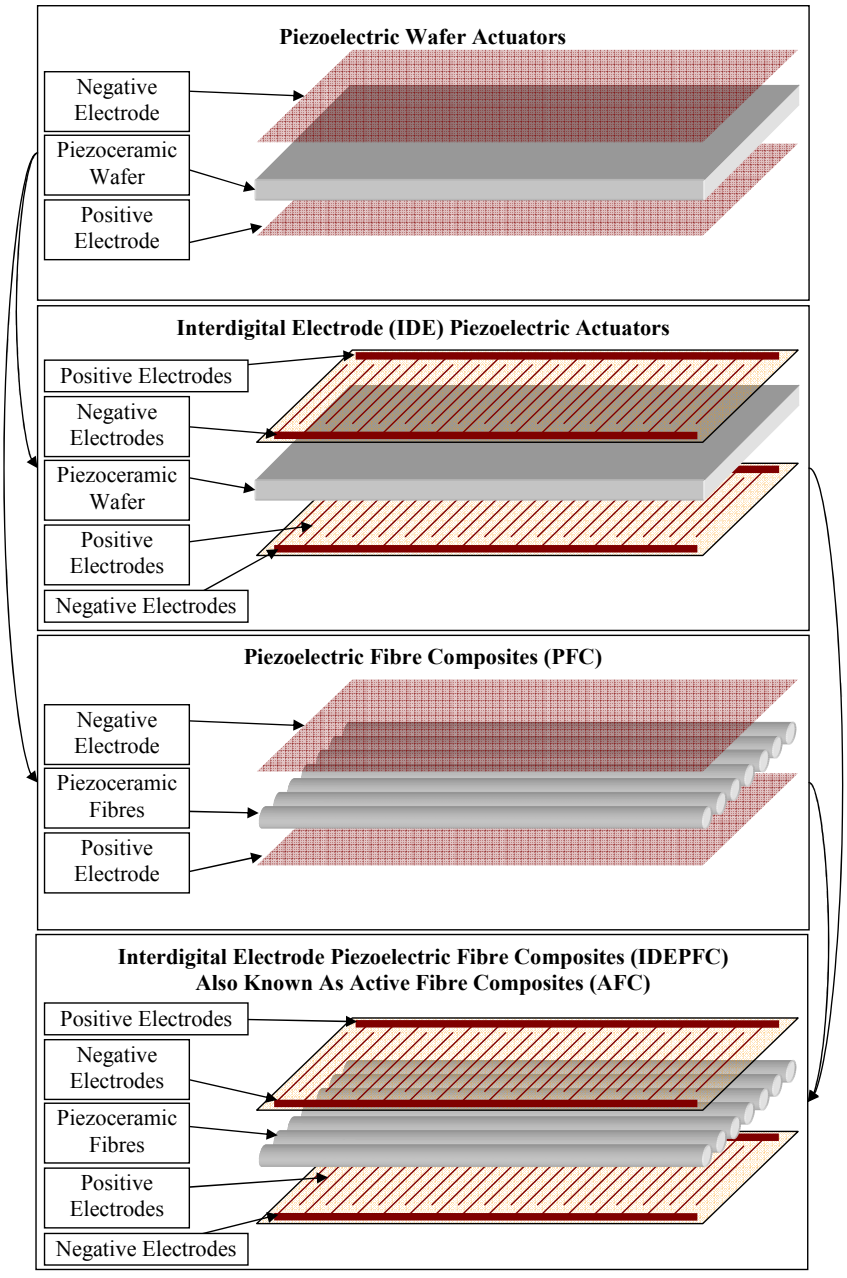

FIGURE 2.6: Progression from piezoceramic wafer to piezoelectric composite and interdigital piezoceramic wafer and then to Active Fibre Composite (AFC).

Macro Fiber Composite (MFC) transducers are a type of AFC transducer that optimises the sensitivity whilst allowing them to be mass produced relatively cheaply. The major difference between the MFC and the AFC is that fibres for an MFC are cut from a piezoceramic wafer using a computer controlled dicing saw and have a square cross-section. This increases the amount of piezoceramic in the electric field and, as the electrodes and the piezoceramic both have flat surfaces, reduces the epoxy between them, thus increasing sensitivity. These transducers not limited to extensional deformation, but only extension along the axis can make use of both interdigital electrodes and the highly sensitive D_{33} mode of deformation.

Piezoelectric patches are simple, flexible and cheap monolithic transducers. Macro Fiber Composites are more complex, but are relatively cheap and are available as a fully assembled product. Macro Fibre Composites are flexible, durable and highly sensitive. As they are thin laminas and extend laterally they cannot be efficiently used as compression transducer and do not have uniform displacement across the contract area, which can cause a problem for the generation of guided waves.

Piezoelectric wafer patches are available from a number of companies world wide at low cost. The method for producing Macro Fiber Composite transducers is patented by NASA Langley Research Center [Wilkie et al., 2003]. Smart Material GmbH is the licensed manufacture. They can be obtained in either D_{33} or D_{31} mode in various different sizes and arrangements.

Chapter 3

Development of 1D Simulation and Experimental Characterisation for Macro Fiber Composite Transducers

3.1 Introduction

A novel device has been identified as suitable for generating and receiving Lamb-equivalent wave modes in pipes [Thien, 2006], with notable practical advantages such as being flexible (compliant to a curved surface), thin and light. These devices are sensitive to and can actuate in-plane strain to a surface. Their size can vary, but they are typically constructed to be from 20 to 90 mm in length and 3 mm to 30 mm in width. This represents a particularly large footprint for a transducer for Long Range Ultrasonic Testing since the waves lengths used are generally of this magnitude. It was expected that their in-plane nature and their size would contribute to a transmission and reception capability that is direction, frequency and wavelength dependent.

In this chapter the frequency response of the MFC transducer is evaluated with consideration for the relationship between MFC length and wavelength. A 1D model for predicting the MFC performance at low frequencies is given, which makes use of external dispersion curve and excitability curve data. Experimental measurement of the MFC performance on a plate and a rod waveguide is presented and compared to the simulated method. The measurement was isolated for a single wave mode using a broadband chirp signal and spectral amplitude measurement through a bank of band-pass filters. This was used to show that thee simulation could predict the mode dependent frequency response for an MFC of a given length.

3.2 MFC Transducers

Generally, methods of testing with ultrasonic guided waves make use of the fundamental wave modes at low frequencies where these are the only wave modes that can exist, because this makes the problem of wave mode control simpler. Surface or plate-like wave modes are possible in all solid structures, and for many of these modes the main axis of vibration is in-plane. For example, the S0 plate wave mode is popular because it tends to offer a wide frequency range where it is non-dispersive and over this range it has predominantly in-plane vibration [Krautkrämer, J. and Krautkrämer, H., 1983].

The relative efficiency for each mode to be excited by a given in-plane or out-of-plane disturbance is known as the excitability and can be expressed as a function of frequency [Wilcox et al., 2001]. An out-of-plane disturbance will preferentially excite modes that are predominantly out-of-plane, whilst an in-plane disturbance will preferentially excite modes that are predominantly in-plane modes. This means there is a requirement for transducers that operate in the plane parallel to the surface of the structure where the transducer is to be placed.

Macro Fiber Composite (MFC) actuators can be used to actuate and sense in-plane displacement. The MFC transducers used in this thesis were provide by Smart Material GmbH and their data sheet is available in Appendix A [Daue, 2011]. At approximately 0.4 mm thick, they are a thin film technology. They have a piezocomposite design to overcome the brittle nature of piezoceramic material, which allows them to be flexible and durable. The piezocomposite design can exhibit uniaxial actuation [Wilkie et al., 2000, Williams et al., 2002]. They also make use of an interdigital electrode approach that allows them to orient the strain and the electric field in the polarisation axis, which is more effective than using a tangential electric field [Nelson, 2002]. The fibres are produced by dicing a piezoceramic wafer into fingers, each with a rectangular cross-section. These fibres are set in parallel within epoxy, which is then enclosed between layers of polyimide that have been etched with the electrode pattern. This assembly is shown in Figure 3.1. The electrode widths and spacing have been optimised for reducing the voltage requirement whilst increasing the actuated length [Bowen et al., 2006].

MFC transducers were originally designed for structural actuation and vibration control [Williams et al., 2002]. They used piezoceramic fibres housed in a polymer matrix, which allow them to use the high efficiency of piezoceramics and yet achieve high flexibility. They also use interdigital electrodes for polarisation and transduction. The d_{33} type interdigital electrode design provides highly efficient transduction [Nelson, 2002]. The manufacturing process for producing these transducers is designed to achieve high reproducibility and low cost production, when high volumes are required [Wilkie et al., 2003]. This manufacturing process separates the MFC transducer from other types of Piezoceramic Fiber Composite Interdigital Electrode (PFCIDE) transducer, which are also known as Active Fiber Composite (AFC) transducers. The MFC transducers for

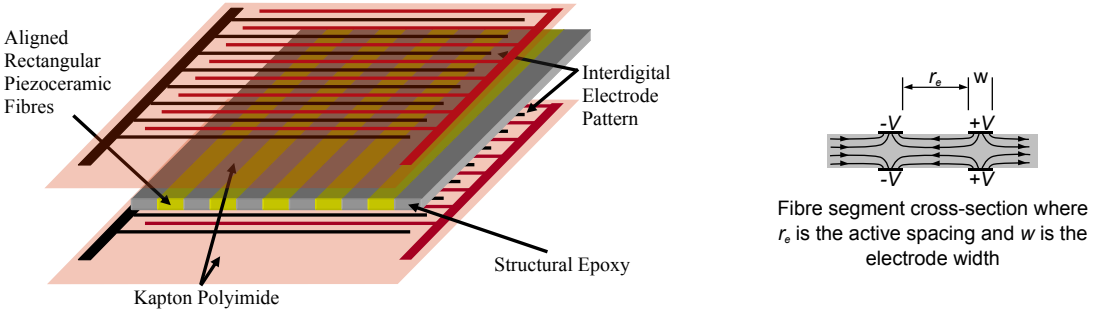

FIGURE 3.1: A) On the left is an illustration showing the expanded make up of a Macro Fiber Composite actuator, and B) On the right is an illustration of the application of an in-plane electric field along the fibre axis for one MFC segment (as given by Nelson [2002]).

this study were provided by ‘‘Smart Materials’’ and the data sheet is provided on their website [Daue, 2011]. Smart Material refer to the MFC described here as the P1 type, they also offer an additional type (known as P2) that is not interdigital, but instead uses an electric field perpendicular to the piezofibres through separate top bottom electrodes. This study is limited to the first type of which there is more supporting literature, although the P2 type is considered in the future work section.

3.3 MFC Wave Mode Dependent Characteristics

Ultrasonic transducers often act over regions with dimensions that are large with respect to the wavelengths excited. For LRUT it is often required that transducers are placed on a surface that is parallel to the plane in which waves propagate. On transmission each point of active contact creates a disturbance in the surface of the structure under test, and the ultrasonic output is the combined output from each of these disturbances. Since the waves generated are in the elastic regime, the total output is the superposition of the output from each of these disturbances. For large transducers this can lead to amplitude variations that are wavelength and direction dependent. Since the velocities of ultrasonic guided waves are frequency dependent, and these velocity-frequency characteristics vary by wave mode, a transducer's directional transmission will be dependent on frequency and different for each wave mode. MFC transducers are made with dimensions that are of the order of a few tens of millimetres, which for many applications of ultrasonic guided waves means they have dimensions that are of a similar size to the wavelengths used.

Ultrasonic waveguides could be classed into two groups: 1D and 2D. 1D waveguides allow propagation in only one axis and include solid rods (e.g. rails, beams, and wires) and hollow rods (e.g. tubular structures and pipelines). 2D waveguides constrain propagation in any direction within a certain plane and include plates (e.g. ship hulls and aircraft wing panels) and surfaces (such as the surfaces of thick structural components). In this chapter a process of MFC actuator characterisation is presented. This process is staged

such that it firstly deals with the 1D scenario for the analysis of the transducer's frequency response and then with the 2D scenario for the analysis of transducer directionality.

3.4 MFC Application To Pipe Testing

MFC actuators have been used as transmitters and receivers of Lamb-like wave modes in steel pipes [Thien, 2006]. In this work an array of four MFC actuators were bonded to a steel pipe at the same position axially and at equidistant positions around the circumference. The MFC actuators were oriented with their fibres aligned in the axial axis of the pipe to match their major axis of operation with the axis of in-plane strain caused by the wave modes of interest, as is shown in Figure 3.2. The pipe had an outer diameter of 64 mm and a wall thickness of 1.6mm.

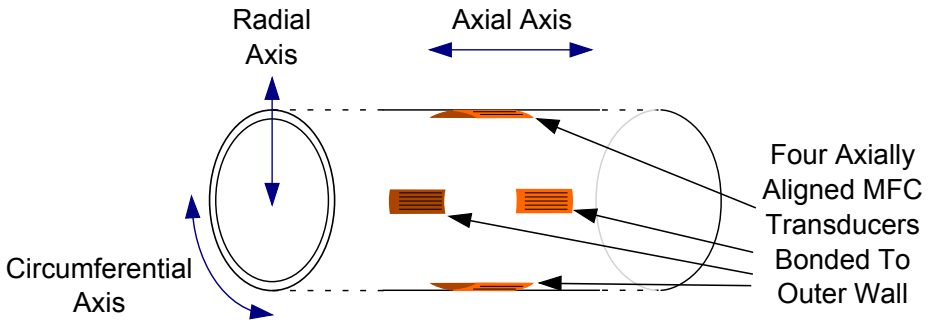

FIGURE 3.2: A sketch showing the positioning and alignment used by Thien [2006] for testing MFC's ability to excite ultrasonic guided waves in pipes.

The MFC actuators are active only for the digitised area containing the fibres, whose length is dictated by the length of the piezoceramic fibres. The fibre length of the MFC actuators used was 85 mm, which is significantly long with respect to the wavelengths that could be expected. Thien demonstrated their use, but did not optimise the size of the MFC or the array layout for single wave mode sensitivity, which would result in signals that are more easily interpreted and are likely to improve defect detection. This optimisation is complicated by the number of possible wave modes that could be excited and received in the pipe of interest. The velocity/frequency characteristics for all possible wave modes between 0 and 120 kHz have been calculated for this thesis based on the steel pipe paramters used by Thien [2006]. These curves were generated using the software Disperse software [Pavlakovic et al., 1997]. This was done to illustrate the complexity of wave mode control problem (Figure 3.3). These graphs are commonly known as dispersion curves. Detail on the naming scheme for the wave mode modes is given in section 2.3.2.

Figure 3.3 shows that Thien used a centre excitation frequency of 70 kHz, which coincides with a frequency where both the L(0,1) and L(0,2) modes are fairly non-dispersive (their velocity does not vary much within a narrow band around this frequency), which is

generally desirable for long range testing. However, they will also have sensitivity to the 19 flexural modes that exist at this frequency, and these modes are mostly dispersive at this frequency. At this frequency the variety of wave modes cover a range of velocities. This example demonstrates how for many ultrasonic guided wave inspection applications there is often one mode of interest and a group of unwanted modes that differ from the mode of interest by wavelength.

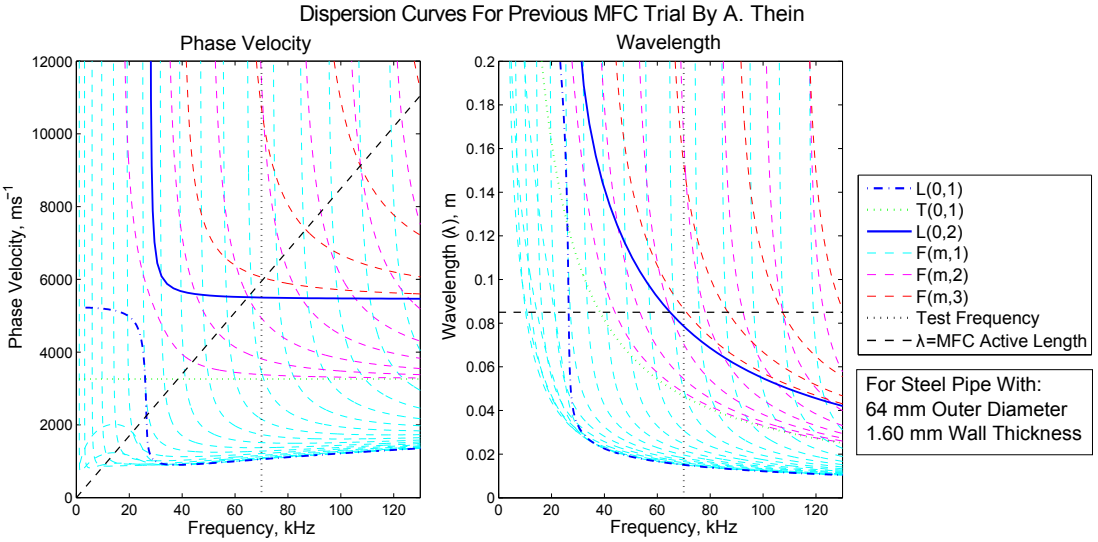

FIGURE 3.3: Phase velocity and wavelength dispersion curves for the pipe used by Thien [2006] for evaluating the application of MFC transducers for generating and sensing Ultrasonic Guided Waves in pipes, with comparison to the active length of the MFC and frequency used. The wave mode naming scheme is described in Section 2.3.2.

3.5 Method for MFC Frequency Response Study

It was hypothesised that, due to their large size, MFC transducers will have sensitivity that is related to the ratio of the active length to wavelength. By confirming this relationship it could be possible to choose the length of the MFC to target a specific wavelength/frequency combination and diminish the sensitivity to the unwanted modes. This chapter explores this hypothesis with experimental measurement and analysis of the MFC's wave mode sensing capability with respect to its size and the wavelengths used. A simplified 1D model of the MFC transducer's sensitivity is used to evaluate the superposition effects that cause this wavelength dependent bias and the results are compared with the experimental measurements. The 1D model is based on the conversion of a voltage varying signal to an actuated surface displacement that excites a wave that is again sensed by another MFC of the same length to create a new voltage varying signal. Experiments on a steel plate and an aluminium bar were used to measure the amplitude of a a wave mode that had been transmitted from an MFC to another MFC. The results of these experiments are used to develop and refine the model for MFCs of varying lengths.

3.6 1D Analytical Model

This section presents a linear analytical model for the transmission and reception of guided waves when an MFC actuator is used. It was hypothesised that the large size of the MFC actuators and the relatively long wavelengths used will have a significant effect on the frequency response of these devices because they are placed on a plane parallel to the wave propagation.

A new set of equations will be derived to give a simplified 1D model, which will be used to explore the mechanism behind this wavelength dependency. This model will be used to produce a transfer function for a specific wave mode for a number of MFC transducers with differing lengths. This is then compared to equivalent experimental results.

Impedance analysis found that the main resonance of these devices was close to 10 MHz (much higher than the frequency of interest) and the impedance characteristics are fairly uniform at the frequency range of interest (approximately 0 to 200 kHz), hence electrical impedance matching and resonant effects are ignored.

3.6.1 Transmission

Most common applications for Long-Range Ultrasonic Testing involve metal structures that are around 3 mm to 25 mm thick, whereas the MFC is thinner at 0.3mm thick. The MFC must be coupled to a surface by either traction (provided by normal force loading) or through bonding to transmit the shear stress between the two objects. The main axis of strain will be in the axis parallel to the MFC fibre alignment; hence the fibre axis should be aligned with the desired main axis of propagation.

On transmission a time varying voltage signal is applied over all electrode pairs of an MFC, which are depicted in Figure 3.4. This figure gives an illustration of a cross-section of an MFC coupled to a solid waveguide. The fibre is aligned along the x-axis, which will be the axis considered for wave propagation. The mechanical system can be considered symmetric about the centre of the piezoceramic fibres and the centre of the fibres will be the origin for the x-axis. The MFC is considered thin in comparison to its length and the wavelengths used, so strain through its thickness is assumed to be uniform.

The transmission of a single frequency is considered. A single frequency signal is a sine wave that exists for all time. The input voltage signal can be represented with a scaled sine function as,

$$V(\omega, t) = A_V(\omega) \cdot \sin\Big(\omega t - \phi(\omega)\Big), \tag{3.1}$$

where ω is angular frequency, t is time, $A_V(\omega)$ is the peak voltage and $\phi(\omega)$ is a phase offset. $A_V(\omega)$ and $\phi(\omega)$ describe the amplitude and phase respectively of the input voltage signal for each angular frequency, which is at the control of the transmission electronics.

Figure 3.4 shows how the piezoceramic fibres are segmented along the x-axis by pairs of electrodes (one on top and one below). Each electrode within each pair has the same voltage, and these pairs alternate in polarity along the fibres. Each segment of the MFC is between a positive and a negative electrode pair.

Whilst the dynamic electric field created within the piezoceramic is three dimensional and spatially dependant, it can be considered to be acting predominantly in the x-axis and approximately uniform. The electrodes are external (they do no penetrate the thickness of the piezoceramic fibres), however the effect of above and below electrodes with equal voltage is to approximate a plate electrode through the thickness, which creates an electric field that is approximately uniform, except in close proximity to the electrodes. This has been assessed with a static charge model of two pairs of point charges where each pair had equal and opposite charge. The relative electric field strength and direction in the region between the electrode pairs is depicted in Figure 3.5. The charges are placed in approximately the same positions as electrodes surrounding an active segment of piezoceramic fibre (of the type illustrated in Figure 3.4). Since this model uses point charges rather than area electrodes, the electric field is strong near the charges, but is seen to be fairly uniform for a significant majority of the active region of the piezoceramic. This means that the electric field developed within the piezoceramic can be assumed to be close to that between two parallel plates with equal voltage, and the classic parallel plate equation (where the electric field is equal to the negative voltage divided by the plate separation distance) can be used to gain the field strength.

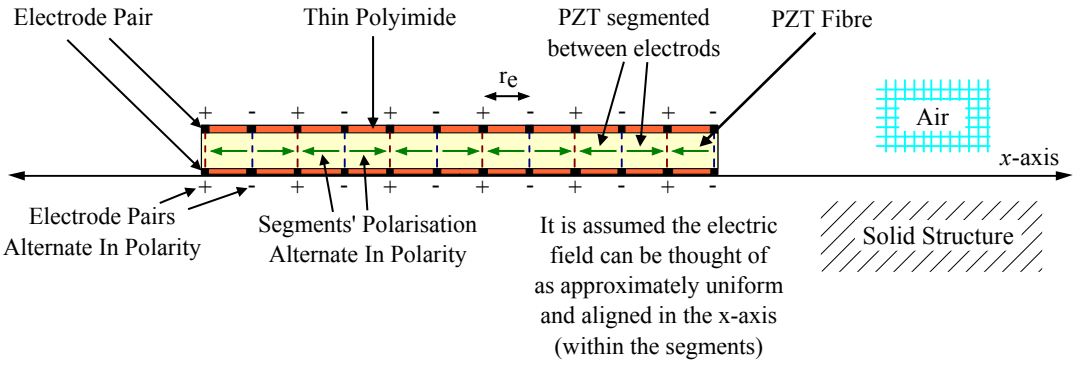

FIGURE 3.4: A depiction of the layout of the MFC represented by the transmission analysis in this section.

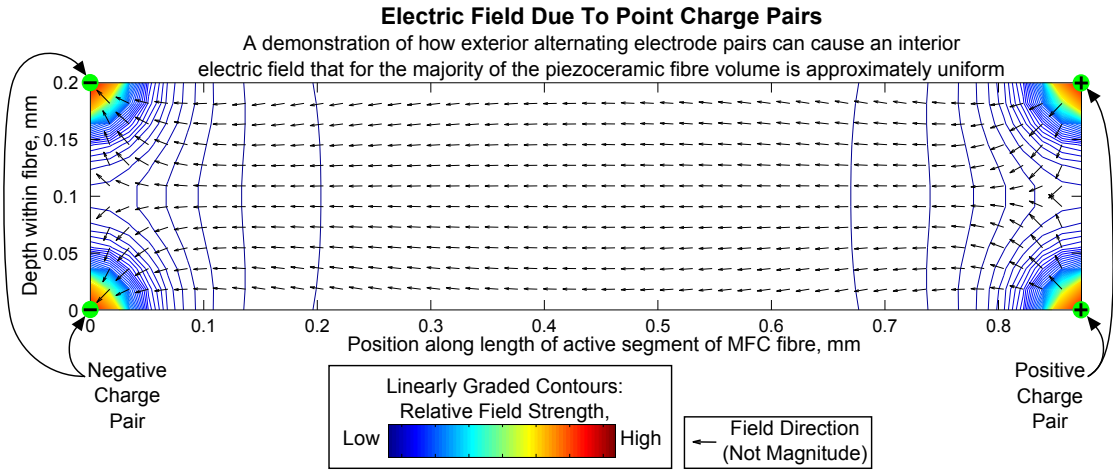

FIGURE 3.5: Two pairs of electric charges (negative on the left and positive on the right) have been modelled with their positions similar to those forming a segment of piezoceramic fibre in an MFC. This shows that for most of fibre there is an approximately uniform electric field aligned in the fibre's major axis.

The uniform electric field strength following from Equation 3.1 is then,

$$E(\omega, t) = \frac{-V(\omega, t)}{r_e} = \frac{A_V(\omega)}{r_e} \cdot \sin\Big(- \omega t - \phi(\omega)\Big), \tag{3.2}$$

where $A_V(\omega)$ is the peak voltage, ω is the angular frequency, t is the time and r_e is the distance between the electrode pairs.

In piezoelectric materials the strain and the charge density are coupled. This coupling is represented with the piezoelectric constitutive coupled equation [Burgt et al., 1974],

$$\begin{aligned} \varepsilon &= s_E \sigma + d' E \\ D &= d\sigma + \zeta_\sigma E \end{aligned} \tag{3.3}$$

where σ is stress, s_E compliance as measured in the absence of an electric field, ζ_σ is permittivity as measured in the absence of stress. D is the charge-density displacement (also known as the dielectric displacement). d is the piezoelectric charge constant for the piezoceramic. d is a material property of the piezoceramic components of the MFC and d' denotes the transverse matrix of d. This is a tensor describing how each direction of electric field can contribute to strain in each direction. Since the MFC principally experiences the electric field and developed strain in the same axis, only the x-axis is considered and a scalar value for d will be used. The polling axis by convention is named the 3-axis [BSE]. The scalar to be used is d_{33} from the d tensor, where the electric field and the strain act in the direction of the polling axis (the major axis of the piezofibres). The d_{33} value for the MFC used is given as 460 pC/N by the manufacturer [Daue, 2011].

The elastic contribution to strain (in Equation 3.3) is $s_E\sigma$ (from Hooke's Law). This gives the piezoelectric contribution to strain caused by an applied electric field, E, as $d_{33} \cdot E$. When E is represented with Equation 3.2 this gives the piezoeletrically induced strain of an MFC active section as,

$$\varepsilon_{tx}(\omega, t) = d_{33} \cdot E(\omega, t) = d \cdot \frac{A_V(\omega)}{r_e} \cdot sin\Big(- \omega t - \phi(\omega)\Big), \tag{3.4}$$

Propagating sound waves lose some intensity with propagation, which will vary by wave mode and frequency. This attenuation is represented with the coefficient $\alpha_n(\omega)$ for each wave mode n and angular frequency ω. The curves for $\alpha_n(\omega)$ can be derived experimentally, by measuring the amplitude of repeat echoes and taking care to achieve mode purity in the measurements.

Since the field is uniform the strain is uniform, and as all the piezoceramic segments experience equal strain, the whole fibre can be thought of as experiencing uniform strain. However, the actual strain of the whole fibre will be less than $\varepsilon_{tx}(\omega, t)$ because the electrode sections experience no strain and the strain is resisted by the stiffness of the structure. An example of this value conversion by a free MFC using a time varying signal is given in Figure 3.6. This figure gives sections of a sine wave, however for the treatment of a single frequency the sine wave should exist for all time. The first of these graphs shows a voltage signal with a peak-to-peak amplitude of 300 V and a frequency of 50 kHz, following Equations 3.4. The middle graphs shows the conversion of voltage to field strength, which is assumed to be uniform within the active regions of the MFCs, in accordance with Equations 3.2, and finally the lowest of the three graphs shows the x-axis strain caused by the reverse piezoelectric effect, following Equations 3.1.

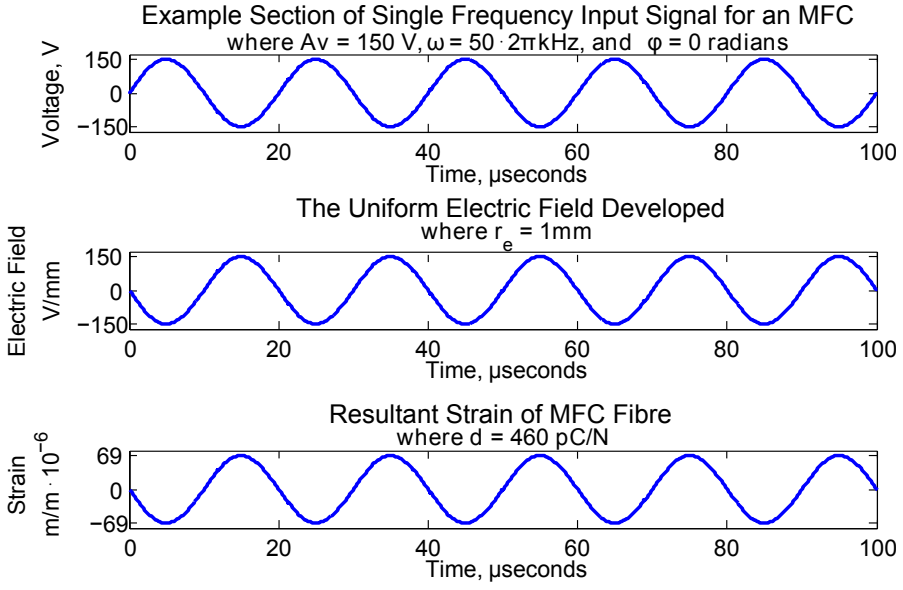

FIGURE 3.6: An example showing a free MFC's conversion of voltage to strain as described with Equations 3.4, 3.2, and 3.1 using a 300 V peak-to-peak, 50 kHz signal.

It is assumed that the MFC is perfectly coupled and symmetric about its centre, hence displacement occurs from the centre outwards. Since the instantaneous strain is the rate of displacement with respect to the position, the displacement is,

$$\begin{aligned} s_n(\omega, t, x) &= \int \varepsilon_{tx}(\omega, t)\, dx \\ = x \cdot \varepsilon_{tx}(\omega, t) = x \cdot d_{33} \cdot \frac{A_V(\omega)}{r_e} &\cdot sin\Big(-\omega t - \phi(\omega)\Big) \\ &\{\text{if } x_{min} < x < x_{max}, \end{aligned} \tag{3.5}$$

where x is the position in the x-axis, within the physical limits of the active fibres named x_{min} and x_{max} for the respective negative and positive extremes. The actuated strain at a distance x along the x-axis is zero outside of the physical limits of the piezoceramic fibres. Figure 3.7 shows two graphs, where the first is an example of the actuated displacement over time when the strain from Figure 3.6 is applied, and the second shows the this displacement for a single point in time so that the linearity is clear.

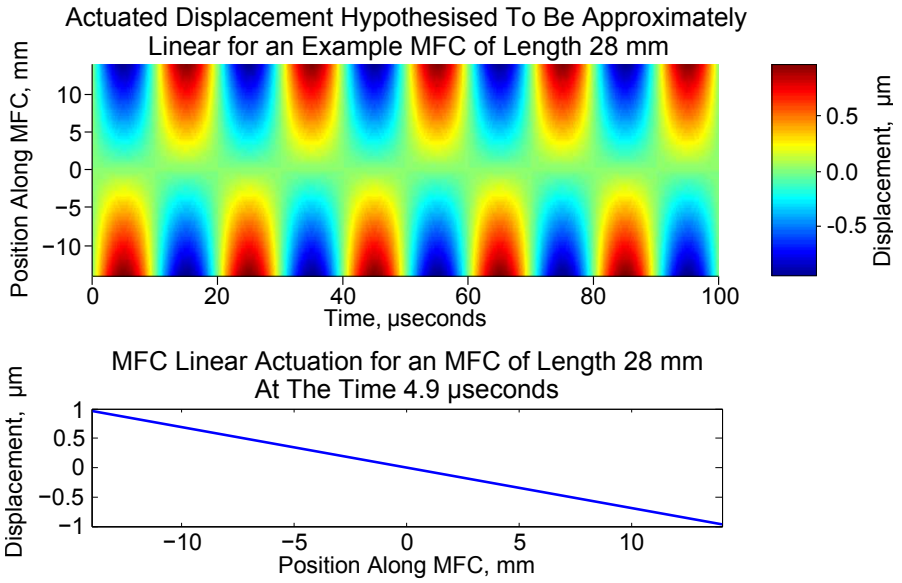

FIGURE 3.7: An example of the modelled linear displacement actuated by the applied strain caused by a time varying sinusoidal voltage signal (as shown in Figure 3.6).

Each point that experiences displacement acts as a source of sound waves. The construction of plate waves happens through the thickness, making phase and amplitude through the thickness dependent on position through the thickness, however the problem can be simplified by considering the wave only at the contact surface where all measurements are taken.

The amplitude at the surface due to the emitted waves can be calculated in relation to the displacement. From each disturbed position, there is an emitted sine wave and the phase of this wave varies with distance (equal to the wavenumber times the distance). Each

wave mode experiences amplitude loss per unit distance that is dependent on frequency, which introduces another amplitude coefficient. Also, each wave mode experiences a different amplitude at the surface due to a point source disturbance, and this ''excitability'' amplitude coefficient is also dependent on frequency. The displacement measured at some distance x_{rx} due to a transmission from a position x for a given input signal is,

$$s_{n,Point}(\omega,t,x,x_{rx}) = \alpha_n(\omega)(x_{rx}-x)\cdot\beta_n(\omega)\cdot x\cdot d_{33}\cdot\frac{A_V(\omega)}{r_e}\cdot\sin\Big(k_n(\omega)(x_{rx}-x)-\omega t-\phi(\omega)\Big) \quad \{\text{if } x_{min}<x<x_{max}, \tag{3.6}$$

where $k_n(\omega)$ is the wavenumber for mode n, $\beta_n(\omega)$ is the excitability of mode n and $\alpha_n(\omega)$ is the attenuation rate coefficient for mode n, all functions of frequency.

$s_{n,Point}(\omega,t,x,x_{rx})$ describes the displacement field from a single point actuated by an MFC. The output displacement field from an entire MFC is the superposition of the output from all points within the MFC, and is given by

$$s_{n,tx}(\omega,t,x_{rx}) = \int_{x_{min}}^{x_{max}} s_{n,Point}(\omega,t,x,x_{rx})\,dx = \beta_n(\omega)d_{33}\cdot\frac{A_V(\omega)}{r_e}\int_{x_{min}}^{x_{max}}\alpha_n(\omega)(x_{rx}-x)\cdot x\cdot\sin\Big(k_n(\omega)(x_{rx}-x)-\omega t-\phi(\omega)\Big)\,dx. \tag{3.7}$$

3.6.2 Reception

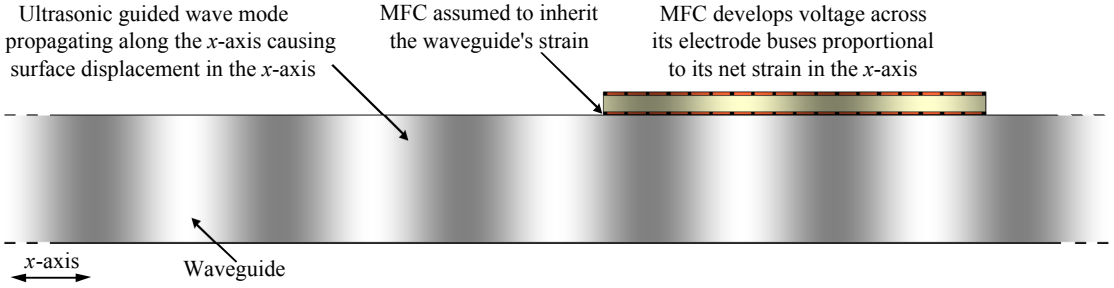

FIGURE 3.8: An illustration showing the MFC reception scenario considered for 1D simulation as part of the evaluation of the wavelength dependent sensitivity of an MFC.

This section offers a linear model of the reception by an MFC of a wave mode that is travelling parallel to a surface on which an MFC is coupled, as illustrated in Figure 3.8. This illustration shows sound propagating along the main axis of a waveguide (the x-axis) on which a coupled MFC transducer is oriented axially to measure the strain caused by this wave.

As with transmission, each frequency will be treated individually. In this section x_{rx} will represent a position within the MFC, between the spatial limits of the MFC x_{min} and x_{max}. For reception, the source of the sound is arbitrary and can be considered originating from a single point at position x_{tx}, which is also on the x-axis.

The surface displacement at position x at time t due to a sinusoidal sound wave of frequency ω from a point x_{tx} is,

$$s_{rx}(\omega, t, x, x_{tx}) = A_n(\omega) \cdot \alpha_n(\omega)(x_{tx} - x) \cdot \sin\Big(k_n(\omega)(x_{tx} - x) - \omega t - \phi(\omega)\Big), \tag{3.8}$$

where $A_n(\omega)$ is the amplitude of mode n as a function of frequency, $\phi(\omega)$ is some initial phase offset, and $\alpha_n(\omega)$ is the rate of attenuation also as a function of frequency. $\alpha_n(\omega)(x - x_{tx})$ gives the attenuation that has occurred during propagation. $A_n(\omega)$ and $\phi(\omega)$ are determined by the source of the sound wave.

When two neighbouring points in a material displace by different amounts the joining material is strained. This is a proportional shape change defined as the change in distance between the two points divided by the original distance between them, which can be expressed as the differential of displacement. The strain in the surface at a point x due to a transmit point x_{tx} is,

$$\varepsilon_{rx}(\omega, t, x, x_{tx}) = \frac{\delta}{\delta x} s_{rx}(\omega, t, x, x_{tx}). \tag{3.9}$$

If the MFC is considered very thin compared to the wavelengths expected and is significantly less stiff than the structure, it is assumed it can be thought of as inheriting the displacement of the surface it is in contact with.

The stress within the piezoceramic fibre will be equal to the strain multiplied by the Young's modulus, Λ, giving stress in the fibre due to a passing wave as:

$$\sigma_{rx}(\omega, t, x, x_{tx}) = \Lambda \cdot \varepsilon_{rx}(\omega, t, x, x_{tx}) = \Lambda \cdot \frac{\delta}{\delta x} s_{rx}(\omega, t, x, x_{tx}) \tag{3.10}$$

As the MFC is segmented by the interdigital electrodes, the strain of the passing wave causes a voltage across each segment and the voltage across the whole MFC is the net voltage across each MFC segment. Every segment has the width r_e and the electrode width is ignored as this makes no contribution and is significantly small. This arrangement is illustrated in Figure 3.9.

Each segment can be ordered from 1 to M. The bounds of any segment m can be given as x_{m_min} and x_{m_max}, where $x_{m\_max} = x_{m\_min} + r_e$. Whilst in reality there is some

inactive space in the region occupied by the electrodes, for simplicity the segments can be thought of as adjacent such that $x_{m-1\_max} = x_{m\_min}$ and $x_{m\_max} = x_{m+1\_min}$.

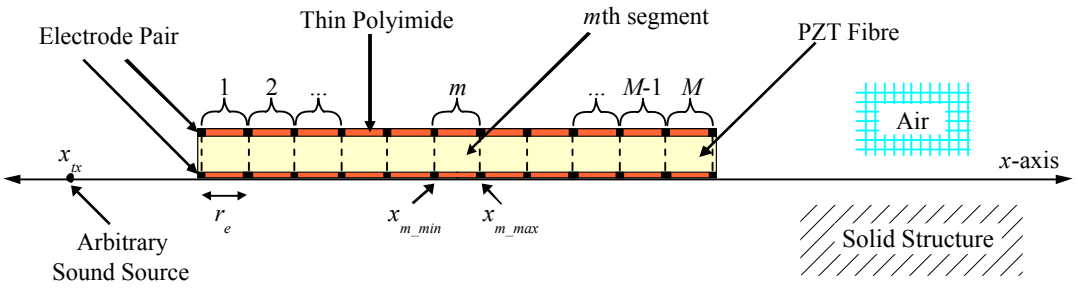

FIGURE 3.9: A depiction of the analytical model of the MFC presented in this section.

Hence, the net strain across the mth segment is,

$$\begin{aligned}\sigma_{m\_rx}(\omega, t, x_{tx}) &= \Lambda \cdot \int_{x_{m\_min}}^{x_{m\_max}} \varepsilon_{rx}(\omega, t, x, x_{tx})\, dx, \\ &= \Lambda \cdot \int_{x_{m\_min}}^{x_{m\_max}} \frac{\delta}{\delta x} s_{rx}(\omega, t, x, x_{tx})\, dx \\ = \Lambda \cdot (s_{rx}(\omega, t, x_{m\_max}, x_{tx}) &- s_{rx}(\omega, t, x_{m\_min}, x_{tx})),\end{aligned} \tag{3.11}$$

The piezoelectric constitutive equation (Equation 3.3) gave the dielectric displacement as the sum of two parts: the piezoelectric component, $d\sigma$, and the dielectric component, $\zeta_\sigma E$. The dielectric displacement caused by stress in turn causes an electric field that is measurable by the electrodes of the MFC, which is,

$$E_m = \frac{d_{33}}{\zeta_\sigma} \sigma_{m\_rx}(\omega, t, x_{tx}), \tag{3.12}$$

which gives the voltage across the mth segment as,

$$V_m = -r_e E_m = -r_e \frac{d}{\zeta_\sigma} \sigma_{m\_rx}(\omega, t, x_{tx}). \tag{3.13}$$

Since every segment has identical electrical characteristics (resistance, inductance and capacitance) the voltage developed across the electrodes buses is simply the mean of the voltage developed across all segments, giving the received voltage as,

$$V_{rx}(\omega, t, x_{tx}) = \frac{1}{M} \sum_{m=1}^{M} \Big(V_m(\omega, t, x_{tx}) \Big). \tag{3.14}$$

This indicates the voltage in the MFC is proportionate to the average of the stress across the segments within the MFC. When the inactive areas under the electrodes are ignored, the sum of the integrals is the same as taking the wider integration; hence this equation can be expressed as,

$$V_{rx}(\omega, t, x_{tx}) = \frac{-r_e}{M} \cdot \frac{d_{33}}{\zeta_\sigma} \cdot \Lambda \cdot \Big(s_{rx}(\omega, t, x_{max}, x_{tx}) - s_{rx}(\omega, t, x_{min}, x_{tx}) \Big) \tag{3.15}$$

where, again, x_{min} and x_{max} are the limits of the active length of the MFC.

3.7 Amplitude In Relation To Fibre Length

3.7.1 Fibre Length Effect On Transmission

There are three aspects of Equation 3.7 that are affected by the length of the MFC. Firstly, since attenuation is greater over longer distances, the sound travelling from the far end of the MFC is attenuated more than the sound travelling from the near side. However, guided wave attenuation rates in most solids at low ultrasonic frequencies are very low and can be considered insignificant over tens of millimetres.

Secondly x is an amplitude factor that ranges from x_{min} to x_{max} where $x_{min} = -1 * x_{max}$. This represents the bipolar displacement of the active fibre's expansion. Amplitude is greatest at the extremes of the fibre length and sound emanating from the first half of the MFC will have inverted phase.

Thirdly, the distance from each transmission point causes a spatial phase delay of $k_n(\omega)(x_{rx} - x)$, where $(x_{rx} - x)$ is the propagation distance from the transmission point. Since Equation 3.7 involves spatial integration, this spatial delay is crucial in the determining the performance of the MFC, particularly since the range of x_{min} to x_{max} is expected to be of a similar order of magnitude to the wavelength.

Whilst attenuation can be ignored, the other two aspects of amplitude that relate to fibre length are significant. These Active Fibre Length (AFL) related effects can be generalised for any combination of wavenumber and fibre length. This allows Equation 3.7 to be reduced (to facilitate the analysis of the superpositional cancellation) to the following,

$$A_{AFL\_tx}(k_n(\omega)) = Amp \int_{x_{min}}^{x_{max}} x \sin\left(k_n(\omega)x\right) dx, \tag{3.16}$$

where $k_n(\omega)$ is the wavenumber and Amp represents the amplitude contributions from non-spatial terms. This leads to an amplitude change that is the result of superpositional cancellation that is dependent on the active length of the MFC with respect to the

transmitted wavelengths (Figure 3.10). Negative values for $A_{FL}(k_n)$ for an MFC with a given active length represent that for some values of $k_n(\omega)$ the phase is inverted. Since $k_n(\omega)$ is different for each wave mode, at a given angular frequency the transmission amplitude of each wave mode will be affected differently.

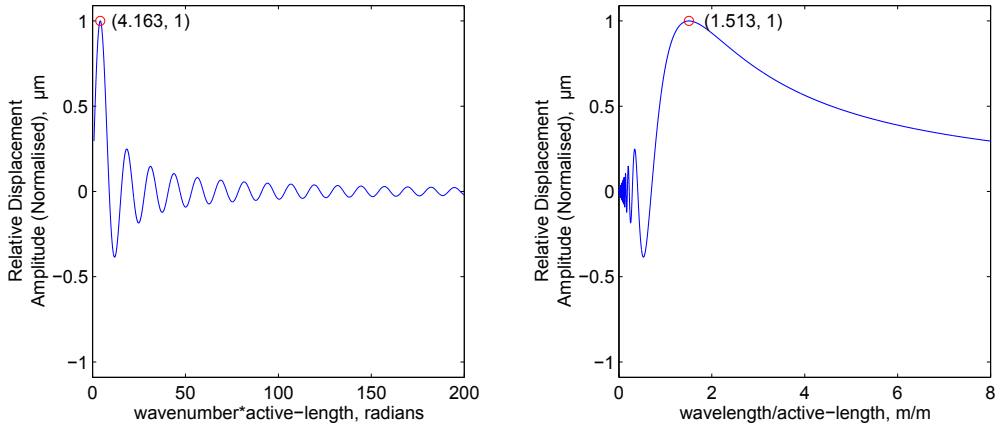

FIGURE 3.10: The hypothesised superpositional amplitude loss across the MFC fibre length on transmission given in relation to wavenumber (left) and wavelength (right). The optimal wavelength/active-length combination has been marked with a red circle.

3.7.2 Fibre Length Effect On Reception

The reception of ultrasonic guided waves with MFC transducers is not the reciprocal process of transmission. On transmission the amplitude is linearly proportionate to position in the MFC (minimal at one extreme, zero in the centre, and maximal at the opposing extreme). This is not the case on reception, since the voltage generated due to strain is uniform across the length of the MFC.

The reception amplitude is affected by the attenuation of the ultrasonic waves. However, as with transmission, the attenuation over the distance of the active length of the MFC is expected to be negligible. When considering the effect of active length on reception amplitude, attenuation will not be considered.

As with transmission, there is expected to be a significant spatial phase delay in the signal across the active length of the MFC due to the phase component $k_n(\omega)(x_{tx} - x)$. The receive amplitude is proportionate to the net strain of the active fibre length of the MFC, which is defined as $L = x_{max} - x_{min}$. Equation 3.15 can be simplified for the analysis of this superpositional cancellation to,

$$A_{AFL\_rx}(k_n(\omega)) = Amp\frac{1}{L}\Big(\sin\left(k_n(\omega)(x_{tx} - x_{max}\right) - \sin\left(k_n(\omega)(x_{tx} - x_{min}\right)\Big), \quad (3.17)$$

where $k_n(\omega)$ is again the wavenumber and *Amp* represents the amplitude contributions from non-spatial terms.

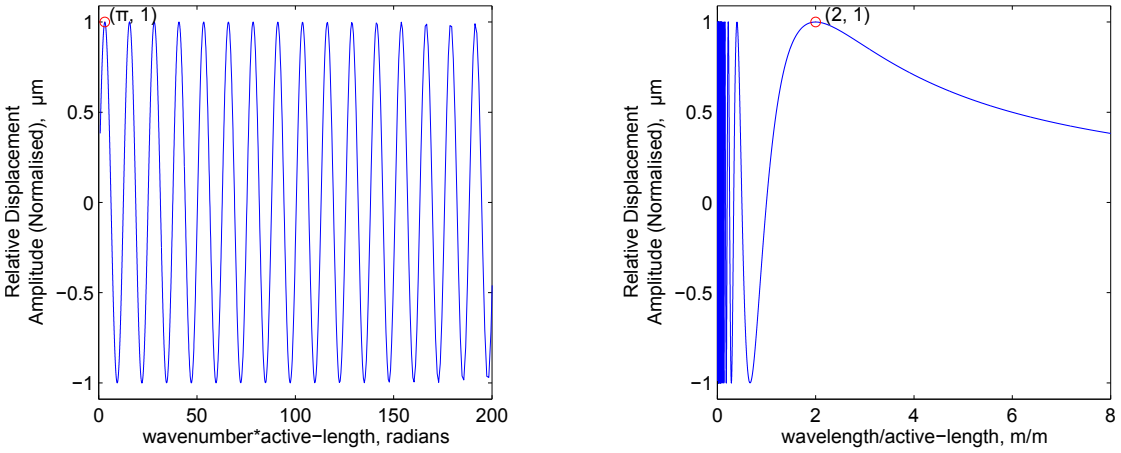

FIGURE 3.11: The hypothesised superpositional amplitude loss across the MFC fibre length on reception given in relation to wavenumber (left) and wavelength (right). The smallest high optimal wavelength/active-length ratio has been marked with a red circle.

As with transmission this can have a profound cancellation effect for some values of k, which has been depicted in Figure 3.11. This shows that amplitude tends towards zero for wavelengths above twice the length of the MFC, which is because (for fixed displacement amplitude) strain is inversely proportional to wavelength. However, the amplitude is not very high for very small wavelengths, because it is compensated by the cancellation due to integration (superpositional cancellation).

Examples of this sampling phenomenon are given in Figure 3.12. This shows the displacement across the MFC due to waves of various wavenumbers and the resultant strain in each MFC segment. Positive and negative regions of strain cancel out. Since the voltage is proportionate to net strain, this wavelength dependent cancellation reduces the observed voltage signal.

3.7.3 Combined Transmission And Reception

It is very common in applications of ultrasonic guided waves that sound waves are transmitted and received with the same type of transducer. This may involve the transmission from one transducer to another located elsewhere (pitch-catch), or similarly this could be a single device used to cast out sound waves and to receive the returned reflections (pulse-echo). If an MFC aligned in the x-axis is used to transmit and another co-aligned MFC at some distance away along the x-axis is used to receive, then the amplitude of the resultant signal will be affected both on transmission and reception.

In the last two sections the amplitude change due to superpositional cancellation on transmission and reception were depicted as coefficients that depend on wavenumber.

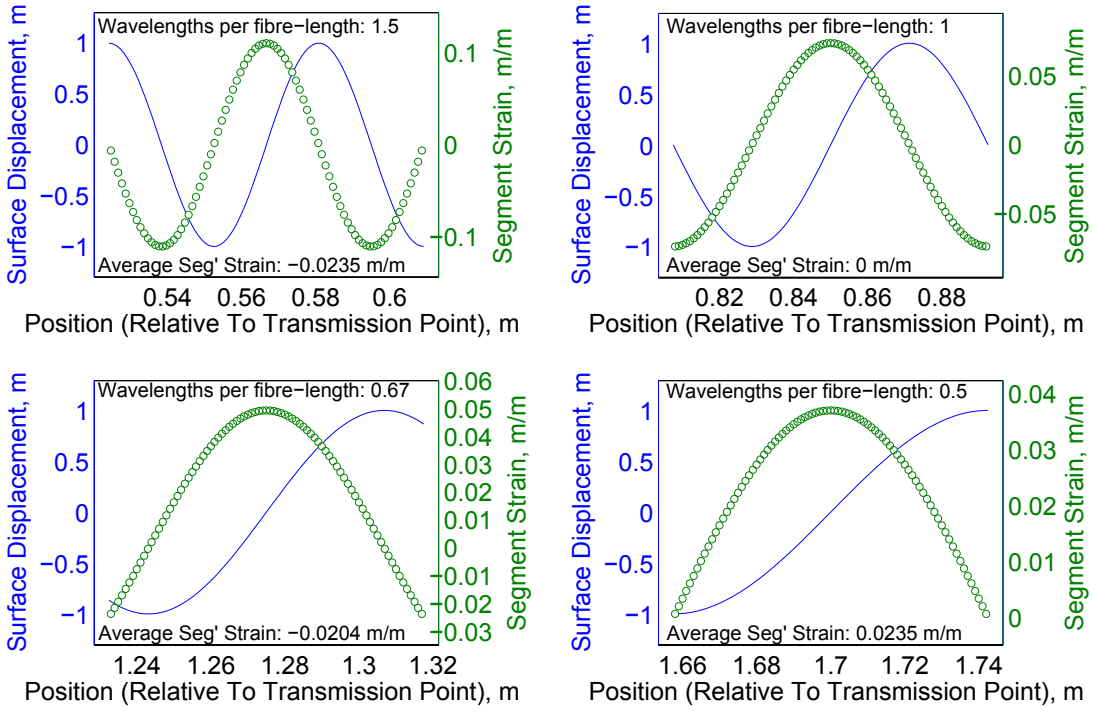

FIGURE 3.12: Here four examples of how axial displacement along the lengths of an MFC due to passing waves result in strain across each of the electroded segments within the MFC. The displacement is arbitrary and uniform for all wavelengths. The examples show the following wavelength to fibre length ratios: 1.5, 1, 0.67, and 0.5.

For transmission, the conversion from a time varying voltage to a time varying displacement signal was described. Whilst for reception, the conversion from a time varying displacement signal to a time varying voltage signal was given. The overall pitch-catch effect can be represented as the product of the two coefficients previously depicted, as is shown in Figure 3.13.

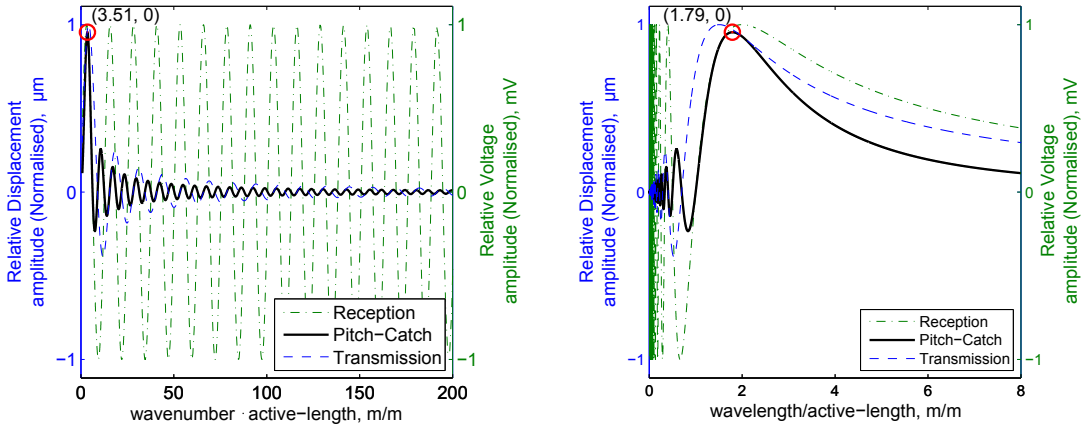

FIGURE 3.13: The result of the combined transmission and reception wavelength dependent amplitude response of an MFC transducer due to superpositional "self cancellation". The peak amplitude has been marked with a red circle.

3.8 Discrete Model

Transmitter hardware often operates on transmission signals that are created as discrete arbitrary waveforms, and reception hardware often yields discretely sampled signals. If the simulation can produced to operate on and produce such wave forms, it will be possible for the simulation to recreate MFC pitch-catch results using the same input that would be used for experimentation and produce output files that can be processed using the same methods. This makes analysis and comparison of the results from both experimentation and simulation more robust. It also yields a model that will have future use in further development, as it will be possible to easily connect it's input and output signals to other simulations or hardware systems.

An input signal will be sampled at a given sample frequency f_s and the highest frequency represented with the signal will be the Nyquist frequency (equal to $f_s/2$). Values for $A_{input}(\omega)$ and $\phi(\omega)$ can be obtained for an arbitrary input signal by using a Fourier transform to transform it into the frequency domain. The values for $k_n(\omega)$ obtained through any process of dispersion curve calculation. This can be either an analytical solution, like the commercial available software Disperse, or using Eigen mode analysis with a Finite Element Model (FEM). Attenuation rate curves can be derived numerically or experimentally [Simonetti, 2003, Luangvila, 2007]. The excitability curves for $\beta_n(\omega)$ can be derived analytically for some structures or can be obtained using Finite Element Analysis (FEA) [Wilcox et al., 2001, Sanderson and Catton, 2011].

3.8.1 Discrete Transmission Model

Equation 3.7 was previously hypothesised to model the sound field generated by an MFC, and this equation demonstrates the idea that the MFC performance will be significantly frequency dependent and wave mode specific. The aim of this model is to predict the wave mode dependent frequency response of the MFC due to the relationship between its size and the wavelengths of the sound transmitted. The interest is in the difference in amplitude over frequency for each wave mode, and so the units of measure for the amplitude are arbitrary. As such, the voltage, electrode spacing, and piezoelectric charge constant can be replaced with an arbitrary amplitude coefficient $A_{input}(\omega)$. Also, an assumption is made that for a simple model attenuation can be ignored. The transmission equation (Equation 3.7) then reduces to,

$$s_{tx}(\omega, t, x_{rx}) = \beta_n(\omega) \cdot A_{input}(\omega) \int_{x_{min}}^{x_{max}} x \cdot \sin\Big(k_n(\omega)(x_{rx} - x) - \omega t - \phi(\omega)\Big)\, dx, \tag{3.18}$$

The active region can be represented as a discrete, regular series of point sources located between x_{min} and x_{max} in the x-axis. These discrete transmission points will be labelled as p_n, each located at position p_x (which is depicted as part of the complete pitch-catch simulation in Figure 3.14 in Section 3.8.3). The combined output of these will be received as a discrete reception point q located at x_q (Equation 3.19). The spatial resolution of transmit points must be such that there are at least two points per wavelength for the cancellation effect to be represented. It is typical for wavelengths of ultrasonic guided waves in most structures to be in the tens of millimetres, and a spatial resolution of one point every millimetre is sufficient for such low frequency applications. The resolution requirement can be tested by running the simulation multiple times each time increasing the spatial resolution. The apparent error will reduce each time and this iterative process can be stopped once the change in the error is deemed less significant than typical experimental error in the corresponding experiments.

$$s_{tx}(\omega, t, x_q) = \beta_n(\omega) \cdot A_{input}(\omega) \sum_{p_n=1}^{N_p} x_p \cdot \sin\Big(k_n(\omega)(x_q - x_p) - \omega t - \phi(\omega)\Big), \tag{3.19}$$

where N_p is the last transmission point.

3.8.2 Discrete Reception Model

Equation 3.15 shows that when considering reception of guided waves that are propagating in the MFC's fibre axis, the MFC is sensitive to the net strain across its active length. In this case it is only necessary to know the difference in displacement between the extremes to know the net strain.

Alternatively, the net strain can be measured as the sum of a set of points along the active length of the receiving MFC. This approach is similar to the discrete transmission model and the same point resolution can be used.

By treating the transducer as a collection of points that cause displacement on transmission and sense displacement on reception, it will be possible to create a pitch-catch simulation that can be easily expanded for any direction in the plane of the contact surface.

Since the MFC is sensitive to strain, the voltage generated at each point is proportionate to the strain at that point. A sound source is given as p that is located at x_p along the x-axis (which, alongside the transmission, is depicted as part of the complete pitch-catch simulation in Figure 3.14 in Section 3.8.3). The strain measured at q_x is the differential

of the displacement caused at x. Equation 3.8 defined the displacement field from an arbitrary source, which is repeated here for the discrete model only without an attenuation coefficient to give the displacement at q from p,

$$s_q(\omega, t, x_q, x_p) = A_{wave\_n}(\omega) \sin\Big(k_n(\omega)(x_q - x_p) - \omega t - \phi(\omega)\Big), \tag{3.20}$$

where $A_{rx\_n}(\omega)$ is the amplitude for mode n as a function of frequency. Since it is the relative amplitude across a frequency range that is of interest, $A_{wave\_n}(\omega)$ can be on an arbitrary scale. The strain at q is the differential of Equation 3.20, which is

$$\varepsilon_q(\omega, t, x_q, x_p) = A_{wave\_n}(\omega) \cos\Big(k_n(\omega)(x_q - x_p) - \omega t - \phi(\omega)\Big). \tag{3.21}$$

As shown in Equation 3.13, the voltage is proportionate to strain by the factors $(r_e \cdot -g_{33} \cdot \eta)$. We can replace $A_{wave\_n}(\omega)$ with $A_{rx\_n}(\omega)$, providing we let $A_{rx\_n}(\omega) = r_e \cdot -g_{33} \cdot \eta \cdot A_{wave\_n}(\omega)$. This gives the voltage at q as,

$$V_q(\omega, t, x_q, x_p) = A_{rx\_n}(\omega) \cos\Big(k_n(\omega)(x_p - x_q) - \omega t - \phi(\omega)\Big). \tag{3.22}$$

The voltage as received by the MFC is the sum of the voltages received across all receive points.

$$V_{rx}(\omega, t, x_p) = A_{rx\_n}(\omega) \sum_{q_n=1}^{N_q} \cos\Big(k_n(\omega)(x_q - x_p) - \omega t - \phi(\omega)\Big), \tag{3.23}$$

where N_q is the last receiver in the range.

3.8.3 Discrete Pitch-Catch Model

It is experimentally difficult to measure in isolation the conversion on transmission or on reception, and so it is useful to combine the model for both. It is possible to produce a new combined equation that simulated the transmission from every transmit point to every receive point (a full matrix approach). However, since this is a 1D model and all sound travels along one path, the composite output from the transmission model can be simulated at an intermediate point. The output signal from the transmission model at the intermediate point can then be used as the input for the reception model. The complete process is outlined in Figure 3.14.

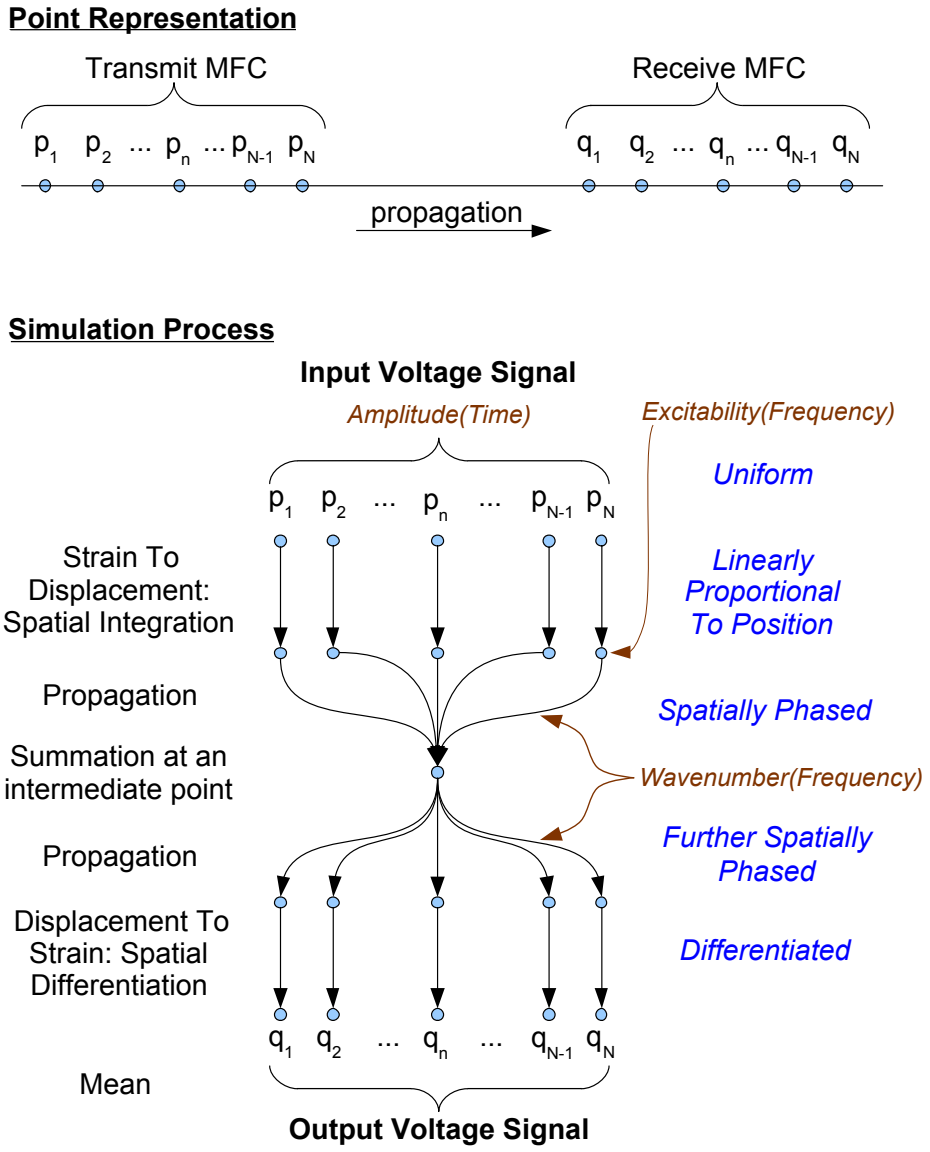

FIGURE 3.14: Pitch-catch simulation using MFC transducers to excite and receive ultrasonic guided waves aligned along the fibre axis. Required input data is given in brown text, whilst spatial effects that determine the effect of superposition are indicated in blue.

3.9 Test Scenario

3.9.1 Waveguide Selection

The model given above describes an MFC's performance as being active length, frequency, wavelength dependent, and wave mode dependent. A scenario of pitch-catch or pulse-echo using MFC transducers for propagation along one axis was required in order to measure the MFC's performance.

A waveguide that allows guided wave propagation in one axis was needed. Round rods and tubes have been tested a great deal for ultrasonic guided waves and, relative to some objects, have wave modes with less complicated vibrational shapes. However, it was decided that it would be difficult to mechanically couple the MFC to the curved surface with uniform coupling pressure, and so a waveguide with at least one flat outer surface was needed.

A narrow plate was first considered, which had a rectangular cross-section with a width that was approximately ten times its thickness. The software ABAQUS\Explicit was used to create a mesh for a bar with a rectangular cross-section and a fixed length. Eigenmode analysis was used to find the modes of resonance for that structure. Since this process gives a number of wavelength and frequency value pairs for different vibrational shapes (resonant modes), the phase velocity curves for the equivalent propagating modes can be derived.

The dispersion curves created for the rectangle case found modes similar to that of round tubes, except there were more modes possible. It was found that many modes that have vibration in the radial direction are polarised either in the direction through the narrow thickness or through the wide thickness. These modes can be termed horizontal (through the wide thickness) and vertical (through the narrow thickness). For each horizontal mode there was an equivalent vertical mode. The horizontal and vertical mode pairs had similar but differing velocity curves. The evaluation of several rectangular shapes found that as the rectangle approaches a square, these mode pairs tend towards having the same velocities. As having fewer modes makes analysis more feasible, this meant that testing with square bars was desirable.

A second experiment was devised in order to demonstrate the generality of the simulation across multiple applications. Another kind of waveguide that has an accessible flat surface is a plate. A plate, unlike a bar, can have a width much greater than its thickness and one so vast that an experiment can be conducted without being influenced by the plate edges.

A bar and a plate were selected because they represented examples of typical engineering components that were suitable for allowing measurement of MFC performance:

Bar: 15.9 mm by 15.9 mm by 5 m - Aluminium.

Plate: 10 mm thick disc with a diameter of 3.44m - Steel.

3.9.2 Bar Waveguide

A bar made from Aluminium Alloy 6082-T6 (Poisson's Ratio: 0.330, Density 2.70 g/cm3, and Modulus of Elasticity 70 GPa) was chosen. The dispersion curves for this bar is

presented in Figure 3.15. Five meters was the longest length available due to limitations in the extrusion process.

There are three fundamental wave modes in these curves. The naming scheme for these square bar modes is created in a similar way to the common nomenclature for plate wave modes [Krautkrämer, J. and Krautkrämer, H., 1983]. The slowest of these has a vibrational shape similar to A0 in plates and so will be termed ‘‘Asymmetric 0’’. One of the fundamental modes is entirely non-dispersive and vibrates entirely circumferentially about its major axis; In this way it is very similar to the first torsional mode in tubes and pipes, and so will be termed ‘‘Torsional 0’’. The final fundamental mode has mainly axial displacement and has a vibrational shape similar to S0 in plates, and thus will be termed ‘‘Symmetric 0’’. There are a great number of higher order modes with complicated vibrational characteristics. As it won’t be necessary to distinguish these modes as the measurements were designed to avoid them, they have not been given descriptive names in the dispersion curve figures.

Symmetric 0, being mainly an axial in-plane mode, is expected to be excitable with an MFC transducer. Also, having the highest velocity curve of the fundamental modes, it will be the easiest mode to isolate for amplitude measurements in a pitch-catch/pulse-echo arrangement.

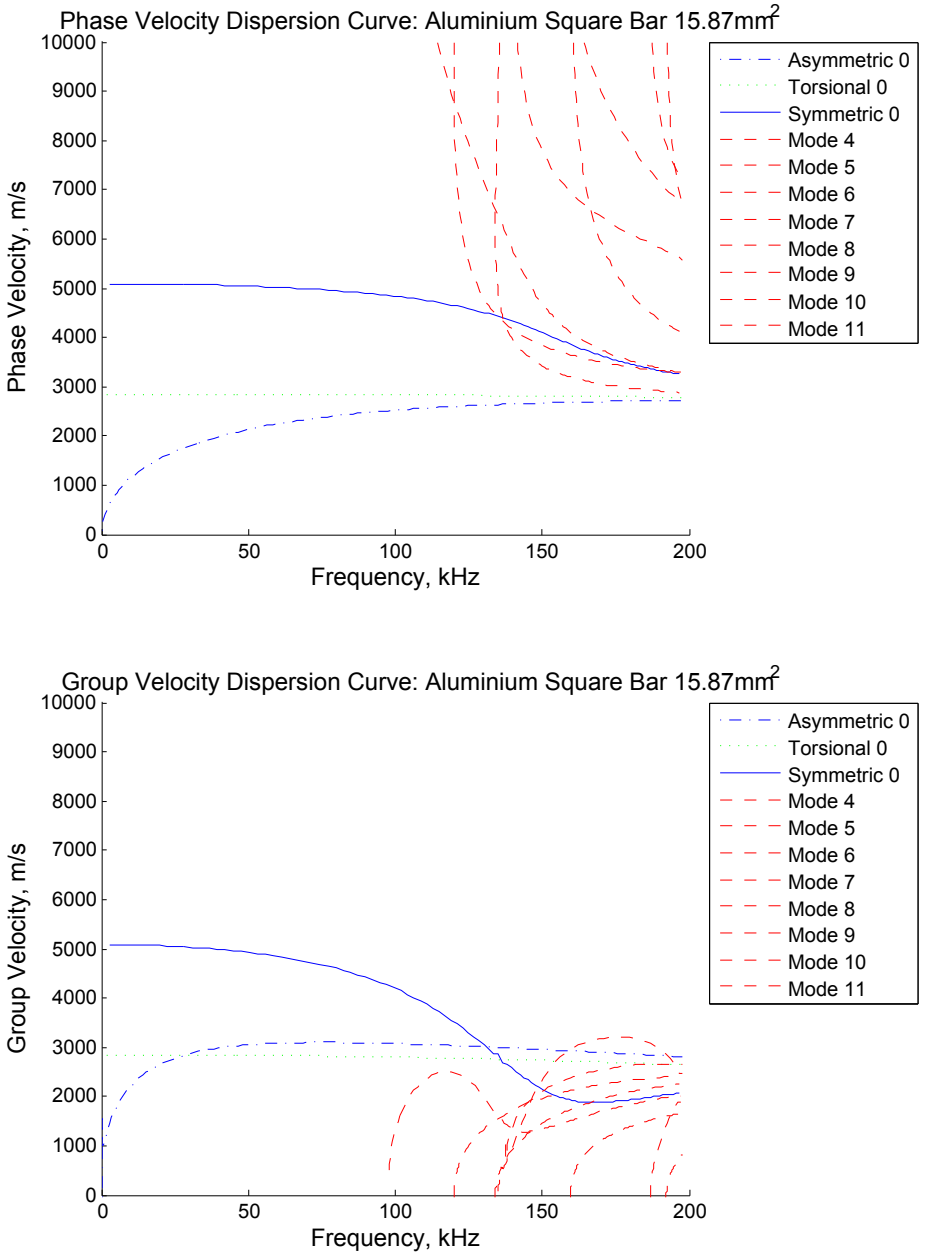

FIGURE 3.15: Dispersion curves for an aluminium alloy square bar with a side length of 15.9mm.

The excitability of a given mode in a given bar can be calculated for a point source acting in-plane along the major axis of the bar [Sanderson and Catton, 2011]. This is likely to vary depending on where along the width of the face of the bar the point source is placed. However, since the Symmetric 0 mode has similar characteristics throughout the width of the bar, it is assumed the excitability is not likely to vary much by position for this mode.

An FEA model was created and solved, again using ABAQUS\Explicit, to measure the level of Symmetric 0 generated by a point source over a frequency range in order to provide an excitability coefficient for the model. Tests were repeated at different frequencies across the desired frequency range and each time a point was excited with a 10 cycle pulse with the same acceleration amplitude. For each frequency the displacement caused by the output sound field of this point source was measured at 30 points along the major axis of the modelled bar. This provided time and spatial data that could be viewed in the frequency domain such that each mode could be distinguished and measured individually. The structure modelled was an aluminium bar with a 15.9 mm by 15.9 mm square cross-section.

It was observed that the dispersion curves for the four bar sizes had very similar characteristics when the wave mode velocities were plotted on a frequency thickness product scale, which indicates that the wave mode characteristic at low ultrasonic frequencies approximately scales with the thickness of the square bars. The excitability curve produced for the 15.9mm^2 bar is given in Figure 3.16.

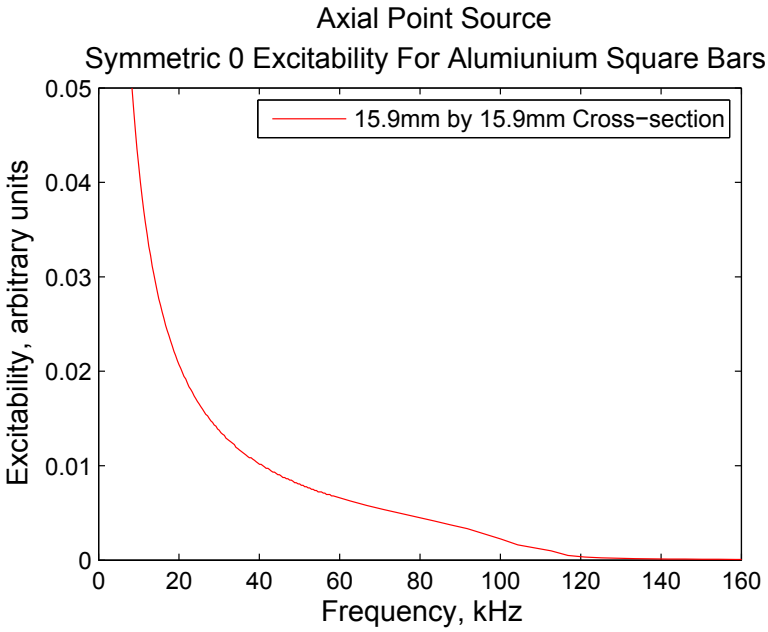

FIGURE 3.16: Symmetric 0 mode excitability in a 15.9mm by 15.9mm aluminium square bar from an in-plane, axially aligned point source placed in the centre on an edge face, as produced by an FEA model.

3.9.3 Plate Waveguide

The plate was made from mild steel (Poisson's Ratio: 0.30, Density 7.9 g/cm3, and Modulus of Elasticity 200 GPa). The width of the disc was determined by the maximum size that could be fabricated by the available suppliers. A homogeneous, defect free sample was required, so a larger plate could not be fabricated by joining smaller ones. The conventional plate wave mode naming scheme is used for this sample (as given by Lamb [1917]). Testing was conducted at frequencies below the cut-off limit for any higher order modes. Only the fundamental asymmetric and symmetric Lamb modes (respectively named S0 and A0) and the fundamental shear horizontal mode (named SH0) exist over the frequency range tested. The dispersion curves for this plate are given up to 200 kHz in Figure 3.17 (including the presence of the higher modes A1 and AH0).

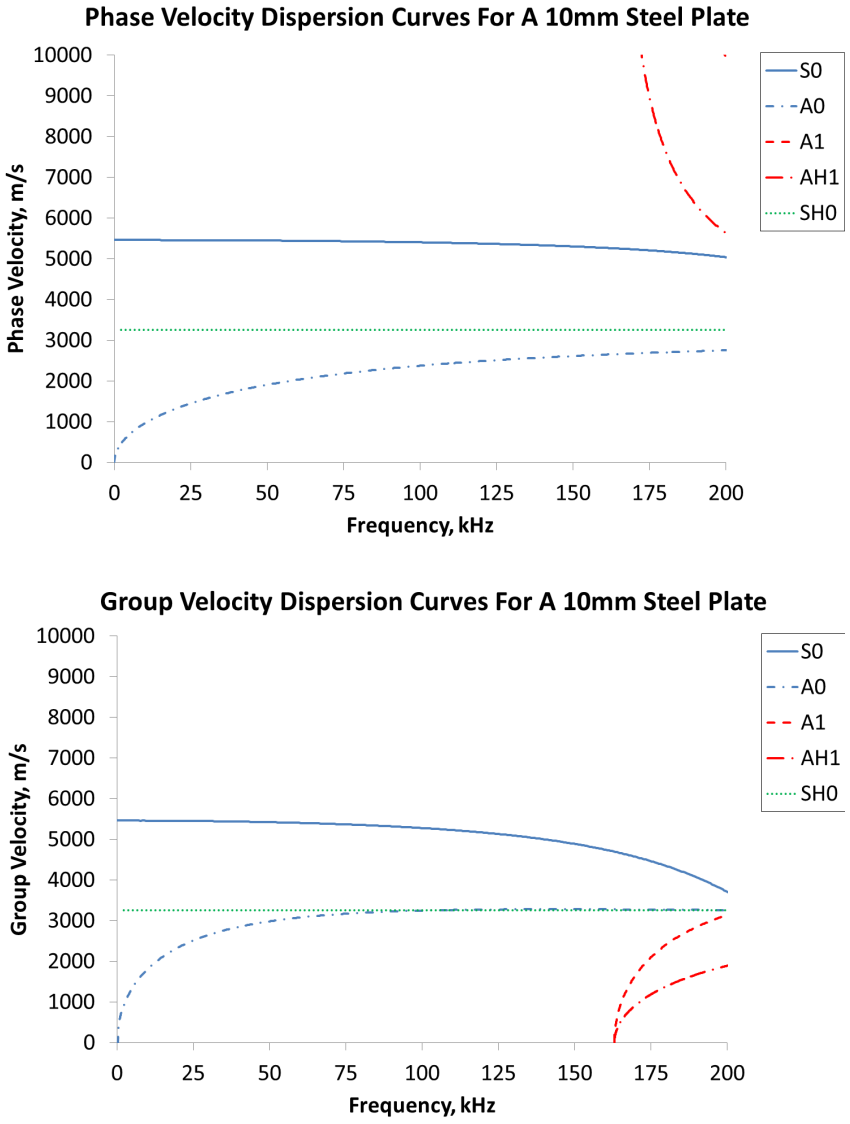

FIGURE 3.17: Dispersion curves for a 10mm thick steel plate, as generated by the software Disperse [Pavlakovic et al., 1997].

3.9.4 Transmit Signal

At high frequencies the velocities of the fundamental wave modes merge with the higher order modes. At these frequencies it would be difficult to distinguish pulses of different wave modes. At low frequencies the pulse length would become so long that wave modes would no longer be distinct. The range of 30 to 110 kHz has been chosen as a suitable middle range for testing of the bars, whilst the range of 30 to 150 kHz was chosen for the plate.

In order to test these ranges, a broadband transmit signal was chosen. In each case the transmit signal is of the form of a linear chirp and is constructed from the following equation:

$$A_{input}(t) = sin\left(2\pi f_1 t + \frac{\pi(f_2 - f_1)}{\tau} t^2\right), \qquad 0 \leq t \leq \tau \tag{3.24}$$

where t is the time, τ is the signal length, f_1 is the lower frequency limit and f_2 is the upper frequency limit. This was used to construct a signal with significantly high and level amplitude between the desired range. The signal for bar testing was constructed using $f_1 = 20$ and $f_2 = 140$, and is depicted in Figure 3.18. The signal for the plate was of a similar form, and was constructed using $f_1 = 20$ and $f_2 = 160$.

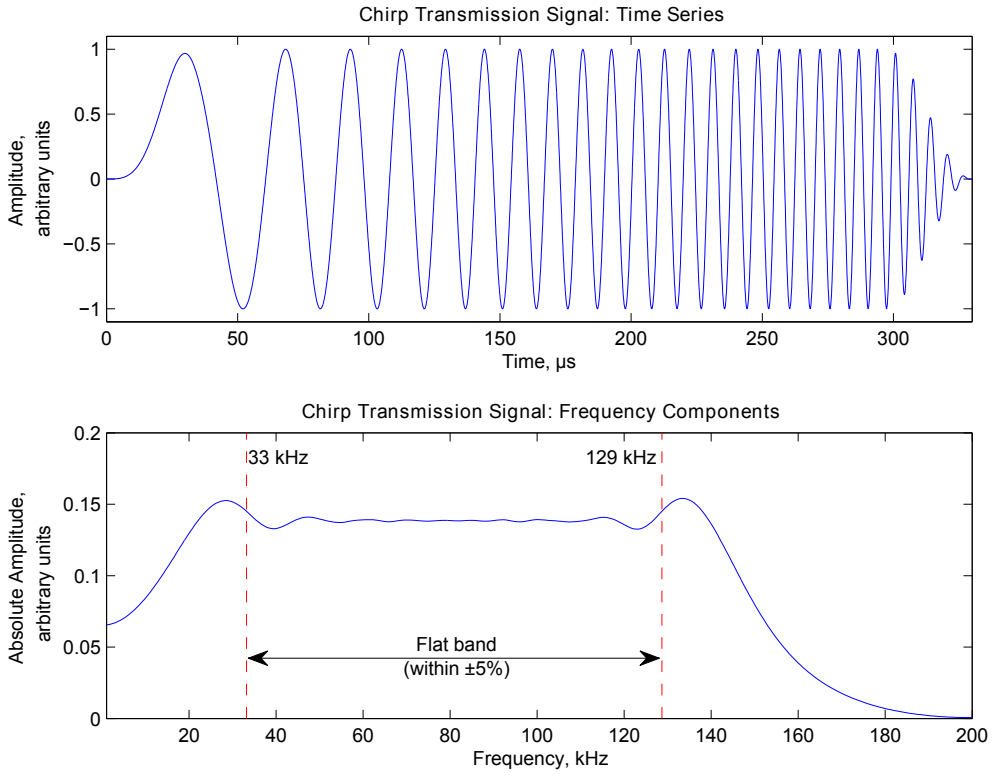

FIGURE 3.18: A linear chirp signal constructed for use in frequency response tests of MFC transducers with aluminium bars.

3.9.5 Experimental Setup: Bar Testing

The aim of the test scenario is to measure the amplitude of the Symmetric 0 mode after it has been transmitted and received by an MFC transducer. To do this, a pulse should be received from one direction only, without interference from other modes. A location was chosen that allows a Symmetric 0 reflection from one end of the bar to arrive well before the reflection from the other end. It was placed sufficiently far away from the near end to allow the Symmetric 0 mode to separate from the slower modes. A process of trial and error found that an MFC position of 1.8 meters from one end to sufficiently meet these criteria (Figure 3.19).

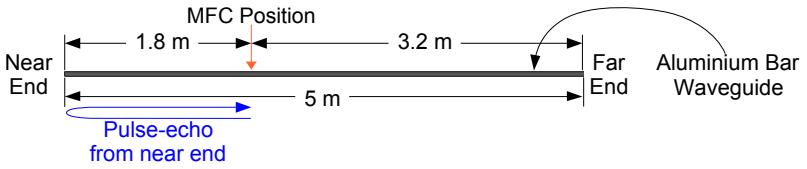

FIGURE 3.19: The experimental setup for measuring the amplitude for a pulse-echo test using an MFC transducer on an aluminium bar.

3.9.6 Experimental Setup: Plate Testing

The approach for the steel plate also involves the measurement of the fastest wave mode from one direction without interference from other signals. The limited size of the plate made it difficult to arrange a pulse echo test where only a single mode could be reflected back to the MFC. In this case it was necessary to conduct pitch catch measurements between two MFCs. A line through the centre of the plate was chosen. An MFC was placed at the position half the radius (1.72m) along this line from the centre. The other was placed at the same distance from the centre, but along the reverse direction along this line. This set up is shown in Figure 3.20.

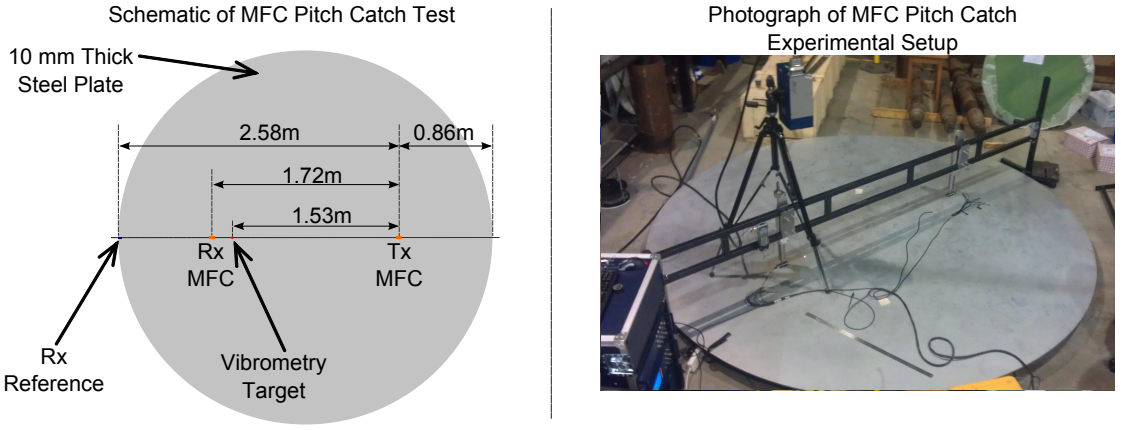

FIGURE 3.20: The experimental setup for measuring the amplitude for a pitch catch test using an MFC transducer on a steel plate.

3.10 Experimental Validation

Both the bar and the plate setup were used to measure the peak-to-peak amplitude of the fastest wave mode as transmitted and received from an MFC transducer. In both cases MFCs were placed such that the piezoelectric fibres were aligned with the axis of propagation. Since the analysis has asserted the length of the MFC is a major factor in determining the frequency response the aim of the measurements is to compare the frequency response with MFC length. The measurements were taken with MFC transducers that initially had a length of 85mm, and were incrementally shortened by steps of 10mm down to a length of 15mm. The shortening was done by guillotine cutting the transducers using a razor blade, and the transmit/receive frequency response was measured for each size.

In the plate case a method of ‘‘dry’’ force coupling the MFC transducers was developed. A steel shaft normal to the contact surface with an in-line force measuring cell was used to press the active area of each MFC transducers to the plate's surface. A 6mm thick layer of closed cell silicone foam was placed between the force loading shaft and the MFC. Since this foam was a low stiffness, two phase material (significantly composed of air) this would acoustically isolate the MFC from the loading mechanism. The foam layer had a contact area of 87mm by 9mm. A pressure of 300 N was found to be sufficiently high to cause an effective signal to noise ratio, but without collapsing the foam material (where it could no longer be regarded as a good insulator).

Since there was a possibility the foam and loading mechanism would affect the performance of the MFC, an alternative approach was used for the bar test. In this case, the MFC was attached with cyanoacrylate adhesive (‘‘Super Glue’’). To reduce the thickness of the adhesive layer, the loading mechanism was applied during the curing period of the adhesive and then removed.

3.11 Results and Analysis

The two experiments yielded a time varying signal for each MFC length tested. The signals for the aluminium bar test are shown in Figure 3.21 and the signals for the steel plate test are shown in Figure 3.22. As these are broadband signals containing responses from various different propagation paths and of various different modes (with amplitude variations across the frequency range for each mode) they appear complex and difficult to interpret. However, in both cases the position of the transducers is such that (at each frequency) the direct S0 pulse arrives before any other signal, and so can be distinctly measured.

The software package Matlab (by Mathworks) was used to create spectrograms of each of the signals captured. These spectrograms are created using a sliding short time Fourier

transform to analyse the spectral content at each point in time. This allows the amplitude contributions across the frequency range to be visualised separately and meaningfully interpreted.

The dispersion curves for the aluminium bar (as shown in Figure 3.15) were used to predict the time of arrival for the direct propagation of the Symmetric 0, Asymmetric 0 and first flexural mode. These predicted arrival times have been added to the aluminium bar test spectrograms to assist interpretation. Since the aim of the experiment is to measure the Symmetric 0 amplitude across frequency, a time band ($\pm$ 100μs) was chosen to fit around the predicted peak arrival time of this mode. The steel plate dispersion curves (Figure 3.17) were used to predict the arrival of the peaks of the fundamental Lamb modes (S0 and A0), and the spectrograms feature these curves and the measurement time band around the S0 curve. Transmitted ultrasonic signals from the MFC were measured using a Polytec PSV400 1D scanning laser vibrometer. As the vibrometry measurements were made for the out-of-plane component of the wave motion and the analysis was for in-plane motion, this data was not used for anything other than to confirm the transmitting MFC was transmitting.

As the plate test was conducted in a pitch-catch arrangement there is a period of time from the beginning of the test where no sound could have reached the receiving MFC (between 0 and approximately 310μs). However, for the duration of transmission there is some electrical cross-talk between the transmit and receive channels, which gives the appearance of noise, but this does not exceed 330μs. There is a slight overlap between the end of the cross-talk and the begging of the direct received signal, but this overlap is not of the same frequency range and so the spectral analysis is not adversely affected.

The spectrograms for the 15mm, 25mm, 35mm, 45mm, 55mm, 65mm, 75mm and 85mm length MFCs when used on the aluminium bar and steel plates are respectively given in Figures 3.23, 3.24, 3.25, and 3.26, 3.27, 3.28. In each spectrogram the horizontal-axis represents frequency (20 to 140 kHz) and the vertical-axis represents arrival time (0.4 to 2.4 μs). Time 0 occurs at the start of the transmission of the output signal (as was shown in Figure 3.18). The spectrogram colour scale represents amplitude from zero to the maximum amplitude with a respective colour range from blue through green, to yellow and then red. Dark red bands indicate the peak arrival of a pulse with high amplitude. These bands tend to be elongated in the horizontal-axis because they are formed from a broadband signal that spans this frequency range. These bands do not have a uniform arrival time because, firstly, the frequency content of the transmit signal is time dependent and, secondly, because the wave velocity is frequency dependent. The predicted time of arrival for the direct reception of the fastest mode is indicated (see legend) and it is observable that this band arrives at the predicted time for all MFC lengths. However, there are maxima and significantly low minima occurring in this band, and where these occur varies with MFC length. As the MFC size is made shorter, it appears that the frequencies at which these maxima and minima occur become lower.

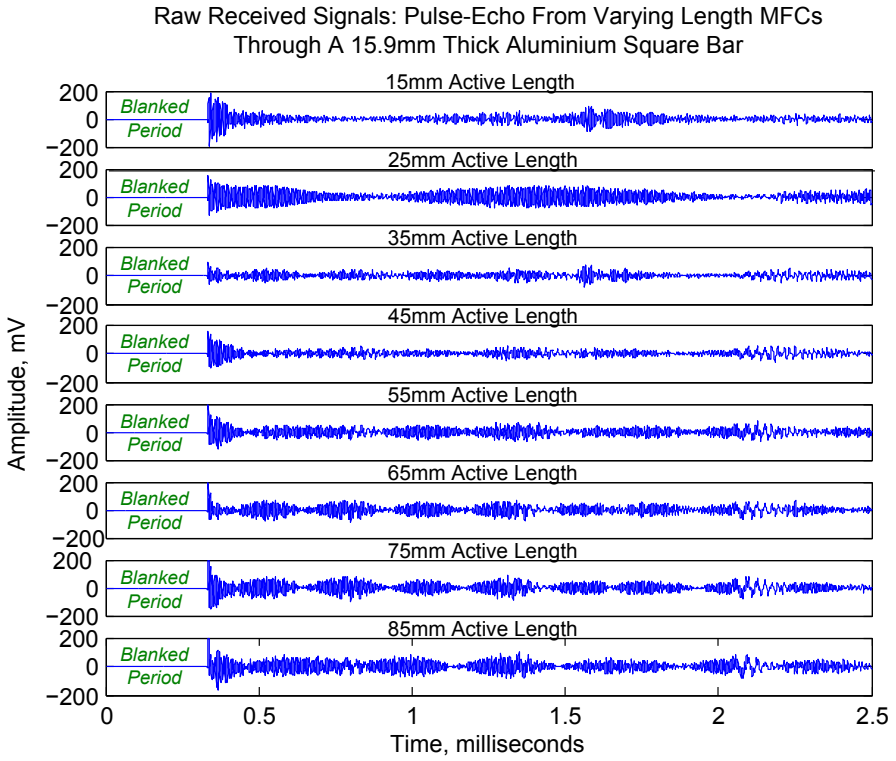

FIGURE 3.21: Signals transmitted received in a pulse-echo test using an MFC adhered to a 15.9mm thick aluminium square bar, where the active length of the MFC was incrementally reduced from 85mm to 15mm by steps of 10mm.

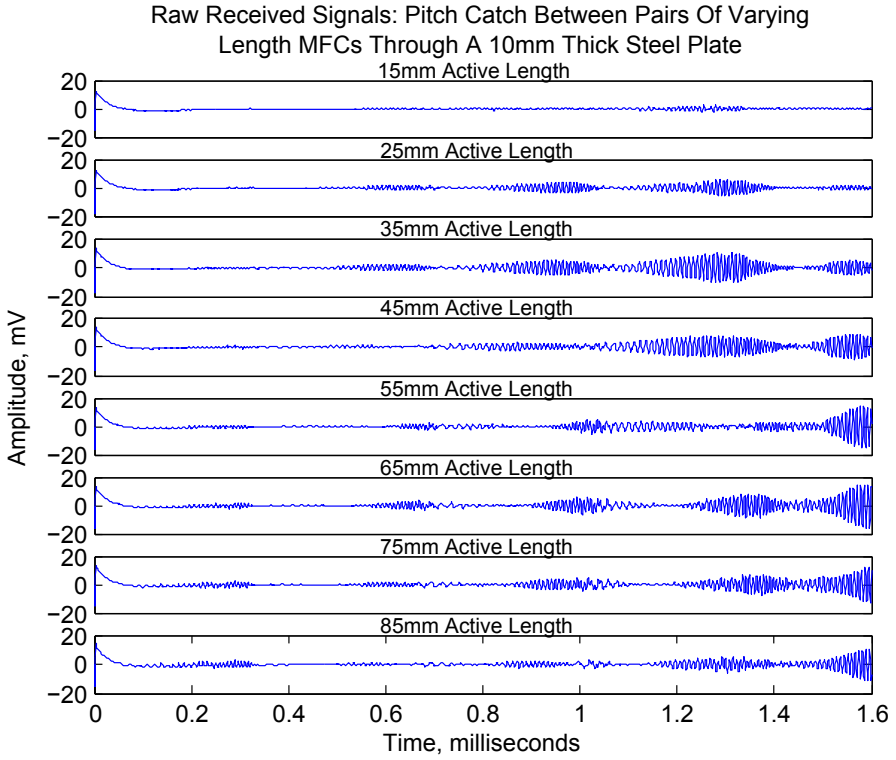

FIGURE 3.22: Signals transmitted from one MFC to another through a 10mm thick steel plate, where the active length of both MFC transducers was incrementally reduced from 85mm to 15mm by steps of 10mm.

The shortest MFC length gives the greatest number of maxima and minima for both experiments for the frequency range given.

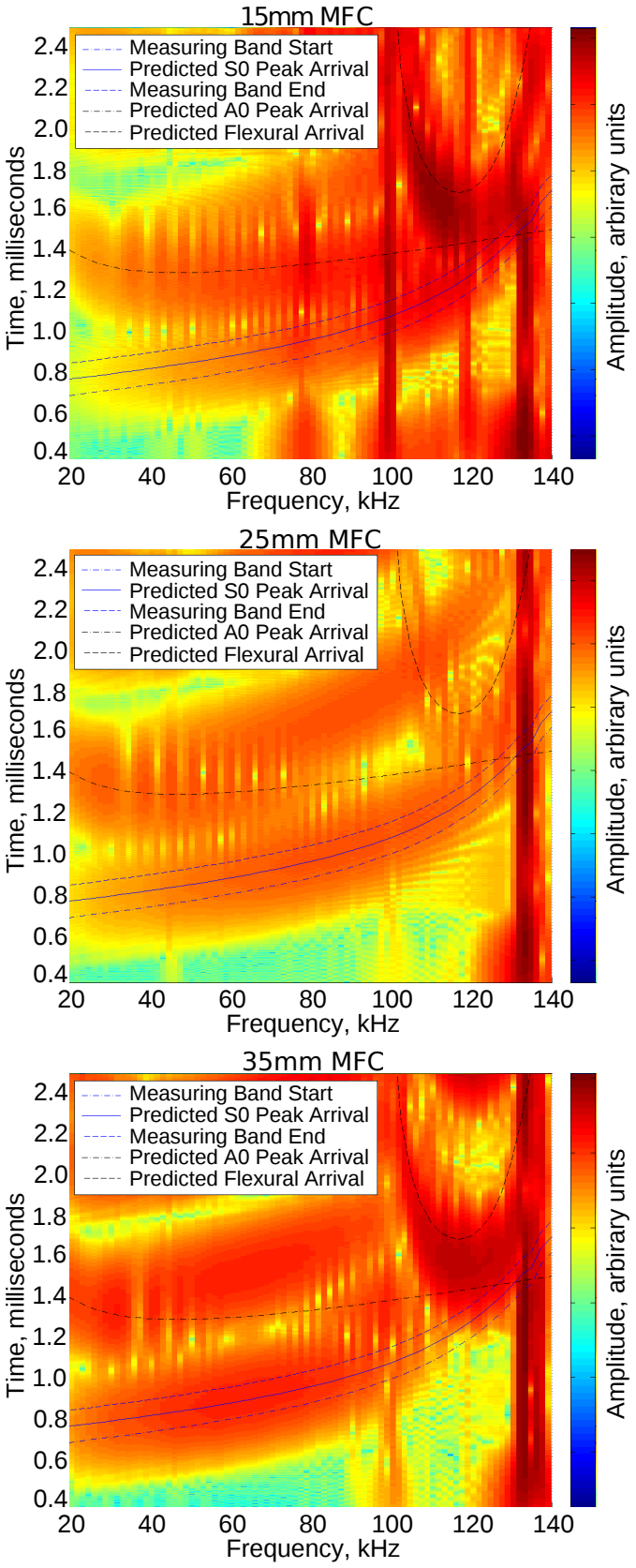

FIGURE 3.23: Spectrograms of signals captured from a pulse-echo test using MFCs of lengths 15mm, 25mm, and 35mm on a 15.9mm thick an aluminium square bar. The signals used are shown in Figure 3.21.

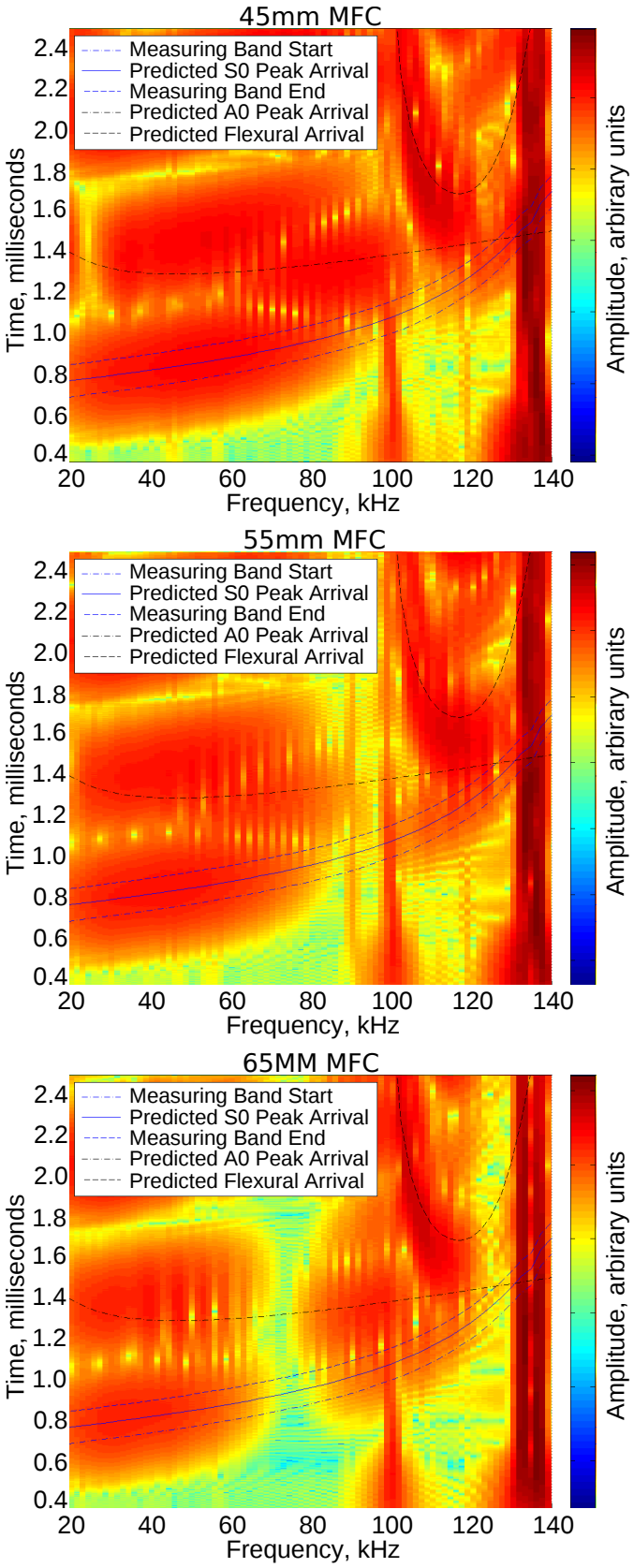

FIGURE 3.24: Spectrograms of signals captured from a pulse-echo test using MFCs of lengths 45mm, 55mm, and 65mm on a 15.9mm thick an aluminium square bar. The signals used are shown in Figure 3.21.

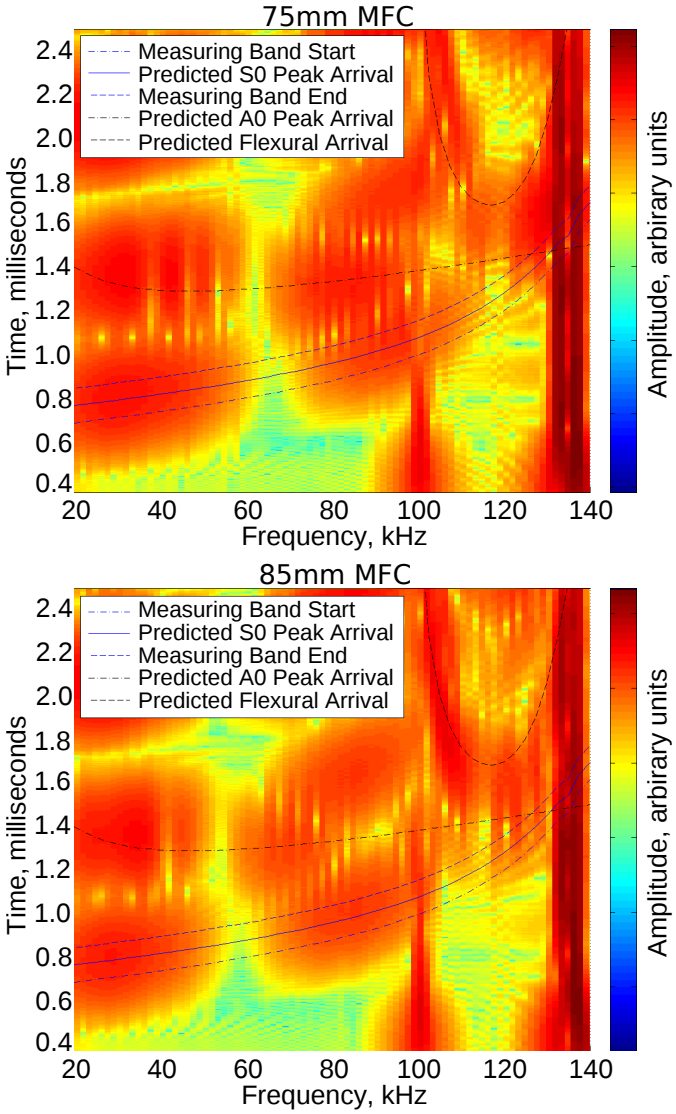

FIGURE 3.25: Spectrograms of signals captured from a pulse-echo test using MFCs of lengths 75mm and 85mm on a 15.9mm thick an aluminium square bar. The signals used are shown in Figure 3.21.

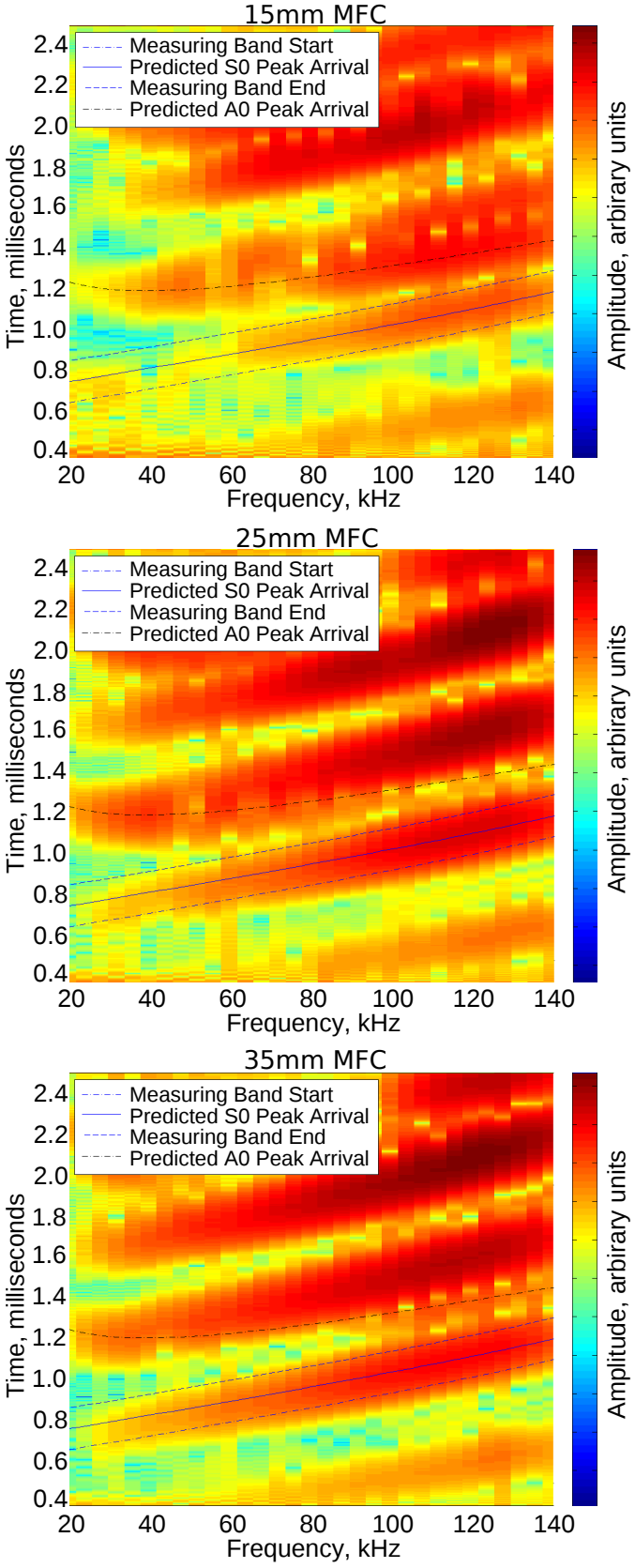

FIGURE 3.26: Spectrograms of signals captured from pairs of different length MFCs in a pitch-catch test on a steel plate. The signals used are shown in Figure 3.22.

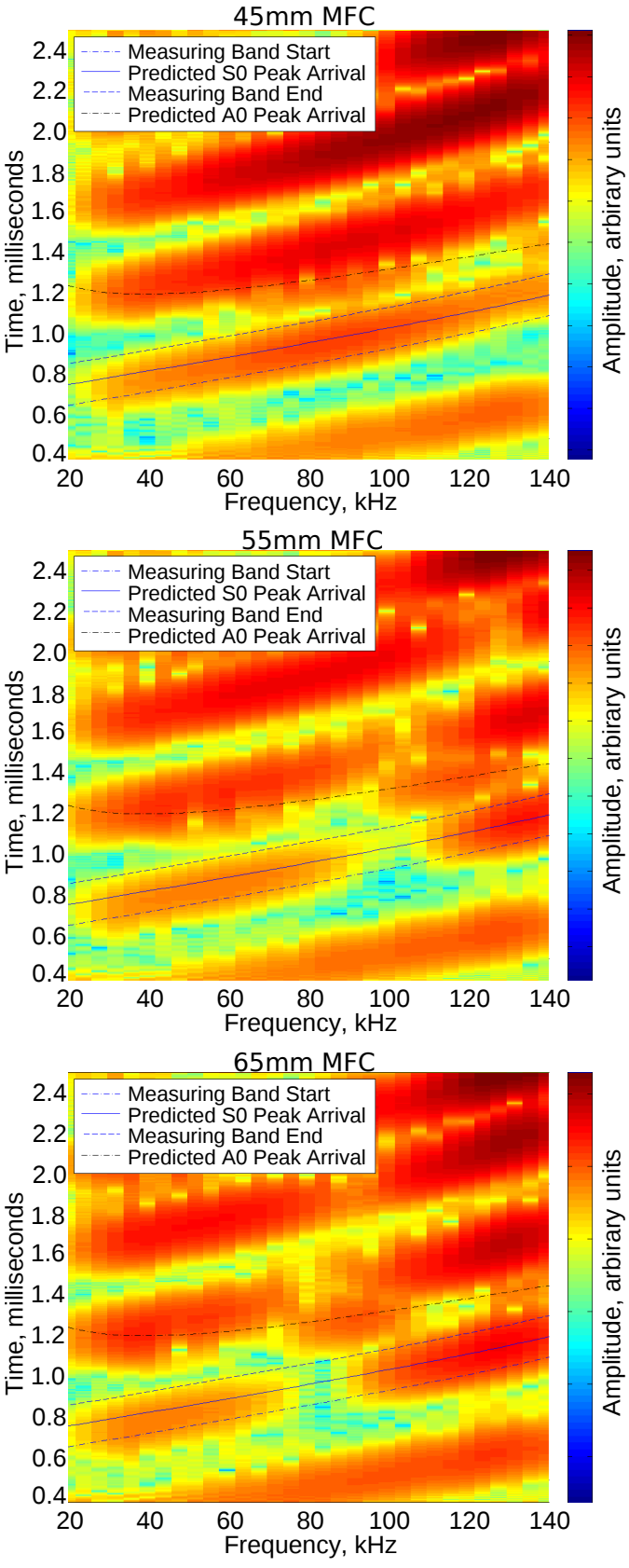
45mm MFC
Measuring Band Start
Predicted S0 Peak Arrival
Measuring Band End
Predicted A0 Peak Arrival
Time, milliseconds
Frequency, kHz
Amplitude, arbirary units
55mm MFC
Measuring Band Start
Predicted S0 Peak Arrival
Measuring Band End
Predicted A0 Peak Arrival
Time, milliseconds
Frequency, kHz
Amplitude, arbirary units
65mm MFC
Measuring Band Start
Predicted S0 Peak Arrival
Measuring Band End
Predicted A0 Peak Arrival
Time, milliseconds
Frequency, kHz
Amplitude, arbirary units

FIGURE 3.27

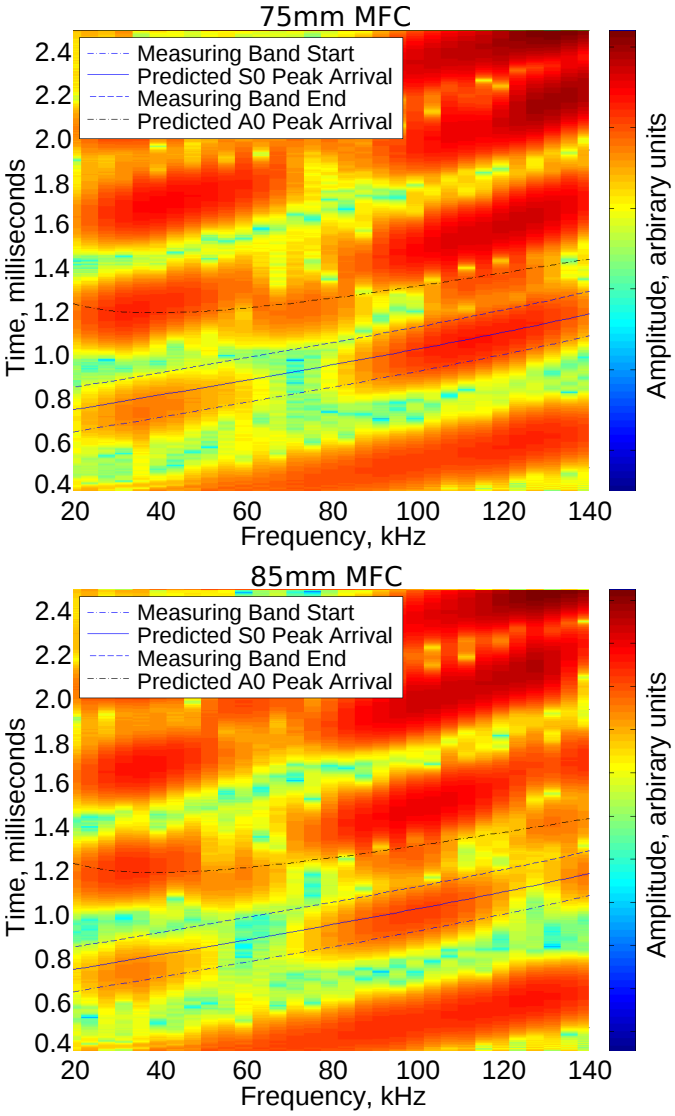
75mm MFC
Measuring Band Start
Predicted S0 Peak Arrival
Measuring Band End
Predicted A0 Peak Arrival
Time, milliseconds
Frequency, kHz
Amplitude, arbirary units
85mm MFC
Measuring Band Start
Predicted S0 Peak Arrival
Measuring Band End
Predicted A0 Peak Arrival
Time, milliseconds
Frequency, kHz
Amplitude, arbirary units

FIGURE 3.28

In order to make the amplitude measurements a bank of band-pass filters were used to split the signals into a set of narrow band signals.

In the case of the aluminium bars this was done to create signals with the centre frequency, f_c, of 20 kHz to 110 kHz at steps 2.5 kHz. This was limited to 110 kHz because the arrival time of Symmetric 0 above this limit overlaps with that of the first flexural and Asymmetric 0 thus obfuscating the signal to be measured. It the plate it to create signals with the centre frequencies of 20 kHz to 150 kHz at steps 2.5 kHz.

For each band a third order Butterworth filter with limits of $f_c \pm 9\%$ was used, as this was observed to give narrow band signals with pulse of around 10 cycles long (the kind commonly used in narrowband LRUT).

An example of how such a broadband signal can be reduced with a bandpass filter to produce a narrowband signal from which amplitudes can be measured is given in Figure 3.29. The amplitude against frequency observable in spectrograms has been measured from the bank of time domain signals created with the set of filters to create an amplitude against frequency curve for each MFC length for both the aluminium bar and the steel plate tests as shown in Figure 3.30 and Figure 3.31 respectively.

The first observation made was that the simulated results rapidly diminished with frequency whereas the experimental results did not. Previously the dynamic strain was assumed to be proportionate to stress and could be used interchangeably for the piezoelectric coupled equation (Equation 3.3) for achieving frequency dependent results with the same overall shape. However, this is not the case since strain is dependent on displacement and stress is dependent on acceleration; the sinusoidal acceleration is propionate to sinusoidal displacement by a factor of ω^2 factor. The model is simply rectified by taking the 2nd order differential of the displacement before the net amount is taken for the length of the MFC.

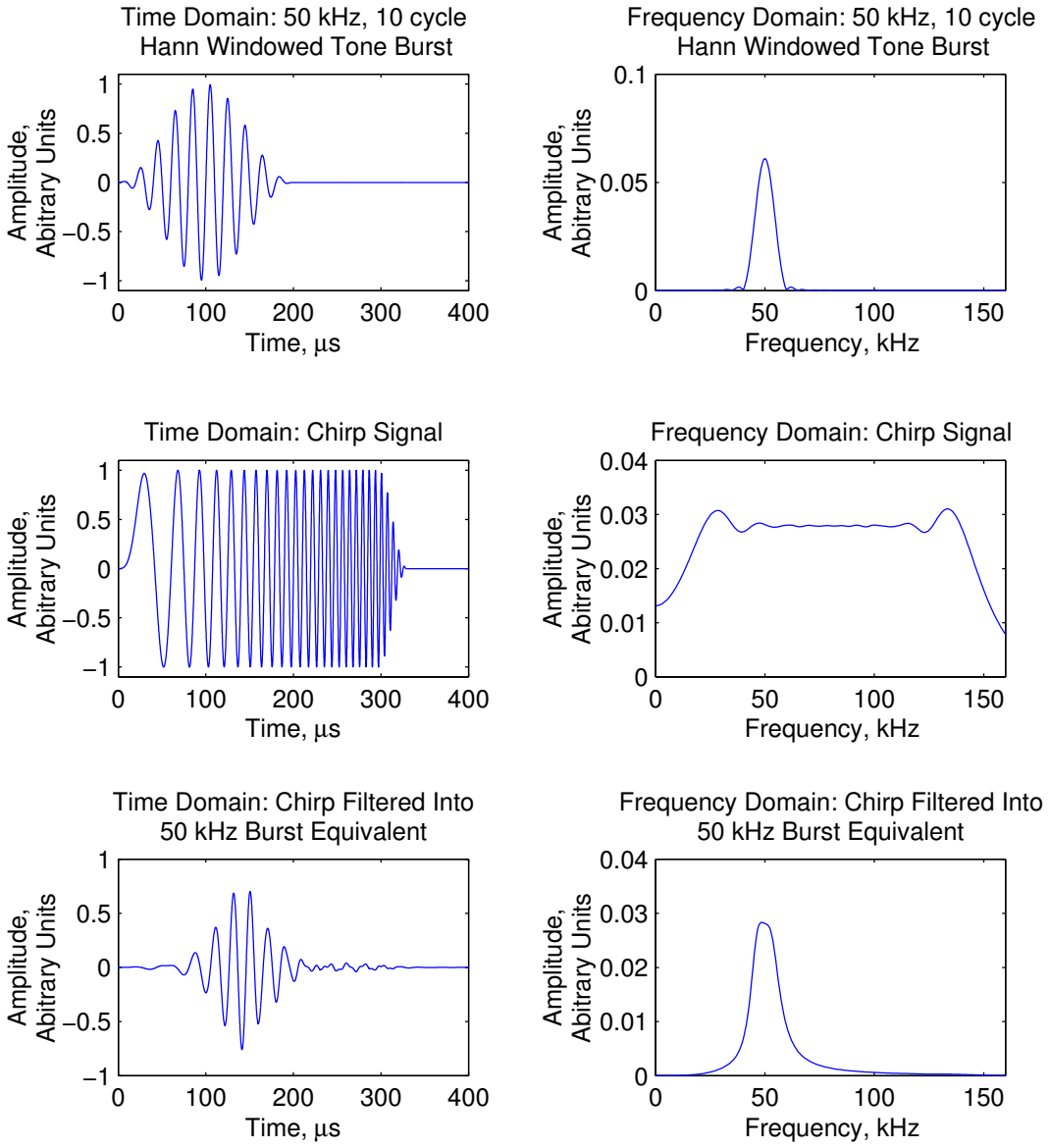

FIGURE 3.29: A comparison of a typical narrow band tone burst used for LRUT with a narrow band signal filtered from a broad band chirp signal.

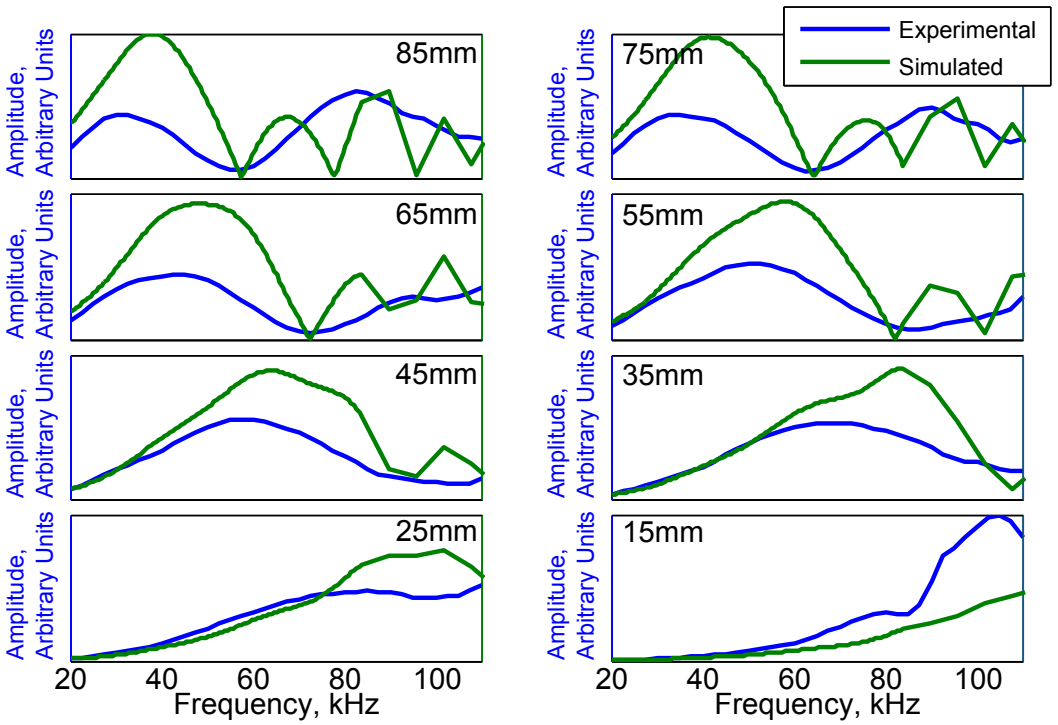

FIGURE 3.30: Measured frequency response by an MFC for the Symmetric 0 mode under a pulse-echo test in a 15.9mm thick aluminium square bar compared to the initial simulation method.

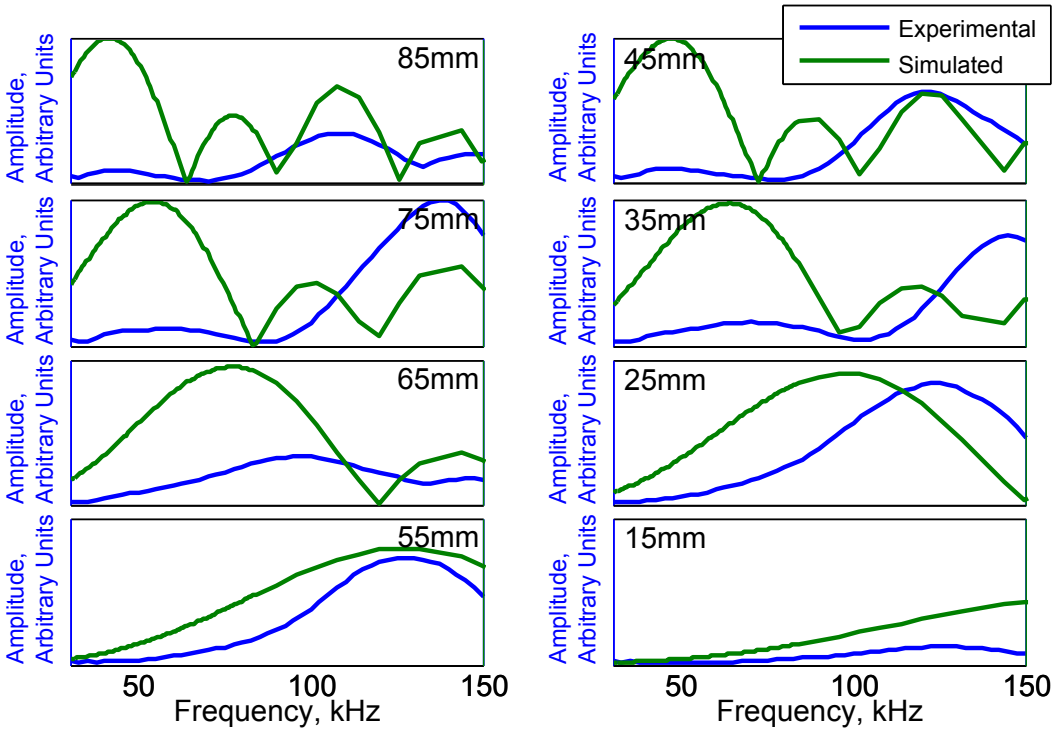

FIGURE 3.31: Measured frequency response by an MFC for the Symmetric 0 mode under a pulse-echo test in a 10mm thick steel plate compared to the initial simulation method.

Analysis of the curves presented in section 3.7.3 found that the matching minima and maxima were those caused by the reception side of the simulation, but there were further predicted minima in the simulation that did not occur. Since the maxima and minima characteristcs in the pulse-echo experimental results were very similar to those predicted by reception, it could be seen that the effect of transmission must either be similar to that of reception or must be uniform for all frequencies (which is unlikely as superpositional effects of some kind must occur due to the MFC transducer's size).

On reception the sampling of the area under the MFC is represented with a definite integral of the acceleration over the active length of the MFC. This is equivalent to taking the difference of the extremes, which likens the MFC to two points of acceleration reception. The equivalent on transmission is to represent transmission as the displacement excitation from two point sources acting in anti-phase separated by the length of the MFC. The transmission model was improved to incorporate reciprocal behaviour to the reception model and the prediction was greatly improved as can be seen in Figure 3.32 and Figure 3.33. The two point anti-phase excitation and the two point reception for the aluminium case have been presented separately in Figure 3.34. The minima occur at the same frequencies for both transmission and reception.

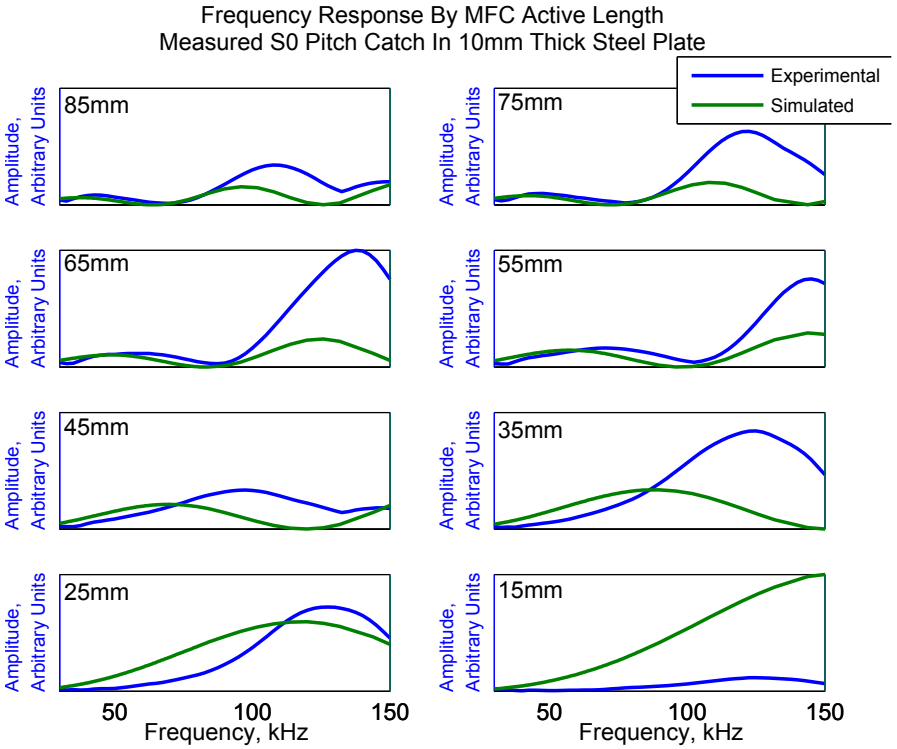

FIGURE 3.32: Measured frequency response by an MFC for the Symmetric 0 mode under a pulse-echo test in a 15.9mm thick aluminium square bar compared to the adapted simulation method.

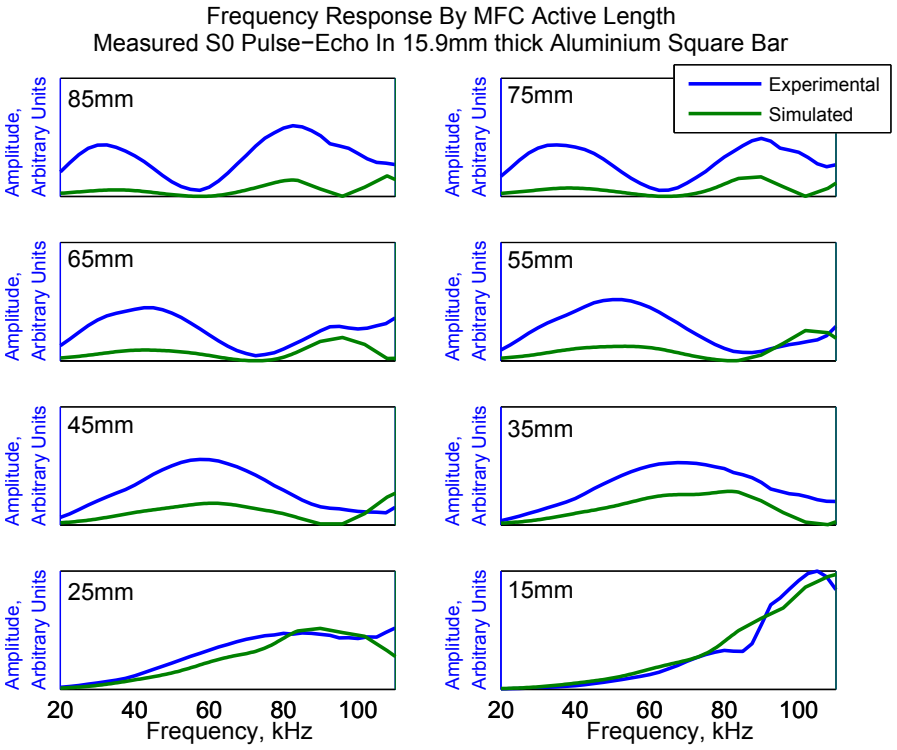

FIGURE 3.33: Measured frequency response by an MFC for the Symmetric 0 mode under a pulse-echo test in a 10mm thick steel plate compared to the adapted simulation method.

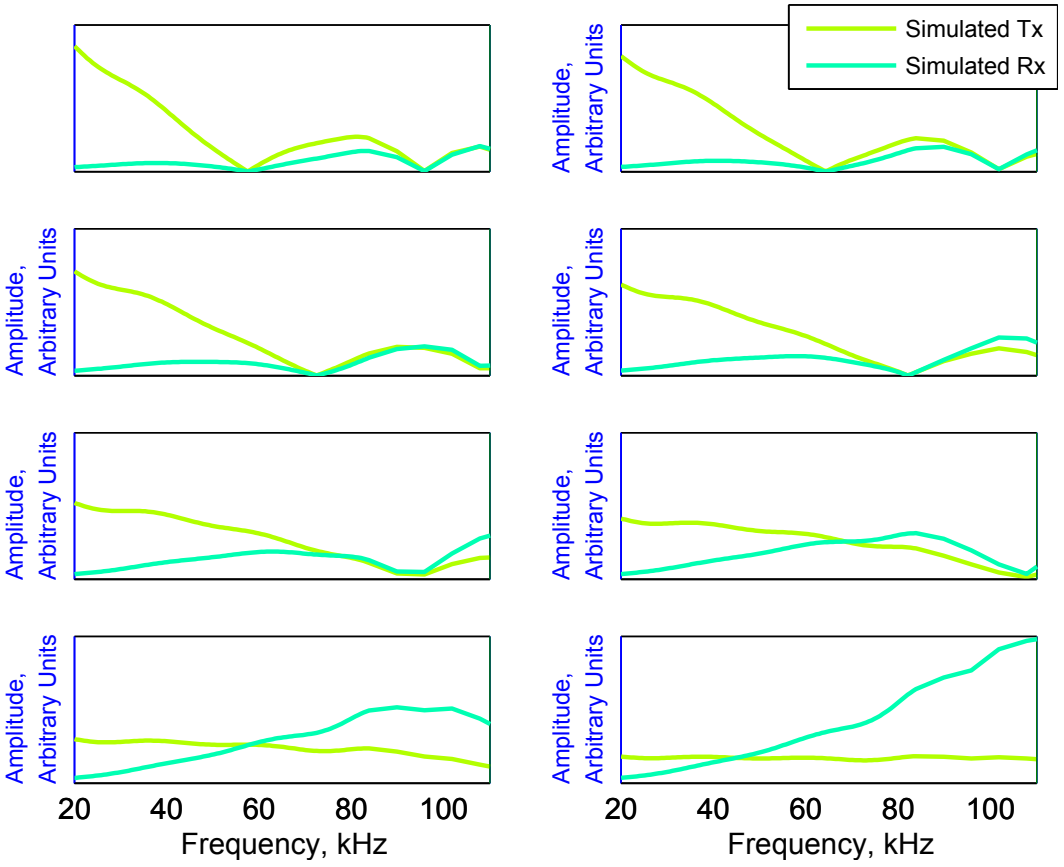

FIGURE 3.34: The simulated frequency response of various length MFCs on an aluminium rod, where the frequency dependence is given for transmission and reception separately.

3.12 Summary

Macro Fibre Composites have been identified as suitable transducers for applications of ultrasonic guided waves. A mathematical model has been used to represent the superpositional effects of an MFC transducer's length on its wave mode sensing capability, which predicted a highly wave length dependent cancellation effect. A chirp transmission method and split spectrum analysis has been developed for measuring frequency response of a transducer type in a pulse echo or pitch catch arrangement, which was then used to confirm the frequency and length dependent performance of MFC transducers.

This model can predict the performance of an MFC of a given length and allows the MFC length to be chosen to have a high sensitivity to a desired mode whilst having a significantly lower sensitivity to unwanted modes. This will help achieve high mode purity with an MFC array, which ultimately can lead to inspection systems being developed with greater defect finding capabilities.

In this chapter the MFC performance has only been considered in the axis parallel to the fibre alignment, which is sufficient for 1D testing, particularly for 1D waveguides such as rods and tubes. However it is also desirable to understand how this wavelength and wave mode dependent sensitivity affects their performance when the ultrasonic guided waves can propagate in any direction within a 2D waveguide. This is dealt with in the next chapter.

Chapter 4

Development of 2D Simulation and Experimental Characterisation for Macro Fiber Composite Transducers

4.1 Introduction

One of the most crucial issues for many long range ultrasonic systems is directional wave mode control. Generally, arrays of transducers are designed such that, through phased transmission, a single or selected set of wave modes is transmitted in a desired direction without significant transmission of other modes or in other directions. This is optimal when a transducer type can be selected for use in the array that has directional characteristics that suit the requirements of the application. An array can be designed to better optimise the wave mode control, if the directional sensitivity of the transducer is known.

In the last chapter, it was described how the length and bipolar nature of the MFC causes interference to occur on transmission and reception. This was considered in one dimension only, where an MFC is placed on a waveguide that is long in one axis only with the MFC fibres parallel to that axis. This is appropriate for the testing of pipes, rods and other 1D waveguides. However, there is also a need for the testing and structural health monitoring of 2D structures, where the waveguide is either a surface or a plate of one or more layers. In this chapter the discrete model of MFC behaviour for a one single dimensional waveguide (from the previous chapter) is developed further to accommodate two dimensional, isotropic waveguides. This Point Source Superposition Model allows the simulation of the output from a transducer giving the directional amplitude for each wave

mode. If a transducer's nature is known, this model can be used to gain an understanding of the transducer's directional wave mode sensitivity. If it is not known, a hypothesis can be made about the transducer's nature and its simulated directional sensitivity can then be compared to experimental measurement. This directional sensitivity information allows arrays of transducers to be optimally designed for wave mode control, which will ultimately lead to greater defect sensitivity for the resultant inspection system.

Another transducer type, a monolithic shear transducer commonly used in commercial LRUT and supplied by PI Ltd. (a reference transducer), will also be evaluated in this chapter [Jackson, 2011]. This transducer has uniform sensitivity and small dimensions compared to the MFC transducer. Unlike the MFC transducer, this transducer is expected to have the directional characteristics of a simple point source when used at low frequencies. The aim of comparing the MFC transducer to this common commercial guided wave transducer was to highlight the significance that the size and bipolar nature of the MFC has on its directional wave mode sensitivity.

This chapter discusses how the transmission amplitude of the three fundamental plate wave modes ($A0$, $S0$ and $SH0$) have been modelled. The simulation results obtained for both these transducer types have been validated experimentally with equivalent tests on a 10 mm thick steel plate. The direction and frequency response maxima and minima for each wave mode may be found relatively easily with this simulation technique. Also, to the best of the author's knowledge, this is the first study to demonstrate the significance of the perpendicular sensitivity of the MFC transducer to Lamb waves and to demonstrate their directional sensitivity to shear-horizontal plate waves.

4.2 Method for MFC Directionality Study

In this chapter the directional characteristics of the MFC transducer and a common commercial transducer are studied and compared. As with the last chapter, a model is used to evaluate the mechanism that associate amplitude sensitivity with MFC geometry and wave mode characteristics. The simulation uses the superposition of results of discrete points, based on the approach in the previous chapter, although in this case the results are compared for varying direction rather than frequency. The experimental technique that uses a large plate with an circumferential array for directional amplitude measurement placed around its perimeter and a test MFC placed in its centre is discussed. The results section in this chapter makes the comparison between the transducers and evaluates the performance of the model.

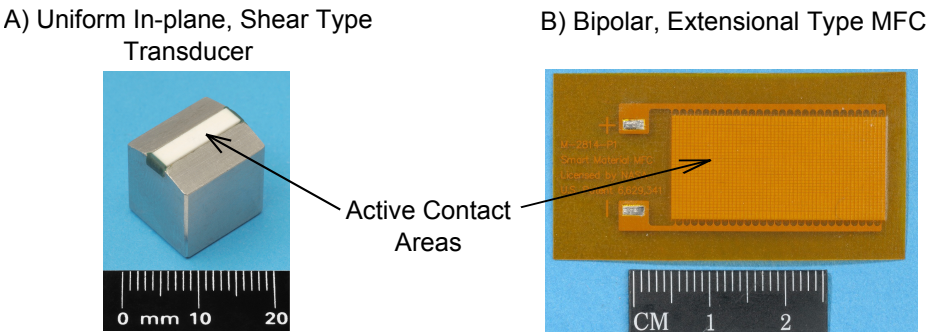

FIGURE 4.1: (A) The uniform in-plane transducer, and (B) the MFC transducer.

4.2.1 Common Commercial Guided Wave Transducer

Since the MFC transducer can be thought of as being bipolar in nature, the common commercial guided wave transducer can be thought of as the monopolar alternative; it has uniform, uniaxial sensitivity. This transducer has been designed to have a significant displacement only along the poling axis and the out-of-plane displacement is assumed to be insignificant. This is achieved by using a polarisation and electrode scheme that gives the transducer a high d_{51} value.

The selected monopolar transducer is relatively small with an active contact area of 10mm by 3mm (Figure 4.1A). A typical MFC, for comparison, has an active area of 28mm, in the fibre axis, and 14mm, in the perpendicular axis, (Figure 4.1B).

4.3 Plate Testing With Ultrasonic Guided Waves

There are many approaches to the testing of plates. Different transducer characteristics are required for the various methods and applications. In every instance, knowledge of the transducers' directional wave mode sensitivity is needed for the frequency range of interest.

Early methods of testing plates with ultrasonic guided waves made use of directional wedge probes, where a narrow beam is used to detect defects along one line, which is then scanned manually over the region to be tested [Ball and Shewring, 1973, Alleyne, 1991]. This has been further developed with different methods of transmission and reception, and with different approaches to defect detection. Fromme et al. [2004] have used thirty two omnidirectional transducers in a localised ring array in order to allow the directional sensitivity to be controllable. These transducers have been designed to be preferentially sensitive to A0, and are presumed to be out of plane transducers. A pulse-echo method was used to create a radial B-Scan (a 2D image where colour intensity represents reflection amplitude and position represents the location of the reflector). This was shown to be effective at detecting a number of different defects in a 5mm steel plate.

Creating defect maps through acoustic waves is a process often referred to as Acoustic Wavefield Imaging (AWI) or ultrasonic tomography.

Thirty two is a considerable number of transducers for one location, not only because of their size, weight and cost, but also because of the requirement for multiplexing electronics. Directional sensitivity has been achieved with a similar arrangement but with fewer transducers by using directional, in-plane transducers [Wilcox et al., 1998]. The transducers, made using a polyvinylidene fluoride (PVDF) film (a piezoelectric polymer), were manipulated by interdigital electrodes placed on film layers either side of the PVDF. The interdigital electrode pattern in this case was based on the surface acoustic wave (SAW) sensor design, where the electrode spacing is equal to half of the desired wavelength. In this work Wilcox et al. created a model for a point source and then used the Huygen's principle to apply this to model the transducers used. This model was validated experimentally. The half wavelength spacing of the electrodes results in the transducer being many wavelengths long. This makes it impractical for low frequency applications, but otherwise effective for generating a desired directional transmission with a narrow wavelength bandwidth. This in turn allows for high wave mode selectivity. A directional ring arrangement of piezoceramic fibre transducers, similar to the MFC transducer, have also been used in a ring arrangement to allow for directional testing with transducers that are small relative to wavelength, and so are practical at low frequencies [Salas and Cesnik, 2009, 2010].

Another approach is to use an array of transducers placed along one axis (known as a linear array) where phasing the transmission from the complete array allows control over the curvature (and so the focal point) of the wave front, which is known as the Synthetic Aperture Focusing Technique (SAFT). There are various ways in which this testing can be performed using, many of which can be done with a single data set through the use of Full Matrix Capture (FMC) techniques. In a recent example of plate testing with linear arrays, Higuti et al. [2010] have tested a defective sample and have shown that, since various techniques produce different noise effects, compounding the results from different methods can be used to reduce misdetection by enhancing the coincidences.

Another approach to plate inspection involves distributed transducer networks (also known as sparse transducer arrays) to perform various methods of ultrasonic guided wave tomography. This is generally done in one of two ways; either the testing is done directly between transducers and the disruption to the propagation across the various possible routes is used to construct an image of wave scattering features, or indirectly by measuring the scatter from these features. The former tends to require many transducers (to ensure there are enough overlapping propagation routes over the region of interest) and can only detect defects internal to the region enclosed by the transducer network [Hay et al., 2006]. However, since the lengths of direct routes are known and the arrival time of the wave mode of interest is predictable, this method can be robust against the presence of uncontrolled wave modes. This may require the amplitude of transmission from

one transducer to a group of receivers to be uniform, which may make omnidirectional transducers the best option. However, there may be regions that are not of interest that contain scattering features that can introduce unwanted signals, in which case transducers can be selected that have directional transmission only in the direction of the desired receivers. Conversely, indirect methods may require relatively few transducers, but care is needed to reduce the influence of unwanted wave modes [Michaels et al., 2005, Michaels, 2008, Clarke et al., 2010]. In this case it is very likely that omnidirectional transducers are desired, because generally the goal here is to achieve wide spanning coverage with few transducers. This technique can also be used to detect defects outside the area bound by the sparse array, although this can be more susceptible to coherent noise [Clarke, 2009]. This coherent noise is mainly complex scatter (caused by transducer sensitivity to undesired wave modes, wave mode conversion by scattering features, and repeat scattering between multiple features) that is not suppressed by the imaging algorithm.

Knowledge of the directional wave mode sensitivity of the transducers used is crucial for all these techniques. This knowledge is needed for transducer selection, the development of the imaging algorithms, and for choosing the transducer placement and orientation. Gao and Rose [2006] have developed a means of optimising the transducer placement to reduce the risk of misdetections. This assumes omnidirectional transducers, however it could be further developed for any transducer, providing the directionality of the transducer is known.

When transducer directionality is not properly understood, both false positive and false negative misdetection can arise for any of the plate testing methods mentioned here. This can be improved through signal processing methods, for example through the filtering of wave modes by their rate of dispersion [Mallett, 2007] or through the aforementioned use of data fusion [Higuti et al., 2010]. However, there will always be a need to have a good understanding of a transducer's directional wave mode sensitivity before it can be considered for any kind of plate inspection application.

4.3.1 MFC Transducer Directional Sensitivity

As far as the author is aware, Raghavan and Cesnik [2007b] were first to assess the directional sensitivity of AFC and MFC transducers analytically with experimental validation. They looked at the $A0$ and $S0$ sound field generated in aluminium structures by solving the 3-D elasticity-based boundary value problems. They demonstrated that the sensitivity to each mode was dependent on the length of the active region. They compared experimental results of $A0$ and $S0$ mode directionality in a 1 mm thick aluminium plate (obtained via laser vibrometry) and equivalent theoretical plots for an MFC transducer and found reasonable agreement, although some lateral transmission was observable that was not accounted for. Birchmeier et al. [2009] used the Finite-Difference

Time Domain (FDTD) method to create a model that included the electromechanical coupling, and the system's geometry and elasticity. They used this for the analysis of the wave field generated by an AFC transducer (similar to an MFC transducer). Both these studies demonstrated a direction, frequency and mode dependent transfer function. Both models closely correlated with the associated experimental work. However, neither included analysis of shear horizontal modes. Also, the experimental work presented in Raghavan and Cesnik includes measurements in the direction perpendicular to the fibre direction, which indicate some, albeit minor, sensitivity to Lamb modes in this direction that were not present in the analytical results. Windisch et al. [2010] have also experimentally evaluated transducer directionality by making measurements through laser vibrometry. This included the evaluation of a fibre composite transducer attached to a 2 mm thick sheeting of aluminium that was used to transmit a narrow band pulse with a centre frequency of 400 kHz. Matt and Lanza di Scalea [2007] evaluated the directionality of MFC transducers for the source location of acoustic events in carbon fibre composite materials using the A0 wave mode. They demonstrated that because of the directional nature of the MFCs, a rosette arrangement could be used to determine the source direction.

Köhler et al. [2009] produced their own AFC transducer, similar to the MFC transducer, which facilitated segmented electrode control. They recognised that for wavelengths that were relatively short compared to the fibre lengths, a transducer that could only utilise uniform strain would be inefficient for sensing and actuation. They found that by segmenting the electrode control they could match the applied strain to the desired mode shape. They presented a method of mode matching for the transduction of Lamb modes along the fibre axis and demonstrated the mode selectivity experimentally.

4.4 Point Source Superposition Model

The active region of a transducer in contact with a structure creates stress at its surface. When applied to an appropriate structure, this disturbance will result in the excitation of ultrasonic guided waves. If the active region is small relative to wavelength, the transducer can be thought of as a point source. Otherwise, the active region can be compartmentalised into subsections that each can be likened to a point source. The total transmission of a transducer can be modelled as the summation of the sound fields from each of these point sources (employing the theory of superposition).

To create the model a set of point sources is selected to represent the transducer and a set of receiver points is chosen for output measurement. A ray tracing approach is used to simulate propagation of an input signal from every transmission point to every reception point. The received signal at each receiver position is the sum of the signals from all transmitter points. This does not require calculation for propagation to intermediate

points or for any other unwanted points, which makes it a relatively simple and fast computation. If the transducer's vibrational shape is known, the output can be simulated and analysed. If this is not fully understood, then a hypothesis should be made about the transducer's vibrational characteristics and this used for simulation. In this case, the simulated output should be validated experimentally to test the hypothesis.

4.4.1 Single Point Source

Before a transducer representation could be constructed using sets of point sources, it was necessary to create a representation for a point source. For isotropic plates, out-of-plane displacement at a point on the surface would cause a wave to be transmitted in all in-plane directions equally. The directional transmission of ultrasonic guided waves from an effective in-plane point source has previously been analysed using Finite Element Analysis (FEA) [Mažeika et al., 2007]. This showed that the Lamb wave transmission amplitude in an in-plane direction is proportional to $\cos\theta$, where θ is the angle between the axis of vibration and the direction under consideration. Whilst this was produced using a modelling method that has been used and validated before, this particular finding was not experimentally validated. Also, only the fundamental Lamb modes were evaluated (the SH0 mode was not considered).

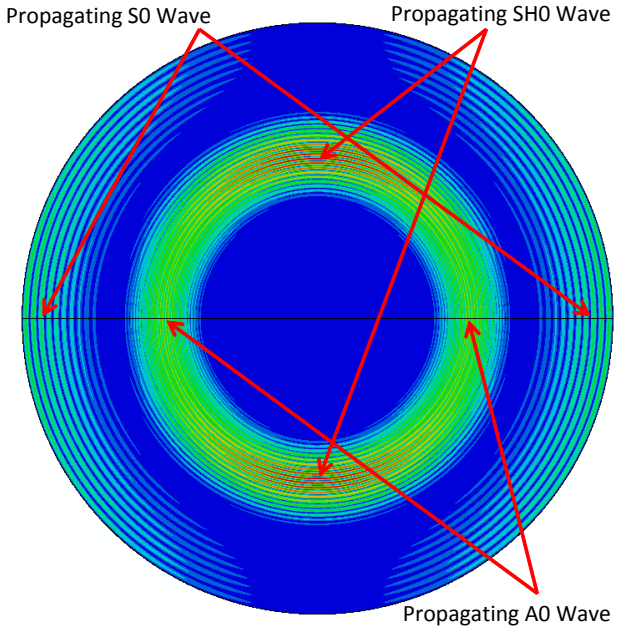

FIGURE 4.2: A Von Mises stress field view from the finite element simulation of the excitation of ultrasonic guided wave modes in a 3.5m diameter, 10mm thick steel plate from a uniaxial in-plane point source. This shows the point in time where the S0 wave mode encounters the plate's perimeter.

For this work, FEA has been used to study the directional characteristics of a point source for all three fundamental plate wave modes ($A0$, $S0$ and $SH0$). A 3D model of a 3.5m diameter round, 10mm thick, steel plate was used, where a single, central point

was excited with a purely in-plane disturbance (Figure 4.2). The model was generated and solved using ABAQUS\Explicit [Dassault Systèmes, 2011]. Three-dimensional brick elements were used with reduced integration to decrease computation time. The mesh was refined sufficiently so that there were at least 8 elements per wavelength in any potential propagation direction. This level of mesh refinement has been previously validated against experimental data [Alleyne, 1991]. The assumed material properties were as follows: Young's modulus: 207 GPa; Poisson's ratio: 0.3; density: 7830 kg/m^3. This model uses appropriate boundary conditions to simulate a line of symmetry in the $0° - 180°$ axis to halve the model size.

The transmitted waves were measured at 32 discrete intervals around the plate's perimeter and stored. Measurements were taken from both the top side and the underside at each angular position. The amplitudes of the output signals were given (by the solver) in Cartesian components and were subsequently converted into radial and circumferential components. The S0 and A0 modes were not expected to have any circumferential component, since the source is perfectly in the centre and these are known to have no shear component. The amplitude of the SH0 wave mode (for each angular position) could be taken as the maximum of the peak-to-peak circumferential stress amplitude. The S0 and A0 wave modes both have radial and out-of-plane components, and could not be separated by measuring in a particular axis. However, since S0 is symmetric through the thickness and A0 is not, these modes can be distinguished. To produce pure S0 signals the out-of-plane signals from the top side were subtracted from the out-of-plane signals from the bottom side. To produce pure A0 signals these out-of-plane signals were added (instead of subtracted). Again, peak-to-peak stress amplitude measurements were taken from the set of pure S0 signals and the set of pure A0 signals. These three directional amplitude measurements have been normalised and displayed in Figure 4.3.

This shows the FEA results confirm the Lamb wave coefficient can be taken as $\cos\theta$ (the projection of displacement to the axis of propagation), and identifies the horizontal shear coefficient to be $\sin\theta$; the shear horizontal directionality is equivalent but orthogonal to the Lamb wave directionality. In this chapter these findings will be used to construct the point source model, which is later validated against experimental measurements.

The relative directional amplitude of a Lamb wave mode, A_{Lamb}, on the surface of the plate produced by an in-plane point source and excited with a sine wave can be calculated as,

$$A_{Lamb} = \cos\theta \cdot A_n \cdot \sin\left(k_n(\omega)x - \omega t\right), \tag{4.1}$$

where A_n denotes the maximum amplitude at the source for the current wave mode, ω the angular frequency, t the time, $k_n(\omega)$ the wave number for the current wave mode as a function of frequency, and x the distance from the source in the 2D plane of the plate.

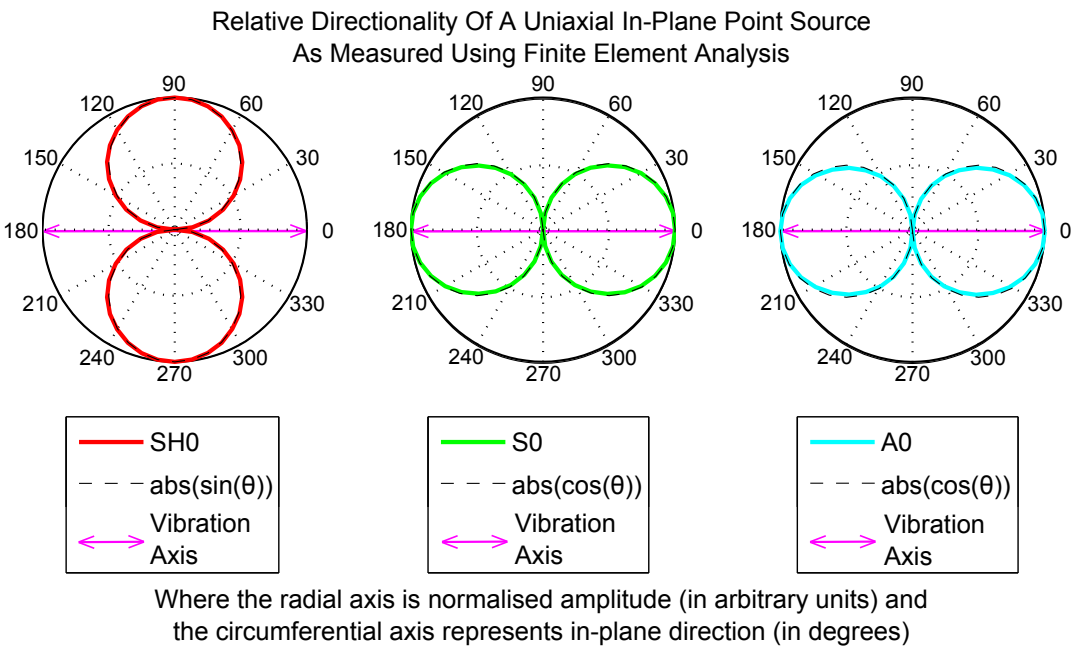

FIGURE 4.3: Results from a Finite Element Model (FEM) of the directional transmission from an in-plane point source.

The relative excitability of each wave mode by an in-plane or out of plane disturbance can be derived numerically [Sanderson and Catton, 2011]. If the relative excitability is known, it can be incorporated into A_n to give the proportionality between modes. However, for the analysis of the directionality of individual wave modes the amplitude is relative, so the value of A_n can be arbitrary and the relative excitability is not used. The relative directional amplitude of a shear horizontal wave, A_{shear}, on the surface of the plate produced by an in-plane point source and excited with a sine wave can be calculated as,

$$A_{shear} = \sin\theta \cdot A_n \cdot \sin\left(k_n(\omega)x - \omega t\right). \tag{4.2}$$

As the Lamb wave directionality coefficient will be negative for angles between $\pi/2$ and $3\pi/2$ radians and the shear horizontal wave directionality coefficient will be negative for angles between π and 2π radians, the corresponding signals will be inverted for these angular ranges, as was observed with FEA.

The propagation of any input signal was simulated by transforming the signal into the frequency domain using a Fast Fourier Transform (FFT), adjusting the phase of each frequency by $k_n(\omega)x - \omega t$, and then transforming the signal back to the time domain using an inverse FFT. Since this adjusts each frequency's phase by $k_n\omega$, this simulation includes the modelling of dispersion, which is where signals are distorted over distance due to the difference in velocity over the frequency spectrum. Then the amplitude was

scaled by $A_n \cdot \sin\theta$ to take account of the directionality. Each wave mode was modelled separately.

The values for $k_n(\omega)$ were provided by the dispersion curves that were generated using the software 'Disperse' [Pavlakovic et al., 1997]. This software was also used to provide the phase and group velocity curves for all possible ultrasonic guided wave modes in a 10mm thick steel plate within the frequency range of interest, as was shown in Figure 3.17.

4.4.2 Multiple Point Source Transducer Model

The continuous displacement across the active region of a transducer can be represented with a discrete, regular grid of point sources. The displacement actuated by a transducer is not always uniform; in fact the direction of displacement and the displacement amplitude is often a function of position within the active region. To represent this non-uniform characteristic the orientation and amplitude of each point source is also determined by position. Each point source may be represented as a vector with position, amplitude and direction.

By representing a transducer as a grid of point sources, the signal transmitted from the transducer to some nominated receive point can be simulated. To do this the single point source simulation described above (in Section 4.4.1) is used to simulate transmission from each transmitter point to the reception point, which results in a bank of signals. The received signals are summed to create a single signal, which is the simulated signal transmitted from the transducer to that point. Amplitude measurements can then be taken from this received signal and amplitudes from different receive locations can be compared.

The tone burst input signals used for each frequency in simulation (and likewise in experimentation) were constructed from a 12 cycle sine wave of the required frequency multiplied by a Hann window (with a length equal to the sine wave). A short pulse length is needed so that reflections appear distinct from one another in the signals, whilst a narrow bandwidth is needed to allow frequency dependent characteristics to be measurable. A Hann windowed tone burst is sufficient for this purpose. Since the main frequency bandwidth of a Hann windowed tone burst is $f_c \pm f_c \cdot (2/N)$ where f_c is the centre frequency and N is the number of cycles, a 12 cycle pulse will have a main lobe bandwidth of $f_c \pm 16.7\%$. 12 cycles thus represents a relatively short pulse length (in time), yet a significantly narrow frequency bandwidth. An example 60 kHz input signal is shown in Figure 4.4A. For each wave mode the simulation produces a signal at each desired location as received from the transducer, which is then used to measure the peak amplitude at this location. As example of a simulated signal is shown in Figure 4.4B.

In the following two sections the point source grid designs for both transducer types are described. The directional sensitivity of each transducer for each of the fundamental wave

modes was measured from simulated signals. This was done by interactively conducting the simulation with the receive point being changed in position. The receive point was fixed at a distance, r, from the centre of the transducer being simulated, whilst the relative angular position, β, was incrementally swept from 0° to 359° by steps of 1°. The relative directional transmission amplitude was then taken as the measured peak to peak amplitude of the simulated signals for each angle of β. The simulations for all directions were conducted for each transducer using the centre frequencies 40, 60 and 80 kHz. At these frequencies, only the fundamental wave modes exist (as shown in Figure 3.17).

4.4.3 Uniform in-plane Transducer Simulation

The transducer in Section 4.2.1 is thought to act uniformly with uniaxial in-plane displacement. Figure 4.5 shows the dimensions of the active region and illustrates the expected homogeneity of the displacement. When the directionality of this transducer was simulated, the active region was represented with a 30 by 9 grid of point sources (one third millimetre separation) with homogeneous orientation and magnitude.

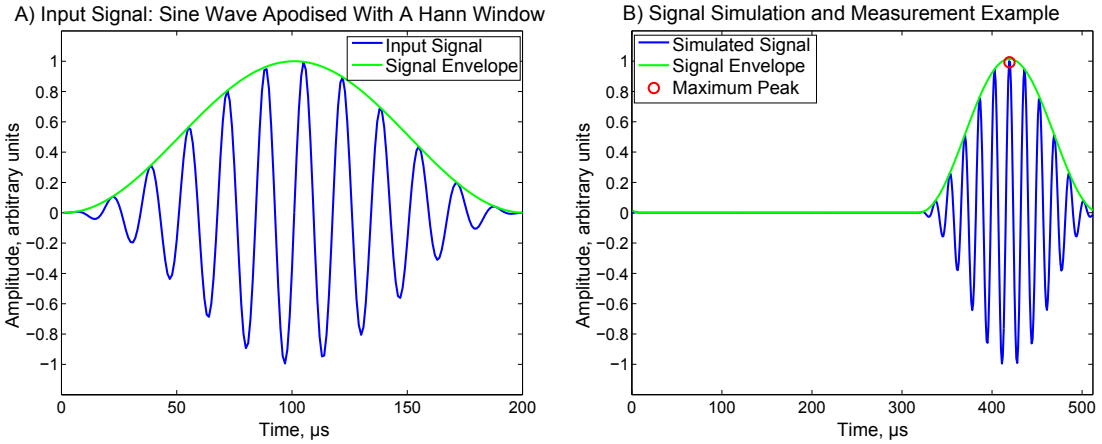

FIGURE 4.4: A) The input signal used for simulation and experimentation. B) An example of the simulation of the transmission of a single wave mode (S0) from an MFC to a point 1.72m away.

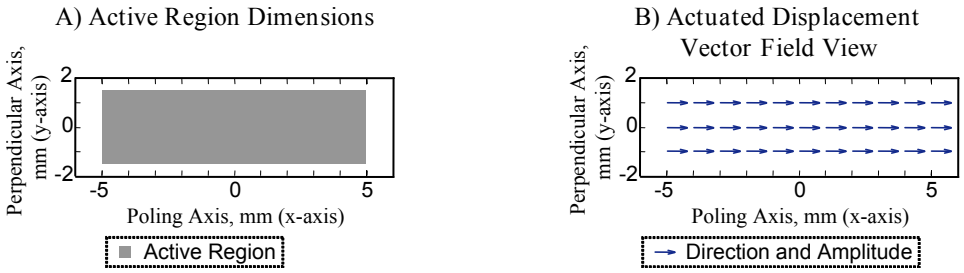

FIGURE 4.5: (A) The dimensions for the active region of the uniform in-plane transducer and (B) the hypothesised displacement field.

4.4.4 MFC Simulation

The X-ray image displayed in Figure 4.6A shows the dimensions of the chosen MFC transducer's active region and the layout of piezoelectric fibres within it. Henceforth, the fibres will be considered to lie along the x-axis, whilst the in-plane, perpendicular direction will be considered the y-axis. On actuation, instantaneous strain is developed uniformly across the active region and some strain occurs in all axes. Given the Poisson's ratio for the active region is 0.312 (similar to that of steel) [Wilkie et al., 2003], it is hypothesised that strain in y is expected to be equal to -0.312 of the strain in x. It was assumed that the out-of-plane displacement would be insignificant owing to the limited thickness of the active layer and therefore this will not be considered. The vibrational characteristics will be different to those hypothesised at some frequencies where resonance occurs, but these were not anticipated at the low ultrasonic frequencies used in this case.

Displacement is the cumulative result of the instantaneous strain and is therefore linear in both x and y. The mechanical loading conditions are expected to be uniform and symmetric about the centre for axes, thus displacement is expected to be zero at the centre of the active region.

For the purpose of modelling, this displacement field was simulated as a discrete, regular grid of point sources with a one third of a millimetre separation distance between points (giving a grid of 84 by 42 points). The amplitude and direction of each point source in the grid is defined by a vector, p_n, given as

$$p_n = \left(A_n \sqrt{(x^2 + (-\nu y)^2)}, \angle \arctan \frac{-\nu y}{x} \right), \tag{4.3}$$

where ν is the Poisson's ratio of the active area, which in this case is 0.312, and A_n again is the displacement amplitude. The hypothesised actuation given by p_n is illustrated in Figure 4.6B.

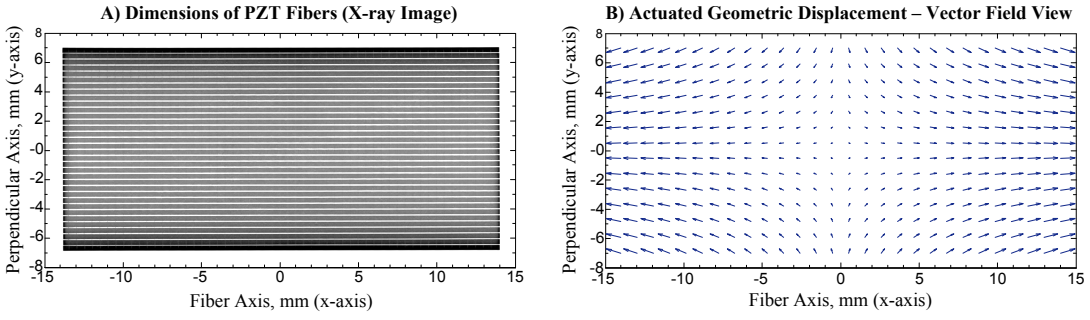

FIGURE 4.6: A) X-ray image showing the fibre arrangement within the MFC active area. B) A vector representation of the hypothesised action of the MFC transducer, in arbitrary magnitude units.

Sound Field Simulation

The aim of this simulation is to measure the transmitted amplitude from each transducer for each wave mode at each desired frequency. However, since it is a fast method, an image of the plate's surface can be created by simulating the signal over a rasterised grid of points to create an animated view of the propagating sound. Doing so perhaps gives a more intuitive view of the transducers output. Figure 4.7 demonstrates the S0 mode sound field after 280 μs as simulated as being transmitted from the MFC transducer. However, reproducing these scanned measurements experimentally is difficult. However, the transducer directionality can be measured from a number of orbital points which greatly reduces simulations time and experimental complexity.

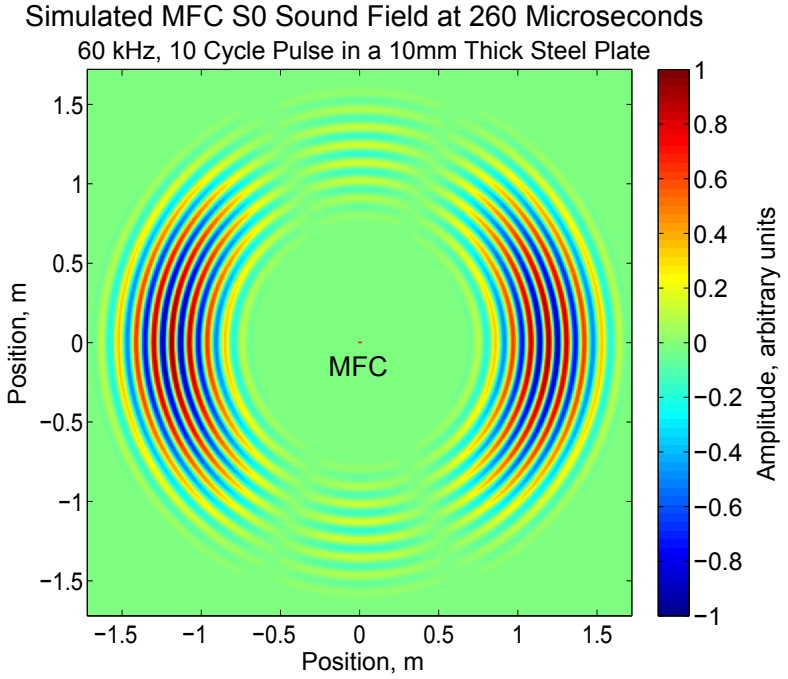

FIGURE 4.7: A demonstration of the sound field at the surface of a 10mm steel plate for the S0 wave mode transmitted from an MFC as modelled by the simulation. The MFC is lying with the fibres parallel to the horizontal axis.

4.5 Experimental Validation

An experiment was devised for measuring the directional transmission of guided waves at low ultrasonic frequencies from a ‘‘test’’ transducer on a circular, 10 mm thick steel plate of 3.44m diameter (as depicted in Figure 4.8). The aim was to produce results that could be used to validate the model and the hypothesised transducer characteristics. The experimental setup involved a test transducer dry-loaded in the centre of the plate, which was used as a transmitter, whilst receivers fixed near the outer rim were used to measure the amplitude transmitted in each direction. The receivers were uniaxial

in-plane transducers similar to the type described in Section 4.2.1. As with simulation, the transmission signals took the form of a 12 cycle tone burst (as described in Section 4.4.2 and depicted in Figure 4.4A) and testing was conducted using the centre frequencies of 40, 60, and 80 kHz. Electrical transmission and reception were achieved using a Teletest Focus^{TM} flaw detector [Jackson, 2011]. Both the uniform in-plane transducer and the MFC transducer models were then evaluated with this test.

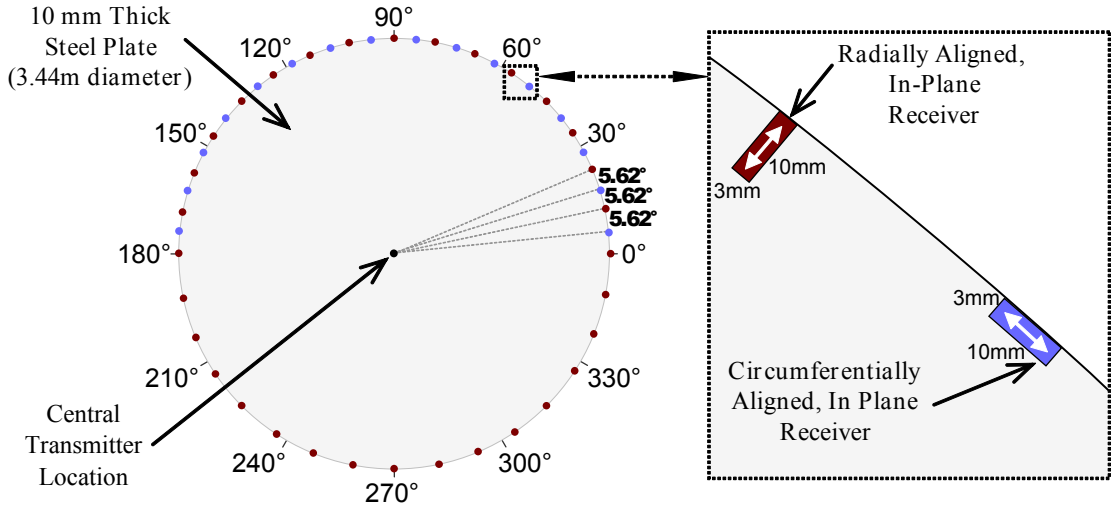

FIGURE 4.8: A plan view of the experimental setup for measuring the directional guided wave mode sensitivity of a centrally located transmitter.

Thirty two piezoelectric receivers were placed around the circumference of the plate. They were placed on the top surface, next to the outer edge, and approximately 11.25° apart. They were aligned radially to be sensitive to Lamb waves transmitted from the central test location.

Sixteen more receivers were added from the 5.6° location through to the 174.4° location, at 11.25° intervals, which were oriented circumferentially to be sensitive to shear horizontal waves transmitted from the centre of the plate. As a symmetric directivity pattern was expected and as the number of available receiver elements was limited, only half the circumference was covered by shear receivers.

All receivers were bonded to the plate using a two-part adhesive (Devweld 530 by ITW Devcon) and coated with cavity wall insulation foam for environmental protection. The plate was supported by 6 ball bearings placed around the outer edge in between receiver positions with the aim of limiting scattering from these supports by keeping their contact area minimal.

The surface at the central location was prepared with a high flatness and low roughness so that coupling conditions could be more repeatable, and a loading mechanism was designed for the transmitting transducer. The loading device was designed to apply a load of 200 N over each transducer in order to ensure good ultrasonic coupling between the structure's surface and the transducer under test. A silicone closed cell foam pad

was used between the loading device and the transducer under test in order to reduce the ultrasonic influence the loading rig would have. The plate dimensions were chosen to allow the various modes under test to arrive at different times, so that it was possible to measure the amplitude of each mode separately.

4.5.1 Receiver Normalisation

Initial testing found that the sensitivity of the fixed receivers varied significantly, making their normalisation essential. The error due to variation in the fixed receivers was dealt with using an averaging process. The test was conducted 16 times with the transmitter under test stepping through rotational increments of 11.25° (equal to the angular step of the receivers). The amplitude for each transmit direction was then taken as the mean of the measurements taken across 16 different receivers. As the circumferentially aligned receivers only covered half the circumference, rotational symmetry was assumed and diametrically opposite positions were used interchangeably for this averaging process.

4.6 Results and Discussion

The 40, 60 and 80 kHz uniform in-plane transducer results are displayed in Figure 4.9. The radial amplitude scales have been normalised. There is a close match between the experimental and the simulated results. All modes display sinusoidal directionality for all frequencies tested. The results are similar for both the Lamb modes studied ($A0$ and $S0$). The Lamb mode directionality appears to vary with the cosine of the angle from the axis of vibration and the shear mode directionality appears to be the sine of this angle. In this sense it is behaving approximately like the theoretical point source described in Section 4.4.1. However, all the experimental results appear to have approximately a $-10°$ angular offset from the numerical results, which is likely to be due to a positioning error in the placement of the piezoelectric element inside the transducer holding rig. Unlike the other two modes, the $A0$ experimental results differ from the simulated results by an omnidirectional positive offset. It was observed that if a value of 0.09 is subtracted from all directions, the shape becomes approximately the same as that of the $S0$ result. As this 9% omnidirectional offset only occurs for the $A0$ results (displayed on the right hand of Figure 4.9) and this mode is the only mode of the three with a significant out-of-plane component, it is likely that this transducer has some unpredicted out-of-plane vibration since SH0 is strong in the 90° and 180° directions. Because of its similarity to the theoretical point source, this transducer has maximal sensitivity to SH0 in the directions where it has minimal sensitivity to Lamb modes. This makes it an appropriate transducer where SH0 waves are desired.

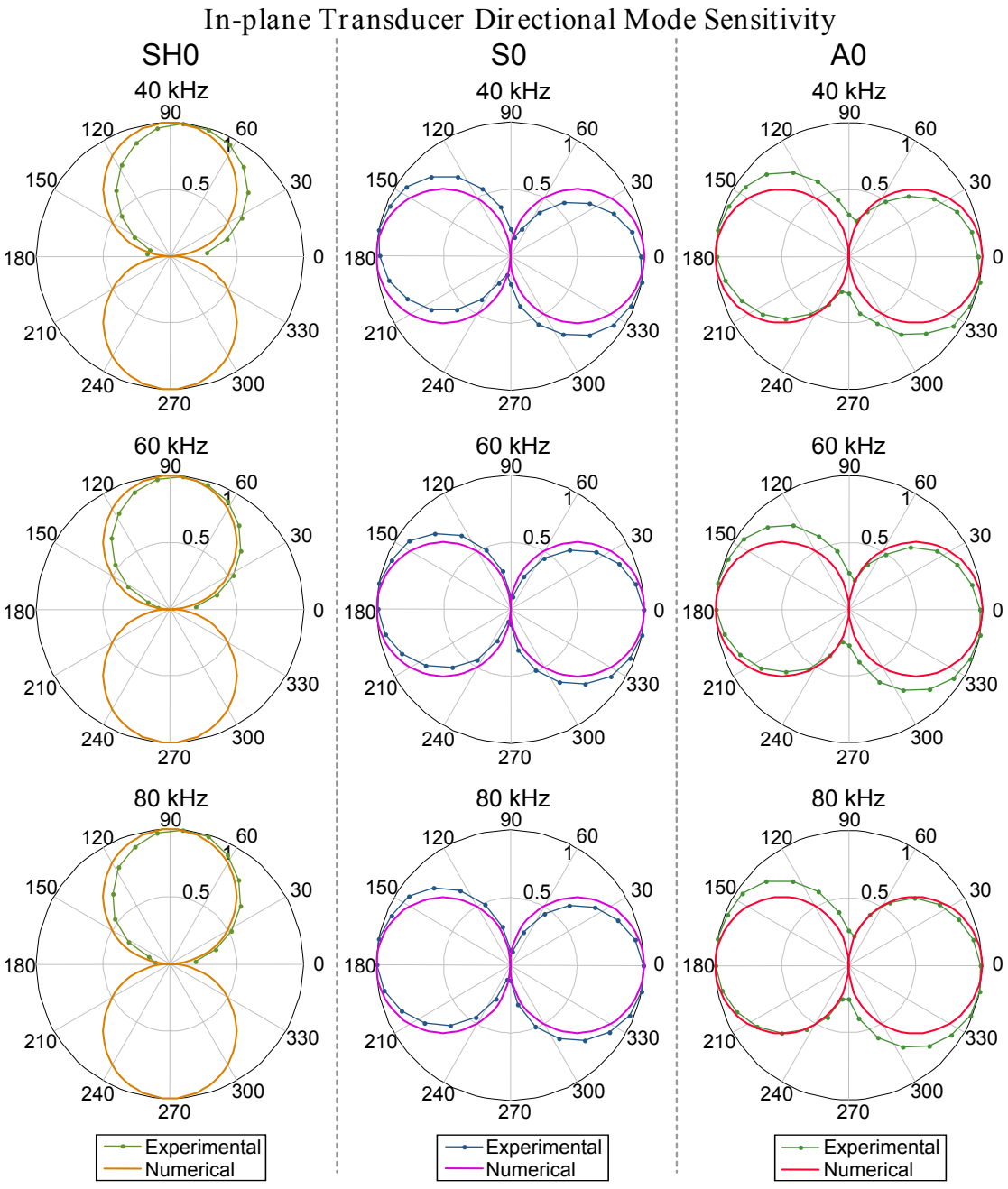

FIGURE 4.9: Experimental and numerical results for the uniform in-plane transducer with the majority of the in-plane displacement in the $0° - 180°$ axis. The circumferential axes give direction and the radial axes give normalised amplitude in arbitrary units.

The MFC transducer results (Figure 4.10) also demonstrate a high degree of similarity between the experimental and numerical results. There is no rotational misalignment in these results and neither does there appear to be any unpredicted out-of-plane sensitivity. The point source superposition model has suitably predicted the directionality of the MFC transducer for each mode.

Unlike the uniform in-plane transducer, the MFC transducer has potentially significant sensitivity to Lamb modes in the direction perpendicular to the main direction of sensitivity ($0° - 180°$ axis). As demonstrated by the $A0$ result at 80 kHz, these ''side lobes'' can be significant at frequencies where the sensitivity along the fibre axis is reduced due to superpositional cancellation. If an array of MFC transducers were to be applied to a plate, these side lobes would need to be taken into consideration in order to avoid lateral sensitivity. The bipolar nature of the MFC transducer also gives rise to self-cancellation of the $SH0$ mode, predominantly in the y-axis ($90° - 270°$ axis). The cancellation of $SH0$ in this axis reduces the maximum achievable amplitude with this mode. In the 10 mm steel plate at low ultrasonic frequencies the maximum $SH0$ sensitivity is achieved in the 45°, 135°, 225°, and 315° directions. This reduced sensitivity to SH0 could be useful when lateral sensitivity is undesired and only Lamb modes are needed. The directional nature of the MFC transducer when transmitting Lamb modes can be beneficial where a narrow beam is required.

Both transducers showed little variation across the frequencies tested, which makes them fairly predictable for low frequency applications for steel plates of this thickness. However, the directional characteristics are expected to vary more drastically when shorter wavelengths are used.

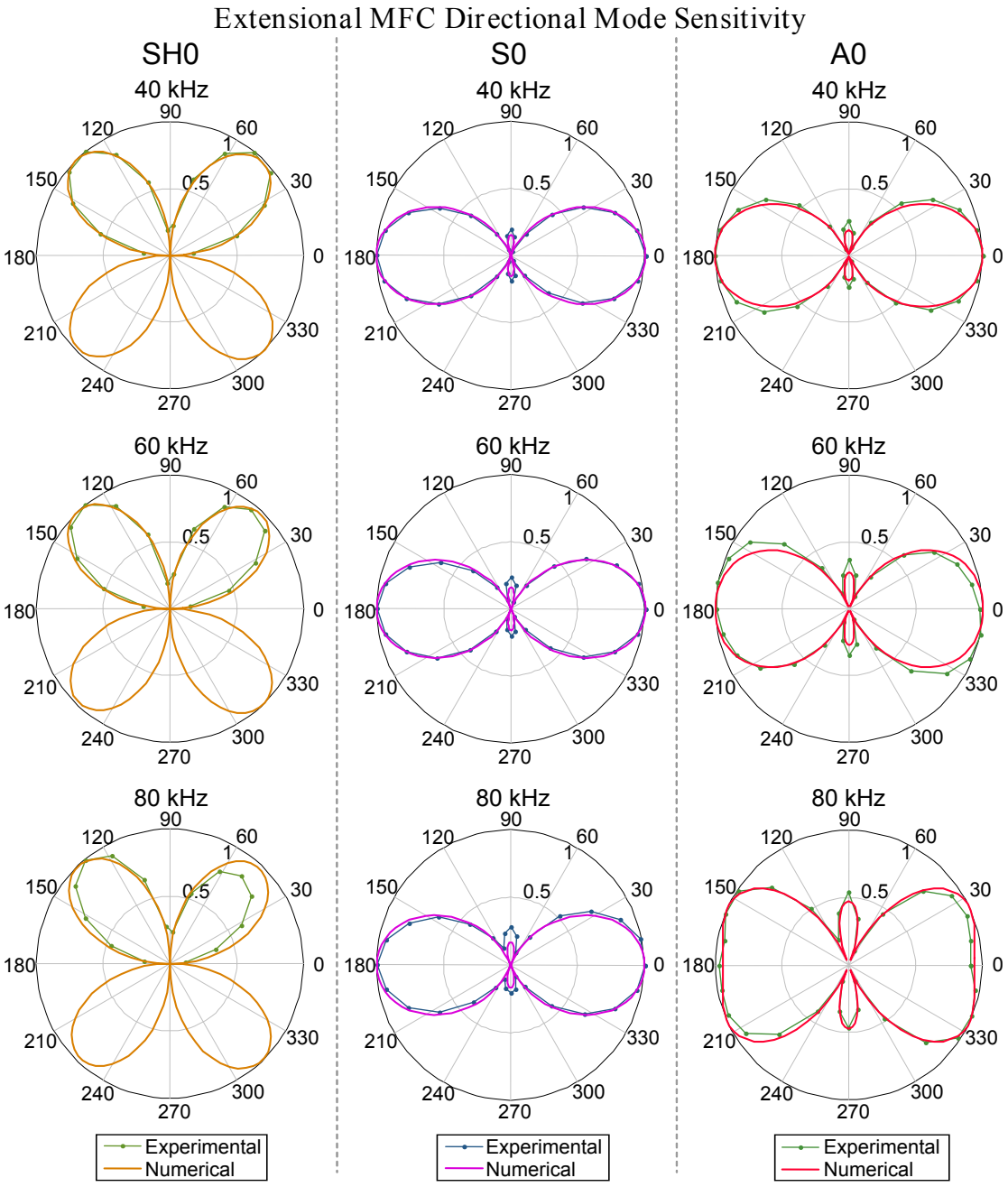

FIGURE 4.10: Experimental and numerical results for the MFC (bipolar) transducer that is predominantly sensitive to in-plane displacement in the $0° - 180°$ axis. The circumferential axes give direction and the radial axes give normalised amplitude in arbitrary units.

4.7 Summary

Through experimentation and simulation, the nature of the uniform in-plane transducer and the nature of the MFC transducer have been evaluated for low ultrasonic frequencies and compared. The experimental and simulated results for both transducer types were a close match. This indicated that the assumed behaviour of the transducers and the simulation are both valid. It was shown that the MFC transducer has significant sensitivity to shear waves in the diagonal directions, but not in the 90° or 270° directions. Unlike the MFC, the uniform in-plane transducer was observed to have a similar directionality to the theoretical point source. The MFCs are more suitable where the use of Lamb waves and directional sensitivity are required.

This approach yields information that can assist the development of transducer arrays. The point source superposition model used for simulation allows the directional wave mode sensitivity to be obtained relatively quickly when a transducer's vibrational behaviour is known. When it is not, the nature of the transducer can be hypothesised and simulated, giving results that can be tested experimentally. It is clear from the presented results that the MFC transducer has significantly different directional behaviour to the commonly available commercial guided wave transducer.

With knowledge of the inherent directional wave mode control of each transducer, it is possible to design an array to further enhance the wave modes of interest whilst reducing others. Enhancements in wave mode control of this kind can lead to improved methods of inspection with greater defect sensitivity.

To the best of the author's knowledge this is the first combined measurement and simulation of MFC wave mode directionality that considered both shear and Lamb modes for all directions. The Lamb mode sensitivity in the in-plane direction perpendicular to the piezo fibre axis is shown to be significant, which demonstrates that their sensitivity in this axis must be considered when MFC arrays are designed. This array design consideration is also required for the diagonal shear wave sensitivity that was measured and simulated.

Chapter 5

Adapting Macro Fiber Composite Transducers for Alternative Wave Mode Sensitivity

5.1 Introduction

The MFC actuator has been evaluated for its use as a transducer for transmitting and receiving ultrasonic guided waves. The MFCs are sensitive to in-plane strain; they are sensitive to a difference in the in-plane displacement between their extremes. On transmission at low frequencies where the MFC is smaller than the wavelength, the MFC acts as an extensional device with its extremes expanding apart. It has been shown in Chapter 3 that this bipolar nature causes the MFC to have a highly wavelength dependent sensitivity. In Chapter 4 it was shown this bipolar nature causes the MFCs to be poor at transmitting shear horizontal waves because the poles cancel the output in the direction that would otherwise be the strongest direction for this wave mode. There are many situations where a transducer is needed that can be selected to transmit and receive Lamb modes of a specific wavelength. However, there are other scenarios where this is not required and in fact shear horizontal modes are most desired [Alleyne et al., 2009]. Since the MFC transducer and transducers like it are not appropriate for shear horizontal modes, these scenarios cannot make use of the benefits of their form, namely their flexibility, low mass and low height.

In this chapter, a method of adapting the MFC transducer to maintain its benefits but to alter its wave mode sensitivity has been developed. The method uses a partial decoupling effect to alter the way ultrasonic guided waves are transmitted and received by the MFC transducer. This decoupling was assessed using finite element analysis. This method also modelled using the same directional, discrete point source modelling approach that has been developed in Chapter 4. This is again validated against an equivalent directional

wave mode measurement experiment. It is shown that the partial decoupling method is successful in significantly changing the MFC's directional wave mode sensitivity at the low ultrasonic frequencies evaluated. The MFC is changed from a bipolar device to act like a monopolar point source transducer. This gives it the advantage of having a high directional sensitivity to shear horizontal waves in a direction where its sensitivity to Lamb waves is low. The use of a weak shear coupling membrane to achieve the decoupling has meant that the MFC can be used as a dry coupled, force loaded device whilst retaining its low weight and flexibility.

5.2 Adaptation

The aim was to adapt the MFC to have strong tangential sensitivity to shear waves, in the same way that the monopolar transducer was found to in Figure 4.9. To maintain a low mass, low height and flexibility, the adaptation could not include the use of rigid interface pieces; instead the use of a film interface was considered. It was hypothesised that the bipolar nature of the MFC transducer could be changed to behave like a monopolar transducer by partially decoupling the active region using a poor coupling material. Previously a proposed nature for the fully coupled MFC (shown in Figure 4.6B) was hypothesised in the last chapter and was found to be accurate at predicting the directional transmission of the fundamental wave modes for wavelengths larger than the MFC length. Since what is required for this adaptation is to alter the bipolar nature to become monopolar, the desired nature of an adapted MFC is to have one side of the actuation caused by a fully coupled MFC. This desired nature is depicted in Figure 5.1.

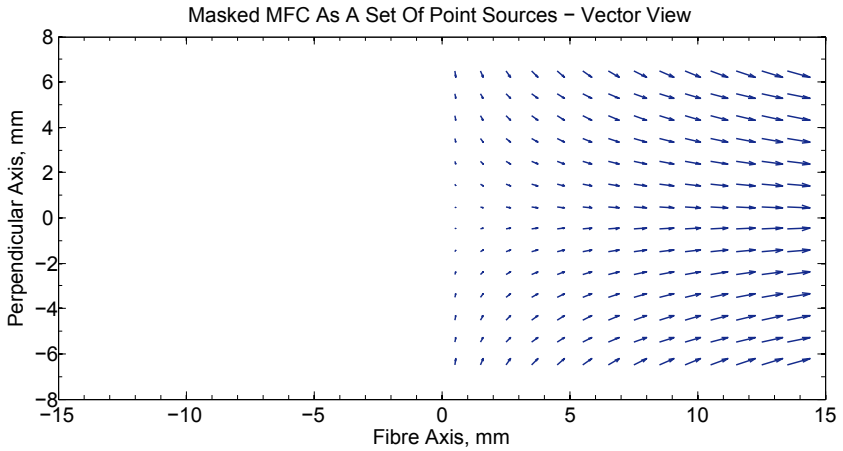

FIGURE 5.1: A prediction of the nature of the actuated vibration by a 50% coupled MFC based on the previous 100% coupled version shown in Figure 4.6B

A poor coupling layer is one that attenuates or reflects a high proportion of sound waves. A high reflection occurs when there is a great acoustic impedance difference between the two materials. When considering material choice alone (without also considering geometry) the decision can be made by comparing the characteristic acoustic impedances

for the two materials. The characteristic acoustic impedance for each material for a shear wave is considered, since the motion of the transducer is carried through to the structure via traction. The shear modulus for mild steel, G_{steel}, is in the region of 75 GPa and the density, ρ_{steel}, is approximately 7910 kg/m^3, giving a characteristic shear wave impedance, $Z_{shear-steel}$, approximately of 770.2 $GPa \cdot s/m$. The week shear coupling material was chosen as latex since this is widely available in a thin, flexible form, and its low density would facilitate a light solution. It was expected to perform well as a week shear coupling material because its shear modulus, G_{latex}, is extremely low being in the region of 0.5 MPa. It has a density, ρ_{latex}, in the region of 950 kg/m^3 and so the characteristic shear wave impedance, $Z_{shear-latex}$, was calculated to be approximately 0.7 $GPa \cdot s/m$. From this the shear wave reflection between a normal incident shear wave at a steel/latex boundary to be:

$$R_{shear} = \frac{Z_{shear-steel} - Z_{shear-latex}}{Z_{shear-steel} + Z_{shear-latex}} = \frac{770.2 - 0.7}{770.2 + 0.7} = 99.8\% \tag{5.1}$$

This calculation shows that an extreme proportion of the sound is reflected causing approximately a -54dB change in amplitude. This calculation is only accurate for bulk waves and when these material properties are accurate. It is unlikely to be accurate when considering the transfer of energy from an ultrasonic guided wave in a relatively thick steel plate to a patch of thin latex. However, it is a strong indication that this material is likely to be effective at decoupling traction between layers.

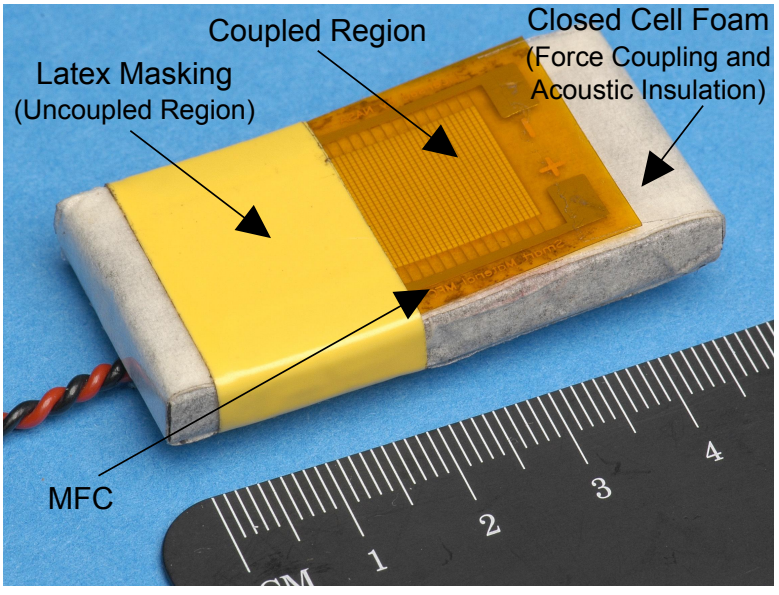

FIGURE 5.2: An example of a masked MFC for partial coupling. The area for good coupling can be coupled directly or, if a uniform MFC height is required, through a shim layer.

A model of the concept was produced (Figure 5.2), an initial test was conducted to confirm it had some lateral sensitivity to shear horizontal waves. The work conducted

within this chapter lead to the patent application (0716047.6 GB) [Mudge and Haig, 2010].

5.3 Decoupling Model

Finite element analysis was used to assess how a latex/steel interface piece would affect the reception characteristics of a in-plane strain sensing transducer like an MFC. The modelling for this scenario could be simplified by assuming a physical system that is infinite in one axis. Here a plate waveguide that was finite in the axis of propagation and of finite thickness, but infinite in the other in-plane axis, was used. Any materials in the transducer assembly were also considered infinite and uniform in this axis. The dynamic strain for the cross-section plane in the two non-infinite axes was modelled. This allowed the interaction between a passing ultrasonic guided wave and a transducer assembly (including coupling interfaces) to be assessed. This was done for a combination of thin interface materials. In each case the piezoceramic laminate was coupled to the plate via an interface layer, so that the interface geometry would not change for the different materials used.

The following interface conditions were modelled:

- Steel shim (Figure 5.4)
- Latex film (Figure 5.5)
- Left side void, right side steel shim (Figure 5.6)
- Left side latex, right side steel shim (Figure 5.7)

A 2m steel plate was chosen, a point at 2 m along was elected as the transmit position and another point at a further 2 m was chosen as the location of the receiving transducer position (Figure 5.3). A 175μm thick piezoceramic (PZT5A) lamina clad top and bottom in a layer of polyimide of thickness 40μm and length 28 mm was chosen as the receiving element. The transmission point was caused to excite an in-plane disturbance (in the non-infinite axis) dynamically described in time by an input signal. The input signal was a narrow band, 10 cycle, Hann windowed toneburst with a centre frequency of 30 kHz. This in-plane disturbance caused both the S0 and the A0 waves modes to be excited in both directions from the transmission point.

In the first model where the interface piece was entirely steel, that aim was to show the strain developed in the piezoceramic layer when no decoupling is applied. The result produced in each model was an animated field view of the cross-section showing in-plane strain in the direction of propagation. This was used because the MFC transducer is sensitive to strain in this axis. The frame from the simulation time of 546 μs from the

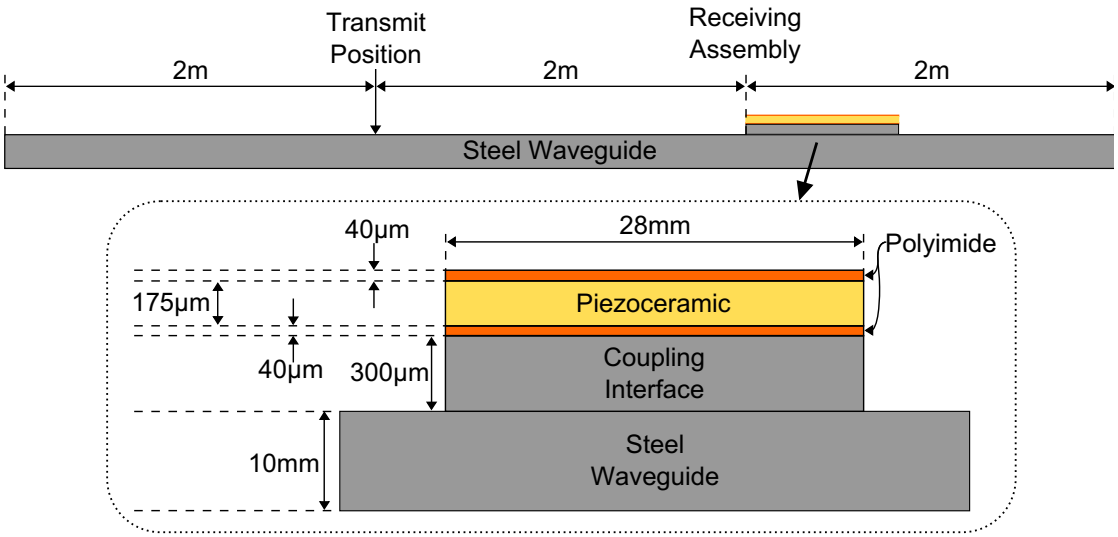

FIGURE 5.3: The schematic of the Finite Element Model used to represent a receiving Macro Fiber Composite transducer.

steel shim model is shown in Figure 5.4, and it can be seen from this example that the strain in the steel shim layer and the piezoceramic layer are similar to the strain developed in the surface of the steel when these layers make contact. At the ends of the piezoceramic lamina the strain is low, but this only occurs for a very short distance.

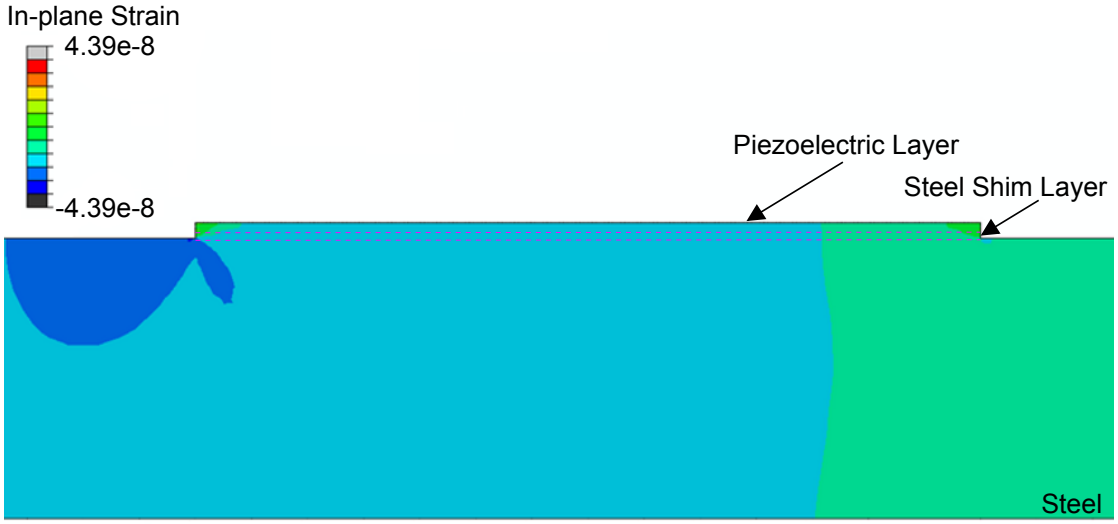

FIGURE 5.4: Finite Element Model showing the strain of a passing S0 wave in a steel plate with a piezoelectric layer (representing the MFC) coupled via a steel shim layer.

Figure 5.5 displays a frame, again at 546 μs, of a model with identical conditions except that the interface material has been changed from steel to latex. The strain developed in the piezoceramic layer this time is very low and it can be seen the latex has been very effective as a decoupling material.

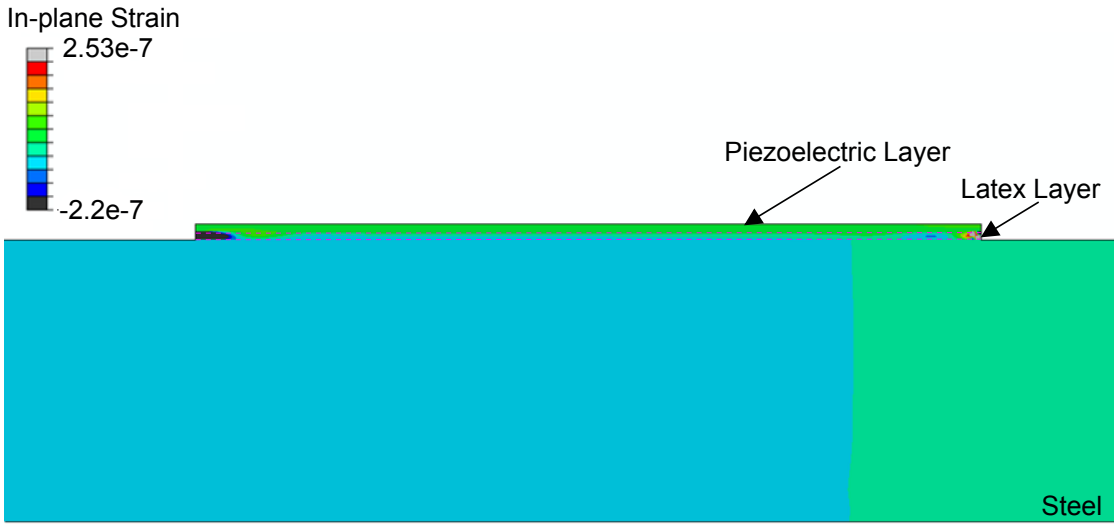

FIGURE 5.5: Finite Element Model showing the strain of a passing S0 wave in a steel plate with a piezoelectric layer (representing the MFC) coupled to it via a latex layer.

The finite element mesh was redefined to split the interface material into a left side and a right side. Two further simulations were run where firstly the left side of the interface was removed (leaving an empty void) and the right side was steel, and again with the left side being latex and the right steel. Frames for the time 546 μs are given for these two cases respectively in Figures 5.6 and 5.7. Here the strain in the piezoceramic is similar for both when the left side of the interface is a void and when it is latex. A void is not practical experimentally because the flexibility of the MFC will mean that it is difficult to keep the waveguide and this side of the MFC apart. This does show that, according to this simulation, the addition of the latex material has little effect on the sound energy existing in the piezoceramic.

The coupled side of the piezoceramic inherits the strain of the waveguide, as was seen with the fully coupled version. Displacement in the right side of the piezoceramic lamina causes sound energy to enter the left hand side causing a ringing effect with high strain.

5.4 Adapted Pulse-Echo Response

The modelling indicated that ringing could be expected in the decoupled portion of the MFC transducer. The frequency dependent characteristics were expected to be more complex. This may cause the MFC to transmit or receive elongated pulses or reduce the working amplitude. To assess the changes in characteristics, another bar test was devised to assess the pulse-echo characteristics when fully coupled and partially decoupled with a latex mask. The primary application for partially masked MFC transducers would be for generating shear horizontal waves. However, since placing an MFC laterally on a small bar is not possible, the initial experiment was conducted using Lamb-equivalent

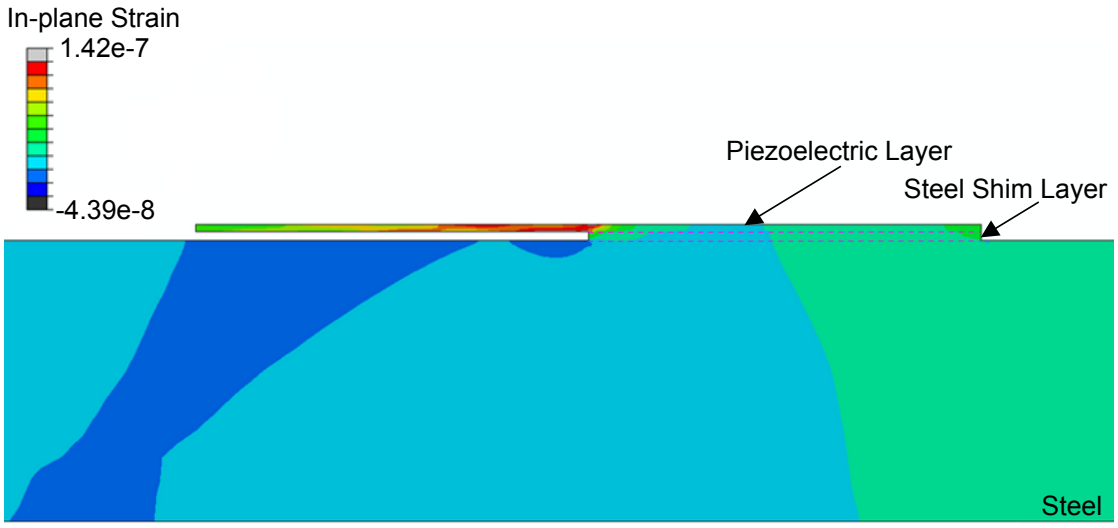

FIGURE 5.6: Finite Element Model showing the strain of a passing S0 wave in a steel plate with a piezoelectric layer (representing the MFC) coupled on one side via a steel shim layer. The other side of the piezoelectric layer is decoupled with a material free gap.

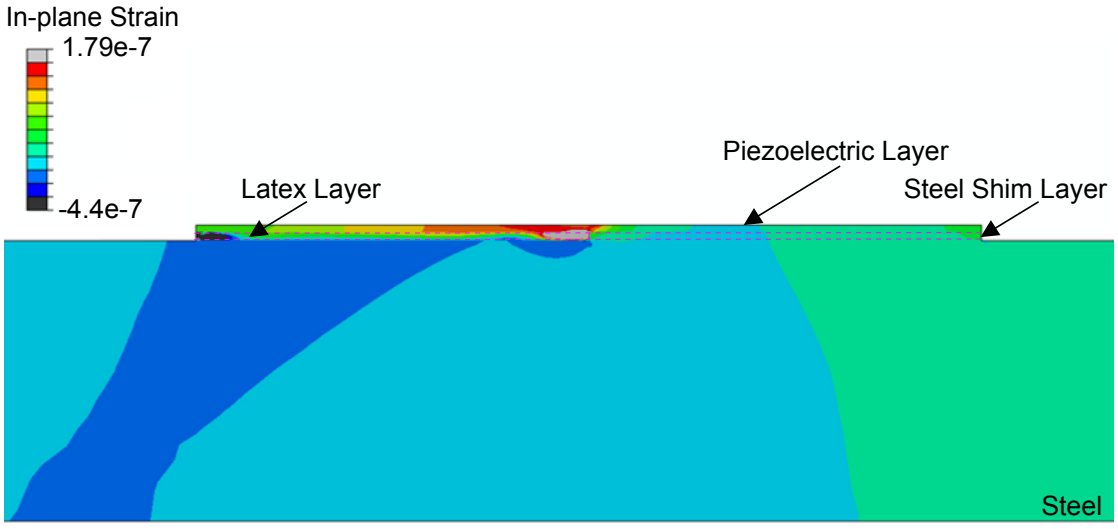

FIGURE 5.7: Finite Element Model showing the strain of a passing S0 wave in a steel plate with a piezoelectric layer (representing the MFC) coupled on one side via a steel shim layer. The other side of the piezoelectric layer is decoupled with a latex layer.

waves. A further plate test to assess their ability to generate the fundamental shear horizontal mode is given in Section 5.5.

If a latex interface piece was placed on only one side of the MFC, then this would result in the undesired bending of the MFC transducer when the coupling load was applied. To avoid this, another interface piece is required on the other side. It was decided that the material of the interface piece for the coupled side should be made of the same material as the waveguide to avoid reducing the coupling efficiency. Latex film was acquired with a thickness of 0.3 mm and steel shim was acquired with a thickness of 0.25 mm. The

latex was taped in place on the waveguide with some tension in it to reduce its thickness to approximately the same as the steel shim. Aluminium shim of this thickness could not be acquired and so a steel shim and a steel bar were used.

The bar was 3.1m long and had a square cross-section with a thickness of 19 mm. An MFC of active length 85 mm and a width of 7 mm was used for experimentation. It was placed with its centre in the middle of one face of the bar at a distance of 1m from one end of the bar. The MFC was aligned with its fibres in the major axis of the bar. A silicone closed cell foam pad of 85 mm by 7 mm and thickness 6 mm was placed over the active area. The pad was compressed with a steel block with a force of 200 N, measured with a load cell supporting the bar.

The method of exciting a chirp signal with a flat amplitude between 30 and 140 kHz that was used in Chapter 3, was used again for this experiment. Two cases were tested where in the first case the MFC was coupled directly to the bar (as was the case in Chapter 3) and in the second test the MFC was coupled via an interface piece with one side of latex and one side of steel.

Spectrograms and the measurement of the Symmetric 0 mode amplitude for both cases are given in Figure 5.8. The short length of the bar has meant that ringing effects from non-propagating modes has affected the measurements at some frequencies (namely 82 and 112 kHz). The overlap between the fundamental asymmetric and symmetric modes above 90 kHz also compromises measurement in this range. Below 70 kHz the measurement of the amplitude of Symmetric 0 is unaffected by these influences.

The amplitude measured from these signals (using the split spectrum method used in Chapter 3) of the Symmetric 0 mode is shown in Figure 5.9 for both cases.

The maxima at 40 kHz in the case where the MFC is directly coupled, is a minima in the partially decoupled case. However, the partially masked MFC is still capable of transmitting and receiving Lamb waves, and the amplitude drop at some frequencies is not significant. This implies that a partially masked MFC can be used for some applications.

5.5 Measurement of Directional Sensitivity

In Chapter 4 a method of both experimentally measuring the directionality of a transducer and modelling its directional performance was presented. This method has been applied to the case of a partially decoupled MFC using the assumption that the disturbance it creates is equivalent to one side of the a fully coupled MFC (as was depicted in Figure 5.1).

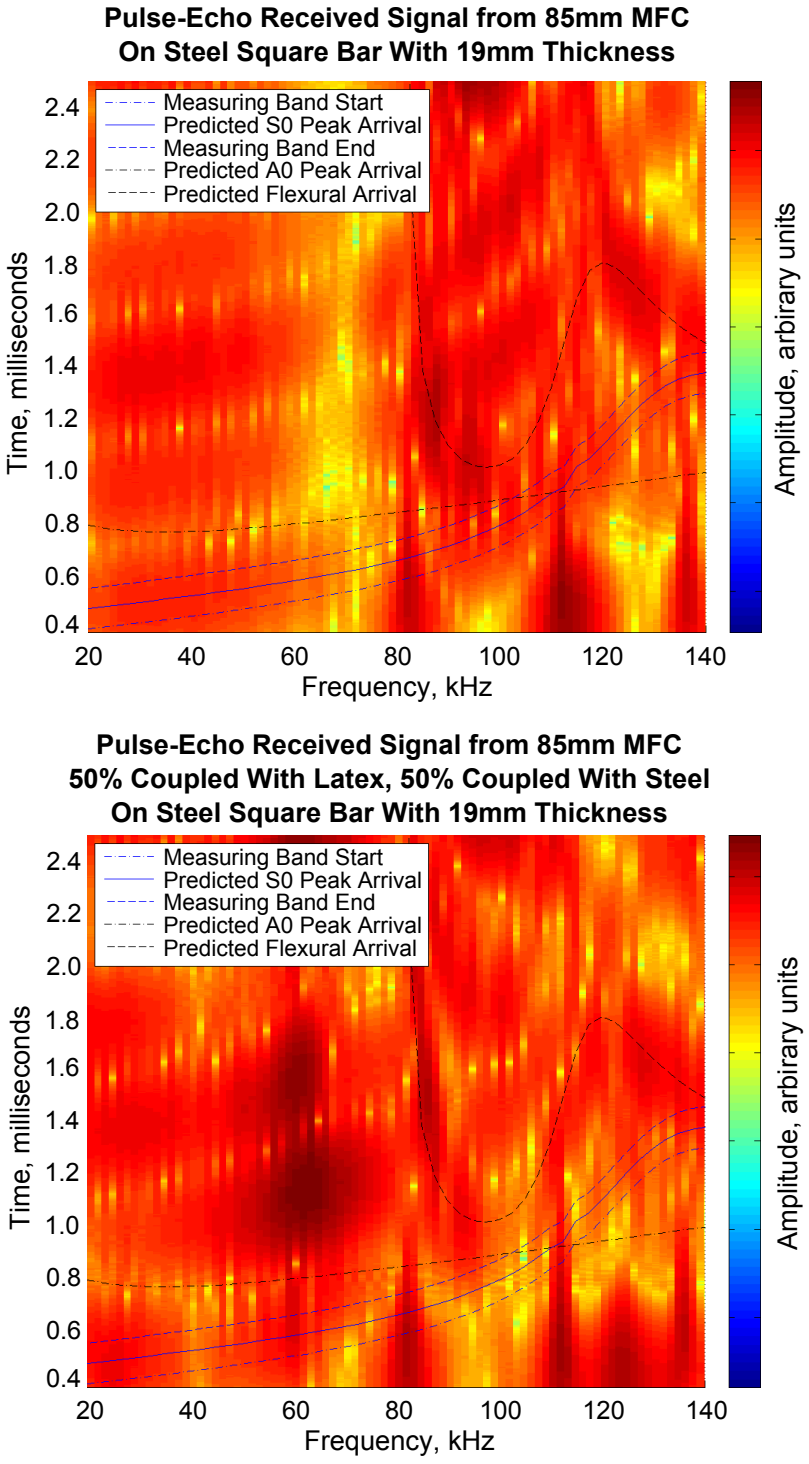

FIGURE 5.8: A comparison of the frequency response of an MFC transmitting the Symmetric 0 wave mode in a steel bar when fully coupled and with 50% of the active area decoupled using a latex masking.

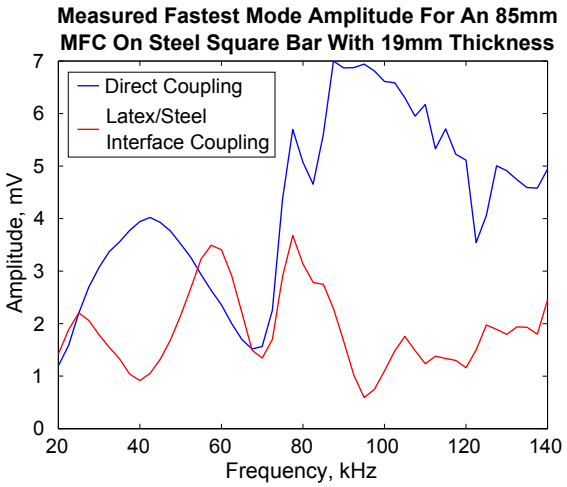

FIGURE 5.9: A comparison of the MFC frequency response for the Symmetric 0 wave mode in a pulse-echo test when either coupled directly or when partially decoupled.

The experimental setup and approach given in Section 4.5 was repeated for the MFC with a partial decoupled interface in place. The MFC had an active area of 28 mm (in the fibre axis) by 14 mm (in the perpendicular axis). The active area was considered in two equal parts where the split between the two occurred in the centre of fibres. This way all fibres began on one side and ended on the other. As before, one side was masked with a latex film.

Measurements were carried out as before using the same averaging method to normalise the measurements. The results for all three fundamental modes for the test frequencies of 40, 60 80 and 100 kHz are given in Figure 5.10. This shows that partially decoupling the MFC with a masking film has dramatically changed the directional wave mode sensitivity.

The fully coupled MFC had no lateral sensitive to shear horizontal waves and had significantly frequency dependent directional sensitivity to the Lamb modes (as was shown in Figure 4.10 in Chapter 4). However, the adapted MFC behaves much more like the monopolar transducer (as was shown in Figure 4.9), in that it behaves like an in-plane point source transducer. It has gained lateral sensitivity to the fundamental shear horizontal wave mode. From the 40 kHz and 60 kHz result, it can been seen that at low ultrasonic frequencies the SH0 output is highest in the lateral directions, and this lateral output is symmetric around the $90° - 270°$ degree axis. Unlike the results presented for the reference transducer there is no rotational offset and so present a closer match to the model prediction.

In this case there is good agreement between the simulation and measured results below 100 kHz. It is interesting to note that as the frequency is set to 80 and 100 kHz, the match with the simulation (using the hypothesised nature of the MFC) becomes less accurate. At these frequencies the measured results demonstrate a rotation of the sensitivity of the

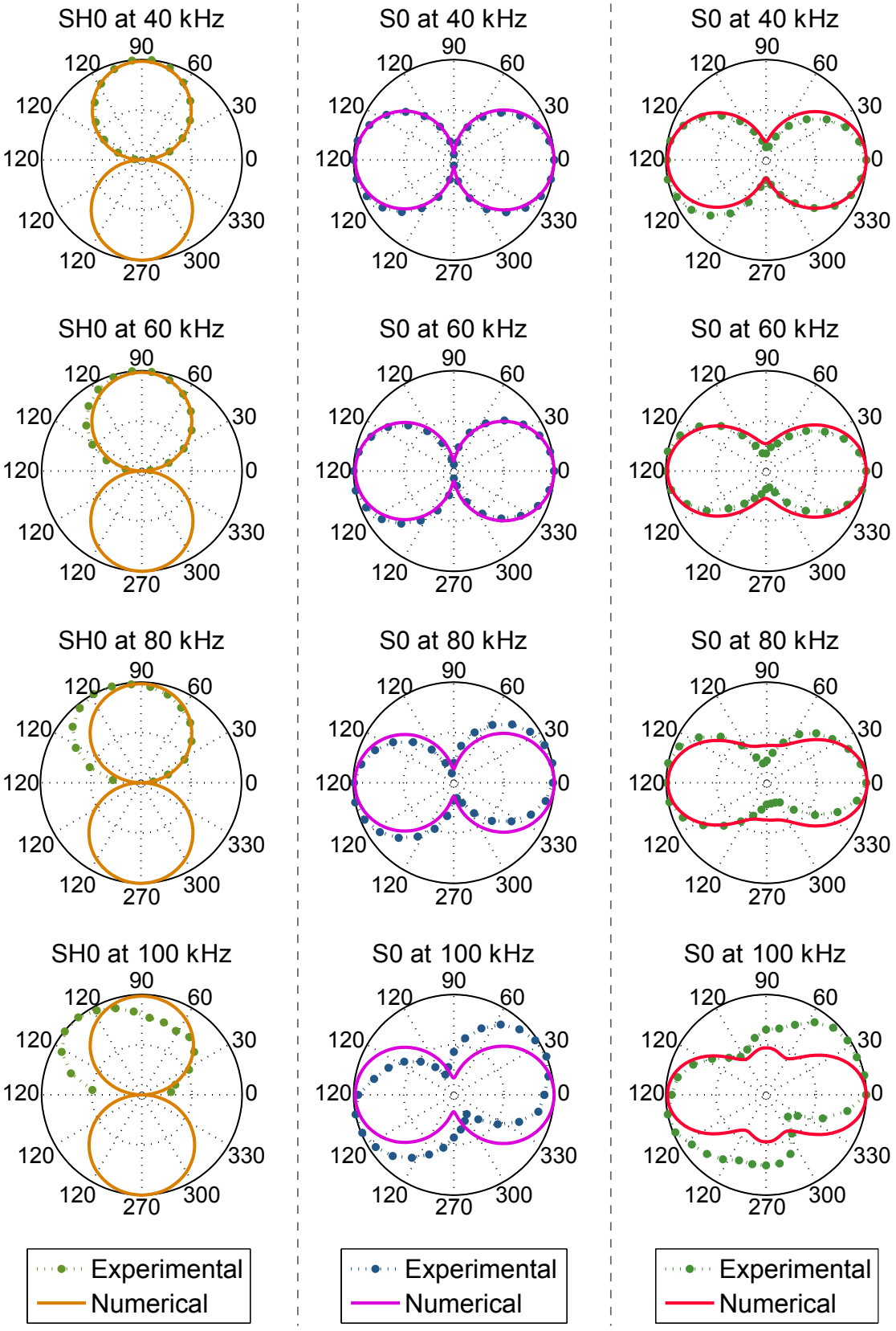

FIGURE 5.10: Experimental and numerical results for the masked MFC (adapted to be monopolar) transducer that is predominantly sensitive to in-plane displacement in the $0° - 180°$ axis. The circumferential axes give direction and the radial axes give normalised amplitude in arbitrary units.

MFC, which implies that the vibrational characteristics change from being orientated mainly in the fibre axis to being aligned in a direction that is diagonal across the MFC.

5.6 Summary

The hypothesis that an MFC will have significantly different wave mode sensitivity to a fully coupled MFC was confirmed. It was demonstrated that a latex membrane could be used to decouple part of the active area of an MFC transducer whilst a coupling pressure over the MFC allowed the rest of the active area to couple as normal. This method of decoupling was assessed using a combination of finite element analysis, analytical simulation and experimental measurement. The model of transducers directional transmission was used for the adapted MFC and found to adequately predict the change in the MFC's performance at the low ultrasonic frequencies evaluated.

This partial decoupling gave rise to directional characteristics similar to the more conventional uniform in-plane transducer, where the transducer has a high sensitivity to shear horizontal modes and a low sensitivity to Lamb modes at right angles to the transducers' main axis of displacement. It was shown that an MFC assembly with a latex masking retains the benefit of being low weight, low height and flexible. This can be used alongside a coupled shim layer to maintain a constant height across the MFC. A patent application has been filed for this method of adapting an MFC or similar transducer [Mudge and Haig, 2010].

This adaptation makes the use of MFC transducers for testing with shear horizontal wave modes feasible, and in the next chapter it is shown how the application of pipe testing using the adapted MFC transducer was achieved and how this may lead to improved inspection equipment.

Chapter 6

Development of Macro Fibre Composite Arrays for Multi-mode Pipe Inspection

6.1 Introduction

In this chapter, MFC arrays that allow inspection using both longitudinal and torsional wave modes are shown to be possible, with performance enhancements over equivalent commercial equipment. Fully coupled MFC transducers, as characterised in Chapters 3 and 4, are used in an arrangement for longitudinal waves, whilst MFC transducers partially decoupled using a latex membrane, as developed in Chapter 5, are used in an arrangement for torsional waves. The wave mode control limits of the arrays are found through experimental measurement and array design criteria for managing wave mode control are discussed. The MFC transducers have form characteristics that offer practical advantages, namely they are thin film devices that have a relatively low weight and are flexible, and so equipment made with them will also have a low profile and weight, which is of benefit to industry. It was shown that with partially decoupled MFC transducers for torsional wave it was necessary to have a high density of transducers to eliminate their sensitivity to circumferential waves over the frequency range of interest. It was also shown that the fully coupled MFC transducers for longitudinal waves do not suffer the same degree of lateral wave transmission and have a lower noise contribution by circumferential waves than partially decoupled MFC transducers (and indeed the conventional in-plane point source transducer that is used in the commercial equipment).

6.1.1 Pipeline Inspection Using Ultrasonic Guided Waves

Mohr and Höller [1976] first considered the non-destructive testing of tubing using ultrasonic guided waves. Further testing was demonstrated by Silk and Bainton [1979], from which the popular naming scheme for ultrasonic guided waves in pipes is taken. A great deal of work, particularly in the last two decades, has been conducted into various methods of manipulating ultrasonic guided waves in pipes for defect detection and sizing [Schneider, 1984, Böttger et al., 1987, Alleyne and Cawley, 1996a, Alleyne and Cawley, 1997, Hirao and Ogi, 1999, Alleyne et al., 2001, Mudge, 2001, Kwun et al., 2001, Rose, 2002, Hay and Rose, 2002]. In the last decade a number of organisations have developed products and services for conducting Long Range Ultrasonic Testing of pipes using guided waves of this kind.

As with plates, there are three fundamental wave modes that can exist in hollow cylinders. This is complemented with a complicated set of higher order modes. A discussion on pipe wave modes and their nomenclature is given in Section 2.3.2 of Chapter 1. Most techniques for pipe testing are based on a pulse-echo method where an array of transducers is used to isolate a single wave mode in transmission and reception. The velocities of the wave modes can be calculated based on the material properties and the tube geometry. Since the velocity is known, the time of arrival of reflected signals can be related to distance. In some applications, multiple wave modes are used together in transmission and/or reception to gain greater sensitivity and sizing capability [Rose et al., 2003, Hayashi et al., 2003, Catton, 2009].

In any case an excitation method must be used that is capable of exciting and receiving the modes of interest without exciting other modes. An additional requirement may be that the equipment should select the direction along the pipe in which to transmit and receive.

6.2 Development Of MFC Arrays for Torsional Waves

The directionality for an MFC without adaptation for the fundamental plates waves was giving in Section 4.6 of Chapter 4. This showed that when the active dimensions of the MFC were lower than a wavelength, the MFC had significant sensitivity in the diagonal axes. This showed that an MFC can be used to generate and receive shear horizontal waves, albeit also with some sensitivity to other modes. Alternatively, in Section 5.5 of Chapter 5 it was shown that, at these same frequencies, an MFC transducer can be adapted using a method of partial decoupling to give the MFC lateral sensitivity (at 90° to the fibre axis) to shear horizontal modes where the sensitivity to the Lamb modes was found to be significantly low.

The author built an MFC based pipe inspection tool using the partially decoupled MFC method, whilst a fellow researcher, Chaston [2009], developed an alternative torsional wave pipe inspection array using MFCs placed with an angular off-set. The performance of both methods is compared here. To put the performance into context, a commonly used commercial tool known as Teletest is also compared [Jackson, 2011].

Each of the two researchers constructed a tool of their own design. Each tool was constructed using 28mm by 14mm P1 MFC transducers as described in the data sheet in Appendix A [Daue, 2011]. The layout of the angled MFC tool can be seen in Figure 6.1 and the layout of the adapted MFC tool can be seen in Figure 6.2. The backing materials for both were closed cell foam found to be effective in initial trials by the author. The design criteria for the angled approach will not be discussed in this thesis. Both tools were developed for the inspection of an 8 inch schedule 20 pipe. Both tools were designed to use the same clamping mechanism, which consisted of an air bladder housed within a steel clamp. The air bladder is placed over the MFC layer and pneumatically loads the MFC array onto the test surface (Figure 6.3).

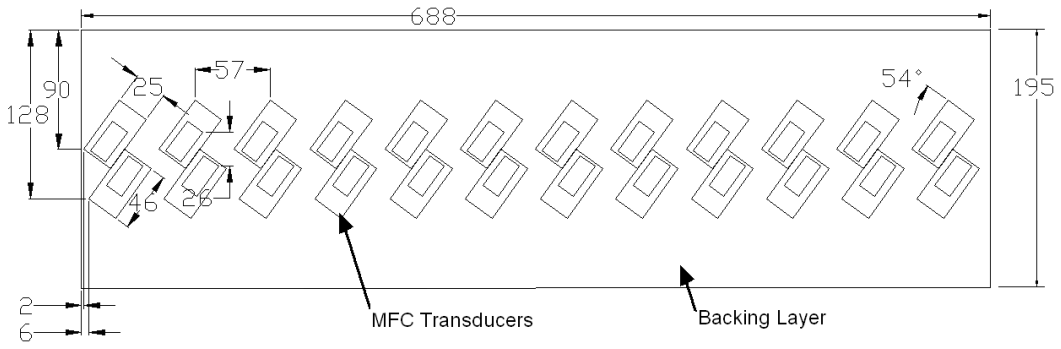

FIGURE 6.1: Layout of the angled MFC transducer array for torsional waves as developed by Chaston [2009]. The MFC transducers used were the 28mm by 14mm P1 type provided by Smart Material GmbH Appendix A

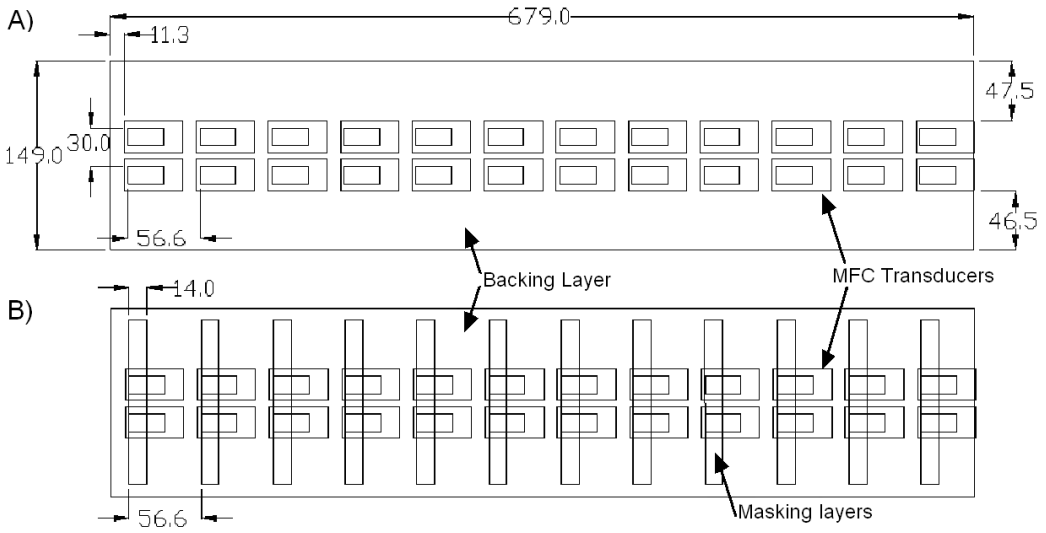

FIGURE 6.2: Layout of the adapted MFC transducer array for torsional waves. The two views show the tool with and without the masking layer. The MFC transducers used were the 28mm by 14mm P1 type provided by Smart Material GmbH Appendix A

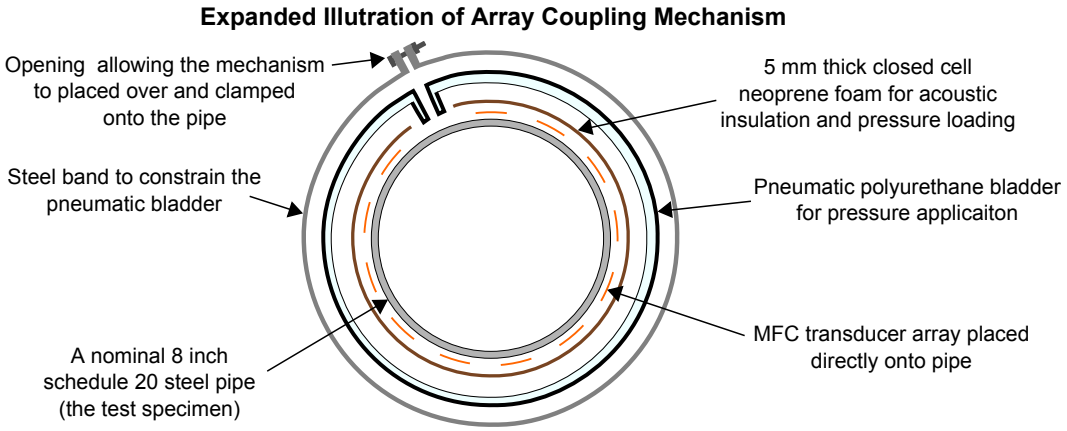

FIGURE 6.3: An illustration showing an expanded view of the pneumatic bladder method for dry force coupling an MFC array around a pipe.

6.2.1 Test Setup

The tool was tested on a pipe as shown in Figure 6.4. The left end of the pipe will be used as a fixed point of reference for all measurements.

The group velocity dispersion curve for an 8" schedule 20 pipe can be seen in Figure 6.5. T(0,1) is the principle shear wave in this test structure and is non-dispersive.

A commercial system was also included in the comparison. This was a tool known as Teletest made for testing with both longitudinal and torsional waves and provided by Plant Integrity [Jackson, 2011]. Having two rings (circular rows oriented circumferentially) in each array allows for transmission in a single direction along a pipe. To achieve

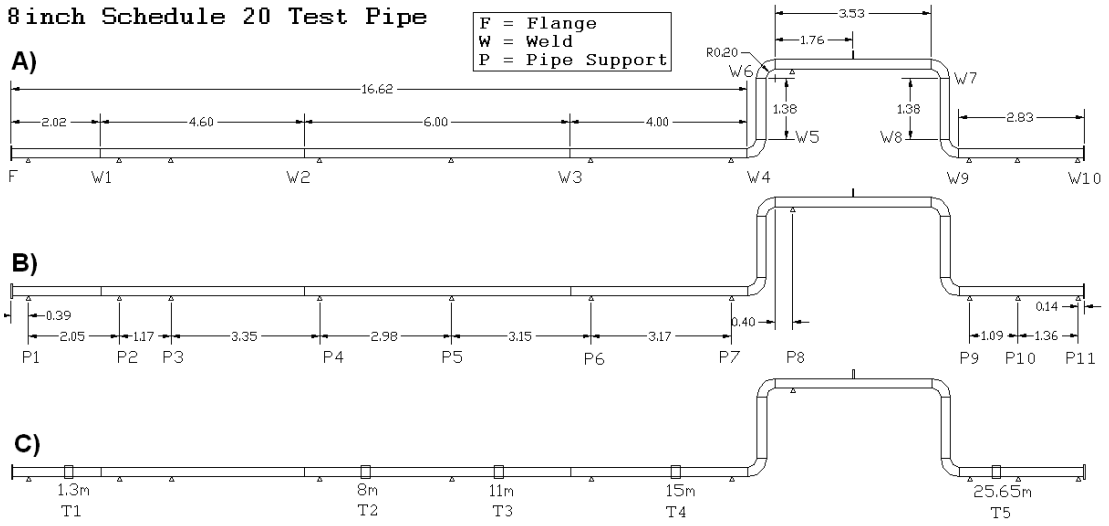

FIGURE 6.4: An 8 Inch Nominal Pipe Size Schedule 20 (Standard ASME B36.10M) Steel Pipe. A) shows the position of the welds, B) shows the position of the pipe supports and C) shows the locations selected to be potential test locations

this, the transmit signal for one ring is inverted and delayed by a time equal to the propagation time between the two rings (e.g. the ring separation distance divided by the phase velocity of the wave at the test frequency). The result is that in one direction the signals from each ring cancel out exactly, but in the other direction they do not for most frequencies. This is why the output performance varies by frequency. The two ring torsional output curves for the 26 mm ring spacing angled MFC tool, the 30 mm spacing masked MFC and Teletest tool can be seen in Figure 6.6. These have been calculated assuming a continuous sinusoidal output from the individual rings. The masked MFC and Teletest output has been calculated assuming two unidirectional rings and the angled MFC tool output has been calculated assuming the two rings of bi-directional transducers act as four unidirectional rings.

6.2.2 Signal Quality

The pipe was inspected with the tool at the 15 m location (see Figure 6.4). The conventional and angled MFC tools were both used with the collar inflated to 60 p.s.i (413.7 kPa). A 10 cycle Hann windowed pulse was used for excitation. Each test shot was taken 64 times and the average of the signal was used so that environmental noise would be reduced.

The lines of transducers in each tool were coupled around the pipe in rings. Each ring of transducers recorded a wave passing at various circumferential positions. The sum of the signals from all transducers in one ring will give the signal for only the axisymmetric modes. The signals from the pairs of rings are combined with an appropriate time delay

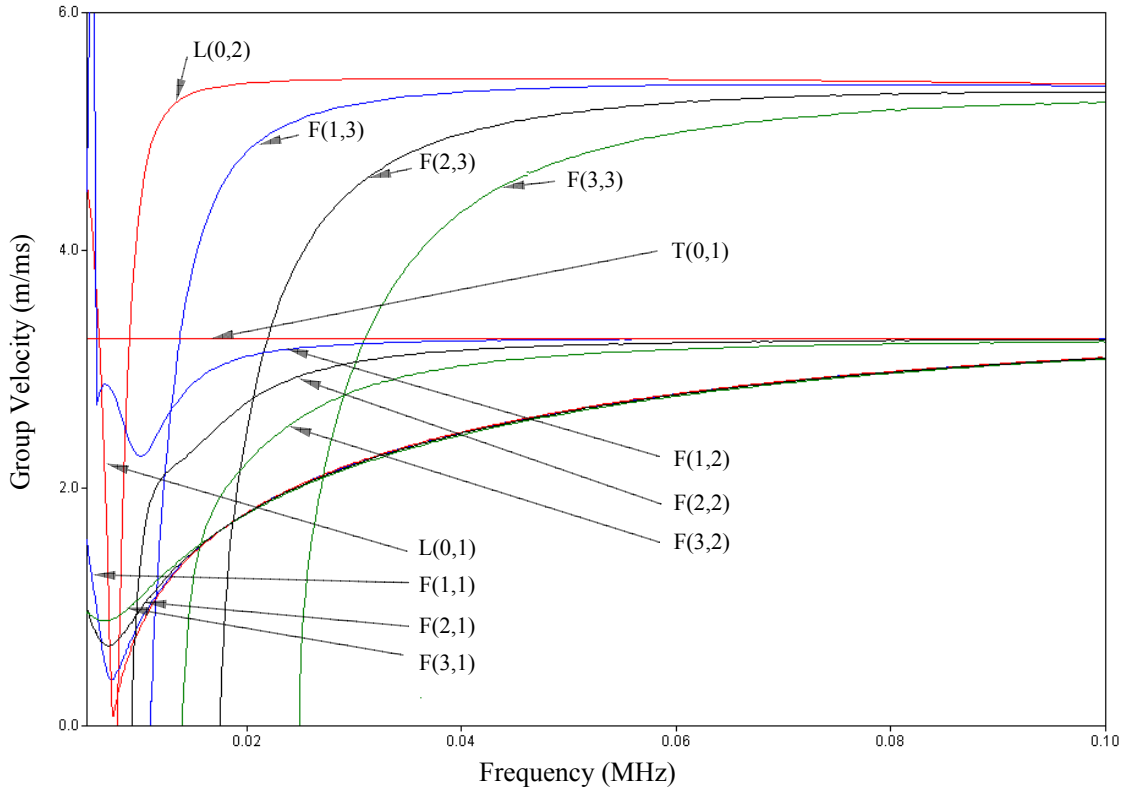

FIGURE 6.5: Group velocity dispersion curves for an 8 inch schedule 20 steel pipe.

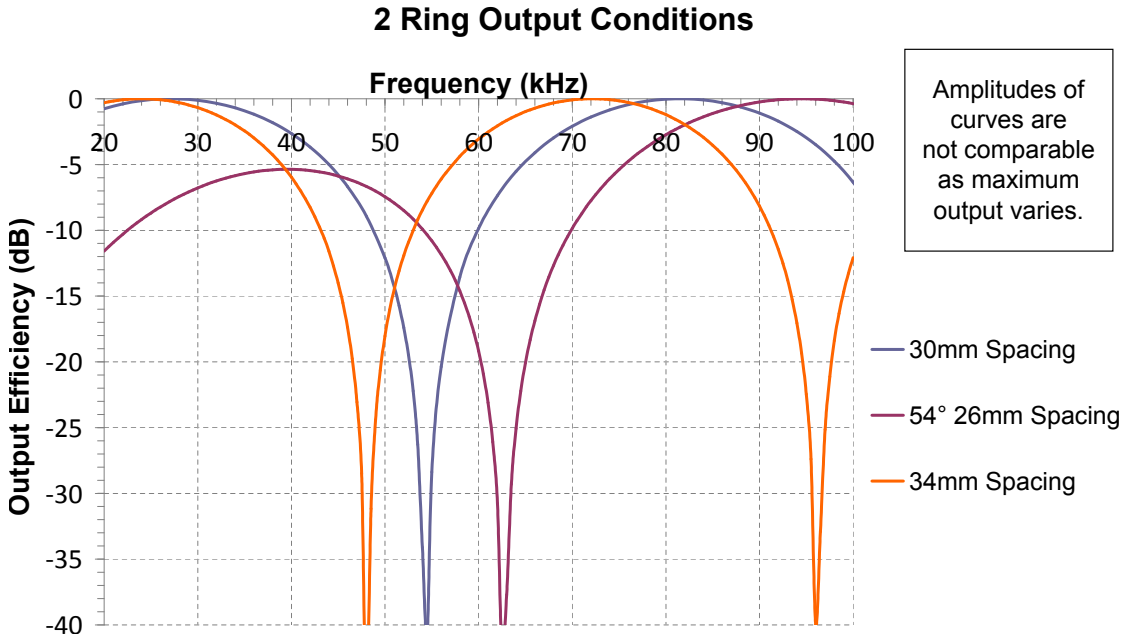

FIGURE 6.6: Calculated array element superposition effect on output amplitude for each tool type.

to eliminate signals from one direction. This reduces the signals to show just symmetric waves from one direction, which should make the identification of features unproblematic.

To understand the best results that each tool can achieve, an example A-Scan (a time varying amplitude signal) has been selected for each at a frequency that shows the highest clarity. Figure 6.7 shows a signal gathered from the commercial tool, Figure 6.8 shows signal gathered from the angled MFC prototype and Figure 6.9 shows signals gathered from the masked monopolar MFC prototype. Each graph is also marked with the predicated arrival times of peaks from each feature near the tool. The signals have been processed to remove peaks from features in the forward direction. Signal clarity can be judged as the amplitude of the peaks that correspond to features in the backward direction against any other period of the signal. Other time periods may include unwanted peaks from the forwards direction, peaks from unwanted modes or incoherent noise. The transmitter/receiver unit cannot receive until transmission has ended which is why all three signals have a blanked period at the beginning.

The signal from the commercial tool shows a number of undesirable features. Firstly, there is a great deal of noise following the blanking period which is likely to be due to the transducers continuing to vibrate after transmission. This shows that the coupling between the transducers and the test piece is poor and the dampening within the transducer is insufficient. This noise will prevent the detection of defects near to the tool, effectively extending the blanked zone. There is also a great deal of incoherent noise, so called due to its consistency throughout the signal. This is likely to be caused by higher order modes generated by the tool. This, again, is a sign of poor coupling as a perfectly coupled tool would not generate these modes. The suppression of the forward signals is good and the amplitude of the peaks is typical of such a tool.

The angled MFC tool shows the peaks from the features in the backwards direction. Unfortunately, peaks in the forwards direction are also detected. Also, other large peaks correspond to the faster longitudinal mode, which occurs in both directions. Most notable is the longitudinal response from the flange showing up at approximately 0.0057 seconds. These three sources of unwanted peaks make any judgement about coherent noise difficult. The overall signal amplitude is lower than that of the commercial tool and defect detection would be more problematic due to the number of unresolved responses.

The adapted MFC tool shows an amplitude increase of over 9 dB in comparison to the commercial tool. The ringing is considerably lower, as is the coherent noise. It is difficult to attribute any peak to a feature in the forward direction or to peaks of the longitudinal mode. In general the masked MFC tool is generating torsional waves at various amplitudes and with very good coupling in comparison to the commercial tool and the angled MFC method.

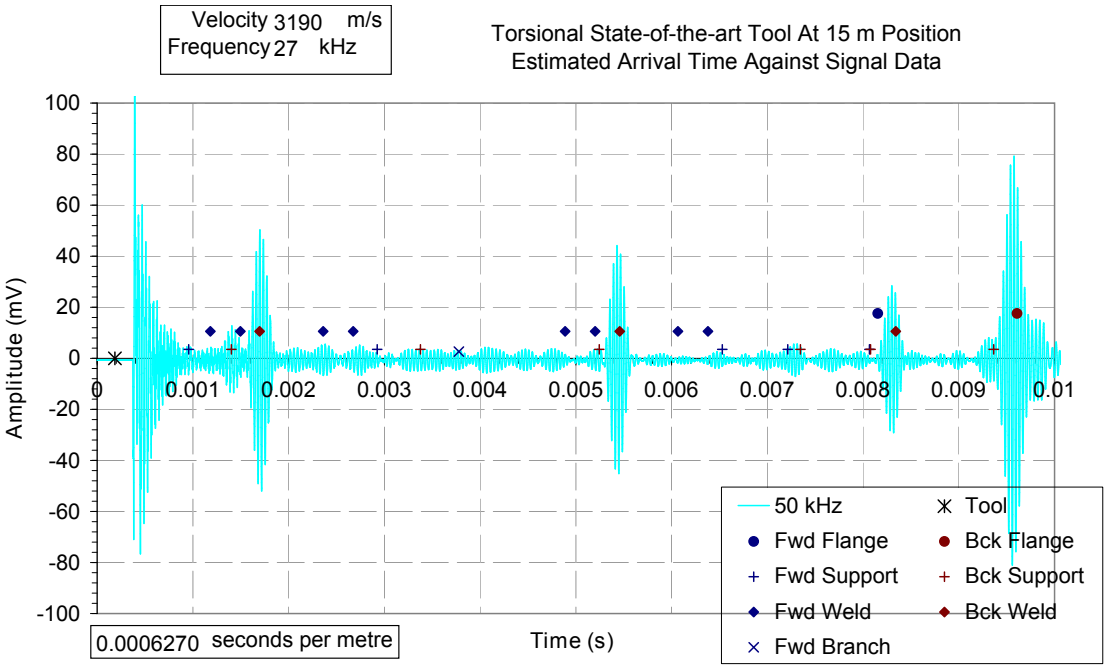

FIGURE 6.7: A-scan signal quality for a commercially available pipe inspection tool using monolithic piezoelectric transducers.

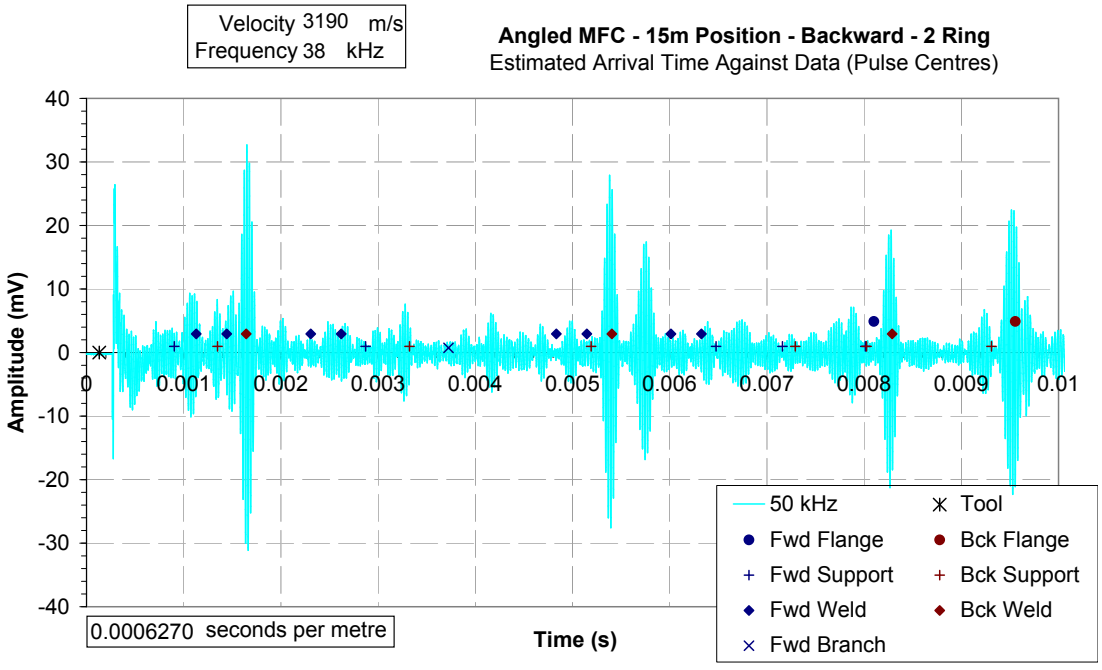

FIGURE 6.8: A-scan signal quality for pipe inspection tool using angled Macro Fiber Composite actuators.

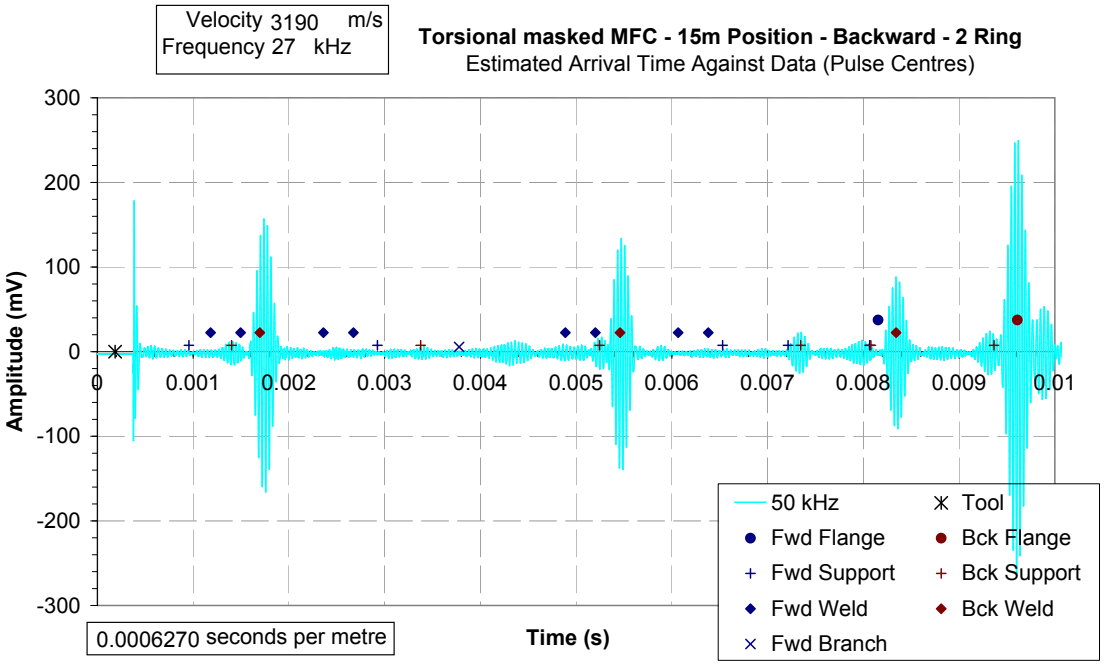

FIGURE 6.9: A-scan signal quality for pipe inspection tool using monopolar adapted Macro Fiber Composite actuators.

6.2.3 Frequency Response

Typically Long Range Ultrasonic Testing of pipework is conducted at a centre frequency within the range of 30 to 100 kHz. It is necessary to examine the ability of each method to excite a torsional wave (an axisymmetric shear wave in a tubular structure) without generating unwanted acoustic signals. Once again the 15 meter position was chosen for all tools tested. As the precision of the direction selection method may be frequency dependent, no directionality was used and only a single ring for transmission and reception was required.

Each tool was mounted into position and a pulse echo A-Scan was recorded for frequencies between 30 and 100 kHz, with 2 kHz iteration steps. Figures 6.10, 6.11 and 6.12 show samples of the data recorded. Figures 6.13, 6.14 and 6.15 show an analysis of the amplitudes recorded within time bands shown in Figures 6.10, 6.11 and 6.12 respectively.

It can be seen in Figure 6.10 that the conventional method is capable of generating and receiving torsional waves throughout the tested frequency range. Amplitude is higher at lower frequencies. At 60 and 70 kHz at least one unwanted wave mode is obfuscating the torsional responses beyond 4 meters from the tool. This is likely to be a high order flexural mode, which could occur if the transducers in the tool were not consistently coupled. It can also be seen that noise following the blanking period occurs at all frequencies shown. Figure 6.13 confirms an essentially linear decrease in signal

amplitude from 30 to 100 kHz. It can also be seen that the issue of unwanted flexural modes occurs between 50 and 80 kHz, with greatest effect at 62 kHz.

The A-Scan data for the angled MFC tool (shown in Figure 6.11) is difficult to compare with those of the conventional tool as the amplitudes of the torsional wave peaks are not significantly greater than those of the longitudinal waves at any frequency. As the longitudinal waves are dispersive, the arrival time of the longitudinal peaks is frequency dependent. This gives rise to complex signals and measurement of noise is difficult. Figure 6.14 confirms the likelihood that at no frequency is the torsional amplitude greater than the longitudinal amplitude. It also shows that amplitude of both modes is low below 50 kHz, although the amplitude of both modes are higher than those seen from the commercial tool.

The A-Scan results for the masked approach, shown in Figure 6.12, show good correspondence with that of the commercially available tool. However, the noise effect of unwanted wave modes is not seen. There is significant noise occurring at 70 kHz. However, as this begins immediately after the blanking period it is unlikely to be due to flexural modes. At other frequencies the period following the blanking period shows little noise, which is an improvement over the commercially available tool. Figure 6.15 shows very high amplitude signals and low noise (particularly between 40 and 66 kHz). Between 68 kHz and 90 kHz the noise pattern seen in Figure 6.12 increases the noise amplitude. At this stage in the experimentation the source of this noise is unknown and is explored in section 6.4. The torsional wave amplitude appears to have two maxima. The amplitude drops at higher frequencies, but is still considerably higher than that of the commercially available tool.

6.2.4 Torsional Tool Summary

The commercially available tool shows that features such as pipe supports, welds and flanges give clear responses for torsional wave, pulse echo testing. It was also shows that two ring arrays facilitate good inspection direction selection. The frequency response of this tool was acceptable between 30 to 50 kHz and 80 to 100 kHz. However, unwanted wave modes made the range 50 to 80 kHz which is poor for inspection. This and other noise issues indicate that the commercially available tool suffers inconsistent coupling efficiency between transducers.

The angled MFC tool demonstrated that it was possible to generate torsional waves with adapted (bipolar) MFC transducers. Selective excitation of torsional waves with good suppression of any longitudinal wave output was not found at any frequency. The presence of longitudinal waves makes the signals gathered for this test difficult to interpret. However, this could potentially be solved should a method of signal processing for eliminating longitudinal waves be developed.

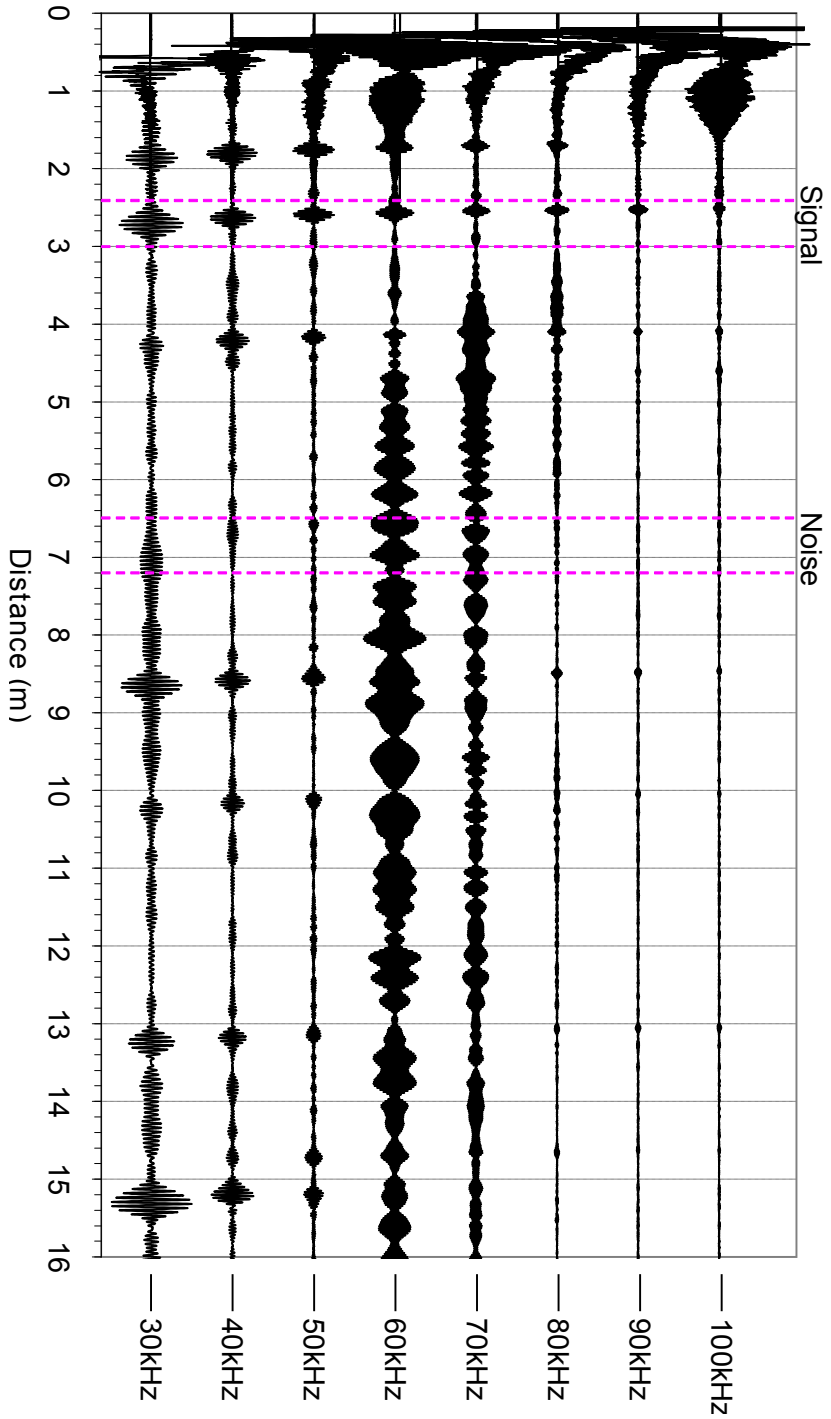

FIGURE 6.10: A series of single ring, pulse-echo tests were conducted that swept through frequencies between 30 and 100 kHz using the commercially available monolithic transducer tool. Here eight sample A-Scans are shown from this range for comparison. Two bands have been identified to aid evaluation; the signal band shows where a peak is expected and the noise band shows where no peak is expected. The time scale has been resolved to a distance scale.

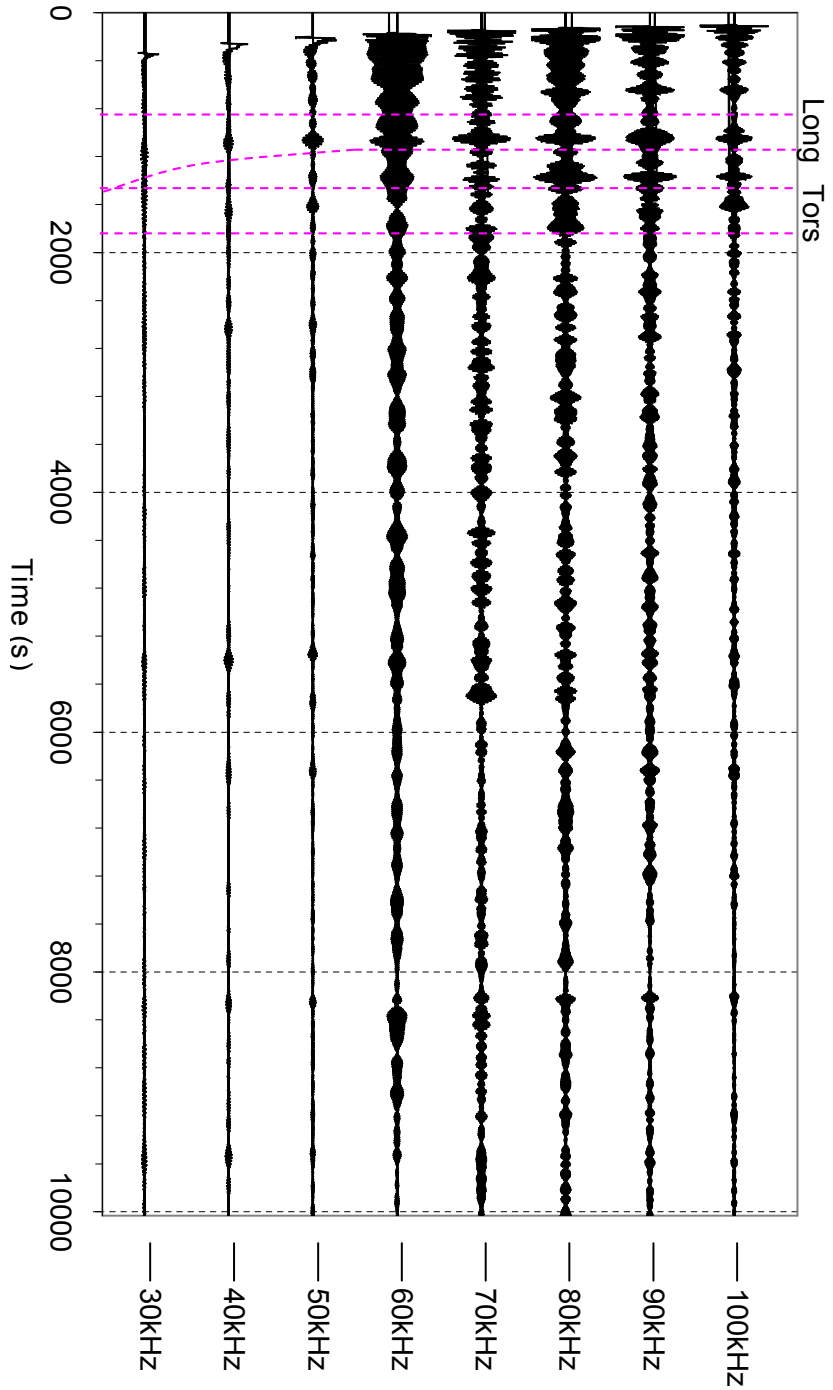

FIGURE 6.11: A series of single ring, pulse-echo tests were conducted that swept through frequencies between 30 and 100 kHz using the angled MFC transducer prototype tool. Here eight sample A-Scans are shown from this range for comparison. Two bands have been identified to aid evaluation; the longitudinal band shows where a longitudinal peak from a weld should arrive and the torsional band shows where a torsional peak from the same weld should arrive. As there are two modes present, it is not possible to resolve the time scale or a distance scale.

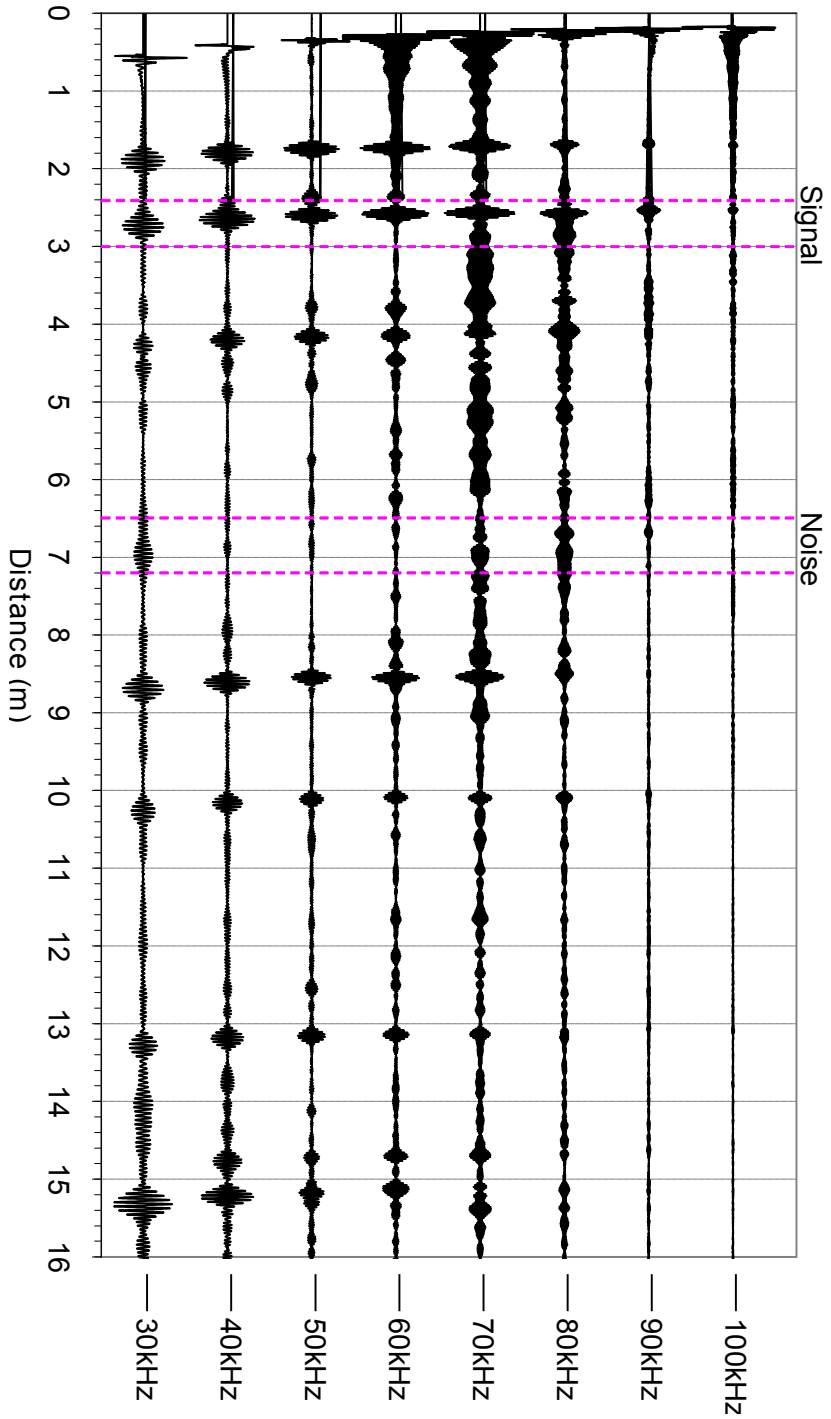

FIGURE 6.12: A series of single ring, pulse-echo tests were conducted that swept through frequencies between 30 and 100 kHz using the masked (monopolar) MFC transducer prototype tool. Here eight sample A-Scans are shown from this range for comparison. Two bands have been identified to aid evaluation; the signal band shows where a peak is expected and the noise band shows where no peak is expected. The time scale has be resolved to a distance scale.

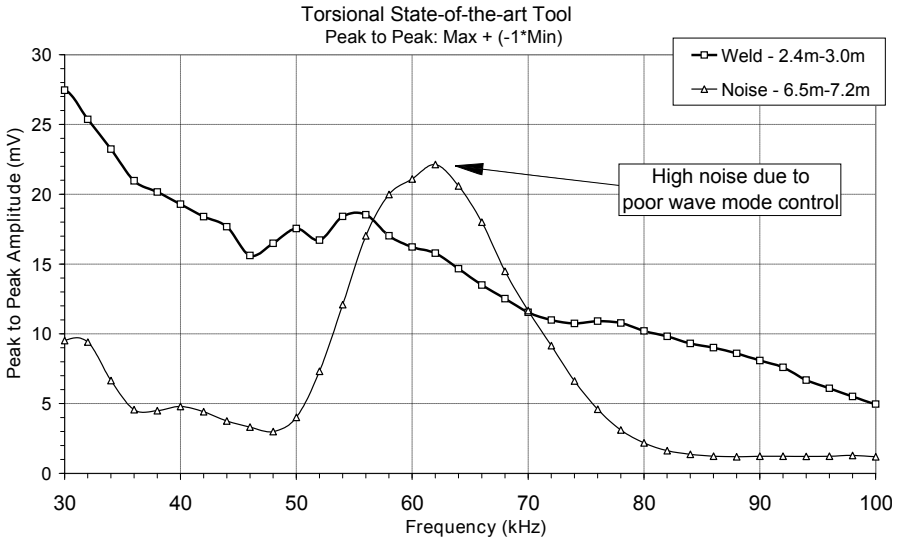

FIGURE 6.13: A series of single ring, pulse-echo tests were conducted that swept through frequencies between 30 and 100 kHz using the commercially available monolithic transducer tool. This graph shows the amplitude (maximum peak to minimum peak) of the signal for two bands; the first band is expected to include a peak corresponding to a weld reflection and the second band is expected not to contain any meaningful peaks. This can be considered a measure of signal to noise.

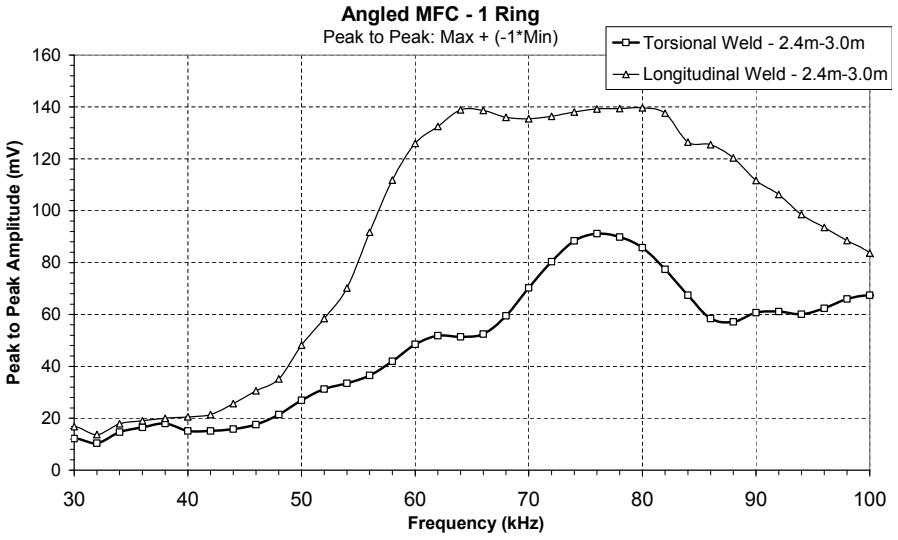

FIGURE 6.14: A series of single ring, pulse-echo tests were conducted that swept through frequencies between 30 and 100 kHz using the angled MFC transducer prototype tool. This graph shows the amplitude (maximum peak to minimum peak) of the signal for two bands; the first band is expected to include a peak corresponding to a longitudinal reflection from a weld and the second band is expected to include a peak corresponding to a torsional reflection from a weld. This can be considered a measure of longitudinal and torsional frequency responses. With two modes present a meaningful measure of noise is infeasible and so not included.

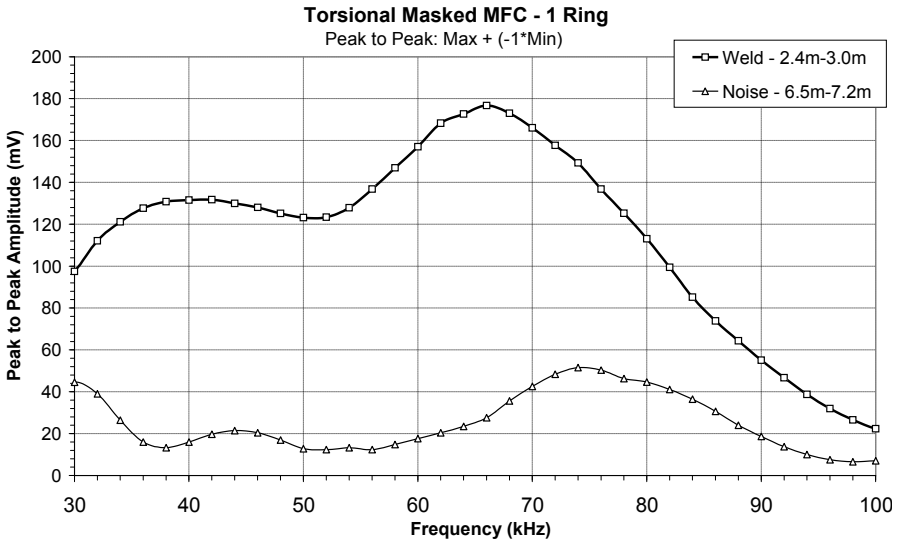

FIGURE 6.15: A series of single ring, pulse-echo tests were conducted that swept through frequencies between 30 and 100 kHz using the commercially available monolithic transducer tool. This graph shows the amplitude (maximum peak to minimum peak) of the signal for two bands; the first band is expected to include a peak corresponding to a weld reflection and the second band is expected not to contain any meaningful peaks. This can be considered a measure of signal to noise.

The prototype tool developed from MFC transducers adapted to work as monopolar devices showed improvement over the commercially available tool. It was shown their sensitivity is much greater. Noise after the blanking period, unwanted wave modes and coherent noise were reduced in comparison to the commercially available tool. An unusual noise range between 68 and 90 kHz is a concern. This noise could not be explained from this work alone and a new direction of experimental research would follow to discover its nature.

6.3 Development of MFC Arrays for Longitudinal Waves

A prototype longitudinal MFC array was constructed using the same approach as that of the torsional array, where an array of MFC transducers was laid out on a backing layer of closed cell foam that could then be coupled to a pipe through a pneumatic collar. A single ring of twelve MFC transducers was used as shown in Figure 6.16.

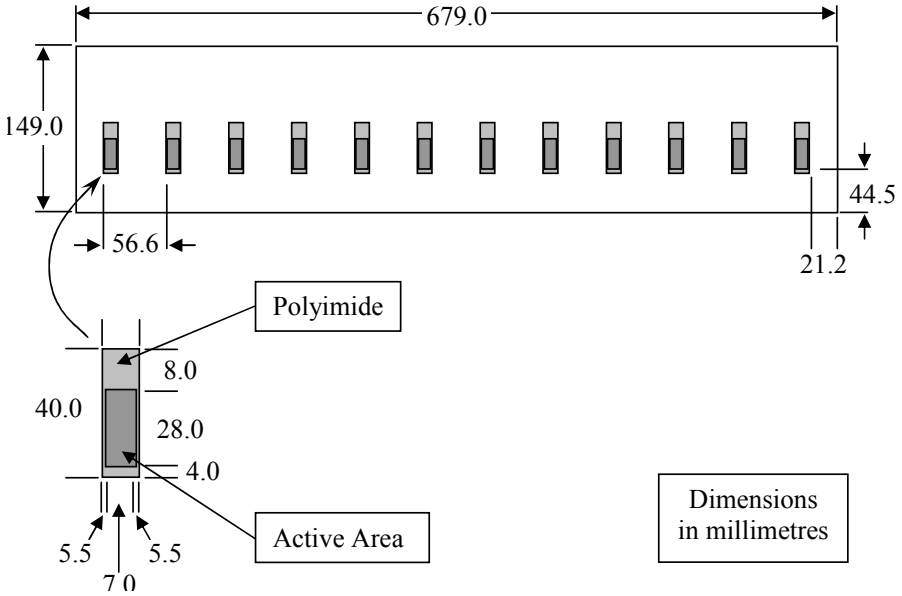

FIGURE 6.16: Layout of the adapted bipolar MFC transducer torsional wave array.

6.3.1 Test Setup

Unfortunately, the test pipe used in the previous test was no longer available for testing, therefore a 5.56 meter long 8 inch schedule 80 pipe was used (Figure 6.17). This pipe contains only three features, two ends and a weld 1.81m from one end. A test location was chosen 4.14 meters from that same end. The pipe has experienced some general corrosion, but no localised defects.

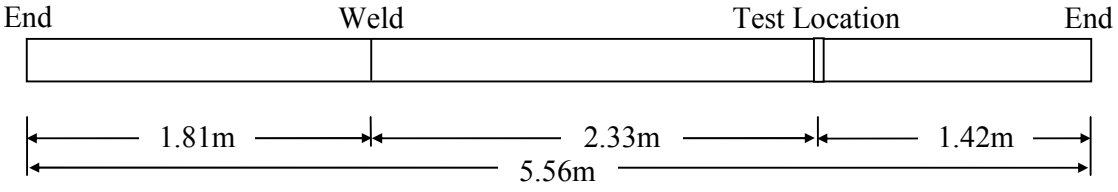

FIGURE 6.17: An 8 Inch Nominal Pipe Size Schedule 80 (Standard ASME B36.10M) Steel Pipe.

The velocities of all wave modes up to order twelve have been calculated using a software package called Disperse [Pavlakovic et al., 1997], which is shown in Figure 6.18. This shows that many high order flexural modes exist within the frequency range desired. In

practise the tools should only generate L(0,1) and L(0,2). However, as there are only twelve transducers in the ring for the MFC tool, high order flexural modes may occur.

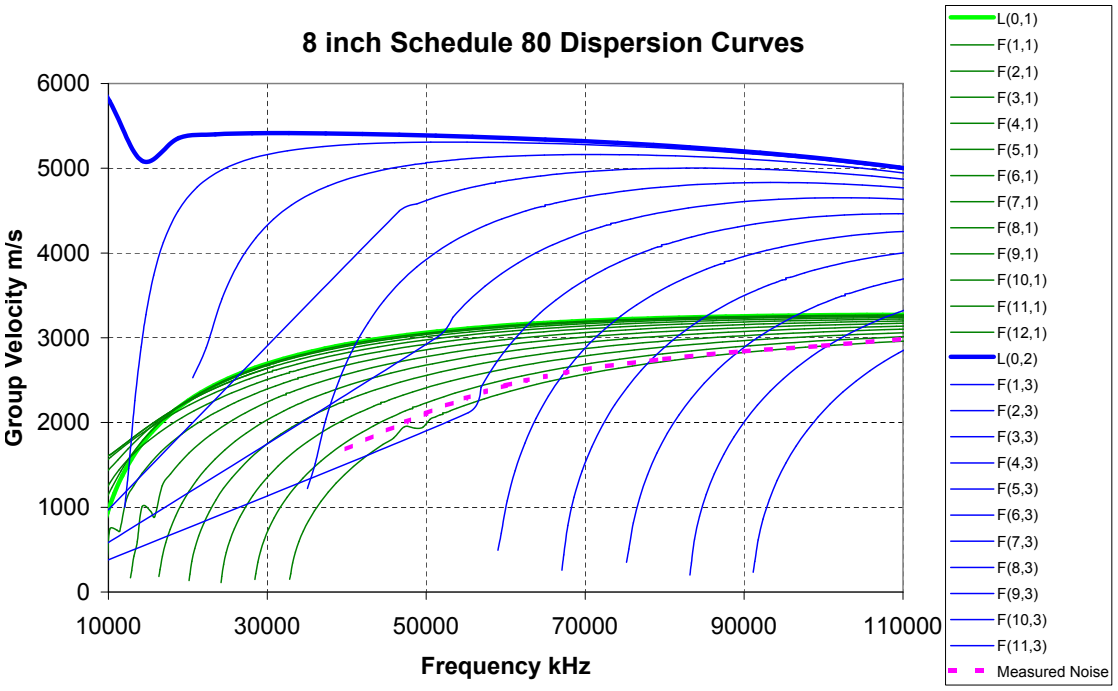

FIGURE 6.18: Group velocity dispersion curves for an 8 inch schedule 80 steel pipe. Also shown is the velocity of the unwanted wave mode recorded in the unmasked MFC prototype tool longitudinal frequency sweep test.

6.3.2 Frequency Response

A test was repeated for each tool, where each tool was mounted at the test location and a single ring was used to transmit and receive. The test repeated over a frequency range from 10 and 110 kHz at 2 kHz steps. This produced a set of signals for each tool varying in time, frequency and amplitude. The dispersion curves (shown in Figure 6.18) have been used to predicted the arrival time of the L(0,1) and L(0,2) pulses as they return from the near end, the weld, the far end, and the combined pulses after they have travelled to both ends. This gives a chart that can be compared with the real signals recorded from this test, shown in Figure 6.19. This figure also shows the time at which the system switched from transmission to reception (the end of the blanking period). The signals collected for the commercially available tool, the unmasked (bipolar) MFC tool and the masked (monopolar) MFC tool are shown in Figures 6.20, 6.21, 6.22 respectively.

The signals for the commercially available tool (shown in Figure 6.20) correlate closely with the predicted arrival bands. It shows that L(0,2) is higher than L(0,1) sensitivity. It also shows that the L(0,2) sensitivity is higher in the low end of the frequency range, particularly below 30 kHz. In practice, testing is rarely conducted below 30 kHz because

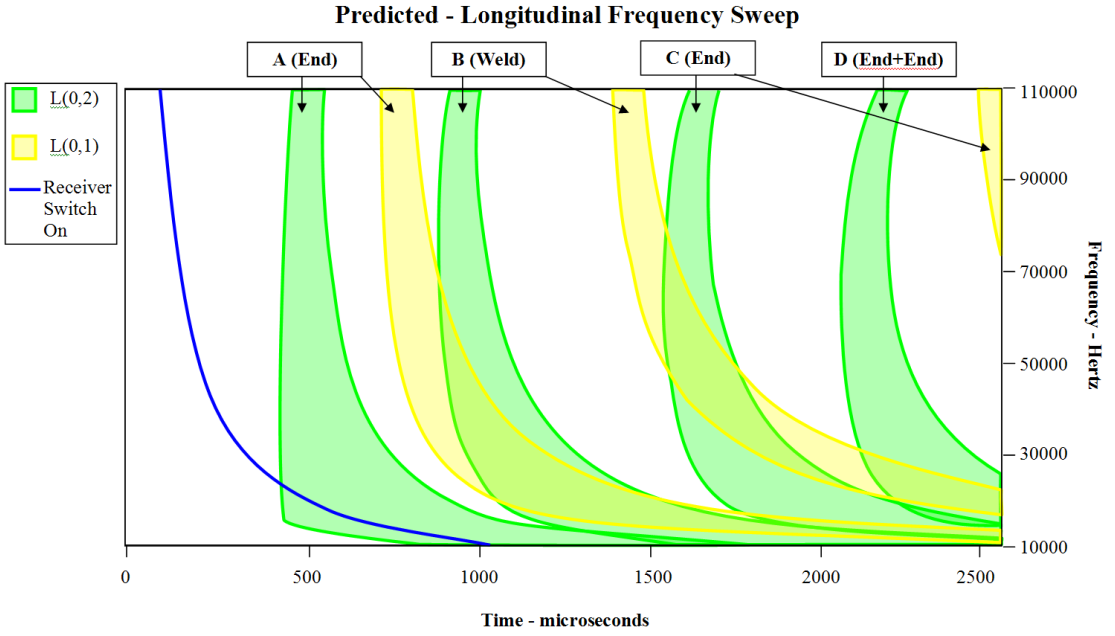

FIGURE 6.19: Predicted pulse arrival times for L(0,1) and L(0,2) for tests conducted on the pipe shown in Figure 6.17 with dispersion curves shown in Figure 6.18. "Receiver Switch On" shows the end of the blanking period where the system is switched from transmission mode to reception mode.

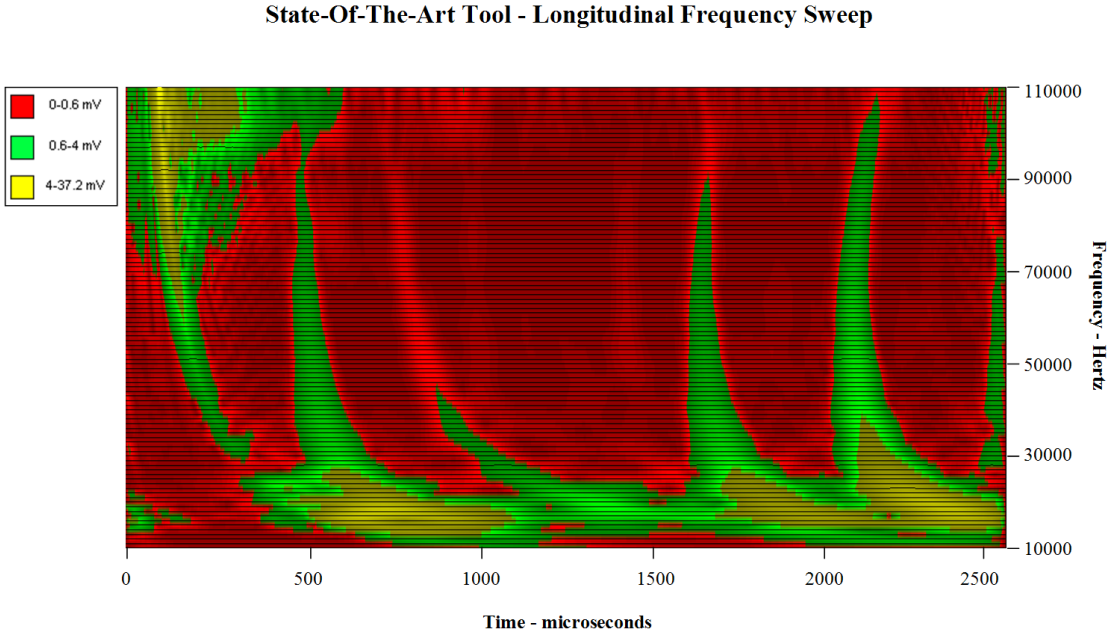

FIGURE 6.20: A twentyfour element ring array, longitudinal, commercially available tool was used to collect A-scans for frequencies from 10 to 110 kHz at 2 kilohertz steps on the pipe shown in Figure 6.17. Horizontal black lines show data intervals. Colouring indicates absolute amplitude.

resolution is low. Noise following the blanking period is high, but there is no clear indication of noise due to high order flexural modes.

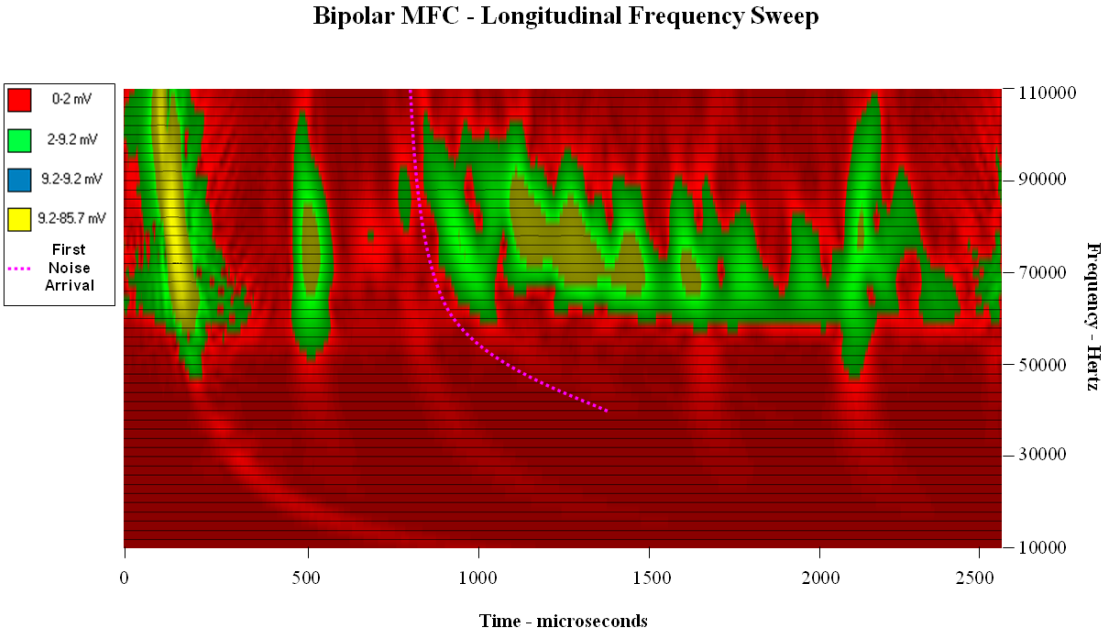

FIGURE 6.21: A twelve element ring array, longitudinal unmasked (bipolar) MFC transducer tool was used to collect A-scans for frequencies from 10 to 110 kHz at 2 kilohertz steps on the pipe shown in Figure 6.17. Horizontal black lines show data intervals. Colouring indicates absolute amplitude. "First Noise Arrival" shows the leading edge of the first pulse of F(1,12) for frequencies between 40 and 110 kHz.

The signals for the unmasked (bipolar) MFC transducer tool (shown in Figure 6.21) gives similar relative sensitivities of L(0,1) and L(0,2). Unlike the commercially available tool the sensitivity is higher above 50 kHz. However there is also significant noise between 50 and 106 kHz. The arrival time of the leading edge of this noise ("first noise arrival" in Figure 6.21) was to compared with the distance of the nearest feature from the tool and used to create a frequency/velocity curve (shown as 'measured noise' on the dispersion curve graph in Figure 6.18). This is in close match to the mode F(1,12), which is dispersive and could account for all the noise. This indicates that a greater number of transducers are required in each ring for this pipe.

Finally, the signals for the masked monopolar MFC tool (shown in Figure 6.22) have similar characteristics to the unmasked MFC tool except that sensitivity is more constant throughout the frequency range and there is very significant noise between 52 and 74 kHz. This noise has similar characteristics to the unexplained noise in the masked MFC tool torsional tool, in that the noise begins from the end of the blanking period and the amplitude cycles up and down with linear decay of the maximum amplitude of each cycle. It is likely that this is one of two physical effects; firstly, it may be due to a resonance introduced by the masking layer or, secondly, it might be due to guided waves travelling circumferentially at the tool location.

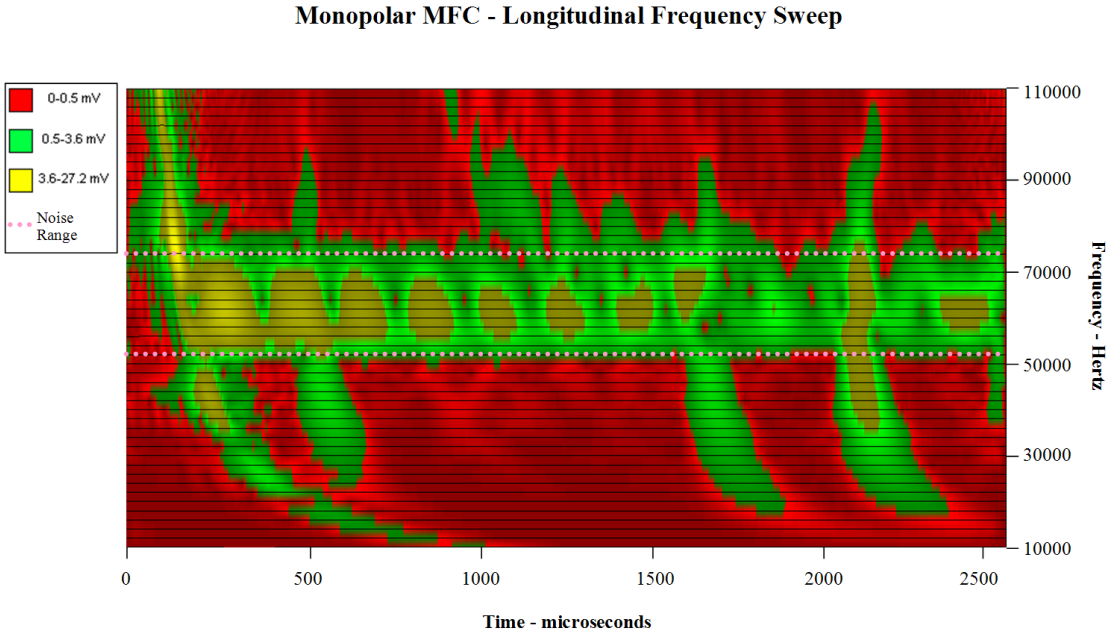

FIGURE 6.22: A twelve element ring array, longitudinal masked (monopolar) MFC transducer tool was used to collect A-scans for frequencies from 10 to 110 kHz at 2 kilohertz steps on the pipe shown in Figure 6.17. Horizontal black lines show data intervals. Colouring indicates absolute amplitude. "Noise Range" shows the 52 to 74 kHz range where currently unexplained noise occurs.

6.3.3 Longitudinal Tool Summary

The design of the longitudinal MFC prototype was flawed in that there were too few transducers allowing F(1,12) to be transmitted and received. Also when the masking was applied the signals gathered included a severe unwanted noise in the range of 52 to 74 kHz. With these two effects it is too difficult to make a fair assessment of frequency response and noise.

6.4 Unwanted Circumferential Waves

Severe noise between 52 and 74 kHz with maximum amplitude at 63 kHz was found for the longitudinal masked tool (Figure 6.22), but this noise is not present in the same tool without the masking (Figure 6.21). It is hypothesised that this is due to horizontal shear waves travelling circumferentially at the tool location and that the sensitivity for transmitted and receiving this mode is dependent on the wavelength and the circumferential transducer separation. Lateral shear waves are not possible without the masking layer and so would not be seen in the data for the unmasked tool.

To measure the presence of circumferential waves a test was devised to measure the output of a single transducer. The twelve transducer of the masked longitudinal tool were applied to an 8inch schedule 80 pipe. An addition masked longitudinal transducer

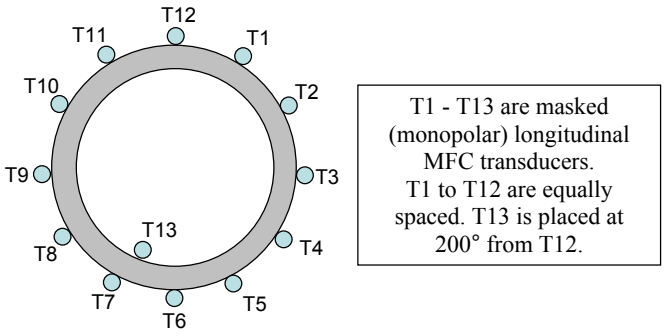

FIGURE 6.23: Transducer configuration for measuring the presence of circumferential waves generated from a single masked MFC transducer.

was applied to the inside wall of the pipe at the same location as the tool. Figure 6.23 shows the relative positions of these thirteen transducers. The top transducer (labelled T12) is used to transmit a 52 kHz, 10 cycle, Hann windowed pulse. Transducers T1-T11 and T13 are used to receive.

Figure 6.24 shows the received signals inside the pipe wall. This confirms that there is an acoustic vibration remaining at the tool location and that it is not isolated to the outer surface.

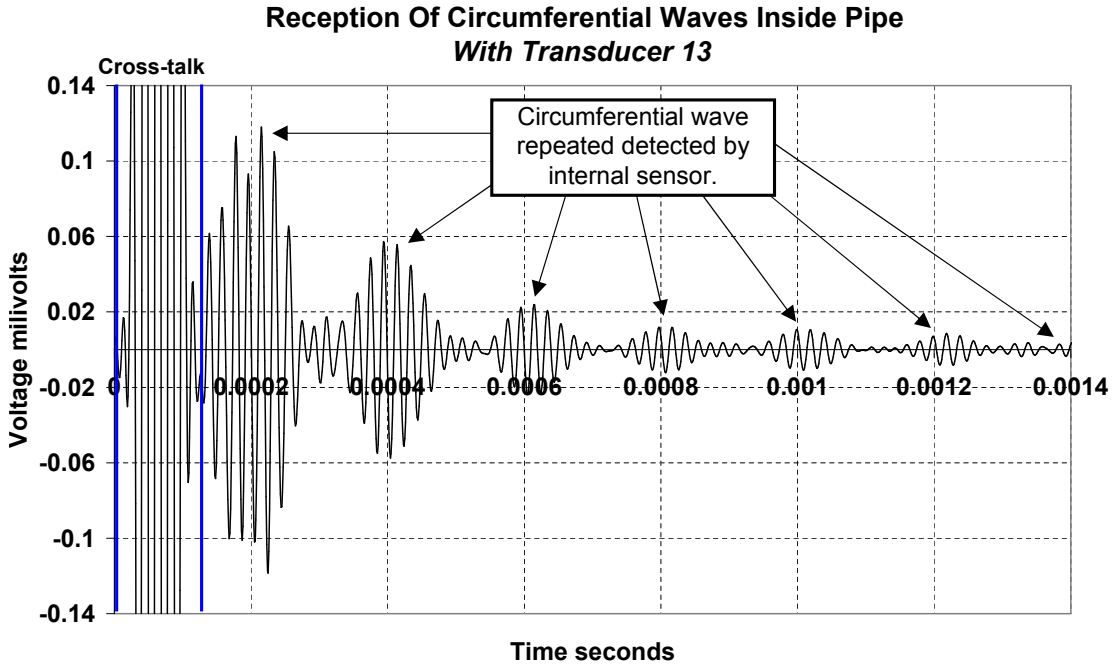

FIGURE 6.24: A masked (monopolar) MFC transducer is longitudinal aligned and used to transmit on the outside wall of an 8inch Schedule 80 pipe. Another transducer was used to receive on the inside wall of the pipe at the 200 degree position to the transmitter and the above signal was recorded. Circumferential waves can be seen to follow an initial period of cross-talk caused by transmission.

In Figure 6.25 the A-Scans of the 12 outer transducers have been processed and put together in a surface plot. The processing of each A-Scan reduced each signal to the envelope of the absolute amplitude. It can be seen that a pulse travels both clockwise

and anticlockwise around the circumference from the transmitting transducer (12). The group velocity of the wave can be approximately measured as the circumference divided by the time between to pulse peaks. As the outside circumference is 0.6882 meters and the time between peaks is 0.0021 seconds, the group velocity is measured to be approximately 3276.2 meters/second. As this speed is a close match to that expected of the shear wave (well known to be 3260 meters/second in a steel plate) and as it is sensed on both sides of the pipe wall, it can be seen the a single longitudinal MFC is transmitting a circumferential shear wave.

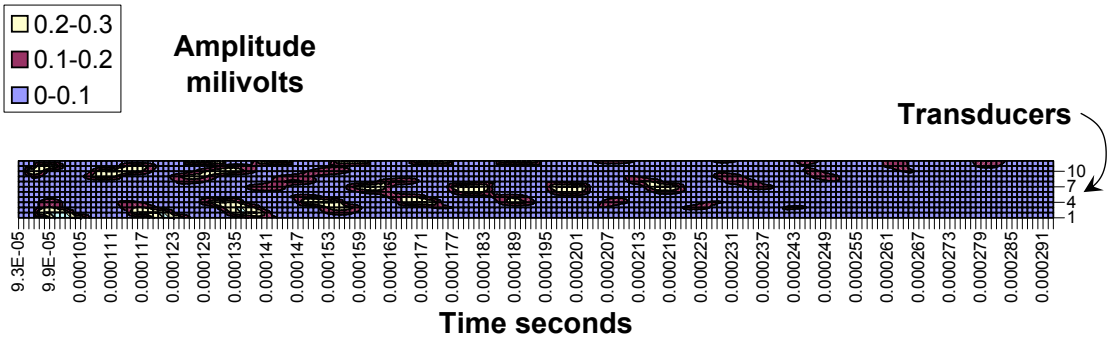

FIGURE 6.25: Comparison of the received signals from 12 equidistant positions around a pipe's circumference shows that a single masked (monopolar) MFC transducer will cause a guided wave to propagate circumferentially.

The tool with twelve of these transducers would only experience these circumferential waves when the circumferential spacing of these transducers did not lead to the cancelation of this mode. Similarly, the amplitude of these circumferential waves would be highest when the circumferential spacing of these transducers is equal to one wavelength. To visualise this effect it would be necessary to compare the frequency response of the noise found (Figure 6.22) with the superposition effect of two transducers separated by 56.6mm. In Figure 6.26 two curves are given. ''Phase Difference'' shows the relative phase of the output of each of a pair of transducers separated by 56.6mm. When they are completely in phase, it can be expected that maximum output from the pair would be experienced. The second curve gives the frequency response of the noise recorded with the masked (monopolar) MFC transducer tool (using a separation of 56.6mm). The noise correlates with relative phase, thus showing that the noise is likely to be the superposition of circumferential shear wave output. This effect is likely to occur when the wavelength is half the transducer spacing too, but notably not double.

6.4.1 Reconsideration of Array Design Criteria

Two initial decisions face an engineer designing LRUT transducer tools; they must choose a frequency range for which the equipment may operate and choose one or more wave modes to transmit and receive. Knowledge of the possible wave modes and the frequency/velocity relationship of each mode is required and can be derived analytically

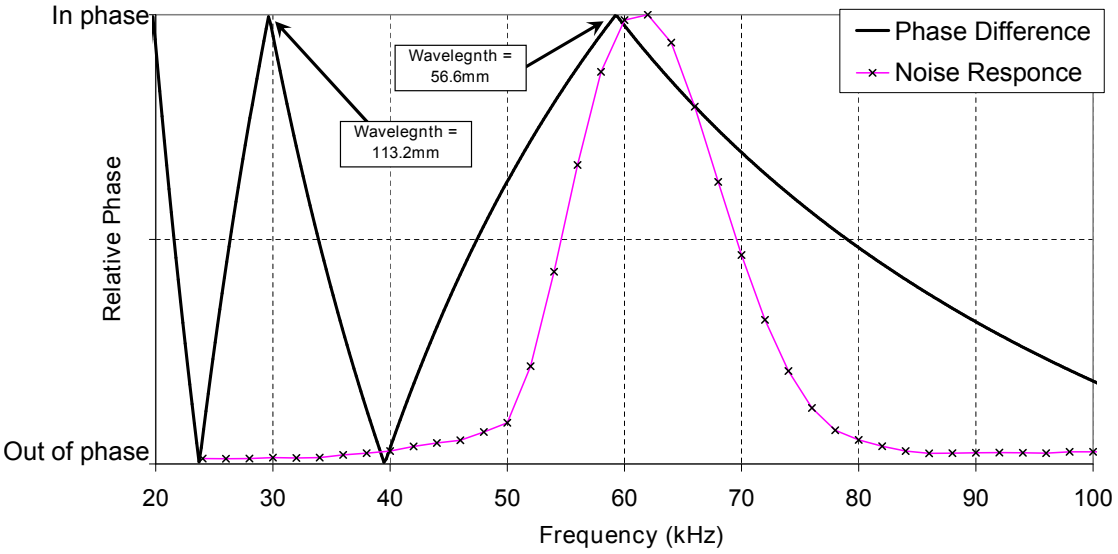

FIGURE 6.26: A comparison of the noise level measured from a longitudinal MFC array (made with the partially decoupled MFCs circumferentially separated by 56.6mm) and the phase delay between two point sources separated by 56.6mm for the circumferential shear horizontal wave mode.

to produce graphs known as Dispersion Curves [Pavlakovic et al., 1997]. It is likely that the approach will need to work with a group of similar acoustic wave guides and the dispersion curves for the extremes need to be considered. Generally a single wave mode is desired and should be excited at a frequency where its velocity variation is low for the local range of frequencies (where it is non-dispersive). It is more feasible to excite a single mode at a frequency where fewer modes exist and thus LRUT is often conducted in at low ultrasonic frequencies (below the cut-off frequency of most modes).

In pipework the diameter and the wall thickness of the pipe affect the dispersion curves. L(0,1) and T(0,1) are present from 0 hertz and typically L(0,2) is present very low in the kHz range. Generally T(0,2) and L(0,3) occur some point above 90 kHz. For L(0,1), T(0,1) and L(0,2) wavelengths can vary between 1000mm and 10mm within the range of 10 to 90 kHz.

To avoid the transmission of flexural wave modes the tool needs to have more transducer per ring than any flexural wave mode has nodes. It was found that twelve transducer of an 8 inch tool is insufficient.

To avoid the transmission of circumferential waves, the circumferential spacing of the transducers in each ring needs to be less than half the wavelength of each mode that the transducer could produce. Transducers in a torsional tool would be capable of transmitting asymmetric and symmetric lamb modes circumferentially and transducers in a longitudinal tool would be capable of transmitting horizontal shear waves circumferentially. The

circumferential separation distance (and therefore the number of transducers per ring) is dependent on the desired frequency range. Again, for pipe inspection it was found that twelve transducer of an 8 inch tool is insufficient.

6.5 Summary

MFC based arrays for pipe inspection were designed, built and tested with a comparison against commercially available equipment. Partially coupled MFC transducers were shown to be capable of transmitting and receiving torsional waves in pipes (specifically the T(0,1) wave mode) and an array was produced that was capable of achieving a high level of mode purity. This demonstrates that the adaptation method developed in Chapter 5 is effective in modifying the MFC transducer sensitivity for the purpose of using shear horizontal wave modes, such as torsional waves in pipes.

Both fully coupled and partially decoupled MFC transducers were used in arrays for pipe inspection with longitudinal waves (specifically the L(0,2) wave mode). It was found that a high density of the partially coupled MFC transducers was needed to avoid the presence of circumferential waves (that can disrupt axial inspection). It was also shown that fully coupled MFC transducers have a low lateral sensitivity to shear horizontal waves (as predicted in Chapter 4), and as such can potentially be used in fewer numbers saving weight and cost.

The design challenges against achieving high mode purity were identified through the development of these arrays and design criteria for achieving a high level of mode control was given.

In comparison to the commercially available equipment, it was shown that MFC transducer arrays can achieve superior results that can lead to improved defect finding capability. As the MFC transducers have form characteristics that offer practical advantages, the equipment made using them can also expect to have a low profile and weight. This work has enabled the use of MFC transducers for portable inspection equipment with potential to improve upon the existing state-of-the-art.

Chapter 7

Conclusions and Future Work

7.1 Conclusions

The long range capability of ultrasonic guided waves allows the development of techniques that can screen large areas of a structure for defects whilst requiring limited access and relatively few sensors. Defect screening of this kind can help prevent structural failure, which otherwise could be catastrophic for human safety and the environment. The research in this thesis was done to improve this technology by developing the application of MFC transducers for ultrasonic guided waves, the way transducers are characterised and how the characterised information can be used to assist with the development of transducer arrays and inspection systems. These improvements lead to greater signal quality, through improved wave mode control and increased amplitude, which leads on to greater inspection range, higher detection reliability and the ability to detect smaller defects.

The Macro Fibre Composite transducer was identified in the literature as having potential benefit to ultrasonic guided wave inspection. This thesis showed that these devices have sensitivity characteristics that vary with a number of application specific parameters, and that these can be predicted and optimised with the experimentally validated models presented. It is shown that the MFC size can be chosen so they have a relatively high sensitivity to a target wave mode, whilst having poor sensitivity to undesired wave modes. The wavelength dependent sensitivity is significant because of the MFC transducers' extensional (or bipolar) nature, and a method of adapting the MFC transducer was developed to alter this nature to yield less variable sensitivity such that the MFC transducer could be used for a wider range of applications.

Pipe inspection arrays were designed and built using both the fully coupled and partially decoupled MFC transducers, and tested in laboratory conditions against state-of-the-art commercial equipment. This testing showed that arrays of MFC transducers can be used

for testing with both longitudinal and torsional waves and that improvement can be achieved upon the state-of-the-art.

7.1.1 Development of Characterisation Methods for Evaluating MFC Transducers

A method of broad-band chirp transmission and split spectrum analysis has been developed for measuring the frequency response of a transducer in a pulse-echo or pitch catch arrangement, which was used to measure the frequency and length dependent performance of MFC transducers (as given in Chapter 3). This was done for an aluminium bar and a steel plate waveguide, which demonstrated that the MFC transducer's performance was dependent on the length of the MFC, the wave mode and the frequency.

This was complemented with the development of a large plate experiment that allowed the directional sensitivity of a transducer to be measured for all three fundamental plate wave modes (A0, SH0 and S0) over a range of frequencies (as given in Chapter 4). This was used to demonstrate how MFC transducers' extensional nature and size gives rise to a complex directional sensitivity for each wave mode, and in particular demonstrated their weak lateral sensitivity to shear horizontal waves. These experiments allow a transducer to be tested for their frequency response for a specific mode and for their directional sensitivity to each wave mode to give a complete wave mode sensitivity characterisation.

A mathematical model was developed to analyse the mechanism that related the MFC behaviour to their frequency and wave mode dependent sensitivity, which was compared with the frequency response measurements (in Chapter 3). The response measurement found that the model gave reasonable agreement when the transmission part of the model was adapted to be reciprocal to the reception part of the model. Further work could be conducted to explore the basis for this adaptation.

This model can predict the performance of an MFC of a given length and allows the MFC length to be chosen to have a high sensitivity to a desired mode whilst having a significantly lower sensitivity to unwanted modes. This analytical and experimental characterisation of MFC transducers allows them to be used optimally for achieving wave mode control, which will enhance long range ultrasonic testing through improved inspection reliability and defect detection capability.

7.1.2 MFC Adaptation through Partial Decoupling With a Weak Shear Coupling Membrane

It was hypothesised that the MFCs' directional wave mode sensitivity could be altered by partially decoupling them in such a way that would give them wave mode sensing characteristics that would be advantageous in some applications. A method of partial

decoupling through the use of a weak shear coupling membrane was developed and this hypothesis was confirmed through a combination of analysis and experimental measurement (given in Chapter 5).

Finite element analysis was used to evaluate the use of a thin, flexible material to decouple a transducer from in-plane tractions at a structure's surface and a latex film was selected as a suitable material. This method was trialled experimentally using the large plate experiment for measuring a transducer's directional wave mode sensitivity, which demonstrated the successful adaptation of the MFC transducer's directional performance.

This partial decoupling gave rise to directional characteristics similar to the more conventional uniform in-plane transducer. The most significant advantage of this adaptation is that it allows MFC transducers to transmit and receive shear horizontal wave modes in a direction in which its sensitivity to Lamb modes is weak. This allows the transmission and reception of shear horizontal with a good degree of mode purity, which is the favoured move for many inspection techniques.

It was shown that an MFC assembly with a latex masking retains the benefit of being low weight, low height and flexible. This can be used alongside a coupled shim layer to maintain a constant height across the MFC. A patent application has been filed for this method of adapting an MFC or similar transducer [Mudge and Haig, 2010].

7.1.3 Development of a Point Source Superposition Model for Directional Transducers

A discrete analytical model was developed that could make predictions about the nature of MFC transducers based on their size, and how superposition effects determine their sensitivity on transmission and reception (as detailed in Chapter 4). In this model a transmitting or receiving MFC transducer could be represented by a set of in-plane point source transducers. This model was used to simulate the characteristics of the MFC transducer with and without the application of a partial decoupling interface layer. These results were compared to the experimental testing done for both the 1D and the 2D cases, and were found to achieve reasonable agreement. This model is fast to run and can be used to validate the hypothesised nature of a transducer, as has been demonstrated here, or, if this nature is known, to evaluate configurations of transducers or transducer arrays.

It was shown that the bipolar nature of the MFC transducer causes it to have only significant sensitivity to shear waves in the diagonal directions (relative to the fibre axis), but not in the 90° or 270° directions. It was also shown that the adapted MFC could be assumed to act as a monopolar MFC, as simulating it as such with this simulation produced accurate predictions about its altered directional sensitivity (as described in Chapter 5).

This approach yields information that can assist the development of transducer arrays. The point source superposition model used for simulation allows the directional wave mode sensitivity to be obtained relatively quickly when a transducer's vibrational behaviour is known. When it is not, the nature of the transducer can be hypothesised and simulated, giving results that can be tested experimentally.

With knowledge of the inherent directional wave mode control of each transducer, it is possible to design an array to further enhance the wave modes of interest whilst reducing others. Enhancements in wave mode control of this kind can lead to improved methods of inspection with greater defect sensitivity.

7.1.4 Pipe Inspection Array using Macro Fiber Composites to Improve upon the State-of-the-art

Transducer arrays have been designed and built using both fully coupled and partially decoupled MFC transducers for the purpose of creating portable pipe inspection equipment that facilitates testing using both longitudinal and torsional wave modes (as is detailed in Chapter 6). This equipment was experimentally compared with a state-of-the-art commercial inspection tool, and the MFC tool's advantages were demonstrated. In particular it was shown that for some frequencies a greater degree of wave mode control could be achieved, which resulted in a higher signal amplitude in comparison to the coherent noise level.

It was found that a high density of the partially coupled MFC transducers was needed to avoid the presence of circumferential waves (that can disrupt axial inspection), but when using fully coupled MFC transducers the effect of circumferential waves was insignificant due to their relatively low sensitivity to lateral waves, which allows them to be used in fewer numbers allowing for lighter and cheaper equipment to be developed. Also, as the MFC transducers have form characteristics that offer practical advantages, the equipment made using them can also expect to have a low profile and weight.

The design challenges against achieving high mode purity were identified through the development of these arrays and design criteria for achieving a high level of mode control was given. The full characterisation of MFC transducers, the method of adapting MFC transducers to provide tailored wave mode sensitivity characteristics and these array design guidelines make it possible to develop optimal arrays for the inspection of pipes of any isotropic material or size.

7.2 Recommendations For Future Work

The plate bar and plate methods developed for measuring a transducer's wave mode sensitivity can be used to characterise transducers and should be used to test a wide range of transducers. In particular it would be valuable to characterise Smart Material's P2 type MFC and compare the results to the performance of the P1 type presented in this thesis. Further transducer characterisation could include the investigation of other parameters on transducer performance, such as coupling force, coupling surface roughness or environmental temperature. These experimental methods can also be used to assess the manufacturing consistency for transducers. This characterisation can be done for a significant number of transducers of the same type to demonstrate how much they vary. Knowledge of the consistency for different transducer types will aid the choosing of a transducer type to be used in a transducer array, since variation across an array is undesirable.

To further aid the use of the point source model for the development of arrays for pipe inspection, it will be advantageous to have excitability curves for all axial and circumferential wave modes (in the low ultrasonic frequency range). This is indeed the case for any structure. The development of a tool for rapidly generating these excitability curves for inclusion in a transducer model would allow for fast transducer evaluation and optimisation. This could be achieved through some means of finite element modelling, although greater speed is likely to be achieved if an analytical method could be devised.

The model presented in Chapter 3 was able to predict the performance of an MFC of a given size for a given wave mode on a given waveguide. This was achieved by treating the transmission as the reciprocal process of reception and by multiplying the predicted amplitude by the cube of the frequency. This was not predicted by the analysis and further work is required to understand the physical mechanism that causes this adaptation to be required. Separate experimental measurement of the transmission and reception may allow this anomaly to be better understood. Currently the model developed in Chapter 3 made use of in-plane excitability curves. If another set of excitability curves were created that described the proportionality of excited modes in terms of their out-of-plane displacement (rather than in-plane), then the simulated performance could be compared with experimental measurements made using a laser vibrometer. Since a vibrometer is a form of non-contact measurement and can be calibrated to make accurate measurements of the surface displacement, this would allow a transducer's transmission performance to be measured separately from its reception performance.

In the MFC prototype pipe inspection device developed in this thesis, the pressure used and the material used to apply the pressure had been selected after analytical consideration, but was not exhaustively optimised and the mechanisms behind achieving optimal results were not thoroughly explored. Future work could involve the assessment of various methods, which could be tested using a combination of finite element modelling

and experimental measurement. A means of protecting the MFC transducer for prolonged use in relatively harsh environments is necessary for them to be used in the widest range of applications. They are flexible devices and may need protecting from excessive flexing. They may also need protection from rough, hard surfaces. These housing considerations for many applications will need to preserve their flexible, low weight, and low profile form. They may also be considered for permanent installation in which case a stable means of long term coupling, which protects them against moisture and damage, should be developed. This development would involve their re-characterisation, since additional materials and changes in coupling may lead to altered behaviour, particularly if the coupling is not kept uniform. This could be done using the characterisation methods developed in this thesis. This would result in a low weight, portable inspection system that has potential to outperform currently available technology.

Appendix A

MFC Data Sheet

The MFC transducers used in this thesis were known as the P1 type MFC transducers and were provided by Smart Material GmbH Daue [2011]. The data sheet for these is given below in Figure A.1.

General technical information for the MFC

High-field (|E| > 1kV/mm), biased-voltage-operation piezoelectric constants:		
d_{33}*	4.6E+02 pC/N	4.6E+02 pm/V
d_{31}**	-2.1E+02 pC/N	-2.1E+02 pm/V
Low-field (|E| < 1kV/mm), unbiased-operation piezoelectric constants:		
d_{33}*	4.0E+02 pC/N	4.0E+02 pm/V
d_{31}**	-1.7E+02 pC/N	-1.7E+02 pm/V
Free-strain* per volt (low-field—high-field) for d_{33} MFC (P1)	~ 0.75 – 0.9 ppm/V	0.75 – 0.9 ppm/V
Free-strain* per volt (low-field—high-field) for d_{31} MFC (P2)	~ 1.1 – 1.3 ppm/V	~ 1.1 – 1.3 ppm/V
Free-strain hysteresis*	~ 0.2	~ 0.2
DC poling voltage, Vpol for d_{33} MFC (P1)	+1500 V	+1500 V
DC poling voltage, Vpol for d_{31} MFC (P2)	+450 V	+450 V
Poled capacitance @ 1kHz, room temp, Cpol for d_{33} MFC (P1)	~ 0.42 nF/cm²	~ 2.7 nF/in²
Poled capacitance @ 1kHz, room temp, Cpol for d_{31} MFC (P2)	~ 4.6 nF/cm²	~ 29 nF/in²
Orthotropic Linear Elastic Properties (constant electric field):		
Tensile modulus, E1*	30.336 GPa	4.4E+06 psi
Tensile modulus, E1**	15.857 GPa	2.3E+06 psi
Poisson's ratio, v12	0.31	0.31
Poisson's ratio, v21	0.16	0.16
Shear modulus, G12 (rules-of-mixture estimate)	5.515 GPa	8.0E+05 psi
Operational Parameters:		
Maximum operational positive voltage, Vmax for d_{33} MFC (P1)	+1500 V	+1500 V
Maximum operational positive voltage, Vmax for d_{31} MFC (P2)	+360 V	+360 V
Maximum operational negative voltage, Vmin for d_{33} MFC (P1)	-500 V	-500 V
Maximum operational negative voltage, Vmin for d_{31} MFC (P2)	-60 V	-60 V
Linear – elastic tensile strain limit	1000 ppm	1000 ppm
Maximum operational tensile strain	< 4500 ppm	< 4500 ppm
Peak work-energy density	1000 in – lb/in3	~1000 in – lb/in3
Maximum operating temperature – Standard Version	< 80°C	< 176°F
Maximum operating temperature – HT Version	< 130°C	< 266 °F
Operational lifetime (@ 1kVp-p)	> 10E+09 cycles	> 10E+09 cycles
Operational lifetime (@ 2kVp-p, 500VDC)	> 10E+07 cycles	> 10E+07 cycles
Operational bandwidth as actuator, high electric field Operational bandwidth as actuator, low electric field	0Hz to 10 kHz 0Hz to 750kHz	0Hz to 10 kHz 0Hz to 750kHz
active Area Density	5.44 g/cm³	5.44 g/cm³
Thickness for all MFC Types	approx 0.3mm	approx. 12 mil

* Rod direction
** Electrode direction

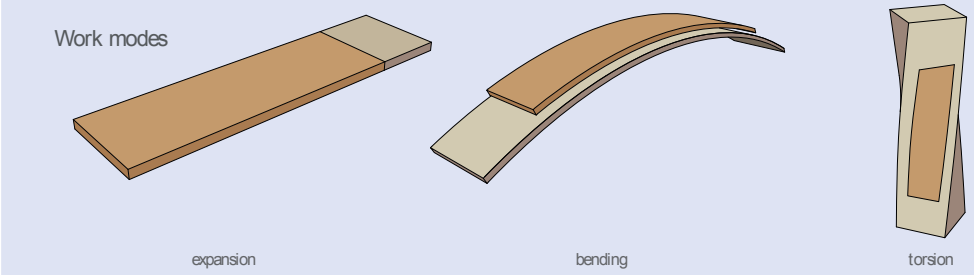

FIGURE A.1: MFC data sheet provided by Smart Material GmbH

References

Piezoelectric properties of ceramic materials and components.

D. N. Alleyne. *The non-destructive testing of plates using ultrasonic Lamb waves*. PhD thesis, Imperial College London, 1991.

D. N. Alleyne and P. Cawley. The interaction of lamb waves with defects. *IEEE Transactions on Ultrasonics Ferroelectrics and Frequency Control*, 39(3):381 -- 397, 1992.

D. N. Alleyne and P. Cawley. The excitation of lamb waves in pipes using dry coupled piezoelectric transducers. *Journal of Non Destructive Evaluation*, 15(1):11--20, 1996a.

D. N. Alleyne and P. Cawley. The effect of discontinuities on the long-range propagation of lamb waves in pipes. *Journal of Process Mechanical Engineering*, 210(3):217--226, 1996b.

D. N. Alleyne, A. M. Lank, M. J. S. Lowe, P. J. Mudge, and P. Cawley. Guided wave inspection of chemical plant pipework. *Proceedings of SPIE*, 2947(1):177--189, 1996.

D. N. Alleyne, B. Pavlakovic, Lowe M. J. S., and P. Cawley. Rapid, long range inspection of chemical plant pipework using guided waves. In *Review of Progress in Quantitative Non-Destructive Evaluation*, volume 20, pages 180--187, 2001.

D. N. Alleyne, T. Vogt, and P. Cawley. The choice of torsional or longitudinal excitation in guided wave pipe inspection. *Insight*, 51(07):373--377, 2009.

D.N. Alleyne and P. Cawley. Long range propagation of lamb waves in chemical plant pipework. *Materials Evaluation*, 55(4):504--508, 1997.

D.N. Alleyne, B. Pavlakovic, M. J. S. Lowe, and P. Cawley. Rapid, long range inspection of chemical plant pipework using guided waves. *AIP Conference Proceedings*, 557: 180--187, July 2000. Review Of Progress In Quantitative Nondestructive Evaluation: Volume 20.

J.M. Allin and P. Cawley. Design and construction of a low frequency wide band non-resonant transducer. *Ultrasonics*, 41:147155, 2003.

Mohammed H. Badi. *Capacitive Micromachined Ultrasonics Lamb Wave Transducers.* PhD thesis, Department of Electrical Engineering, Stanford University, 161 Packard Building, 350 Serra Mall, Stanford, CA 94305-9505, 2004.

D. F. Ball and D. Shewring. Some problems in the use of lamb waves for the inspection of cold-rolled steel sheet coil. *Nondestructive Testing*, 6(3):138--145, 1973.

F. Benmeddour, S. Grondel, J. Assaad, and E. Moulin. Study of the fundamental lamb modes interaction with symmetrical notches. *NDT & E International*, 41(1):1--9, 2008a.

F. Benmeddour, S. Grondel, J. Assaad, and E. Moulin. Study of the fundamental lamb modes interaction with asymmetrical discontinuities. *NDT & E International*, 41(5): 330340, 2008b.

M. Birchmeier, D. Gsell, M. Juon, A. J. Brunner, R. Paradies, and Dual J. Active fiber composites for the generation of lamb waves. *Ultrasonics*, 49(1):73--82, 2009.

W. Böttger, H. Schneider, and W. Weingarten. Prototype emat system for tube inspection with guided ultrasonic waves. *Nuclear Engineering and Design*, 102(3):369--376, 1987.

C. R. Bowen, L. J. Nelson, R. Stevens, M. G. Cain, and M. Stewart. Optimisation of interdigital electrodes for piezoelectric actuators and active fibre composites. *Journal Of Electroceramics*, 16(4):263--269, 2006.

C. M. v.d. Burgt, D. G. J. Fanshawe, J. F. Fiedeldij, I. Flinn, D. J. Grevink, G. D. van Grol, P. J. Hulyer, J. Koch, W. Laurich, and A. Petersen. *Piezoelectric Ceramics.* Mullard, London, 1974.

G. Busch and P. Scherer. A new siegnette-electric substance. *Naturwiss*, 23:737--738, 1935.

Michel Castaings and Peter Cawley. The generation, propagation, and detection of lamb waves in plates using air-coupled ultrasonic transducers. *The Journal of the Acoustical Society of America*, 100(5):3070--3077, 1996.

P. Catton. *Long Range Ultrasonic Guided Waves for the Quantitative Inspection of Pipelines.* Engd, Brunel University, 2009.

A. M. Chaston. *Development Of A Transducer To Be Used In Long Range Ultrasonic Testing.* Engd, Cardiff University, 2009.

Y. Cho, D. D. Hongerholt, and J. L. Rose. Lamb wave scattering analysis for reflector characterization. *IEEE Transactions on Ultrasonics Ferroelectrics and Frequency Control*, 44(1):44--52, 1997.

T. Clarke. *Guided wave health monitoring of complex structures.* PhD thesis, Imperial College London, 2009.

T. Clarke, P. Cawley, P. D. Wilcox, and A. J. Croxford. Evaluation of the damage detection capability of a sparse-array guided-wave shm system applied to a complex structure under varying thermal conditions. *IEEE Transactions on Ultrasonics Ferroelectrics and Frequency Control*, 56(12):2666 -- 2678, 2009.

T. Clarke, F. Simonetti, and P. Cawley. Guided wave health monitoring of complex structures by sparse array systems: Influence of temperature changes on performance. *Journal of Sound and Vibration*, 329(12):2306--2322, 2010.

E. Le Clézio, M. Castaings, and B. Hosten. The interaction of the s0 lamb mode with vertical cracks in an aluminium plate. *Ultrasonics*, 40:187192, 2002.

D. Damjanovic and R. E. Newnham. Electrostatics and piezoelectric materials for actuator applications. *Journal of Intelligent Material Systems and Structures*, 3(2): 190--208, 1992.

Dassault Systèmes. *ABAQUS version 6.10 User's Manual*, 2011.

T. Daue. Macro fibre composite (mfc) data sheet. Technical report, Smart Material GmbH, 2011. www.smart-material.com, last accessed Jan 2011.

L. J. Demer and L. H. Fentnor. Lamb wave techniques in nondestructive testing. *International Journal of Nondestructive Testing*, 1:251--283, 1969.

A. Demma, P. Cawley, and M. Lowe. A. g. roosenbrand. *Journal of the Acoustical Society of America*, 114(2):611--625, 2003.

A. Demma, P. Cawley, M. Lowe, A.G. Roosenbrand, and B. Pavlakovic. The reflection of guided waves from notches in pipes: A guide for interpreting corrosion measurements. *NDT&E International*, 37:167180, 2004.

F. Firestone. Flaw detecting device and measuring instrument, 1942.

F. Firestone and J. Frederick. Refinements in supersonic reflectoscopy. polarised sound. *The Journal Of The Acoustical Society Of America*, 18(1):200--211, 1946.

H. Florian and S. Ragossnig. Piezoelectric component and method for the production thereof, 2007.

P. Fromme, P. D. Wilcox, J. S. Lowe, and P. Cawley. On the sensitivity of corrosion and fatigue damage detection using guided ultrasonic waves. In *IEEE Ultrasonics Symposium*, volume 2, pages 1203--1206, August 2004.

H. Gao and J. L. Rose. Ultrasonic sensor placement optimization in structural health monitoring using evolutionary strategy. In *Review of Progress in Quantitative Nondestructive Evaluation, AIP Conference Proceedings*, volume 820, pages 1687--1693, 2006.

D. C. Gazis. Three-dimensional investigations of the propagation of waves in hollow circular cylinders. i. analytical foundation. *The Journal Of The Acoustical Society Of America*, 31(5):568--573, 1959a.

D. C. Gazis. Three-dimensional investigations of the propagation of waves in hollow circular cylinders. ii. numerical results. *The Journal Of The Acoustical Society Of America*, 31(5):573--578, 1959b.

K. F. Graff. *Wave Motion in Elastic Solids*. Clarendon Press, Oxford, 1991. ISBN-10: 0486667456.

T. N. Grigsby and E. J. Tajchman. Properties of lamb waves relevant to the ultrasonic inspection of thin plates. *IRE Transactions on Ultrasonic Engineering*, 8:26--33, 1961.

T. Hay and J. Rose. Flexible pvdf comb transducers for excitation of axisymmetric guided waves in pipe. *Sensors and Actuators A: Physical*, 100(1):18--23, 2002.

T. R. Hay, R. L. Royer, Gao H., X. Zhao, and J. L. Rose. A comparison of embedded sensor lamb wave ultrasonic tomography approaches for material loss detection. *Smart Materials and Structures*, 15(4):946 -- 951, 2006.

T. Hayashi, K. Kawashima, Z. Sun, and J. Rose. Analysis of flexural mode focusing by a semianalytical finite element method. *Journal of the Acoustical Society of America*, 113(3):1241--1248, 2003.

A. Heinzmann, E. Hennig, B. Kolle, D. Kopsch, S. Richter, H. Schwotzer, and E. Wehrsdorfer. Properties of pzt multilayer actuators. In *Actuator 2002 Conference Proceeding*, Bremen, Germany, June 2002.

R.T. Higuti, O. Martinez-Graullera, C.J. Martin, A. Octavio, L. Elvira, and F.M. De Espinosa. Damage characterization using guided- wave linear arrays and image compounding techniques. *IEEE Transactions on Ultrasonics, Ferroelectrics and Frequency Control*, 57(9):1985--1995, 2010.

M. Hirao and H. Ogi. An sh-wave emat technique for gas pipeline inspection. *NDT & E International*, 32(3):127--132, 1999.

M. Hirao and H. Ogi. An sh-wave emat technique for gas pipeline inspection. *NDT & E International*, 32(3):127--132, 1999.

C. W. Horton and M. V. Mechler. Circumferential waves in a thin-walled air-filled cylinder in a water medium. *The Journal Of The Acoustical Society Of America*, 51 (1B):295--303, 1971.

G. E. Hudson. Dispersion of elastic waves in solid circular cylinders. *Physical Review*, 63:4651, 1943.

D. Hutchins, D. Schindel, A. Bashford, and W. Wright. Advances in ultrasonic electrostatic transduction. *Ultrasonics*, 36:1--6, 1998.

P. Jackson. Teletest focus^{TM}. Technical report, Plant Integrity Ltd., 2011. www.plantintegrity.com, last accessed Jan 2011.

J. Jin, S. Quek, and Q. Wang. Design of interdigital transducers for crack detection in plates. *Ultrasonics*, 43(6):481--493, 2005.

Shaju John, Jayant Sirohi, Gang Wang, and Norman Wereley. Comparison of piezoelectric, magnetostrictive, and electrostrictive hybrid hydraulic actuators. *Journal of Intelligent Material Systems and Structures*, 18(10):1035--1048, 2001.

E. Kannan, B. Maxfield, and K. Balasubramaniam. Shm of pipes using torsional waves generated by in situ magnetostrictive tapes. *Smart Materials And Structures*, 16(6): 2505--2515, 2007.

H. Kim, K. Jhang, M. Shin, and J. Kim. A noncontact nde method using a laser generated focused-lamb wave with enhanced defect-detection ability and spatial resolution. *NDT & E International*, 39(4):312--319, 2006.

B. Köhler, B. Frankenstein, F. Schubert, and M. Barth. Novel piezoelectric fiber transducers for mode selective excitation and detection of lamb waves. In D. O. Thompson & D. E. Chimenti, editor, *Proceedings of the 35th Annual Review of Progress in Quantitative Nondestructive Evaluation*, volume 1096 of *American Institute of Physics Conference Series*, pages 982--989, March 2009. doi: 10.1063/1.3114365.

Krautkrämer, J. and Krautkrämer, H. *Ultrasonic Testing of Materials*. Springer-Verlag, 1983. ISBN: 9783540117339.

H. Kwun and K. Bartels. Magnetostrictive sensor technology and its applications. *Ultrasonics*, 36:172--178, 1998.

H. Kwun, S. Y. Kim, and G. M. Light. Long-range guided wave inspection of structures using the magnetostrictive sensor. *Journal For The Korean Society Of NDT*, 21: 383--390, 2001.

H. Lamb. On waves in an elastic plate. In *Proceedings Of The Royal Society*, A93, page 114128, London, 1917.

B. C. Lee and W. J. Staszewski. Modelling of lamb waves for damage detection in metallic structures: Part i. wave propagation. *Smart Materials And Structures*, 12(5): 804814, 2003a.

B. C. Lee and W. J. Staszewski. Modelling of lamb waves for damage detection in metallic structures: Part ii. wave interactions with damage. *Smart Materials And Structures*, 12(5):815824, 2003b.

K. R. Leonard and M. K. Hinders. Lamb wave tomography of pipe-like structures. *Ultrasonics*, 43(7):574583, 2005.

J. Li and J. L. Rose. Natural beam focusing of non-axisymmetric guided waves in large-diameter pipes. *Ultrasonics*, 44:3545, 2006.

Z. Liu, C. He, B. Wu, X. Wang, and S. Yang. Circumferential and longitudinal defect detection using t(0, 1) mode excited by thickness shear mode piezoelectric elements. *Ultrasonics*, 44:e1135e1138, 2006.

R. Long, M. Lowe, and P. Cawley. Attenuation characteristics of the fundamental modes that propagate in buried iron water pipes. *Ultrasonics*, 41:509519, 2002.

M. J. S. Lowe, D. N. A., and P. Cawley. Defect detection in pipes using guided waves. *Ultrasonics*, 36:147--154, 1998.

K. Luangvila. *Attenuation of Ultrasonic Lamb Waves with Applications to Material Characterization and Condition Monitoring.* PhD thesis, Georgia Institute of Technology, 2007.

R. Mallett. Signal processing for non-destructive testing. EngD Thesis, Brunel Univerisity, August 2007.

E. V. Malyarenko and M. K. Hinders. Ultrasonic lamb wave diffraction tomography. *Ultrasonics*, 39(4):269--281, 2001.

R. L. Mancuso. Some studies on ultrasonic testing with lamb waves. Technical report, General Electric Co. Hanford Atomic Products Operation, Richland, Washington, USA., 1957.

H. M. Matt and F. Lanza di Scalea. Macro-fiber composite piezoelectric rosettes for acoustic source location in complex structures. *Smart Materials and Structures*, 16: 1489--1499, 2007.

L. Mažeika, R. Kažys, and A. Maciulevičius. Optimization of transducer arrays parameters for efficient excitation of lamb waves. *Ultragarsas (Ultrasonics)*, 62(4):7--15, 2007.

A. H. Meitzler. Mode coupling occurring in the propagation of elastic pulses in wires. *The Journal Of The Acoustical Society Of America*, 33(4):435--445, 1961.

J. E. Michaels. Detection, localization and characterization of damage in plates with an in situ array of spatially distributed ultrasonic sensors. *Smart Materials and Structures*, 17:1--15, 2008.

T. E. Michaels, J. E. Michaels, B. Mi, and M. Ruzzene. Damage detection in plate structures using sparse ultrasonic transducer arrays and acoustic wavefield imaging. In *AIP Conference Proceedings*, volume 760, pages 938--945, 2005.

W. Mohr and P. Höller. On inspection of thin walled tubes for transverse and longitudinal flaws by guided ultrasonic waves. *IEEE Transactions on Sonics and Ultrasonics*, 23 (5):369--374, 1976.

R. Monkhouse, P. Wilcox, and P. Cawley. Flexible interdigital pvdf transducers for the generation of lamb waves in structures. *Ultrasonics*, 35(7):489--498, 1997.

R. Monkhouse, P. Wilcox, M. Lowe, R. Dalton, and P. Cawley. The rapid monitoring of structures using interdigital lamb wave transducers. *Smart Materials and Structures*, 9(3):304--309, 2000.

E. Morgan and P. Crosse. The acoustic ranger, a new instrument for tube and pipe inspection. *NDT International*, 11(4):179--183, 1978.

R. W. Morse. Dispersion of compression waves in isotropic rods of rectangular cross-section. *Journal of the Acoustical Society America*, 20:833--838, 1948.

P. Mudge. Field application of the teletest long-range ultrasonic testing technique. *Insight*, 43(2):74--77, 2001.

P. Mudge and A. Haig. 0716047.6 gb - acoustic transducer assembly, 2010.

P. J. Mudge. Teletest long range ultrasonic testing technique performance details, document reference: Ttp/01, may 2001. Technical report, TWI Ltd., 2000.

P. B Nagy and L. Adler. Nondestructive evaluation of adhesive joints by guided waves. *Journal of Applied Physics*, 66(10):4858--4663, 1989.

A. H. Nayfeh and D. E. Chimenti. Propagation of guided waves in fluid-coupled plates of fibre-reinforced composite. *The Journal Of The Acoustical Society Of America*, 83 (5):1736--1743, 1988.

L. J. Nelson. Smart piezoelectric fibre composites. *Materials Science and Technology*, 18 (11):1245--1256, 2002.

J. Oliver. Elastic wave dispersion in a cylindrical rod by a wide-band short-duration pulse technique. *The Journal Of The Acoustical Society Of America*, 29(2):189--971, 1957.

B. Pavlakovic, M. J. S. Lowe, D. N. Alleyne, and P. Cawley. Disperse: a general purpose program for creating dispersion curves. In D. O. Thompson & D. E. Chimenti, editor, *Review of Progress in Quantitative Non-destructive Evaluation*, volume 16, pages 185--192, New York, 1997. Plenum Press.

P. Pertsch, S. Richter, D. Kopsch, N. Krämer, J. Pogodzik, and E. Henning. Reliability of piezoelectric multilayer actuators. In *Actuator 2006 Conference Proceeding*, Bremen, Germany, June 2006.

A. Raghavan and E.S. Cesnik. Review of guided-wave structural health monitoring. *Shock and Vibration Digest*, 39(2):91--114, 2007a.

A. Raghavan and E.S. Cesnik. 3-d elasticity-based modelling of anisotropic piezocomposite transducers for guided wave structural health monitoring. *Journal of Vibration and Acoustics*, 129(6):739--751, 2007b.

J. Rose. A baseline and vision of ultrasonic guided wave inspection potential. *Journal of pressure vessel technology*, 124(3):273--282, 2002.

J. Rose, Z. Sun, P. Mudge, and M. Avioli. Guided wave flexural mode tuning and focusing for pipe testing. *Materials Evaluation*, 61(2):162--167, 2003.

J. L. Rose. *Ultrasonic Waves in Solid Media*. Cambridge University Press, 1999. ISBN-10: 0-521-64043-1.

J. L. Rose. Guided wave testing of water loaded structures. *Materials Evaluation*, 61(1): 23--24, 2003.

K. I. Salas and C. E. S. Cesnik. Guided wave excitation by a clover transducer for structural health monitoring: theory and experiments. *Smart Materials and Structures*, 18:1--27, 2009.

K. I. Salas and C. E. S. Cesnik. Guided wave structural health monitoring using clover transducers in composite materials. *Smart Materials and Structures*, 19(1):1--25, 2010.

R. Sanderson and P.P. Catton. An analytical model for guided wave array design for structures of any cross section. *IEEE Transactions on Ultrasonics, Ferrorelectric and Frequency Control*, 58(5):1016--1026, May 2011.

H. Schneider. The nondestructive testing of tubes and pipes for nuclear application. *Nuclear Engineering and Design*, 81(1):69--76, 1984.

S. Sherrit and B. Mukherjee. Electrostrictive materials: Characterization and applications for ultrasound. In *SPIE Conference Proceedings*, volume 3341, pages 196--207, 1998.

H. J. Shin and J. L. Rose. Guided waves by axisymmetric and non-axisymmetric surface loading on hollow cylinders. *Ultrasonics*, 37:355--363, 1999.

M. G. Silk and K. F. Bainton. The propagation in metal tubing of ultrasonic wave modes equivalent to lamb waves. *Ultrasonics*, 17(1):11--19, 1979.

Simonetti. *Sound propagation in lossless waveguides coated with attenuative materials*. PhD thesis, Imperial College London, 2003.

W-J. Song, J. L. Rose, and H. Whitesel. An ultrasonic guided wove technique for damage testing in a ship hull. *Materials Evaluation*, 61(1):94--98, 2003.

R. W. Soutas-Little. *Continuum Mechanics*. EOLSS, 2012. Chapter "History of Continuum Mechanics".

W. Staszewski, B. Lee, L. Mallet, and F. Scarpa. Structural health monitoring using scanning laser vibrometry; part i lamb wave sensing. *Smart Materials and Structures*, 13(2):251--260, 2004.

A. B. Thien. Pipeline structural health monitoring using macro-fiber composite active sensors. Master's thesis, University Of Cincinnati, 2006.

J. Tressler, S. Alkoy, and R. Newnham. Piezoelectric sensors and sensor materials. *Journal of Electroceramics*, 2(4):257--272, 1998.

A. V. Turik, A. A. Yesis, and L. A. Reznitchenko. Comparison of piezoelectric, magnetostrictive, and electrostrictive hybrid hydraulic actuators. *Ferroelectrics*, 359(1): 111--116, 2007.

K. Uchino. Acoustic transduction - materials and devices. Technical Report 4, Pennsylvania State University, Materials Research Lab, University Park, Pennsylvania, 2000. Available through U.S. National Technical Information Service.

I. A. Viktorov. *Rayleigh and Lamb waves: physical theory and applications*. 1967.

X. Wang, P. W. Tse, C. K. Mechefske, and M. Hua. Experimental investigation of reflection in guided wave-based inspection for the characterization of pipeline defects. *NDT & E International*, 43:365374, 2010.

P. Wilcox, M. J. S. Lowe, and P. Cawley. Mode and transducer selection for long range lamb wave inspection. *Journal Of Intelligent Material Systems And Structures*, 12: 553--565, 2001.

P.D. Wilcox, P. Cawley, and M.J.S. Lowe. Acoustic fields from pvdf interdigital transducers. In *IEE Proceedings in Science, Measurements and Technology*, volume 145, pages 250--259, September 1998.

W. Wilkie, R. Bryant, R. Fox, R. Hellbaum, J. High, A. Jalink, B. Little, and P. Mirick. Method of fabricating a piezoelectric composite apparatus, 10 2003.

W. K. Wilkie, R. Bryant, J. High, R. Fox, and R. Hellbaum. Low-cost piezocomposite actuator for structural control applications. In *SPIE 7th International Symposium On Smart Structures And Materials*, Newport Beach, California, U.S., 2000.

R. B. Williams, G. Park, D. J. Inman, and W. K. Wilkie. An overview of composite actuators with piezoceramic fibers. In *Conference on structural dynamics Number 20*, volume 4753 of *SPIE proceedings*, Los Angeles, USA, February 2002.

T. Windisch, B. Köhler, and N. Meyendorf. Comparison of guided wave sensors for shm sensor networks. In *Smart Sensor Phenomena, Technology, Networks, and Systems*, volume 7648 of *Proc. SPIE*, 2010.

D. C. Worlton. Applications of lamb waves in ultrasonic testing. In *Symposium on Nondestructive Tests in the Field of Nuclear Energy*, pages 260--265, Chicago, Ill., April 1957.

D. C. Worlton. Experimental confirmation of lamb waves at megacycle frequencies. *The Journal of Applied Physics*, 32(6):967--971, 1961.

J. Zemanek. An experimental and theoretical investigation of elastic wave propagation in a cylinder. *The Journal Of The Acoustical Society Of America*, 51(1B):265--283, 1971.